

**BREAKTHROUGH ANALYSIS OF A
STRUCTURED ADSORBENT BED**

by

VORAPOJ NETPRASAT

B.A.Sc., The University of British Columbia, 2000

A THESIS SUBMITTED IN PARTIAL FULFILLMENT OF
THE REQUIREMENTS FOR THE DEGREE OF
MASTER OF APPLIED SCIENCE

in

THE FACULTY OF GRADUATE STUDIES
(DEPARTMENT OF CHEMICAL AND BIOLOGICAL ENGINEERING)

We accept this thesis as conforming
to the required standard

THE UNIVERSITY OF BRITISH COLUMBIA

April, 2004

© Vorapoj Netprasat, 2004

Library Authorization

In presenting this thesis in partial fulfillment of the requirements for an advanced degree at the University of British Columbia, I agree that the Library shall make it freely available for reference and study. I further agree that permission for extensive copying of this thesis for scholarly purposes may be granted by the head of my department or by his or her representatives. It is understood that copying or publication of this thesis for financial gain shall not be allowed without my written permission.

VORAPOT NETPRASAT

Name of Author (please print)

21/04/2004

Date (dd/mm/yyyy)

Title of Thesis: BREAKTHROUGH ANALYSIS OF
A STRUCTURED ADSORBENT BED

Degree: M. A. Sc.

Year: 2004

Department of CHEMICAL AND BIOLOGICAL ENGINEERING
The University of British Columbia
Vancouver, BC Canada

Abstract

The objectives of the present study were to compare the adsorption isotherms of various gases on various adsorbents using gravimetric, volumetric, and chromatographic methods: to determine whether the Langmuir isotherm model is appropriate for the N_2 adsorption isotherms up to 300 kPa on zeolite NaX and zeolite LiX; to identify the dominant dynamic behaviour through a laminate bed of these and other adsorbents and to determine the effect of flowrate on the magnitude of the axial dispersion or mass transfer resistance within the laminated bed of adsorbent.

The gas adsorption isotherms of CO, and CO₂ on zeolite 13X were obtained using the volumetric, gravimetric, and chromatographic methods. The isotherms obtained from the volumetric and gravimetric methods showed good agreement. The gravimetric method was used to measure adsorption isotherms of N_2 up to 300 kPa for N_2 on zeolite LiX relevant in the air separation industry. The N_2 adsorption capacity of zeolite LiX, obtained in the present study, was higher than the N_2 adsorption capacity of NaX or 13X used traditionally for air separation.

The chromatographic method was used to determine the dispersion and mass transfer coefficients in a laminated bed of adsorbent. The results suggested that at low interstitial velocities, $v < 1.7$ cm/sec, dispersion dominated, while at high interstitial velocities, $v \gg 1.7$ cm/sec, macropore and micropore mass transfer resistance dominated. Estimated dispersion and external fluid film mass transfer resistances were consistent with literature values. However, the micropore diffusivity obtained was lower than that reported in available literature data. The difference was most likely due to the

inaccuracy in the results obtained using only two particle sizes. Furthermore, from the mass transfer resistances obtained for PSA with short cycle times using laminate beds, fast PSA with cycle time of 0.6 to 3 seconds is possible.

Table of Content

Abstract	ii
List of Tables	viii
List of Figures	x
Nomenclature	xiv
Acknowledgement	xx
Chapter 1: Introduction	1
1.1 Background	1
1.2 Motivation for the Study	5
1.3 Objectives	8
Chapter 2: Literature Review	9
2.1 Adsorption	10
2.1.1 Pressure Swing Adsorption	12
2.2.2 PSA with Short Cycle Time	15
2.2.3 Adsorbent Development in Air Separation	20
2.2 Gas Adsorption Isotherms	23
2.2.1 Background	23
2.2.1.1 Henry's Law	24
2.2.1.2 The Langmuir Isotherm	25
2.2.1.3 Freundlich and Langmuir Isotherms	26
2.2.2 Isotherm Measurement Methods	27
2.2.2.1 Volumetric Method	27

2.2.2.2 Gravimetric Analysis	28
2.2.2.3 Breakthrough Analysis.....	28
2.2.2.4 Comparison Between Isotherm Measurement Methods	32
2.3 Bed Configurations	33
2.3.1 Packed Bed.....	33
2.3.2 Monolithic Bed	35
2.4 Experimental Methods in Measuring Gas Adsorption Dynamics	38
2.4.1 Zero Length Column.....	40
2.4.2 Permeation	40
2.4.3 Frequency Response Method.....	41
2.4.4 Chromatography method	42
Chapter 3: Experimental	50
3.1 Procedure and Apparatus	50
3.1.1 Gas isotherm measurement.....	50
3.1.1.1 Gravimetric Analysis	50
3.1.1.2 High Pressure Gravimetric Measurement.....	54
3.1.1.3 Volumetric Adsorption Isotherm Measurement	56
3.1.1.4 Breakthrough Analysis.....	58
3.1.2 Chromatographic Method	59
3.1.3 Pressure Drop Through Structured Adsorbent Bed	61
3.2 Materials.	62
3.2.1 Adsorption Isotherm	62
3.2.2 Kinetic Parameters.....	63

Chapter4: Adsorption Isotherm Measurements	65
4.1 Introduction.....	65
4.2 CO and CO ₂ adsorption isotherms.....	65
4.3 N ₂ Adsorption Isotherms.....	77
4.4 Heats of Adsorption.	90
Chapter 5: Dispersion and Mass Transfer in Structure Adsorbent Bed.....	94
5.1 Introduction.....	94
5.2 Henry's Constant Estimates.....	96
5.3 Dispersion and Mass Transfer Estimates.....	101
5.4 Macropore and Micropore Mass Transfer	109
5.6 Parametric Study	121
Chapter 6: Conclusions and Recommendations for Future Work	127
6.1 Conclusions.....	127
6.2 Recommendations for Future Work.....	128
Reference:.....	129
Appendix 1 :Isotherm Measurements Data.....	135
Appendix 2: Summary of Breakthrough Data	145
Appendix 3: Breakthrough Curves for Breakthrough Experiments	149
Appendix 4: Mass Transfer Resistance Comparison.....	154
Appendix 5: Calculation of Mass Transfer Resistance.....	155
Appendix 6: Pressure Drop Through the Structured Adsorbent Bed	157
Appendix 7: Detailed Experimental Procedures.....	159
Low pressure (atmospheric) gravimetric method	159

High pressure (up to 3 bar) gravimetric method	159
Volumetric method	160
Programming a sample file	160
Desorption breakthrough experiment	161
Running breakthrough measurements.....	161
Breakthrough method used to estimate dispersion and mass transfer coefficients.....	163
Appendix 8: F test.....	165
Appendix 9: Heat Adsorption Calculations	174
Appendix 10: Matlab™ Program.....	178

List of Tables

Table 1.1	Usage of hydrogen, nitrogen, and oxygen.	1
Table 2.1	Advantages and disadvantages in adsorption dynamics measurement method.....	39
Table 3.1	Adsorbents used in the present study.....	63
Table 4.1	Comparison of Langmuir adsorption constants at 30 °C determined using the volumetric gravimetric, and desorption breakthrough methods on zeolite NaX.....	67
Table 4.2	F-test comparison between volumetric and gravimetric data for CO and CO ₂ adsorption on zeolite NaX at 30 °C.	73
Table 4.3	F-test comparison of N ₂ adsorption on zeolite NaX by volumetric and gravimetric methods.....	78
Table 4.4	Langmuir constants for N ₂ on zeolite LiX.....	80
Table 4.5	Langmuir constants for high and low pressure data for N ₂ on QP	87
Table 4.6	F-test comparison for significant difference between low and high pressure N ₂ adsorption isotherms on QP vs. both sets of data.	89
Table 5.1	Summary of Adsorption structure dimensions.....	96
Table 5.2	Henry constants and their 95% confidence intervals.....	100
Table 5.3	Comparison of gas adsorbed at 101 kPa and 24 °C between gravimetric and chromatographic method	100
Table 5.4	Dispersion coefficients estimated for structured adsorbent beds.....	105
Table 5.5	Lumped mass transfer resistances estimated using HETP/2υ vs. 1/υ ² at low flow rate.	106
Table 5.6	Lumped mass transfer rates estimated using Plate theory at high flow rate and their 95% confidence intervals.....	109

Table 5.7	Individual mass transfer coefficients.	112
Table 5.8	Fluid film mass transfer coefficient.	113
Table 5.9	Fluid film mass transfer coefficient compared with literature value.	114
Table 5.10	SSE and F-values from the F-test for predicted data from Matlab™ program and measured data.....	121

List of Figures

Figure 2.1	Skarstrom cycle	14
Figure 2.2	PSA with short cycle Process (source: Sircar & Hanley, 1995).....	16
Figure 2.3	Brunauer classification of isotherms	24
Figure 2.4	General equilibrium relationship.....	29
Figure 3.1	Flowsheet of gravimetric apparatus used for adsorption isotherm measurement.....	51
Figure 3.2	Schematic of the gravimetric analyzer unit.....	52
Figure 3.3	Graphical representation of high pressure TGA.....	55
Figure 3.4	Schematic diagram of ASAP 2010.....	57
Figure 3.5	Breakthrough experiment for mass-spectrometer system	58
Figure 3.6	Breakthrough experimental set up with TCD for low flow rate experiments	60
Figure 3.7	Breakthrough experiment set up with TCD for high flow rate experiments.....	61
Figure 3.8	Graphical representation of the structured adsorbent	64
Figure 4.1	CO and CO ₂ adsorption isotherms on zeolite NaX at 30 °C obtained by the volumetric and gravimetric methods.....	66
Figure 4.2	Measured and fitted adsorption isotherms for CO at 30 °C on zeolite NaX	68
Figure 4.3	Measured and fitted adsorption isotherms for CO ₂ at 30 °C on zeolite NaX.....	69
Figure 4.4	Comparison of the CO adsorption isotherms for zeolite NaX based on Langmuir parameters obtained from volumetric, gravimetric, and desorption breakthrough method at 30 °C.....	70

Figure 4.5	Comparison of the CO ₂ adsorption isotherms at 30 °C for zeolite NaX based on Langmuir parameters obtained from volumetric, gravimetric, and desorption breakthrough method	71
Figure 4.6	$(q^*-q'_o)/(q_o-q'_o)$ vs. $(c-c'_o)/(c_o-c'_o)$ for CO.	75
Figure 4.7	$(q^*-q'_o)/(q_o-q'_o)$ vs. $(c-c'_o)/(c_o-c'_o)$ for CO ₂	76
Figure 4.8	C/C_o vs. $1/\sqrt{vt-z}$ plot for CO at 30 °C.	77
Figure 4.9	Measured N ₂ adsorption isotherms on zeolite NaX obtained by the volumetric and gravimetric methods.	79
Figure 4.10	N ₂ adsorption isotherms for zeolite LiX obtained by the gravimetric method.	81
Figure 4.11	ln K vs. 1/T for the extrapolation of Henry's constant of N ₂ isotherm on zeolite NaX.	83
Figure 4.12	ln b vs. 1/T for the extrapolation of Langmuir constant, b of N ₂ isotherm on zeolite LiX.	84
Figure 4.13	N ₂ adsorption isotherm on NaX at 25 °C.	85
Figure 4.14	N ₂ adsorption isotherm on LiX at 25 °C.	86
Figure 4.15	Comparison of extrapolated high pressure isotherm data with measured high pressure data for N ₂ on QP.	88
Figure 4.16	ln K vs. 1000/T used to determined heat of adsorption of N ₂ , CO, and CO ₂ on QA2 adsorbent from the data measured volumetrically.	91
Figure 4.17	ln K vs. 1000/T used to determined heat of adsorption of N ₂ on zeolite NaX adsorbent from the data measured gravimetrically.	92
Figure 4.18	ln b vs. 1000/T used to determined heat of adsorption of N ₂ on zeolite LiX adsorbent using Langmuir parameter, b.	93

Figure 5.1	μ vs. $1/F$ for high X-sectional area structure for N_2 at 24 °C and 101 kPa.	97
Figure 5.2	μ vs. $1/F$ for mid X-sectional area structure for N_2 at 24 °C and 101 kPa.	97
Figure 5.3	μ vs. $1/F$ for low X-sectional area structure for N_2 at 24 °C and 101 kPa.	98
Figure 5.4	μ vs. $1/F$ for high voidage structure for N_2 at 24 °C and 101 kPa.....	98
Figure 5.5	μ vs. $1/F$ for thick adsorbent sheets structure for N_2 at 24 °C and 101 kPa.	99
Figure 5.6	HETP/ $2v$ vs. $1/v^2$ for high X-sectional area structure for N_2 at 24 °C and 101 kPa.....	102
Figure 5.7	HETP/ $2v$ vs. $1/v^2$ for mid X-sectional area structure for N_2 at 24 °C and 101 kPa.....	102
Figure 5.8	HETP/ $2v$ vs. $1/v^2$ for low X-sectional area structure for N_2 at 24 °C and 101 kPa.....	103
Figure 5.9	HETP/ $2v$ vs. $1/v^2$ for non adsorbing structure for N_2 at 24 °C and 101 kPa.	103
Figure 5.10	HETP/ $2v$ vs. $1/v^2$ for high voidage structure for N_2 at 24 °C and 101 kPa.	104
Figure 5.11	HETP/ $2v$ vs. $1/v^2$ for thick adsorbent sheets structure for N_2 at 24 °C and 101 kPa.....	104
Figure 5.12	HETP vs. interstitial velocity plot used to determine the lumped mass transfer coefficient for $v > 7$ cm/s.....	108
Figure 5.13	$\frac{1}{kK}$ vs. $(\alpha R_p)^2$ used to determine macropore and micropore mass transfer coefficients.....	110
Figure 5.14	$\frac{1}{kK}$ vs. $(\alpha R_p)^2$ used to determine macropore and micropore mass transfer coefficients.....	112

Figure 5.15	Predicted breakthrough curve and raw data for high X-sectional area structure with flow = 100 SCCM.....	115
Figure 5.16	Predicted breakthrough curve and raw data for mid X-sectional area structure with flow = 100 SCCM.....	116
Figure 5.17	Predicted breakthrough curve and raw data for non-adsorbing structure with flow = 100 SCCM.....	117
Figure 5.18	Predicted breakthrough curve and raw data for low X-sectional area structure with flow = 100 SCCM.....	118
Figure 5.19	Predicted breakthrough curve and raw data for high voidage structure with flow = 100 SCCM.....	119
Figure 5.20	Predicted breakthrough curve and raw data for thick adsorbent sheets structure with flow = 100 SCCM.....	120
Figure 5.21	Predicted breakthrough curve for change in external fluid film coefficient, k_f	122
Figure 5.22	Predicted breakthrough curve for change in macropore mass transfer coefficient, D_p	123
Figure 5.23	Predicted breakthrough curve for change in micropore mass transfer coefficient, D_c	124
Figure 5.24	Predicted breakthrough curve for change in dispersion coefficient, D_L	125

Nomenclature

		Units
a	= Langmuir constant	$\text{mmol g}^{-1} \text{ kPa}^{-1}$
A	= Percent open frontal area of a monolith	%
A_w	= Wall correction term for Equation [2.28]	-
A_1	= Molecular diffusion term in Equation [2.53]	cm
A_2	= Eddy diffusion term in Equation [2.53]	cm
A_3	= Mass transfer resistances term in Equation [2.53]	cm
b	= Langmuir constant	kPa^{-1}
B	= Monolith channel cross section constant	-
B_w	= Wall correction term for Equation [2.28]	-
c	= Concentration	mol/L
c'_o, c_o	= Initial ($t < 0$) and final ($t \geq 0$) steady state values of c	
CMS	= Carbon Molecular Sieve	-
d	= Diameter	μm or m
d_{ch}	= Monolith channel diameter	cm
d_h	= Hydraulic diameter	cm
d_p	= Particle diameter	μm or m
D/d_p	= Tube to particle diameter ratio	-
D_c	= Micropore diffusivity	cm^2/sec
D_L	= Axial dispersion coefficient	cm^2/sec
D_m	= Molecular dispersion coefficient	cm^2/sec
D_p	= Macropore diffusivity	cm^2/sec
d.f.	= Degree of freedom	-

erfc	=	Error function	-
E	=	Electric field	
f	=	Friction factor	-
F_{stats}	=	F factor defined as F_1/F_2 or volumetric flow rate	-
F	=	Volumetric flow rate	cm^3/sec
F factor	=	F_{stats} obtained from Statistical F-test	-
F_1	=	SSE/d.f. of data set 1	-
F_2	=	SSE/d.f. of data set 2	-
F_b	=	Buoyancy force	N
$F_{\text{critical}, \alpha=0.05}$	=	F values from F distribution table at 95% confidence interval	-
FR	=	Frequency Response	-
g_0	=	Gravitational constant	m/sec^2
HETP	=	Height Equivalent Theoretical Plate	cm or m
k	=	Mass transfer coefficient	sec^{-1}
k_f	=	External fluid film mass transfer coefficient	cm/sec
k_1	=	Coefficient of wall effect correction term	-
k_2	=	Coefficient of wall effect correction term	-
K	=	Henry constant (expressed on a particle volume basis)	-
K'	=	Henry constant	-
K_c	=	Dimensionless equilibrium constant, expressed on a solid volume basis	-

K_o	=	Pre-exponential factors in $K = K_o \exp(-\Delta U/RT)$ and $K' = K'_o \exp(-\Delta H/RT)$	-
K_1	=	Coefficient of pressure correlation	-
m	=	Initial mass of the sample	kg or g
L	=	Length	cm or m
$Li, Me^{2+}X$	=	Zeolite X with Li and metal ion with 2+ charge	-
$Li, Me^{3+}X$	=	Zeolite X with Li and metal ion with 3+ charge	-
N	=	Amount of gas adsorbed	mmol/g
Me^{2+}	=	Metal cation with 2+ charge	-
p	=	Pressure	kPa
PSA	=	Pressure Swing Adsorption	-
q	=	Amount of gas adsorbed or sorbate concentration	mmol/g
q^*	=	Equilibrium value of q	mmol/g
q'_o, q_o, q'	=	Initial, final, and surface value of q	mmol/g
q'_L	=	Surface value of gas adsorbed	mol/L
q_s	=	Amount of gas adsorbed at saturation	mmol/g
\bar{q}_L	=	Value of gas adsorbed over crystal particle	mol/L
r	=	Radius	μm or m
r_c	=	Radius of a zeolite crystal	μm or m
R	=	Universal gas constant	$kPa \cdot m^3 / (mol \cdot K)$
R_p	=	Particle radius	μm or m
Re	=	Reynolds number	-

s	=	Second	sec
Sc	=	Schmidt number	-
SCCM	=	Standard cubic centimeter per minute	cm ³ /min
Sh	=	Sherwood number	-
SSE	=	Sum of square of errors defined as [Y(predicted) - Y(average)] ²	-
T	=	Temperature	K or °C
t	=	Time	sec
TGA	=	Thermogravimetric analyzer	-
v	=	Interstitial velocity	cm/sec
V _f	=	Volume of fluid	cm ³
V _s	=	Volume of sorbate	cm ³
w(c)	=	Concentration profile velocity	cm/sec
W	=	Mass flow rate	g/sec
W _{flow}	=	Weight of sample with He flow	g
W _{static}	=	Weight of sample without He flow	g
W _t	=	Sample weight after adsorption	g
U _g	=	Kinetic energy of sorbate in the bulk phase	kJ
U _s	=	Kinetic energy of sorbate in the adsorbed phase	kJ
z	=	Length of the adsorption column	cm or m
ZLC	=	Zero Length Chromatography	-

GREEK LETTERS

β	=	Dimensionless variable defined as $1 - \frac{q_o}{q_s}$ or $(1 + bc_o)^{-1}$	-
δ	=	ratio of external film resistance and axial dispersion in (Equation [2.55]) and (Equation [2.56])	-
ε	=	Force Potential (characteristics of the particular molecular species) or bed voidage	kJ or -
ε_p	=	Particle voidage	-
ϕ	=	Potential energy	kJ
ϕ_D	=	Energy due to Dispersion	kJ
ϕ_P	=	Energy due to Polarization force	kJ
ϕ_Q	=	Energy due to Quadruple force	kJ
ϕ_R	=	Repulsion energy	kJ
ϕ_α	=	Polarization energy	kJ
ϕ_ε	=	Sorbate-sorbate interaction energy	kJ
ϕ_μ	=	Dipole interaction energy	kJ
γ_1, γ_2	=	Constants in axial dispersion equation (Equation [2.52])	-
μ	=	Dipole moment or viscosity or mean residence time	C*m or Pa*s or sec
ρ	=	Density	kg/m ³
ρ_f	=	Fluid density	kg/m ³

σ	=	Force Constants (characteristics of the particular molecular species)	$\frac{\text{N}}{\text{m}}$
σ^2	=	Variance	sec^2
τ	=	Dimensionless time constant	-
v	=	Interstitial velocity (superficial velocity/voidage)	cm/s
ξ	=	Dimensionless bed length	-
$\frac{\xi}{\tau}$	=	Dimensionless variable defined as $\frac{(bq_s)z}{(vt - z)} \left(\frac{1 - \varepsilon}{\varepsilon} \right)$	-
ψ	=	Dimensionless pressure drop	-
ΔH_R^O	=	Heat of reaction at standard conditions	kJ/mol
ΔH_o	=	Heat of adsorption at low coverage	kJ/mol
Δp	=	Change in pressure	kPa
ΔU	=	Change in internal energy	kJ

Acknowledgement

I would like to express my sincere appreciation to Dr. Kevin Smith for his invaluable guidance and support throughout my research.

I would like to thank Questair Technologies for the financial and technical support for this research, especially Dr. Jim Sawada.

I would like to acknowledge the graduate students in Dr. Smith's research group for their help and support throughout the years, especially Sevan Bedrossian, Yi Zhang, Ching Tian Tye, and Jamie Mckay.

Chapter 1: Introduction

1.1 Background

Hydrogen, nitrogen and oxygen are chemicals of vital importance to many industrial manufacturing processes. In the production of these chemicals, a mixture of gases must be separated to obtain a sufficiently pure hydrogen, nitrogen or oxygen product. High purity hydrogen, nitrogen and oxygen are needed in many applications ranging from fuel cells to medical air. Some of the uses of these three chemicals are listed in Table 1.1.

Table 1.1 Usage of hydrogen, nitrogen, and oxygen.

Chemical	Usage
Hydrogen	Production of ammonia, methanol, gasoline, heating oil, rocket fuel, fertilizers, glass, refined metals, vitamins, cosmetics, semiconductor circuits, soaps, lubricants, cleaners, and fuel cells.
Nitrogen	Production of ammonia, fertilizer, carrier gas or purging gas in semiconductor production, refrigerant, and cryogenic freezing.
Oxygen	Oxygen therapy to cure stress, respiration, combustion to fuel a flame and increase its heat to remove impurities in steel production, used in variety of oxidation processes.

Ammonia and methanol plants are the major and most important consumers of hydrogen. In 1996, CMA (Chemical Manufacturing Association) reported that ammonia and methanol plants consumed 264 billion (STP) m^3 and 36.9 billion (STP) m^3 , respectively, of the 420 billion (STP) m^3 hydrogen produced worldwide, accounting for over 70 percent of hydrogen consumption. The cost of hydrogen through pipeline and for large on-site production is

approximately US\$ 0.070 per (STP) m^3 , thus making hydrogen production a US\$ 30 billion per year industry. Furthermore, in 1996, the demand for hydrogen was predicted to grow at the rate of 3 percent a year over the next 5 years.

Ammonia production is the major consumer of nitrogen. 80 % of the ammonia produced from nitrogen is used in fertilizer manufacture. The cost of nitrogen through pipeline is approximately US\$ 0.039 per (STP) m^3 , hence making nitrogen production a US\$ 2 billion per year industry, since the total worldwide nitrogen production was estimated to be 45 billion (STP) m^3 in 1991 (Hardenburger, 1996).

Oxygen is also used in many industrial applications. In 1991 the largest uses of oxygen in the United States, accounting for 95% of production, were: steel, 40%; chemicals, 24%; metal welding and cutting, 7%; coal gasification, 7%; nonferrous metals, 7%; petroleum refining, 6%; and health, 4% (CMA, 1992). During the same year, worldwide annual production of oxygen was estimated to be about 70 billion (STP) m^3 and was predicted to grow at the rate of 3-5 percent a year over the next 10 years (CMA, 1992). The cost of oxygen in 1991 was approximately US\$ 0.053 per (STP) m^3 making oxygen production a US\$ 4 billion per year industry.

There are many ways to manufacture hydrogen, nitrogen and oxygen. The main commercial processes for the on-site production of hydrogen are steam reforming of hydrocarbons, partial oxidation of coal, coke, and residue oil, and the electrolysis of water. Hydrogen is also produced as a by-product of various chemical processes especially ethylene cracking and catalytic reforming. Hydrogen is primarily produced by the steam reforming process using natural gas and water (Equation [1.1]). In the U.S., more than 95% of on-site hydrogen production is supplied by steam reforming of light hydrocarbons such as methane (Baade and Parekh, 2001). In 2000, worldwide hydrogen production was 240 billion (STP) m^3

from natural gas, 150 billion (STP) m³ from oil, 90 billion (STP) m³ from coal, and 20 billion (STP) m³ from electrolysis (DOE, 2002).



The steam reforming process (Equation [1.1]), which is endothermic with $\Delta H_R^O = +206$ kJ/mol, is widely used in the chemical industry for hydrogen production. This reaction takes place between 788-880 °C with steam to carbon ratio of 2.5-4 to ensure adequate reaction rate and high hydrogen formation, which is favoured at high temperature and low pressures (1.4-2.8 MPa).

Carbon monoxide produced from the steam reforming reaction can further react with water in the water-gas-shift reaction, which has $\Delta H_R^O = -41$ kJ/mol (Equation [1.2]) to produce hydrogen and carbon dioxide using nickel catalyst at 343-371 °C.



In both reactions, the products consist primarily of hydrogen and CO and CO₂, hence, there is a need for separation of hydrogen from these gases. Many existing chemical plants or refineries produce hydrogen with purity ranging from 95-97 % from the steam reforming process, followed by absorption and methanation of any remaining carbon oxides. However, this purity is too low for some applications such as hydrogen fuel cells. Consequently, the purity of hydrogen can be and usually is increased to above 99.9% by pressure swing adsorption (Baade and Parekh, 2001).

The primary method of nitrogen production is by the liquefaction and fractional distillation of air (cryogenic distillation), and by pressure swing adsorption (PSA) of air. Commercially, high purity nitrogen with 1 ppm residual oxygen is produced from cryogenic distillation while lower purity nitrogen of up to 99.8% nitrogen with 0.2% residual oxygen is produced by PSA (Hardenburger, 1996).

The principal methods of oxygen production are by cryogenic distillation and by PSA of air. Commercially, worldwide production of 99.5% pure oxygen is by cryogenic distillation in air separation plants (Ansel et al., 1996). Oxygen at about 90-95% purity is produced from air by PSA at lower cost than cryogenic distillation since it is less energy intensive. Storms (1997) compared the power requirement and oxygen production cost from cryogenic distillation and PSA. The power requirement for 50-2000 tons/day cryogenic distillation plant and 10-100 tons/day PSA plant is 350-400 kWh/ton and 250-600 kWh/ton, respectively. He further compared oxygen production costs at low production of 20 tons/day. The result is that oxygen produced by cryogenic distillation costs \$US 75-85 per ton and by PSA \$US 40-55 per ton. Storms (1997) concluded that for low to medium oxygen production (20-50 tons/day) and purity (80-95%), PSA is more cost effective than cryogenic distillation. In the past few years, PSA has gained popularity and market share in oxygen production. In 1999, Tosoh industry reported that oxygen generation by PSA accounted for approximately 20 % of the market compared to less than 5% in 1991.

Due to an increasing importance of PSA in hydrogen, nitrogen and oxygen production, there is a need to further improve the PSA process. PSA is an adiabatic process, in which impurities in a gas stream are removed by adsorption onto suitable adsorbents such as activated carbon or zeolite (hydrogen purification), carbon molecular sieve or 5A zeolite (nitrogen production), and 5A zeolite or 13X zeolite (oxygen production) in a fixed bed of adsorbent under high operating pressure with low pressure drop. Adsorbents are usually regenerated, first by depressurizing the bed, then, purging with some of the product gas at low pressure. In order to obtain continuous products, at least two adsorbers must be used; one to receive feed gas at high pressure, hence, generating products while at the same time, another is regenerated by depressurizing the adsorbent bed. The two adsorbers are cycled between adsorption and

regeneration modes of operation to obtain continuous product flow, hence the name pressure swing adsorption.

1.2 Motivation for the Study

Attempts have been made to improve the conventional PSA process in order to increase productivity and hence lower capital and operating costs. For a conventional PSA, two adsorbers in parallel are needed and the cycle time, which is defined as the time taken for the adsorption and desorption of the gas, is often long, ranging from 3 to 4 minutes (Jones and Kelly, 1981), leading to high operating cost and little product, e.g., the Lindox process (1970) produced 40 tons/day of 90% pure oxygen with 38% recovery (percentage of oxygen produced over oxygen fed) and power requirement of about 1.7 kWh/100 SCF (standard cubic feet) or 60 kWh/100 m³, which translates to 460 kWh/ton oxygen. The high cost has led to the development of the short cycle time PSA process. Jones et al. (1980) is one attempt to reduce capital and operating costs of PSA by introduction of PSA with short cycle time using only one adsorbent bed. PSA with short cycle time involves two steps: (1) adsorption at relatively high pressure, e.g. 300-500 kPa during which specific components are attached to the adsorbents (2) desorption, during which these components are removed by pressure reduction. Unlike the conventional PSA, PSA with short cycle time only requires one adsorber and adsorbed components are removed by the difference in pressure between the adsorption and desorption cycle. The process requires a large pressure difference, usually between 100 to 300 kPa and short cycle time (5 to 20 seconds). The pressure difference can be achieved by using small adsorbent particles between 100 to 500 μm . Several advantages arise from PSA with short cycle time relative to conventional PSA:

- (1) PSA with short cycle time is more compact than PSA since cycle times are much shorter resulting in higher production rates.

- (2) The cost of the PSA with short cycle time is much lower than the PSA system due to a more compact single adsorber.
- (3) No purge flow is required during desorption.

However, the major drawback of this system is the energy cost to produce a large pressure difference. Furthermore, a recent study by Alpay et al. (1994) showed that the product enrichment is limited for small particle sizes by axial dispersion and pressure dynamics of the system, and for larger particles, by macropore mass transfer resistance (resistance within pores of the particles/pellets, but not the crystals). In a packed bed, small particles are used in order to reduce macropore mass transfer resistance, however, Keefer et al. (1992) stated that small particles tend to stick together and pack unevenly causing significant axial dispersion, hence preventing reduction in adsorber length. Consequently, the cycle time can not be reduced much below 3 seconds.

Even though PSA with short cycle time can produce a larger quantity of products compared to PSA, this process is limited to small scale use only, since the pumping cost to create the large pressure difference is high at larger scale. Storms (1997) reported the power requirement for 10-100 tons/day oxygen production as 250 to 600 kWh/ton. The operating cost of PSA with short cycle time process clearly increases dramatically at higher production rate when compared to the operating cost of the cryogenic process. For 50-2000 tons/day oxygen production, the power requirement for the cryogenic process ranges from 350-400 kWh/ton. The power requirement for the PSA system more than doubles when production is increased 10 times from 10 tons/day to 100 tons/day, but the power requirement for cryogenic distillation only increases by 15% when the production is increased from 50 to 2000 tons/day.

To overcome this large pressure difference and obtain even shorter cycle times, QuestAir Technologies Incorporation has developed a PSA system with cycle times of 0.2 to 6 seconds by introducing a structured adsorbent bed instead of a conventional packed bed. The structured

adsorbent bed resembles a monolith or parallel passage bed using multiple layers with adsorbent sheet thickness ranges from 50-300 μm , deposited on a solid substrate where the particle thickness and channel height can be varied independently (i.e., the adsorbent particle size). The monolith structure provides a large voidage in the bed, hence reducing pressure drop drastically when compared to a conventional packed bed PSA. The cycle time for the structured adsorbent bed is short since reduced particle diameter is used, hence, reducing macropore mass transfer resistance. Keefer et al. (1992) and Keefer (2000) claimed that high dispersion due to clustering of small particles limits the cycle time of short cycle PSA using a conventional packed bed to 3 seconds whereas, the cycle time of the PSA process using a structured adsorbent bed can be lower 0.2 second. Furthermore, PSA using a structured adsorbent bed has an advantage over PSA using a packed bed since it does not require a large pressure difference. As with the conventional packed bed, the structured adsorbent bed operated at high flowrate and even shorter cycle time is constrained by mass transfer and axial dispersion resistances that become significant at these small particle sizes. There is a need to identify the magnitude of the dominant mass transfer resistances when using the structured adsorbent bed, especially at high flow rates. The motivation behind this work is, therefore, to study the dynamics of such structured adsorbent bed configurations to identify the magnitude of the dominant resistances at different flow rates, i.e., determining the flow rate range that axial dispersion or mass transfer resistances are significant. Moreover, at high flow rates, mass transfer resistances are expected to dominate over axial dispersion. Consequently, the flow rate at which the dominant mass transfer resistance occurs, whether it is external fluid film, macropore, or micropore resistance (mass transfer resistance within the crystal structures) needs to be identified. In addition to identifying the adsorption dynamics in the structured adsorbent bed, the expected reduction in pressure drop will be verified. Furthermore, since the design of any adsorption column requires adsorption capacity of a given adsorbent to be known, this study also aimed at measuring the

adsorption isotherms of various gas components in the QuestAir adsorbent of interest, at pressure up to 300 kPa. High-pressure adsorption isotherms up to 300 kPa are required since the inlet pressure of around 300 kPa is normally used in the PSA process. The focus of these measurements, however, is a comparison of the various measurement methods such as gravimetric, volumetric, and desorption breakthrough method, and determining the most appropriate method for the adsorbents in this study.

1.3 Objectives

The objectives of the present study may be summarized as follows:

- 1) To compare the adsorption isotherms of various gases on various adsorbents using gravimetric, volumetric, and chromatographic methods
- 2) To determine whether the Langmuir isotherm model is appropriate for the N₂ adsorption isotherms up to 300 kPa on zeolite NaX and zeolite LiX.
- 3) To identify the dominant dynamic behaviour through the structured adsorbent bed and to determine the effect of flowrate on the magnitude of the axial dispersion and the mass transfer resistance.

Chapter 2: Literature Review

Diffusion of gases in porous solids such as zeolites has been studied extensively in the past few decades. Zeolites are of great importance in the petrochemical industry because they have high activities, especially for acid catalyzed reactions, high surface area, and uniform pore size distribution in the range of nm. However, these zeolite crystals must be pelletized in order to be of any practical industrial use. Binding the crystals into pellets in turn creates diffusion resistance to gas within the pellets, which could control the kinetics of an adsorption process or a chemical reaction. These two processes can either be controlled by the rate of adsorption/chemical reaction or by the rate of mass transfer. In order to study the mass transfer rate of processes involving zeolitic materials, it is important to make a distinction between two different mass transport phenomena, namely, diffusion of gases within the pellets (macropore diffusion) and diffusion of gases within the crystals (micropore diffusion). Understanding diffusion and the external fluid film mass transfer are very important in most industrial applications because in many cases, reaction rates and adsorption rates are fast relative to mass transfer rates. Hence, in many applications, whether, catalytic cracking or gas adsorption, mass transfer is the rate controlling step.

The first step in designing a separation process is to determine the most suitable adsorbent having the best separation factor with a high adsorption capacity. These adsorbent properties can be determined by measuring adsorption isotherms of the gases of interest, and volumetric, gravimetric, or chromatographic methods are available to make these measurements. However, the overall rate of the process can often be dictated by mass transfer resistances as mentioned above. Hence, the dynamic behaviour of the adsorbate-adsorbent system also plays a significant role in designing and optimizing the separation process. Dispersion and mass transfer resistances including external fluid film, macropore and micropore resistance are parameters of

interest in this study. These parameters will be extracted using a chromatographic method of analyzing the dynamic response of the adsorbents, placed in structured adsorbent bed configurations.

2.1 Adsorption

The interaction (dispersion, repulsion, and electrostatic forces) between a gas molecule (usually a specie that gets adsorbed or adsorbate) and a solid (the adsorbing specie or adsorbent) results in a reduction in the potential energy of that gas molecule. Consequently, gas molecules tend to concentrate in regions around the surface of a solid, leading to higher gas density around the surface relative to the bulk density of the gas.

The potential energy (ϕ) of adsorption comprises van der Waals forces (dispersion (attraction) -repulsion) and electrostatic interactions (polarization, dipole, and quadrupole interactions). For an ionic adsorbent such as zeolite (cationic adsorbent), the overall potential is given by the sum of the six terms

$$\phi = \phi_D + \phi_R + \phi_P + \phi_\mu + \phi_Q + \phi_S \quad \text{Equation [2.1]}$$

At low coverage any effects of interaction between neighbouring adsorbed molecules can be neglected. Under low coverage conditions, a simple relationship exists between heat of adsorption and the potential energy.

$$-\Delta H_o = U_g - U_s + RT - \phi \quad \text{Equation [2.2]}$$

where $U_g - U_s + RT$ is the difference in kinetic energy between sorbate in the bulk gas and the adsorbed phase.

However, in most cases, the difference in kinetic energy is often small and can be neglected, hence

$$\phi \approx \phi_{\min} \approx \Delta H_o \quad \text{Equation [2.3]}$$

Forces between sorbate and adsorbent are what make adsorption possible and the type of forces between the gas and the solid are dictated by the nature of both species. There are two types of adsorption: physisorption and chemisorption. Physisorption involves weak forces such as van der Waals interactions and/or electrostatic forces (dipole or quadrupole interactions) occurring if the adsorbent has an ionic structure, such as a zeolite. Since chemisorption involves significant electron transfer between sorbate and adsorbent, it is limited only to monolayer coverage of the surface. For physisorption, multiple molecularayers are possible. The adsorption forces depend on the nature of the adsorbing molecule and the nature of the surface which has different affinities for different substances. This “selectivity” provides the basis for equilibrium selective adsorption used in adsorption separation processes.

Adsorption processes may be categorized according to the nature of the adsorption selectivity: kinetic or equilibrium. For N₂ production from air, the separation occurs on kinetically selective 4A zeolite. The pore size of zeolite 4A is approximately 40 nm, the kinetic diameter of O₂ and N₂, are 34.6 to 36.4 nm, respectively. The difference in diffusion rates makes O₂ the preferentially adsorbed component despite an insignificant difference in equilibrium selectivity. Ruthven and Derrah (1971) and Ruthven and Boniface (1985) determined the macropore diffusivity of N₂ and O₂ at 303 K in zeolite 4A to be 3.4×10^{-13} and 3.5×10^{-10} cm²/s respectively. They also determined the micropore diffusivity to be 3.8×10^{-11} cm²/s for N₂ and 3.6×10^{-9} cm²/s for O₂. The difference in the diffusion time of about 100 times leads to kinetically selective adsorption of O₂ on zeolite 4A.

An example of equilibrium selective adsorption is the production of O₂ from air by PSA. Even though O₂ can be obtained from the N₂ PSA process, the purity is not sufficiently high for most applications (less than 90% pure). Hence O₂ PSA uses adsorption of N₂ based on equilibrium selectivity. Generally, 5A zeolite and NaX zeolite are used for this separation process. Diffusion of both O₂ and N₂ are rapid so that the separation occurs by equilibrium

selective adsorption of N_2 , which is 3.0 to 3.5 times greater than oxygen (Sorial et al., 1983). Substantially higher selectivity has been reported for thoroughly dehydrated CaX and various ionic forms of chabazite (Coe et al, 1990). Furthermore, in the 1990s, use of Li containing zeolites such as LiX, $Li,Me^{2+}X$ and $Li,Me^{3+}X$ has increased the selectivity and yield for O_2 (Coe et al, 1993 and Fitch et al., 1995). The separation of O_2 and N_2 is, therefore associated with the differences in the gas molecule-solid cation interactions. In the case of air separation using zeolite X, the selective adsorption of N_2 is due to the polarizability and the electronic quadrupole moment of N_2 . The polarizability of N_2 is about 10% larger than that of O_2 while the quadrupole moment of N_2 is 3.68 times that of O_2 (Mullhaupt and Stephenson, 1995).

Even though O_2 PSA is an equilibrium selective adsorption process, mass transfer dynamics may also be important if the mass transfer resistance limits the rate of adsorption. For a PSA process with short cycle time, the rate of mass transfer becomes important since it may limit the maximum number of PSA cycles. Consequently, it is important to determine the magnitude and the type of mass transfer resistance (external fluid film, macropore, or micropore) that limits the PSA cycle frequency. For O_2 PSA, the adsorption rates on 5A and 13X zeolite are controlled by macropore diffusion (Ruthven et al, 1994). Ruthven et al (1994) reported the macropore diffusion rate for two different size fractions of zeolite 5A at 193 K as 0.0016 s^{-1} for $R = 1.03\text{ mm}$ and 0.0083 s^{-1} for $R = 0.42\text{ mm}$. As shown by Ruthven et al (1994), the increase in pellet size greatly decreases macropore diffusion rate. Hence, in order to obtain high PSA cycle frequency, zeolite pellet size must be reduced since macropore diffusion is rate limiting.

2.1.1 Pressure Swing Adsorption

Whether the separation selectivity is a result of equilibrium or kinetic adsorption, PSA cycles can expect to have the following elementary steps:

1. Pressurization:

- Pressurization with feed from the feed end or;
- Pressurization with raffinate product from the product end before feed pressurization.

2. High pressure adsorption:

- Product is withdrawn at constant column pressure or;
- The column pressure is allowed to decrease while the raffinate product is drawn from the product end.

3. Blowdown:

- Countercurrent blowdown to a low pressure or;
- Cocurrent blowdown to an intermediate pressure prior to countercurrent blowdown

4. Desorption at low pressure:

- Countercurrent desorption with product purge or;
- Countercurrent desorption without external purge
- Evacuation

5. Pressure equalization

- The high and low pressure beds are either connected through their product ends or the feed and product ends of the high-pressure bed are connected to the respective ends of the low pressure bed

6. Rinse

- The bed is purged with adsorbed species after high-pressure adsorption at feed pressure in the direction of the feed

The first generation air separation using the PSA process was developed by Skarstrom (1960). The cycle uses two-packed adsorbent beds in order to provide continuous flow of products with the following four steps per cycle as illustrated by Figure 2.1:

1. Pressurization;
2. Adsorption;
3. Countercurrent blowdown; and
4. Countercurrent purge

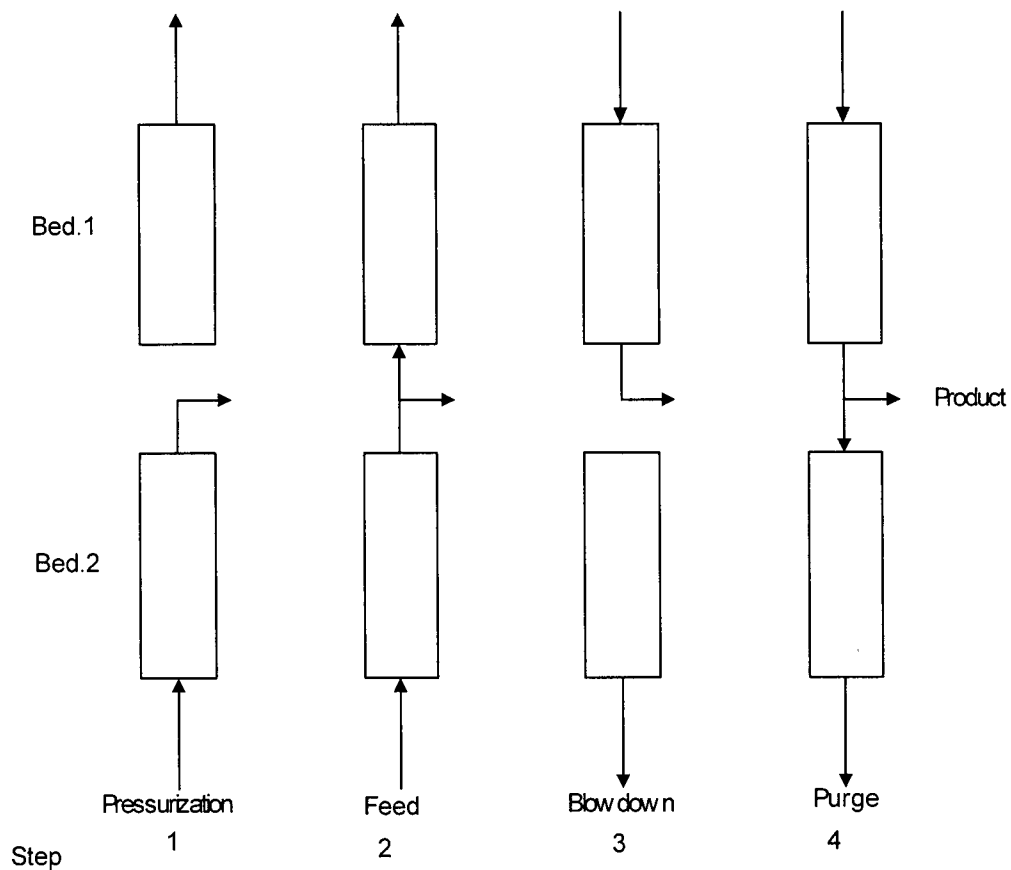


Figure 2.1 Skarstrom cycle

In step 1, bed 2 is pressurized to high pressure with feed from the feed end while bed 1 is blown down to atmospheric pressure in other end (top). In step 2, high pressure feed flows

through bed 2. The more strongly adsorbed component is adsorbed in the bed while the weak sorbate leaves at a pressure just below the feed. A fraction of the product is withdrawn as product and the rest is used to purge bed 1 at low pressure. The direction of the purge flow is countercurrent with respect to the feed to bed 1. Step 3 and 4 are the same as Steps 1 and 2 but with the beds interchanged.

The Skarstrom cycle was further improved by Berlin (1966). Berlin modified the cycle by adding a pressure equalization step. In this modified cycle, after the first bed has been purged and the second bed has completed the high-pressure adsorption step, instead of blowing down the second bed directly, the pressure in the two beds are equalized by connecting them through their product ends. Hence the first bed is partially pressurized with product from the second bed. After the pressure equalization step is completed, the beds are disconnected and the first bed is pressurized with feed gas. Since, the first bed is partially pressurized by the product from the second bed, the pressure equalization step conserves energy.

2.2.2 PSA with Short Cycle Time

In order to reduce the capital cost and increase production rate using the PSA process, a pressure swing adsorption with short cycle time was developed by Turnock and Kadlec (1971) and commercialized by Jones et al. (1980). They used one adsorbent bed filled with 5A zeolite to separate O_2 and N_2 from air by N_2 adsorption. The separation is realized by the pressure difference during adsorption and desorption. Sircar and Hanley (1995) described a model for PSA with short cycle time in terms of a linear driving force assuming that the time for adsorption and desorption are equal. From this model, they concluded that the rapid cycling between the adsorption pressure and desorption pressure leads to a greater rate of adsorption for a given adsorption capacity and better cycle efficiency. Sircar and Hanley's process consists of two

layers, A and B, of the same zeolite adsorbent separated by a perforated screen, as illustrated in Figure 2.2. Each layer of adsorbent is subjected to two steps as follows:

1. Pressurization with air feed where N_2 is selectively adsorbed, producing oxygen rich product. Some of the O_2 produced is used later as countercurrent purge gas.
2. Countercurrent depressurization of the bed follows by countercurrent purge with the O_2 -enriched gas from step 1 (to clean out the residual N_2).

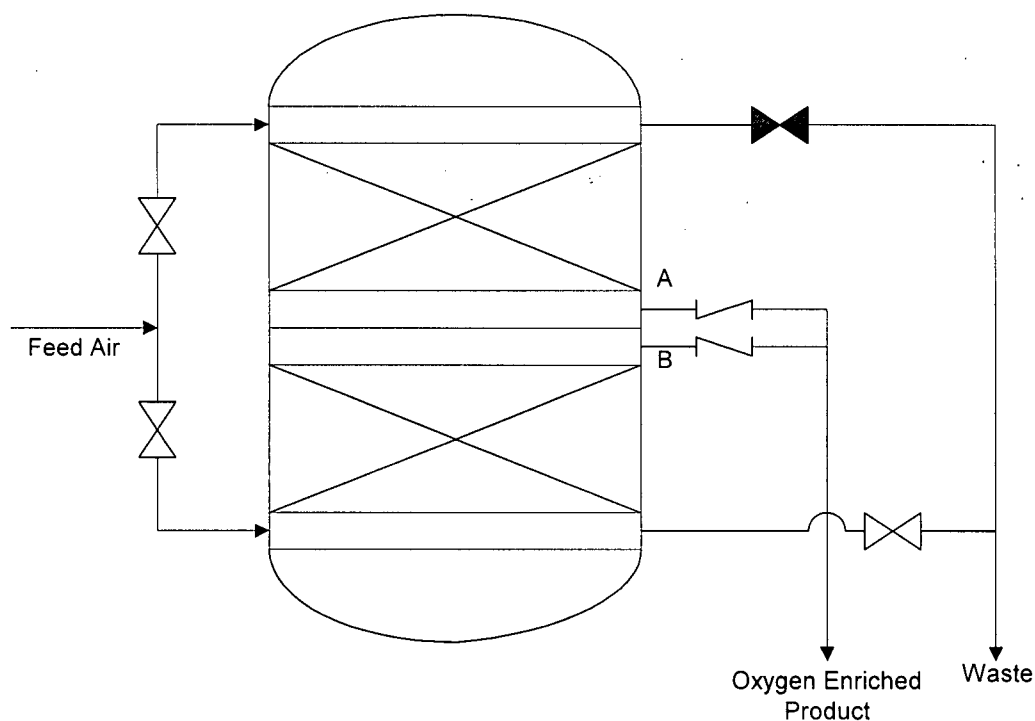


Figure 2.2 PSA with short cycle Process (source: Sircar & Hanley, 1995)

The sequence of operation is as follows: layer A undergoes step 1 for 3-10 seconds while layer B undergoes step 2 at the same time. Then, the sequence is switched such that layer A undergoes step 2 and layer B undergoes step 1 for 3-10 seconds. For a complete cycle consisting of adsorption, then desorption, the cycle time is between 6 to 20 seconds. This allows a

continuous flow of oxygen product. Furthermore, to ensure a dry gas, a layer of dessicant can be placed before each adsorbent layer to remove moisture from the feed. Dry feed gas is desired since the adsorbents are highly hydrophilic. Due to shorter cycles compared to conventional PSA, Sircar and Hanley (1995) claimed that the O_2 production rates are ten to twenty times more than the conventional PSA process and the oxygen recovery is better than in a Skarstrom cycle.

In an attempt to improve separation performance of PSA with short cycle time, Alpay et al. (1994) studied the effects of particle size and the following operating conditions on O_2 production using 5A zeolite:

1. Feed gas pressure
2. Cycle time
3. Feed to cycle time ratio
4. Product delivery rate

By assessing the separation performance in terms of product O_2 purity (percentage of O_2 in the product) or O_2 recovery (moles of O_2 collected as product per mole of O_2 supplied as feed) or adsorbent productivity (moles of O_2 collected as product per unit time per unit weight of adsorbent), they made the following observations:

1. Feed gas pressure:

High feed gas pressure gives high O_2 purities, and subsequently high adsorbent productivities due to the increased amount of N_2 adsorbed during the pressurization step, but O_2 recovery is low due to the high feed flow rate.

2. Cycle time:

The cycle time of the process controls the rate of pressurization and depressurization of the bed. Although large cycle time allows gas equilibrium to

be established between bulk gas and adsorbed phase concentrations, low frequency pressure swing results in loss of separation capabilities. Short cycle times, however, give rise to gas localization in the feed region of the bed, i.e., the entire length of the adsorber is not fully utilized resulting in loss of separation capacity. Hence, there exists an optimum cycle time for maximum product O₂ purity, which was 3 seconds for their studies.

3. Feed to cycle time ratio:

For small particles (between 150 and 425 μm), a feed to cycle time ratio of 0.5 gave the optimum product O₂ purities.

For large particles (between 425 and 710 μm), a small feed to cycle time ratio is desirable for maximum O₂ purities since such a ratio results in a relatively small feed gas flow rate and a low pressure swing cycle within the bed. Hence, increasing the gas residence time within the bed allowing more time for N₂ to get adsorbed, i.e., reducing the macropore mass transfer limitation.

4. Product delivery rate:

Increasing delivery rate results in decreasing gas residence time since the gas exits the adsorber quicker, i.e., increasing influence of mass transfer limitation.

Furthermore, the effect of countercurrent purge is decreased because the pressure at the product end of the adsorber reaches atmospheric pressure quickly during depressurization causing less of the adsorbed N₂ to flow out of the bed from the product end to the feed end. As a result, O₂ purity is decreased.

5. Particle size:

The separation capacities of a process employing small particles are reduced by the ineffective pressure swing within the low permeability bed, while for large particles, macropore diffusional limitations reduce the process separation capacities. In their study, a particle size of approximately 300 μm gave the highest product purities.

More recently, Zhange et al., (1998) studied the effects of operating conditions on N_2 and CO_2 separation by PSA with short cycle time in which CO_2 is the heavy phase and the desirable product. Increasing the adsorption time increased the time for feed gas flow rate, N_2 productivity, N_2 purity, and feed gas pressure, but decreased CO_2 recovery since more CO_2 was adsorbed by the adsorbent. Increasing the time for countercurrent purge increased purity, the pressure in the N_2 surge tank, but decreased recovery and productivity. Increasing desorption time increased recovery and productivity, but decreased purity and pressure. Increasing the feed pressure increased the purity, recovery and productivity at the same time. Furthermore, they compared the performance of a single bed PSA with short cycle time to a double bed PSA with short cycle time where two identical adsorbers were used. Their results showed that CO_2 purity (89.5% for single bed and 93.5% for double bed), CO_2 recovery (70% for single bed and 72.3% for double bed), and productivity (1.95 kg CO_2 /kg adsorbent/day for single bed and 2.07 kg CO_2 /kg adsorbent/day for double beds) were higher for the double bed system.

Furthermore, Keefer (1992) claimed that there is a particle size limitation to the use of finely granular adsorbents for the PSA with short cycle time. In order to reduce the macropore diffusion mass transfer resistance small particles are desirable, however, if the particles are too small, they tend to cluster and pack unevenly giving rise to higher axial dispersion. As a result, cycle frequency exceeding 20 cycles per minute is not practicable since the increased axial dispersion prevents a reduction in adsorber length. To overcome this problem, Keefer (1992) introduced a structured adsorbent bed consisting of thin layers of zeolite supported on a

fibreglass or stainless steel substrate with empty channels between each layer parallel to the gas flow. Keefer (1992) claimed that the structured adsorbent bed had higher surface area and lower pressure drop than a conventional packed adsorbent bed. Hence, a reduction in power requirement due to lower pressure drop and a cycle frequency of 100-300 cycles per minute is possible. To ensure faster and efficient pressure swing adsorption, Mattia (1984) introduced an adsorber mounted on a rotary adsorber assembly which has the advantage that no pneumatic valves to control the feed or product flow are needed. Hence, the valve switching (open/close) does not limit the cycle frequency since the feed or product flow is switched from one bed to the next by rotating the adsorption beds to the valveless feed and product delivery lines. Keefer et al. (2000) used six structured adsorbent beds in the rotary adsorber. However, for large PSA units, the rotary adsorber may not be usable since the weight of the rotating assembly is limited and a complete seal of the large rotary adsorber assembly may be difficult. Because of the small and compact size of structured adsorbent beds, Keefer (2000) claimed that these beds could be mounted on rotary adsorbers to give high frequency pressure swing adsorption and high production rate.

2.2.3 Adsorbent Development in Air Separation

In recent years, adsorbent development for O₂ production using the PSA process has focused on zeolite X rather than zeolite A, since zeolite A possesses a smaller pore structure (8-ring opening) while zeolite X has a large pore structure (12-ring opening). Consequently, micropore diffusivity in zeolite X is more rapid than zeolite A. Ruthven and Xu (1992) reported the micropore diffusivities of N₂ at 200 K in 13X zeolite and 5A zeolite as 2.0×10^{-6} cm²/s and 1.2×10^{-7} cm²/s, respectively, while Karger et al. (1997) reported micropore diffusivities of N₂ at 208 K in 13X zeolite as 3.0×10^{-5} cm²/s. The Skarstrom cycle using 5A or 13X zeolite as the

adsorbent was used to preferentially adsorb N_2 from an air stream, producing 90% pure O_2 product. For oxygen production using only one zeolitic adsorbent, the maximum O_2 purity is 95-96 % since O_2 and Ar are adsorbed with almost the same affinity and consequently, N_2 can only be separated from O_2 and Ar. However, higher O_2 purity is needed for welding and cutting in the steel industry and this can be achieved using two different adsorbents. In 1996, both BOC and Sumitomo Seika Co., Ltd filed patents for high purity oxygen production using carbon molecular sieve (CMS) and 5A zeolite. The process involves using CMS to selectively adsorb N_2 and O_2 , hence separating them from Ar. The mixture of N_2 and O_2 is then passed through a 5A zeolite to produce pure oxygen. Hayashi et al. (1996) claimed that an O_2 purity of over 99 % could be achieved.

The performance of a PSA process depends on the type of adsorbents, i.e., its adsorption capacity and its selectivity. Gaffney (1996) has reviewed the development of new adsorbents for the O_2 PSA process. The first generation O_2 PSA systems used NaX (13X) or CaA (5A) zeolites. In the 1980s, CaX type adsorbents exhibiting higher N_2 selectivity became widely used in O_2 production. In 1989-1990, lithium based adsorbents were developed. These materials have the desirable combination of high capacity and a near linear isotherm for N_2 adsorption, hence, zeolite LiX is currently a preferred air separation adsorbent. Zeolite X with Li^+ and Na^+ or Me^{2+} cations where Me^{2+} cations are metal cations with positive 2 charge, have fairly constant N_2 capacity up to 75% Li in cations content. This is because at low Li content, Li^+ first occupies the sites in the center of the six-rings of the zeolite. Above 75% Li^+ content, the sites in the six-rings are all filled up, hence, Li^+ starts to fill up the sites on the 12-O-rings in the supercage. Li^+ located at these sites is what makes the N_2 adsorption capacity increase rapidly above a Li^+ content of 75%. N_2 capacity increases dramatically as the Li content increases from 75% to 100% (at Li content of 100%, N_2 capacity is three times higher than at Li content of 75%). Unfortunately, the high cost of LiX zeolite due to the high cost of Li salts and unfavorable ion

exchange thermodynamics limits the use of LiX zeolite with high lithium content. This has led to the development of low silica LiX zeolites by Kimer (1993). The same N₂ capacity can be achieved at lower lithium content using these low silica zeolites.

More recently, Rege and Yang (1997) reported on PSA performance for O₂ production using LiX with 100 % Li content and NaX zeolite as adsorbent. They optimized the product recovery by keeping the purity and productivity of O₂ constant while varying the inlet and outlet pressure ratio. They reported that superior recovery can be achieved with LiX at lower pressure ratio; 60 % recovery can be realized at the pressure ratio of 2 for LiX while only 50 % recovery can be achieved with NaX at pressure ratio of 4.

Yang et al. (1996) studied the effects of LiX, LiAgX, and AgX zeolite adsorbents on the performance of PSA for O₂ production. They reported that the adsorption capacity for N₂ is higher for AgX than LiAgX and LiAgX is higher than LiX. However, since AgX has a high N₂/O₂ selectivity at low total pressure (as low as 10 kPa), N₂ desorption will be difficult, hence AgX is not suitable for PSA air separation. They further reported that N₂/O₂ selectivities were higher for LiAgX at high total pressure and lower for LiAgX at low pressures, due to a relative selectivity reversal. This result, combined with the higher N₂ capacity for LiAgX could make LiAgX a more superior adsorbent than LiX.

For N₂ PSA, carbon molecular sieve (CMS) and zeolite 4A are the adsorbents that adsorb O₂ preferentially to N₂ via kinetic separation and are used in industrial adsorption system. This kinetic separation of O₂ from air occurs because O₂ is adsorbed on CMS or zeolite 4A approximately 100 times faster than N₂. However, in recent years, attempts have been made to develop an equilibrium selective adsorption of O₂ from air to produce N₂. Choudary et al. (2000) attempted to use CeX zeolite while Yang et al. (2002) attempted to use NaCeX zeolite. Unfortunately, the results from both Choudary et al. (2000) and Yang et al. (2002)'s work showed little O₂ selective adsorption. Choudary et al. (2000) only obtained O₂/N₂ selectivity of

1.5 while Yang et al. (2002) attempted to vary Ce/Na ratio yielded a maximum O₂/N₂ selectivity of 1.79.

2.2 Gas Adsorption Isotherms

2.2.1 Background

The selectivity of an adsorbent is most often determined experimentally by measuring adsorption isotherms for different gases. There are five commonly observed forms of adsorption isotherm according to Brunauer's classification, as illustrated in Figure 2.3. A Type I isotherm is characteristic of chemisorption, where saturation is reached after all surface sites are occupied, or to physical adsorption in a microporous material where saturation is achieved after micropore filling is complete. Type II and III behaviour corresponds to adsorption on macroporous adsorbents with strong and weak adsorbate-adsorbent interactions, respectively. Type IV and V represent mono- and multilayer adsorption plus capillary condensation. Since the microporous materials used in PSA processes almost always follow type I and type II isotherms, the isotherm models discussed in section 2.2 will be restricted to these two cases.

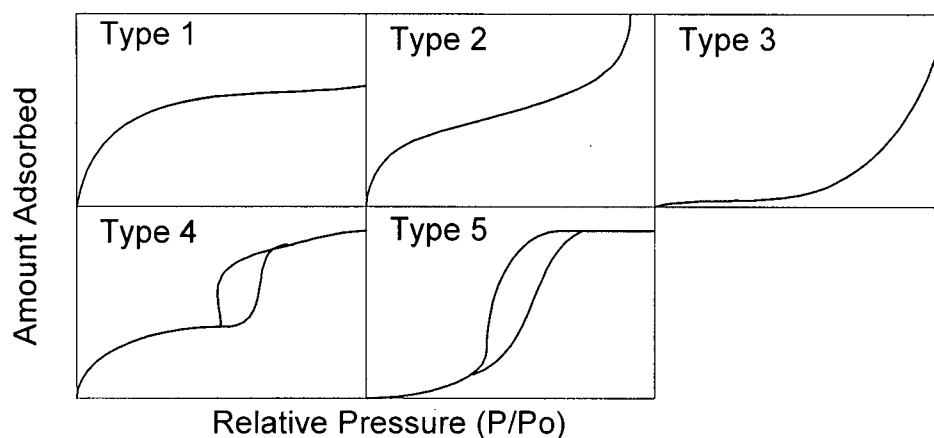


Figure 2.3 Brunauer classification of isotherms

2.2.1.1 Henry's Law

At sufficiently low concentration, the initial slope of a type I isotherm is linear, hence, it can be modeled by the simple linear model or Henry's law:

$$q = K'p \text{ or } q = Kc \quad \text{Equation [2.4]}$$

Where q is the amount adsorbed, p and c are pressure and concentration, respectively, and K' or K is referred to as the "Henry's law" constant or simply the Henry constant or the adsorption equilibrium constant. The temperature dependence of Henry's constant follows the van't Hoff relation:

$$K' = K'_0 e^{-\Delta H/RT}; \quad K = K_0 e^{-\Delta U/RT} \quad \text{Equation [2.5]}$$

where $\Delta H = \Delta U - RT$ is the change in enthalpy on adsorption. Since physical adsorption from the gas phase is an exothermic process, equilibrium favors adsorption at lower temperatures and

desorption at higher temperatures. It follows that ΔH and ΔU are negative, and the Henry constant decreases with increasing temperature.

2.2.1.2 The Langmuir Isotherm

Most microporous adsorbents follow a type I isotherm which can be adequately represented by the ideal Langmuir model where the adsorption isotherm curves level off as the adsorption sites are being filled up.

$$\frac{q}{q_s} = \frac{bp}{1 + bp} \quad \text{Equation [2.6]}$$

where q = amount adsorbed

q_s = amount adsorbed at saturation, i.e., all the adsorption sites are filled up

p = pressure

b = Langmuir constant; $q_s b$ = Langmuir constant, a .

This model is derived from a mass balance of occupied and unoccupied sites of the adsorbent. Equation [2.6] shows the correct asymptotic behaviour at low and high concentration. At low pressure, $(1+bp) \rightarrow 1$ and Equation [2.6] reduces to Henry's law where $q_s b = K$. At high pressure, $(1+bp) \rightarrow bp$ and hence $q \rightarrow q_s$. The model parameters (b and q_s) can be determined from the slope and intercept of a plot of $(1/q)$ vs. $(1/p)$ or by curve fitting the q vs. $q_s bp/(1+bp)$ curve with a parameter estimation algorithm. At low sorbate pressure, the temperature dependence of the Henry's constant follows the van't Hoff equation.

$$\ln K = -\frac{\Delta H}{R} \frac{1}{T} + \frac{\Delta S}{R} \quad \text{or} \quad K = K_o \exp\left(-\frac{\Delta H}{R} \frac{1}{T}\right) \quad \text{Equation [2.7]}$$

where $K_0 = \frac{\Delta S}{R}$

The van't Hoff relation (Equation [2.7]) can be obtained from the following Gibbs free energy equations.

$$\Delta G = \Delta H - T\Delta S \quad \text{Equation [2.8a]}$$

$$\Delta G = -RT \ln K \quad \text{Equation [2.8b]}$$

The enthalpy change during adsorption can be determined by plotting $\ln K$ versus $(1/T)$. From Equation [2.6] and Equation [2.7], q_s is independent of temperature and the change in enthalpy is independent of concentration. Rege and Yang (1997) reported the heat of adsorption of N_2 on LiX and NaX to be 23.4 kJ/mol and 18.0 kJ/mol, respectively.

The ideal Langmuir isotherm has two advantages: it makes a good approximation of many adsorption systems and it reduces to Henry's law in the low concentration limit, which is a requirement for thermodynamic consistency in any physical adsorption system. For these reasons, Langmuir isotherms are widely used in PSA systems for qualitative and semiquantitative purposes. Furthermore, Langmuir isotherm in the form of a generalized Langmuir isotherm can be extended to include the adsorption on heterogeneous system.

$$\frac{q}{q_s} = \left(\frac{bc^n}{1 + bc^n} \right)^{m/n} \quad \text{Equation [2.9]}$$

2.2.1.3 Freundlich and Langmuir Isotherms.

The Type I isotherm can also be modeled by the Freundlich equation:

$$q = bc^{1/n}, \quad n > 1.0 \quad \text{Equation [2.10]}$$

where b and n = Freundlich constants

The Freundlich isotherm is based on a distribution of affinities among the surface adsorption sites, but it is probably better regarded as an empirical expression.

2.2.2 Isotherm Measurement Methods

In order to select appropriate adsorbents to be used in pressure swing adsorption, adsorption isotherms must be measured. There are many experimental techniques which can be used to obtain these isotherms. In the present study, gravimetric and volumetric adsorption methods as well as desorption breakthrough (or the chromatographic method) have been used to determine the adsorption isotherm.

2.2.2.1 Volumetric Method

The volumetric method of determining an adsorption isotherm generally involves measuring the volume adsorbed by monitoring change in fluid phase concentration or bulk concentration. In a gaseous system, the fluid phase concentration is measured by monitoring the change in pressure. For a gas adsorption isotherm, the known amount of adsorbate is introduced into the adsorbent chamber of known volume to pressurize the chamber at a fixed pressure and a fixed temperature followed by equilibration of gas between the bulk and the adsorbed phase. After the system is allowed to come to equilibrium, the pressure is measured and compared to the original pressure. If the pressure decreases, a known amount of adsorbate is added to obtain the original pressure. On the other hand, if there is no change in pressure, then the bulk gas is assumed to be in equilibrium with the adsorbed gas at that pressure and temperature. The entire adsorption isotherm can be obtained by measuring the adsorbed volume at other pressures. To account for the volume in of gas in the bulk phase, a blank sample tube can be run at the same conditions as the isotherm measurement and this volume can be subtracted from the total volume in the bulk phase and adsorbed phase to obtain the volume of gas adsorbed by the adsorbents.

2.2.2.2 Gravimetric Analysis

The gravimetric method measures the weight change of a sample when exposed to different pressures of adsorbate at a fixed temperature. The amount adsorbed can be calculated by

$$N = \frac{W_t - F_b}{m \times M_w} \quad \text{Equation [2.11]}$$

where W_t is the sample weight after adsorption, M_w is the gas molecular weight, m is the initial mass of the sample, and F_b is the total buoyancy force. In a typical thermogravimetric apparatus, the buoyancy force can be obtained by monitoring the weight change in the sample with and without He flow, assuming that helium does not adsorb onto the sample.

$$F_b = W_{\text{flow}} - W_{\text{static}} \quad \text{Equation [2.12]}$$

where W_{flow} = weight of sample with He flow

W_{static} = weight of sample without He flow

2.2.2.3 Breakthrough Analysis

Unlike the gravimetric or volumetric methods, breakthrough analysis does not generate experimental isotherms which can be fitted with Langmuir or other isotherm models. However, by measuring the desorption dynamics of a pre-adsorbed adsorbate from a bed of adsorbent, the adsorbate concentration profile through the bed can be determined. The concentration profile along the length of the bed yields Langmuir isotherm parameters, a and b where $a = q_s b$.
(Ruthven, 1984)

The general nature of a concentration front or mass transfer zone traveling down the length of a packed column is entirely dependent on the equilibrium isotherm. However, the shape of the concentration front is dictated by kinetic effects and dispersion. Usually, an equilibrium relationship over the concentration range under consideration can be classified as linear, favourable, and unfavourable. These three forms of equilibrium relationship arise from plotting a dimensionless adsorbed phase versus fluid phase concentration, $(q^* - q_o')/(q_o - q_o')$ and $(c - c_o')/(c_o - c_o')$ as illustrated in Figure 2.4.

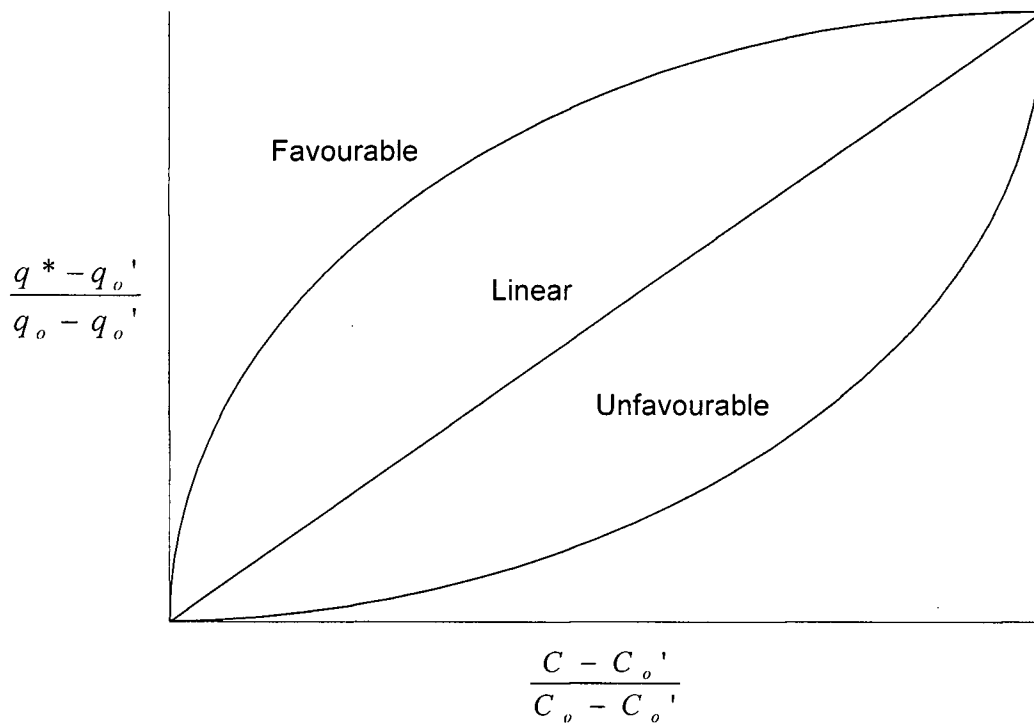


Figure 2.4 General equilibrium relationship

The three general equilibrium relationships in Figure 2.4 correspond to:

Favourable	$\frac{q^* - q_o}{q_o - q_o} > \frac{c - c_o}{c_o - c_o}$	
Linear	$\frac{q^* - q_o}{q_o - q_o} = \frac{c - c_o}{c_o - c_o}$	Equation [2.13]
Unfavourable	$\frac{q^* - q_o}{q_o - q_o} < \frac{c - c_o}{c_o - c_o}$	

Usually, the adsorption isotherm is favourable, therefore, the desorption isotherm will be unfavourable. In desorption, the mass transfer zone is therefore dispersive meaning that the concentration profile spreads and becomes more dispersed as it travels down the length of the bed. Since the profile spreads in direct proportion to the distance traveled, this is referred to as “proportionate pattern” behaviour. Assuming that the column is long enough so that equilibrium is reached at the end of the packed column, it is possible to extract adsorption isotherm parameters for a given system.

For isothermal plug flow of a trace component in an inert carrier system used in packed bed configuration, the material balance is

$$v \frac{\partial c}{\partial z} + \frac{\partial c}{\partial t} + \left(\frac{1 - \varepsilon}{\varepsilon} \right) \frac{\partial \bar{q}_L}{\partial t} = 0 \quad \text{Equation [2.14]}$$

and assuming mass transfer equilibrium:

$$\left(\frac{\partial \bar{q}_L}{\partial t} \right)_z = \left(\frac{\partial q^*_L}{\partial t} \right)_z = \frac{dq^*_L}{dc} \left(\frac{\partial c}{\partial t} \right)_z \quad \text{Equation [2.15]}$$

with a Langmuir adsorption model, whose derivative with respect to concentration is

$$\frac{dq^*_{L}}{dc} = \frac{bq_s}{(1+bc)^2} \quad \text{Equation [2.16]}$$

Substituting Equation [2.15] and Equation [2.16] into Equation [2.14] yields the concentration profile velocity propagating down the length of the column:

$$w(c) = \left(\frac{\partial z}{\partial t} \right)_c = - \frac{(\partial c / \partial t)_z}{(\partial c / \partial z)_t} = \frac{v}{\left[1 + \left(\frac{1-\varepsilon}{\varepsilon} \right) \left(\frac{dq^*_{L}}{dc} \right) \right]} \quad \text{Equation [2.17]}$$

By substituting Equation [2.15] into Equation [2.17], followed by integration, the concentration profile down the length of the bed can be determined:

$$\frac{c}{c_o} = \frac{\beta}{(1-\beta)} \left[\left(\frac{\xi}{\tau} \right)^{1/2} - 1 \right], \quad \frac{1}{\beta^2} > \frac{\xi}{\tau} > 1 \quad \text{Equation [2.18]}$$

where the dimensionless variables are defined as

c/c_o = concentration/initial concentration

$$\beta = 1 - \frac{q_o}{q_s} = (1 + bc_o)^{-1} \quad \text{and} \quad \frac{\xi}{\tau} = \frac{(bq_s)z}{(vt - z)} \left(\frac{1-\varepsilon}{\varepsilon} \right)$$

or

$$\frac{c}{c_o} = \left(\frac{1}{bc_o} \right) \left[\sqrt{\frac{bq_s z}{vt - z} \left(\frac{1-\varepsilon}{\varepsilon} \right)} - 1 \right] \quad \text{Equation [2.19]}$$

The plot of c/c_0 versus $1/\sqrt{vt} - z$ yields the Langmuir isotherm parameters (b, q_s) from the intercept and the slope, provided ϵ is known.

2.2.2.4 Comparison Between Isotherm Measurement Methods

Adsorption isotherms are normally obtained by either volumetric or gravimetric measurement. Both methods are time consuming since they require several points to directly and adequately define the adsorption isotherm. Physical adsorption isotherms are often rectangular or Langmuir (Type 1) and more data points are needed so that the curvature of the isotherm can be accurately defined. Furthermore, some isotherms have a steep slope in the linear region, hence, if an inadequate number of data points are taken, the curved region of the isotherm might only be represented by one data point or even worse no data point. Depending on what type of adsorbents and/or gas is used, either volumetric or gravimetric methods might be more advantageous. For adsorption of small molecules such as hydrogen, the volumetric measurement might be more advantageous since buoyancy force correction is important in gravimetric methods. If the mass of adsorbed gas is comparable to the buoyancy force exerted on the sample, accurate results may not be obtained (Robens et al., 1999). In the volumetric measurement, the system free space (dead volume) must be determined and this is usually done with He at 77 K or ambient temperature, under the assumption that the adsorbent does not adsorb He. However, a small error in the dead volume measurement may introduce significant errors in the isotherm measurement.

Analysis of the desorption of pre-adsorbed adsorbent can also be used to determine the adsorption isotherm. However, this method does not generate the adsorption isotherm directly. Rather parameters of the Langmuir isotherm are extracted from the desorption profile and this could be quite cumbersome and inaccurate since the method requires large quantities of data to be collected and the desorption curve must be carefully generated. Also, the adsorbent used in

the breakthrough experiment must be bound into larger particles to avoid significant pressure drop through the system. Inert materials are used as binders during pelletization introducing errors into the adsorption isotherm obtained.

2.3 Bed Configurations

Traditionally, absorbents in most adsorption processes are contacted by the fluid phase in a packed bed, resulting in significant pressure drop at high flow rate. From a process economic point of view, high pressure drops result in higher pumping cost. Alternatively, reducing flow rate to reduce pressure drop results in longer residence time and less productivity. If high flow rate is maintained, then large particles must be used due to a significant increase in pressure drop, which results in an increase in mass transfer resistance. An alternative approach to a packed bed of adsorbent particles is to use adsorbent placed in a structured monolith. The monolith reduces pressure drop, and hence, higher flow rate can be used without significantly increasing particle size or mass transfer resistance.

2.3.1 Packed Bed

Pressure drop in flow through a packed bed has been investigated by several investigators, some of which include Chilton and Colburn (1931) and Ergun (1952). Usually, a dimensionless friction factor (f) is used to correlate pressure drop to particle size and flow rate.

$$f = \left(\frac{2R_p}{L} \right) \frac{\Delta p}{\rho_f (\varepsilon v)^2} \quad \text{Equation [2.20]}$$

where Δp is the pressure drop, ρ_f = fluid density, and εv is the superficial fluid velocity. Two commonly used correlations for the friction factor are:

Chilton-Colburn (1931)

$$\text{Re} < 40 \quad f = 805/\text{Re} \quad \text{Equation [2.21]}$$

$$\text{Re} > 40 \quad f = 38/\text{Re}^{0.15}$$

Ergun (1952)

$$f = \left(\frac{1 - \varepsilon}{\varepsilon^3} \right) \left[\frac{150(1 - \varepsilon)}{\text{Re}} + 1.75 \right] \quad \text{Equation [2.22]}$$

where Re (Reynolds number) = $vd_p\rho/\mu$ where v = velocity, d_p = particle diameter, ρ = density, and μ = viscosity

As can be seen from Equation [2.20] and [2.22], pressure drop is a function of both velocity and Reynolds number, i.e., particle size. The smaller the particle size and the higher the velocity, the higher the pressure drop, especially for the velocity since it shows a square relationship with the pressure drop. Hence, increasing velocity (flowrate) will increase the pressure drop significantly. Furthermore, in order to keep the pressure drop low, catalyst particles will have to be larger, resulting in higher mass transfer resistance.

Eisfeld and Schnitzlein (2001) reported recently on the influence of walls on pressure drop in packed beds. Among 24 correlations they attempted to fit to 2300 data points, the Reichelt (1972) correlation (Equation [2.23]), which is based on the Ergun equation, yielded the best fit. Furthermore, they showed that for tube-to-particle diameter ratios (D/d_p) of less than 10, the Ergun equation normally over predicts the pressure drop whereas, the pressure drop predicted by the Reichelt equation is lower than the Ergun equation and it also shows good agreement with experimental data. Eisfeld and Schnitzlein (2001) reported that the Reichelt equation can be used to calculate pressure drop in the following ranges: $0.01 < \text{Re} < 17635$, $1.624 < D/d_p < 250$, and $0.330 < \varepsilon < 0.882$.

$$\psi = \frac{K_1 A_w^2 (1-\varepsilon)^2}{\text{Re} \varepsilon^3} + \frac{A_w}{B_w} \frac{1-\varepsilon}{\varepsilon^3} \quad \text{Equation [2.23]}$$

with the wall correction terms

$$A_w = 1 + \frac{2}{3(D/d_p)(1-\varepsilon)^2}$$

$$B_w = \left[k_1 \left(\frac{d_p}{D} \right)^2 + k_2 \right]^2$$

where Re = Reynolds number

ε = voidage

k_1 and k_2 = the coefficient of pressure drop correlation or the wall correction term

ψ = the dimensionless pressure drop

2.3.2 Monolithic Bed

The monolithic bed consists of thin (wall thickness could be as low as 0.1 mm) parallel layers of substrate such as ceramic, metal, plastic, or fiberglass, whose surface is deposited with the adsorbent material. This leads to one of the most important advantages of the monolithic bed, which is that it has a large open frontal area resulting in little flow resistance and hence a low pressure drop. Metal monoliths can be made with very thin walls, with open frontal areas approaching 90% of the total cross sectional area.

The basic equation for pressure drop can be derived from the energy balance, assuming constant temperature as developed by Heck et al. (2001):

$$\frac{-1}{\rho} \frac{dP}{dL} = \frac{2f v^2}{g_c d_{ch}} \quad \text{Equation [2.24]}$$

where P is the total pressure (atm); f is the friction factor, dimensionless; d_{ch} is the monolith channel diameter (cm); g_c is the gravitational constant (980.665 cm/s^2); L is the length (cm); v is the interstitial velocity in channel (cm/s); and ρ is the gas density.

The interstitial velocity (v) in the channel can be calculated as

$$v = W/(\rho A \epsilon) \quad \text{Equation [2.25]}$$

where W is the mass flowrate; A is the cross-sectional area of the monolith; and ϵ is the voidage.

Integration of Equation [2.24] yields:

$$\Delta P = \frac{2fL\rho v_{ch}^2}{g_c d_{ch}} \quad \text{Equation [2.26]}$$

where d_{ch} is the hydraulic diameter of the monolith channel (cm).

Based on Equation [2.20] and Equation [2.26], the pressure drop for both the packed bed and the monolithic bed have a square relationship with velocity (flowrate). However, adsorbent particles deposited on the surface of the monolithic bed can be much smaller than those in packed beds, leaving more voidage within the bed, hence, reducing the pressure drop.

Besides the advantage of lower pressure drop in a monolithic bed, mass transfer resistance in a monolithic bed is lower than in a packed bed since smaller particles are deposited on fine layers of substrate giving more surface area. As a result, there is more contact area and less diffusion within these smaller particles. However, external fluid film resistance between the bulk and solid phase in the monolithic bed may contribute more to mass transfer resistance than in packed beds.

Gas-to-solid or external fluid film mass transfer rates in monolithic catalysts or adsorbents have been reported in the literature. Hawthorn (1974) combined the numerical

solution of the developing laminar flow with the analytical solutions for fully developed laminar flow to obtain the following equation

$$Sh = B \left(1 + 0.095 \text{Re} Sc \frac{d}{L} \right)^{0.45} \quad \text{Equation [2.27]}$$

where Re = Reynolds number

Sc = Schmidt number

d = diameter

L = length

B = channel cross-section constant: B = 3.66 for circular channels B = 2.98 for square channel

Hayes and Kolaczowski (1994) examined the experimental results of Bennett et al. (1991) and Ullah et al. (1992) for gas-solid mass transfer. They claimed that the experimental values of Sh number from these two works were lower than analytical values. They pointed out that the assumption of a negligible kinetic effect by Bennett et al. (1991) and negligible internal mass transfer by Ullah et al. (1992) were not valid.

Recently, Uberoi and Pereira (1996) proposed an empirical model for the gas-solid mass transfer in monolith channels:

$$Sh = 2.696 \left(1 + 0.139 \text{Re} Sc \frac{d}{L} \right)^{0.81} \quad \text{Equation [2.28]}$$

and, Holmgren and Andersson (1998) correlated gas-solid mass transfer in square monolith channels with rounded corners as:

$$Sh = 3.53 \exp \left(0.0298 \text{Re} \frac{d_h}{L} Sc \right) \quad \text{Equation [2.29]}$$

where d_h = hydraulic diameter, i.e., $4(\text{cross-sectional area})/(\text{wetted perimeter})$.

Holmgren and Andersson (1998) claimed that this expression predicts higher Sh numbers compared with the analytical values for laminar flow. They discussed the discrepancy between the correlation value and analytical value as being due to turbulent effects as follows:

- The turbulent-to-laminar transition will take place over some distance in the channel.
- Turbulence is generated by the monolith walls at the entrance.
- The surface roughness of the channel walls will generate some turbulence in the flow near the walls.

2.4 Experimental Methods in Measuring Gas Adsorption Dynamics

In designing any gas separation process, it is important to determine the dynamic behaviour of the system since it identifies the magnitude and type of mass transfer resistance in the adsorption system. Thus, for example, if macropore mass transfer resistance is rate limiting and is of the same magnitude as the cycle time, then the mass transfer rate can be increased by reducing the pellet size in order to increase the cycle frequency, which in turn increases the productivity. Some of the methods developed over the years to measure micropore and macropore diffusivities include zero length column (ZLC), permeation, frequency response (FR), and the Chromatographic method. These methods have their advantages and disadvantages as summarized in Table 2.1 below:

Table 2.1 Advantages and disadvantages in adsorption dynamics measurement method

Method	Advantages	Disadvantages
ZLC	<ul style="list-style-type: none">• Direct Measurement of micropore diffusivity	<ul style="list-style-type: none">• Limited to slower process due to intrusion of time delay• Need sensitive Detector
Permeation	<ul style="list-style-type: none">• Very easy to collect and analyze data	<ul style="list-style-type: none">• Difficult in mounting pellet especially when micropore diffusivity is desired
FR	<ul style="list-style-type: none">• Few experiments are needed to obtain full adsorption dynamics	<ul style="list-style-type: none">• Difficult and expensive to setup• Data Analysis is very difficult since several intergrations of data are needed
Chromatography	<ul style="list-style-type: none">• Easy to set up and data collection	<ul style="list-style-type: none">• Data Analysis is cumbersome since integration of several hundreds of data points are often desired

Since the chromatographic method is the easiest method to set up and is readily available for this study, it will be used to determine adsorption dynamics of the monolithic bed. Furthermore, the chromatographic method has gained a general acceptance as a reliable method to extract the magnitude of mass transfer resistances. (Ruthven et al., 1992) However, brief summaries of the other methods are provided below.

2.4.1 Zero Length Column

The ZLC method was developed in the late 1980s by Eic and Ruthven (1988) to reduce the effect of axial dispersion on the measurement of diffusivities by using a very small sample of adsorbent.

A few milligrams of adsorbent is placed between two porous sintered discs. The individual crystals are dispersed approximately as a monolayer across the area of the sinter to ensure good contact with the purge gas stream, hence minimizing the effects of external resistance to heat and mass transfer. The method involves letting a small sample to equilibrate at a low uniform sorbate concentration, preferably within the Henry's law regime. After the system reaches equilibrium, desorption is achieved by purging with an inert gas at a flow rate high enough to maintain zero sorbate concentration at the external surface of the particles or crystals.

2.4.2 Permeation

The permeation method involves measuring flux through a slab under conditions such that concentrations at both faces of the slab are known. There are two different permeation methods; one in which the flux is measured under a known pressure gradient and the Wicke-Kallenbach method in which flow through the slab is at constant pressure, driven by a concentration difference between the faces. With a known slab thickness, the effective

diffusivity can be calculated from measuring the composition and flow rate of the gas streams leaving both sides of the slab, thus determining net fluxes in both directions. However, in order to determine the micropore diffusivity, a single crystal must be mounted, hence, limiting the usefulness of this method for steady state measurements. It is possible to extract the micropore diffusion coefficients from transient measurements.

2.4.3 Frequency Response Method

There are three types of transient response method, each of which use a different input perturbation, namely: step, pulse or harmonic. For the step change, whether it is concentration or volume, individual system dynamics such as macropore and micropore diffusivities cannot readily be separated because only the magnitude of the step change can be varied. Pulse perturbation in which both the width of the pulse and time elapsed between pulses can be varied, it is possible to better access the multiple dynamic processes in a complex system. However, this approach lacks the relaxation time introduced by harmonic oscillations. Harmonic oscillations or perturbations, often known as frequency response, allows the solution of the governing equations in the frequency domain. In addition to these advantages, pulse perturbation gives an additional degree of freedom, namely the frequency of oscillations.

The approach is to introduce a periodic perturbation by making a small change in volume, usually $\pm 1\%$ of system volume, hence producing a response with lower amplitude and phase lag (shift), which is monitored by a pressure transducer. The magnitude of the amplitude attenuation and phase lag yields the dynamics of the system when fitted with a proper model. The harmonic perturbation of volume can usually be introduced using bellows or moving plate devices coupled mechanically to rotary motors or coupled with electromagnetic devices. The system pressure must be monitored because adsorbent responds to change in pressure through adsorption, diffusion, or reaction processes. This can be done by using either pressure gauges

with rapid response or a mass spectrometer. However, the monitoring device needs high accuracy and very rapid response time in order to establish a signal attenuation, phase lag between induced volume change and pressure response, and fluctuations at each forcing frequency. Typically the frequency range used for this method is 0.01 Hz to 10 Hz.

2.4.4 Chromatographic method

The chromatographic method used to measure diffusivity is based on measurements of the dynamic response of an adsorption column to a perturbation in the sorbate concentration at the inlet, which could either be a pulse or a step change. Exactly the same information can be obtained from either a step or a pulse input, hence, the choice of the type of input is determined more on a practical convenience rather than from a theoretical base. In a typical chromatographic experiment, a steady state flow of inert or non-adsorbing specie is established through a small packed bed containing the adsorbent. At time zero, a stream of low concentration sorbate is introduced into the system, hence, inducing a step change. The effluent concentration is then monitored continuously. With this method, two parameters can be determined. From the mean retention time, the adsorption equilibrium or Henry's constant can be calculated while the effects of mass transfer resistances and axial mixing in the column can be derived from the shape of the breakthrough curve. By varying experimental conditions, it is possible to separate the axial dispersion and mass transfer resistances. Hence, under favourable circumstances, macropore and micropore diffusivities can be determined.

To analyze and interpret the data from a chromatographic experiment, a mathematical model must first be established. By matching the experimental response to the appropriate mathematical model, the kinetic and equilibrium parameters can be determined. From the basic continuity equation, derived from a mass balance on an element of a typical chromatographic column with isothermal and negligible pressure drop assumptions, the general form of the

modeling equation of the dynamic response of a chromatographic column is given by Ruthven (1984):

$$-D_L \frac{\partial^2 c}{\partial z^2} + v \frac{\partial c}{\partial z} + \frac{\partial c}{\partial t} + \left(\frac{1-\varepsilon}{\varepsilon} \right) \frac{\partial \bar{q}_L}{\partial t} \quad \text{Equation [2.30]}$$

where D_L = dispersion coefficient

v = interstitial velocity

ε = voidage

With the following boundary conditions for a step input

$$c(z,0) = q(z,0) = 0, \quad c(0,t) = c_0 \quad \text{and} \quad \frac{\partial \bar{q}_L}{\partial t} = kK(c - c^*)$$

While it is convenient to obtain analytical solutions of the chromatographic response in the time domain, it is not necessary because moment analysis can be used to obtain the kinetic and equilibrium parameters, hence avoiding complex analytical solutions, which are derived from the inversion of a Laplace transform. Moment analysis involves matching the moments of the experimental and theoretical response curves.

From the breakthrough data, the mean and the variance of the response to a step input can be calculated from the 1st and 2nd moment equations of a step input as follows:

$$1^{\text{st}} \text{ moment} \quad \mu = \bar{t} = \int_0^{\infty} (1 - c/c_0) dt \quad \text{Equation [2.31]}$$

$$2^{\text{nd}} \text{ moment} \quad \sigma^2 = 2 \int_0^{\infty} (1 - c/c_0) t dt - \mu^2 \quad \text{Equation [2.32]}$$

From a simple overall material balance, the retention time is always given by

$$\mu = \frac{L}{v} \left[1 + \left(\frac{1-\varepsilon}{\varepsilon} \right) K \right] \quad \text{Equation [2.33]}$$

where L = length of adsorption pack, and K is the Henry's constant.

According to Equation [2.33], with the value of μ calculated from Equation [2.31], the Henry's constant can be calculated from the slope of the plot μ vs. $1/v$ with known values for the column length and voidage.

A useful equation for the second moment for gaseous systems where K is often large is given as (Haynes and Sarma, 1973):

$$\frac{\sigma^2}{2\mu^2} = \frac{D_L}{vL} + \frac{\varepsilon v}{L(1-\varepsilon)} \frac{1}{kK} \left[1 + \frac{\varepsilon}{(1-\varepsilon)K} \right]^{-2} \quad \text{Equation [2.34]}$$

By rearranging and multiplying by L/v

$$\gamma = \frac{\sigma^2}{2\mu^2} \frac{L}{v} = \frac{D_L}{v^2} + \frac{\varepsilon}{(1-\varepsilon)} \frac{1}{kK} \left[1 + \frac{\varepsilon}{(1-\varepsilon)K} \right]^{-2} \quad \text{Equation [2.35]}$$

where

$$\frac{1}{kK} = \frac{R_p}{3k_f} + \frac{R_p^2}{15\varepsilon_p D_p} + \frac{r_c^2}{15KD_c}$$

k = total mass transfer coefficient

k_f = external fluid film mass transfer coefficient

D_p = macropore diffusivity

D_c = micropore diffusivity

R_p = particle radius

r_c = crystal radius

In Equation [2.35], $\frac{R_p}{3k_f}$ is the external fluid film mass transfer resistance while $\frac{R_p^2}{15\varepsilon_p D_p}$

is the macropore mass transfer resistance and $\frac{r_c^2}{15KD_c}$ is the micropore mass transfer resistance.

External fluid film mass transfer resistance is the mass transfer resistance between the bulk fluid and the surface of the adsorbent. Macropore mass transfer resistance is the diffusional resistance within the pores of the pellets. Micropore mass transfer resistance is the resistance within the pores of the crystals. From Equation [2.35], by plotting γ vs. $1/v^2$, the axial dispersion, D_L , and the overall mass transfer coefficient, k , can be calculated from the slope and the intercept. From a number of chromatographic or breakthrough experiments, the kinetics and equilibrium parameters can be obtained by varying the flow rate of the sorbate. However, varying the sorbate flow rate is not sufficient to obtain the individual mass transfer resistances, namely, macropore and micropore diffusivities. In principle, the use of higher moments is possible to obtain the additional equation needed to solve the axial dispersion and mass transfer coefficients simultaneously, but the accuracy in determining the higher moments limits this approach. Furthermore, evaluation of higher moments does not provide additional information concerning mass transfer resistances, but can provide the relative importance of axial dispersion and mass transfer resistance.

Fortunately, it is possible to determine each mass transfer resistance by performing experiments with two or more particle sizes. For most gaseous system of commercial interest, $K \gg 1$ and hence the effect of mass transfer resistance will dominate over axial dispersion provided

$$\frac{v^2}{kKD_L} \gg 1.0 \quad \text{Equation [2.36]}$$

where

$$\frac{1}{kK} = \frac{R_p}{3k_f} + \frac{R_p^2}{15\epsilon_p D_p} + \frac{r_c^2}{15KD_c}$$

In order to extract the micropore diffusivities, it is necessary to ensure that

$$\frac{r_c^2}{15KD_c} \gg \frac{R_p}{3k_f} + \frac{R_p^2}{15\varepsilon_p D_p} \quad \text{Equation [2.37]}$$

This condition can be achieved by reducing the gross particle size and can be confirmed experimentally by making replicate experiments with different particle size. When small particles are used, it is desirable to make measurements in the low Reynolds number region to avoid problems with channeling and high order dependence of axial dispersion. In this low Reynolds number region, it can be assumed that $D_L \approx D_m$, hence, Equation [2.36] becomes

$$\frac{1}{kK} \approx \frac{D_m}{\nu^2} \quad \text{Equation [2.38]}$$

When micropore diffusivity becomes dominant, Equation [2.38] becomes

$$\frac{D_c}{r_c^2} \ll \frac{\nu^2}{15KD_m} \quad \text{Equation [2.39]}$$

From the above equation, it is clear that the measurement of micropore diffusivity becomes difficult for a system with high equilibrium constant.

As for the measurement of macropore diffusivity, it is possible to eliminate the contribution of micropore resistance if a non-porous material is used instead of the adsorbent or if a non-penetrating gas is used (gas molecules that are bigger than the micropores themselves). However, the non-porous material used must possess the same dimension as the adsorbents, which may be difficult to replicate.

Alternatively, the mass transfer parameters can be separated by performing the experiment at low flow rate such that the Reynolds number is low. At these conditions, the correlation of Ranz and Marshall (1952) is valid: $Sh \equiv 2k_f R_p / D_m = 2 + 0.6Sc^{1/3} Re^{1/2} \approx 2$, i.e., $k_f = D_m / R_p$ can be substituted into Equation [2.35] (Ruthven, 1984).

$$\frac{\sigma^2}{2\mu^2} \frac{L}{v} \approx \frac{D_L}{v^2} + \frac{\varepsilon}{(1-\varepsilon)} \left(\frac{R_p^2}{3D_m} + \frac{R_p^2}{15\varepsilon_p D_p} + \frac{r_c^2}{15KD_c} \right) \left[1 + \frac{\varepsilon}{(1-\varepsilon)K} \right]^{-2} \quad \text{Equation [2.40]}$$

$$\text{where } \frac{1}{kK} = \frac{R_p^2}{3D_m} + \frac{R_p^2}{15\varepsilon_p D_p} + \frac{r_c^2}{15KD_c}$$

From Equation [2.40], if the total mass transfer resistance, $\frac{1}{kK}$ for two or more different particle size is known, the plot of $\frac{1}{kK}$ vs. R_p^2 can be used to separate micropore diffusivity from other mass transfer resistances. The intercept will give the micropore resistance while the slope will give the external fluid film resistance and macropore resistance, which can be separated by calculating the molecular diffusion.

An alternative approach to the differential mass balances in an element of the column described earlier, is the tanks-in-series model developed by Martin and Synge (1941). If an ideal mixing cell in which mass transfer occurs between fluid phase and adsorbed phase is considered, a transient mass balance for the two phases gives

$$\varepsilon v c_o = \varepsilon v c + V_f \frac{dc}{dt} + V_s \frac{d\bar{q}_L}{dt} \quad \text{Equation [2.41]}$$

$$(1-\varepsilon)l \frac{d\bar{q}_L}{dt} = k \left(q^*_L - \bar{q}_L \right) \quad \text{Equation [2.42]}$$

After performing Laplace transforms on Equation [2.41] and [2.42], the transfer function is

$$\frac{\bar{c}}{\bar{c}_o} = \left[1 + \frac{sl}{v} \left(1 + \frac{\left(\frac{1-\varepsilon}{\varepsilon} \right) K}{1 + (s/k)} \right) \right]^{-1} \quad \text{Equation [2.43]}$$

where $K = q^*/c$. For N identical stages in series

$$\frac{\tilde{c}}{c_o} = \left[1 + \frac{sl}{v} \left(1 + \frac{\left(\frac{1-\varepsilon}{\varepsilon} \right) K}{1 + (s/k)} \right) \right]^{-N} \quad \text{Equation [2.44]}$$

If van der Laan's theorem (1958) is used, the moments may be found as

$$\frac{\sigma^2}{2\mu^2} = \frac{1}{2N} + \frac{v}{Nl} \left(\frac{\varepsilon}{1-\varepsilon} \right) \frac{1}{kK} \left[1 + \frac{\varepsilon}{(1-\varepsilon)K} \right]^{-2} \quad \text{Equation [2.45]}$$

Equation [2.45] is identical to Equation [2.44] provided that $N = L/l = vl/2D_L$, where N is the number of equivalent theoretical plates (HETP).

$$HETP = \frac{\sigma^2}{\mu^2} L = 2 \frac{D_L}{v} + 2v \left(\frac{\varepsilon}{1-\varepsilon} \right) \frac{1}{kK} \left[1 + \frac{\varepsilon}{(1-\varepsilon)K} \right]^{-2} \quad \text{Equation [2.46]}$$

To account for the velocity dependence of axial dispersion at high flow rate, we assume that the axial dispersion with the dependency on velocity is

$$D_L = \gamma_1 D_m + \gamma_2 R_p v \quad \text{Equation [2.47]}$$

Then, combining Equation [2.46] with Equation [2.47] gives

$$HETP = \frac{A_1}{v} + A_2 + A_3 v \quad \text{Equation [2.48]}$$

where $A_1 = 2\gamma_2 R_p$, $A_2 = 2\gamma_1 D_m$, $A_3 \approx 2[\varepsilon/(1-\varepsilon)]/kK$ assuming $K \gg 10$.

From Equation [2.48], A_1 describes molecular diffusion, A_2 describes eddy diffusion, and A_3 describes the mass transfer resistances including the external fluid film, macropore diffusion, and micropore diffusion.

After having determined kinetic parameters such as dispersion coefficient, external fluid film mass transfer coefficient, macropore mass transfer coefficient, and micropore mass transfer coefficient, it is possible to substitute these parameters back into an analytical expression to predict breakthrough curves. An overall effective rate coefficient (k') including both the axial dispersion and mass transfer resistance can be written as:

$$\frac{1}{Kk'} = \frac{D_L}{v^2} \left(\frac{1-\varepsilon}{\varepsilon} \right) + \frac{R_p}{3k_f} + \frac{R_p^2}{15\varepsilon_p D_p} + \frac{r_c^2}{15KD_c} \quad \text{Equation [2.49]}$$

A simple linear adsorption rate model, based on the linear driving force (LDF) for the rate expression, $\frac{\partial \bar{q}}{\partial t} = k(q^* - \bar{q})$ or $\frac{\partial \bar{q}}{\partial t} = k'(c - c^*)$, with the overall effective rate coefficient defined above can be used to predict breakthrough response curves and concentration profiles. The dimensionless parameters for this simple model are defined as follows (Ruthven, 1984):

$$\tau' = k'(t - z/v) \quad \xi' = \frac{k'Kz}{v} \left(\frac{1-\varepsilon}{\varepsilon} \right) \quad \delta = \frac{kKD_L}{v^2} \left(\frac{1-\varepsilon}{\varepsilon} \right)$$

The first two terms of these dimensionless parameters can be used in approximate solutions to predict the response curves as follows:

$$\frac{c}{c_o} = \frac{1}{2} \operatorname{erfc} \left(\sqrt{\xi'} - \sqrt{\tau'} - \frac{1}{8} \sqrt{\xi'} - \frac{1}{8} \sqrt{\tau'} \right) \quad \text{Equation [2.50]}$$

or for an asymptotic form for large ξ'

$$\frac{c}{c_o} = \frac{1}{2} \operatorname{erfc} \left(\sqrt{\xi'} - \sqrt{\tau'} \right) \quad \text{Equation [2.51]}$$

Chapter 3: Experimental

3.1 Procedure and Apparatus

The following sections describe the experimental procedures and apparatus used for the gravimetric, volumetric and breakthrough (desorption) isotherm measurements. The experimental procedure and apparatus used for the chromatographic method to determine mass transfer coefficients is similar to that used for the isotherm measurement by breakthrough and will be described in section 3.1.2.

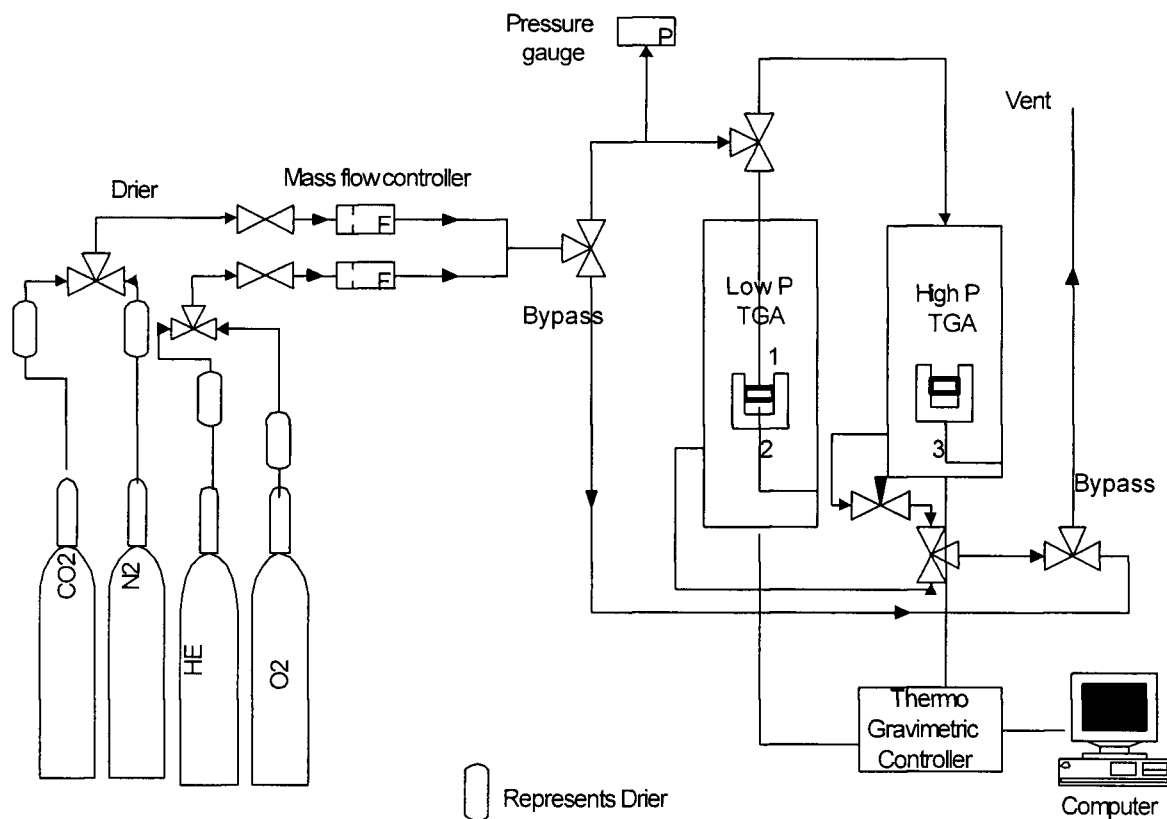
3.1.1 Gas isotherm measurement

In order to design an adsorption column, it is important to measure how much gas an absorbent can take up at different pressures and temperatures, i.e., it is desirable to measure gas adsorption isotherms for different adsorbents under study. In this study, gas adsorption isotherms up to a total partial pressure of 101 kPa for different adsorbents were measured using three different methods: gravimetric, volumetric, and desorption breakthrough analysis. The results from these methods are compared. The isotherm data up to the total pressure of 101 kPa were fitted as Langmuir isotherms and extrapolated to higher pressure (300 kPa). In order to confirm that the Langmuir model fit the data at higher pressure (up to 300 kPa), a gravimetric analyzer was modified to obtain isotherm data to pressures of 300 kPa.

3.1.1.1 Gravimetric Analysis

A Perkin Elmer Thermogravimetric Analyzer (TGA) model TGS-2, consisting of a high temperature furnace capable of reaching 1000 °C, a Pt sample pan and stirrup wire, housed in a glass chamber, was used to obtain isotherms up to 100 kPa. The unit includes a blower to cool the sample, microbalance electronics housed in a metal dome, and a Perkin-Elmer System 4

temperature controller. A second Perkin Elmer TGA was modified to measure the adsorption isotherm up to 300 kPa. For both systems, the flow rate was controlled using two Brooks mass flow controllers (5850E series: 0-500 SCCM) to control helium flow and the test gas flow rate (N_2 , CO , CO_2 , O_2 , and H_2). Figure 3.1 shows a flowsheet of the gravimetric unit set-up. Figure 3.2 provides a graphical representation of the gravimetric analyzer.



- 1- adsorbent
- 2- thermocouple for low pressure TGA system
- 3- thermocouple for high pressure TGA system

Figure 3.1 Flowsheet of gravimetric apparatus used for adsorption isotherm measurement.

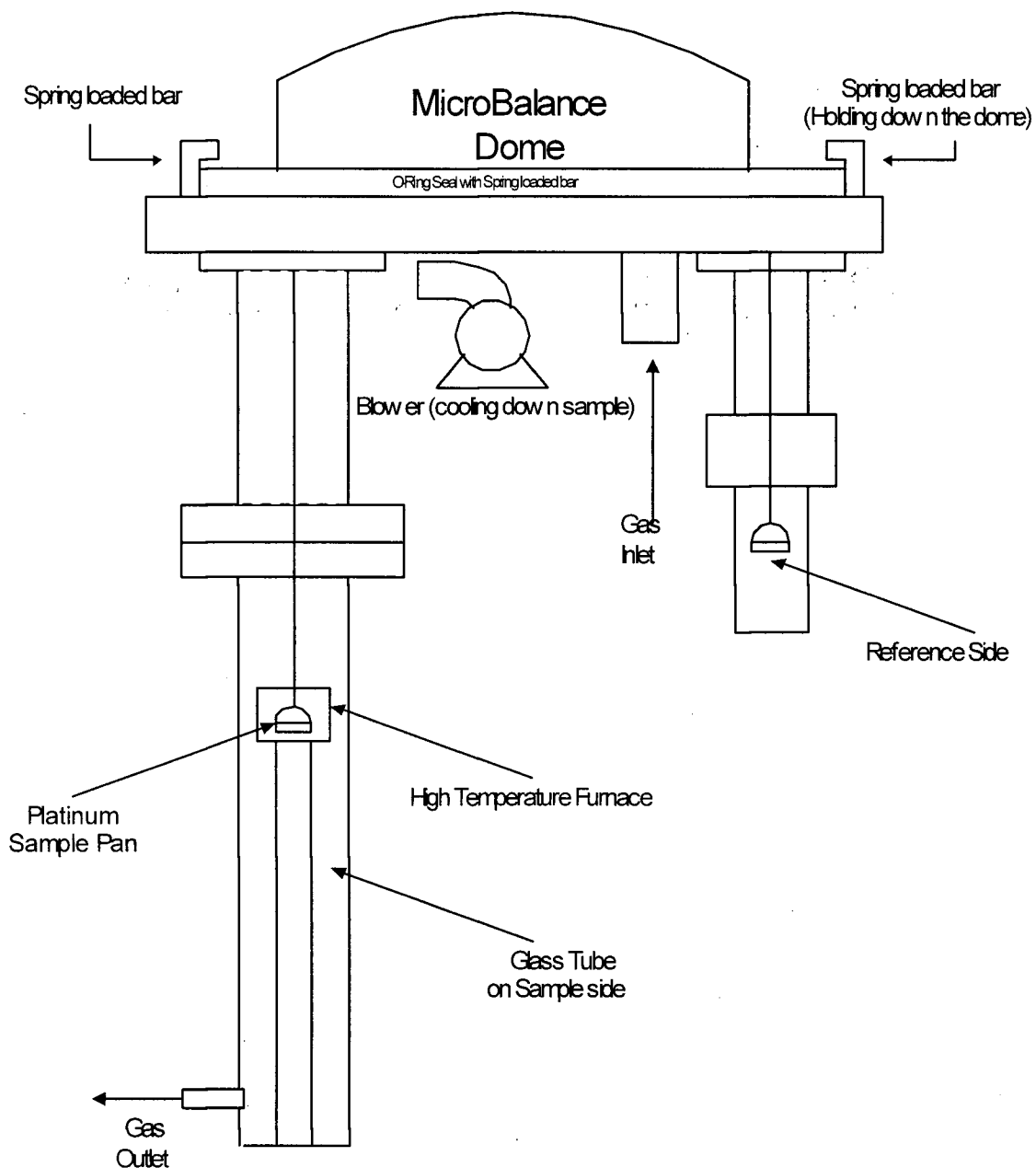


Figure 3.2 Schematic of the gravimetric analyzer unit

All experiments for the low pressure gravimetric measurement were conducted at a total gas flow rate of 400 mL (STP)/min. Prior to measurement, approximately 20 mg of adsorbent was placed on the sample side of the microbalance and its weight was measured. The sample was preheated to 450 °C at a ramp rate of 10 °C/min and then held at that temperature for 4 hours. The water content of the He gas was reduced to about 2-3 ppm using a 5A zeolite

moisture trap placed in the gas feed line prior to the gas entering the gravimetric unit. After the sample was activated, the temperature was reduced to the desired temperature for the isotherm measurement, at which point the dry sample weight was recorded. The gas composition was set using the two mass flow controllers while maintaining a total flow rate of 400 mL (STP) /min. The sample weight was continuously monitored until the weight change was < 0.003 mg. The difference between the measured sample weight after adsorption and the dry sample weight was taken as the gas adsorbed at that gas composition. The amount of gas adsorbed was corrected for residual water in the He gas using the water adsorption rate measured prior to the gas adsorption measurement since the He gas carrier contains a few ppm of water that could not be ignored. The residual water adsorption rate in the He gas was measured by monitoring the weight change of the sample while flowing pure He through the dry sample for a few minutes. This water adsorption rate was then used to correct for the residual water in the He gas during the adsorption experiments. The procedure was repeated at other gas compositions. Further experimental details can be found in Appendix 7.

Similar experimental procedures were followed for the high-pressure gravimetric measurements. However, a different sample activation procedure was followed. Initially, the high-pressure unit was incapable of high temperature sample activation due to a temperature limitation on the microbalance wires. Hence, the samples were activated in the low-pressure unit (at 400 mL (STP)/min and 450 °C with 10 °C/min heating rate) and then transferred to the high-pressure unit. The sample was then reheated to 275 °C to try to desorb any moisture adsorbed on the sample during the transfer process. Unfortunately, the heating at 275 °C was not sufficient to thoroughly dry the sample. To overcome this difficulty, a cooling jacket was added to the high pressure TGA to maintain the seals on the TGA dome below their maximum allowable temperature. With this modification, the same (sample pre-treatment) procedures as low-

pressure measurements could be followed. Further detail of the experimental procedure can be found in Appendix 7.

3.1.1.2 High Pressure Gravimetric Measurement

Glass components of the low pressure gravimetric unit, including the sample tube on the sample side of the analyzer and its o-ring connection, were replaced with aluminium in order to measure isotherms up to 300 kPa. The glass components on the low pressure analyzer were connected with O- rings sealed with vacuum grease, whereas the aluminium connections on the high pressure unit consisted of flanges, bolts and gaskets to maintain a high pressure seal. The inlet and outlet of the low pressure gravimetric unit connected to plastic were also modified to connect with 1/8" stainless steel Swagelok tubing.

The dome containing the microbalance mechanism is located at the top of the gravimetric unit and was sealed with an O-ring and spring loaded bars that press down on the dome. The modified unit was sealed by a metal ring, which was bolted down with 12 equally spaced bolts around the dome.

The heat was supplied to the sample in the low-pressure unit by means of high temperature heating dome or furnace. The sample, suspended from a hang down wire was located just inside the heating dome. For the high-pressure system, the heating dome was removed and the heat was supplied by two band heaters with a power of 200 Watts each. The band heaters were wrapped around the aluminium tube (sample side), in which the sample was located. Unfortunately, the heat provided by the band heater was also conducted through the aluminium tube to the dome where the microbalance mechanism was located. Since the epoxy sealing the dome and the signal wires from the microbalance could not withstand temperatures above approximately 92 °C, the temperature on the upper part of the aluminium tube (sample side) had to be reduced below this temperature. A stainless steel water-cooling jacket was used

to reduce the temperature of the sample side aluminium tube below 90 °C. Figure 3.3 shows the diagram of the high pressure gravimetric unit.

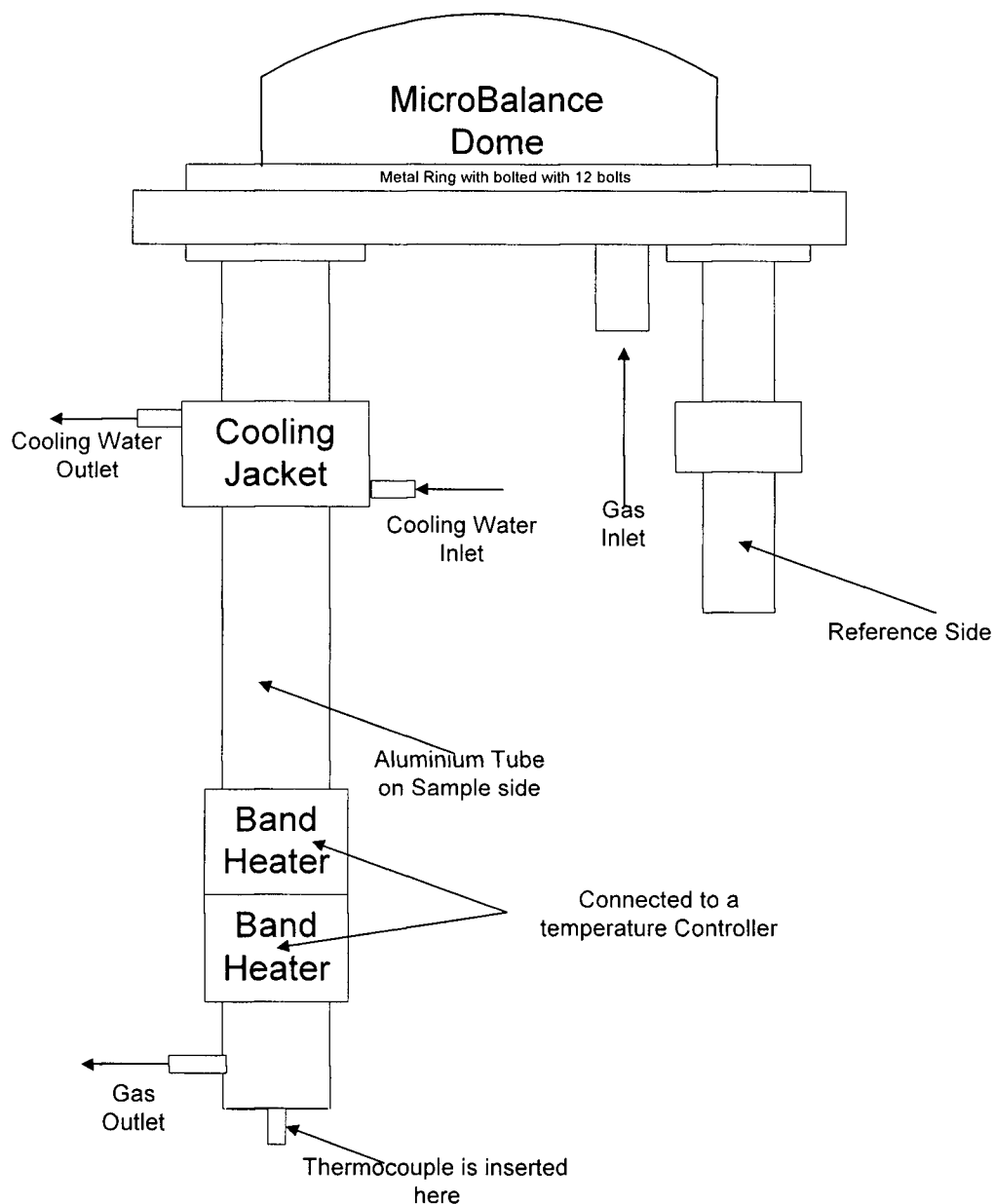


Figure 3.3 Graphical representation of high pressure TGA

3.1.1.3 Volumetric Adsorption Isotherm Measurement

The Micromeritics accelerated surface area and porosimetry system (ASAP 2010) was used to obtain gas adsorption isotherms by the volumetric method. The ASAP 2010 consists of two sample preparation ports, one analysis port, in-line cold traps, and a sample saturation pressure tube. The sample preparation ports consist of two straight glass tubes connected with two U-shaped sample tubes, which are heated by heating mantles capable of reaching 350 °C. The analysis port was made of a quartz sample tube heated by the analysis bath dewar (furnace), which can be moved up and down by the dewar elevator. A cold trap is located between the sample preparation ports and the sample analysis port for trapping impurities from either the sample in the sample preparation ports or sample analysis port during sample evacuation. The vacuum pump used for evacuation is capable of reaching and maintaining a vacuum of around 2 μm Hg in the manifold, the sample preparation ports and the sample analysis port. The saturation pressure tube injects doses of analysis gas into the sample tube until the equilibrium pressure between adsorbent and surrounding does not change for two consecutive doses.

The principle behind the volumetric method of gas adsorption isotherm measurement is that the known amount of adsorbate is introduced into the adsorbent chamber to pressurize the chamber at a fixed pressure and temperature, followed by equilibration of the gas between the bulk and the adsorbed phase. After the system is allowed to come to equilibrium, the pressure is monitored and compared to the original pressure. If the pressure decreases, a known amount of adsorbate is added to obtain the original pressure. On the other hand, if there is no change in pressure, then the bulk gas is assumed to be in equilibrium with the adsorbed gas at that pressure and temperature. The entire adsorption isotherm can be obtained by measuring the adsorbed volume at other pressures. To account for the volume of gas in the bulk phase, a blank sample tube can be run at the same conditions as the isotherm measurement and this volume can be

subtracted from the total volume in the bulk phase and adsorbed phase to obtain the volume of gas adsorbed by the adsorbents. Figure 3.4 shows the schematic diagram of the ASAP 2010.

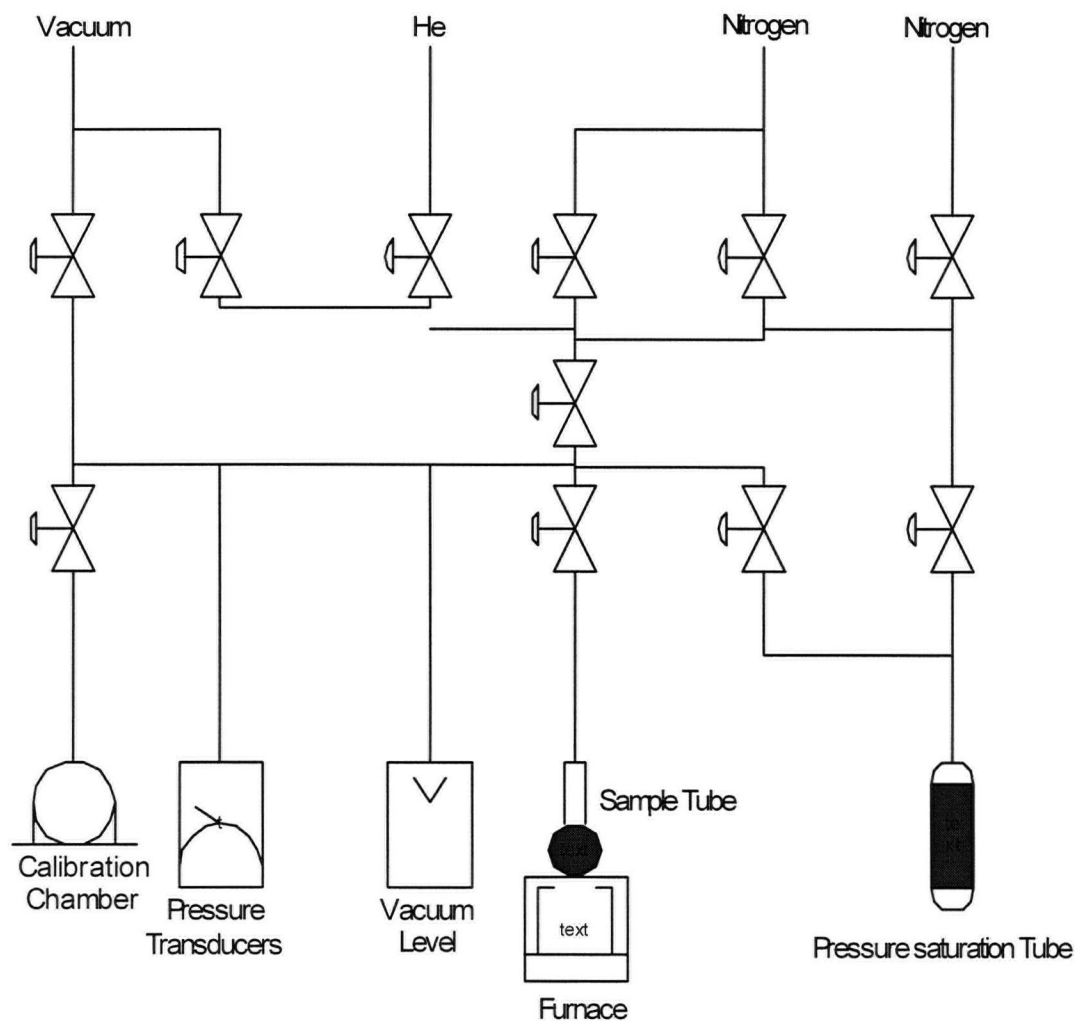


Figure 3.4 Schematic diagram of ASAP 2010

A Micromeritics ASAP2010 adsorption unit was used to obtain the volumetric adsorption data. Approximately 350 mg of sample was placed on quartz wool inside a U-shaped quartz sample tube. The sample tube was then degassed at 350 °C under 3-10 $\mu\text{m Hg}$ for 14 hours. The sample was transferred to the sample analysis port (without exposure to ambient air) and heated to the required adsorption temperature. After the sample transfer, the unit was programmed to measure the adsorption isotherm at different adsorbate partial pressure. Detailed experimental procedures can be found in Appendix 7.

3.1.1.4 Breakthrough Analysis

Desorption breakthrough curves were obtained using the experimental set up shown in Figure 3.5, that consists of the following:

- Two moisture traps to reduce the moisture content of the gas used in the experiments.
- Two Brooks mass flow controllers (5850E series, 0-100 SCCM and 0-500 SCCM) controlled by a Brooks microprocessor control & read out unit, Model 0154E.
- An Omega pressure transducer to detect the inlet pressure.
- An Anglo Scientific Instruments Dataquad mass spectrometer (MS) and vacuum chamber.
- A computer with Labtech Notebook program to log the measured data.

A schematic diagram of the experimental set up is shown in Figure 3.5.

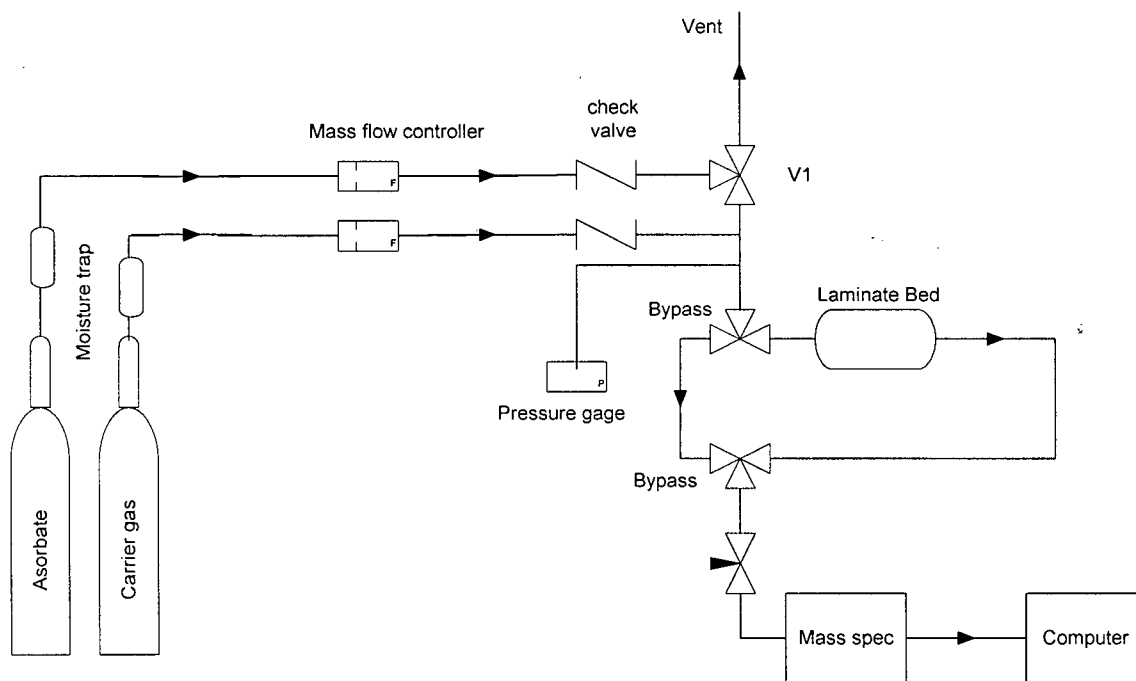


Figure 3.5 Breakthrough experiment for mass-spectrometer system

Two moisture traps consisting of 5A zeolite were used to dry He and the adsorbent gas of interest. The desired flowrate of the gases was controlled by the two mass flow controllers. The He carrier gas was mixed with the test gas in the line before the inlet to the adsorbent bed. Eighty percent by volume of test gas was used for the analysis. An Omega pressure transducer was used to measure the inlet pressure. The outlet gas was analyzed by the mass spectrometer connected to Labtech Notebook for data logging. The exit gas was monitored, but not logged until adsorption was complete. After the adsorbent was saturated with test gas, 400 mL of He was switched to desorb adsorbed gas in the bed while the exit gas was continuously monitored by the mass spectrometer and logged. The data logging ceased when all the gas had been desorbed, as indicated by a constant pressure reading on the mass spectrometer. Further details of the experimental procedure are provided in Appendix 7.

3.1.2 Chromatographic Method

The apparatus used for the chromatographic method was similar to that used for the breakthrough curve for the desorption experiment, except that the total gas flow consisted of 5 % test gas in He. The pressure was monitored at the inlet and outlet of the adsorbent bed and the change in sorbate concentration was measured by a thermal conductivity detector (TCD). The sole purpose of switching from the MS to the TCD was that at high flow rate, sampling rates of more than one per second were required and this could be achieved with the TCD whereas the MS response time was of the order of one second.

The apparatus for the chromatographic method was used in two configurations; one for high flow experiments and the other for low flow experiments. The apparatus for high flow rate experiments used three mass flow controllers (0-500 SCCM (STP), 0-100 SCCM (STP), and 0-20 SCCM (STP)) controlled by a Brooks microprocessor control and read out unit (model 0154E), a rotameter (0-4880 SCCM (STP)), adsorbent pack, and pressure transducers. It was

necessary to put one mass flow controller at the outlet of the adsorption pack since the filament of the thermal conductivity detector (TCD) used was not able to withstand flow rate exceeding 300 SCCM (STP). Hence, the mass flow controller was placed after the adsorption pack's outlet flow to reduce the flow rate below 300 SCCM (STP). The low-flowrate setup consisted of the same components except that the rotameter was not used. Schematic diagrams for both systems are shown in Figure 3.6 and Figure 3.7. Detailed experimental procedures can be found in Appendix 7.

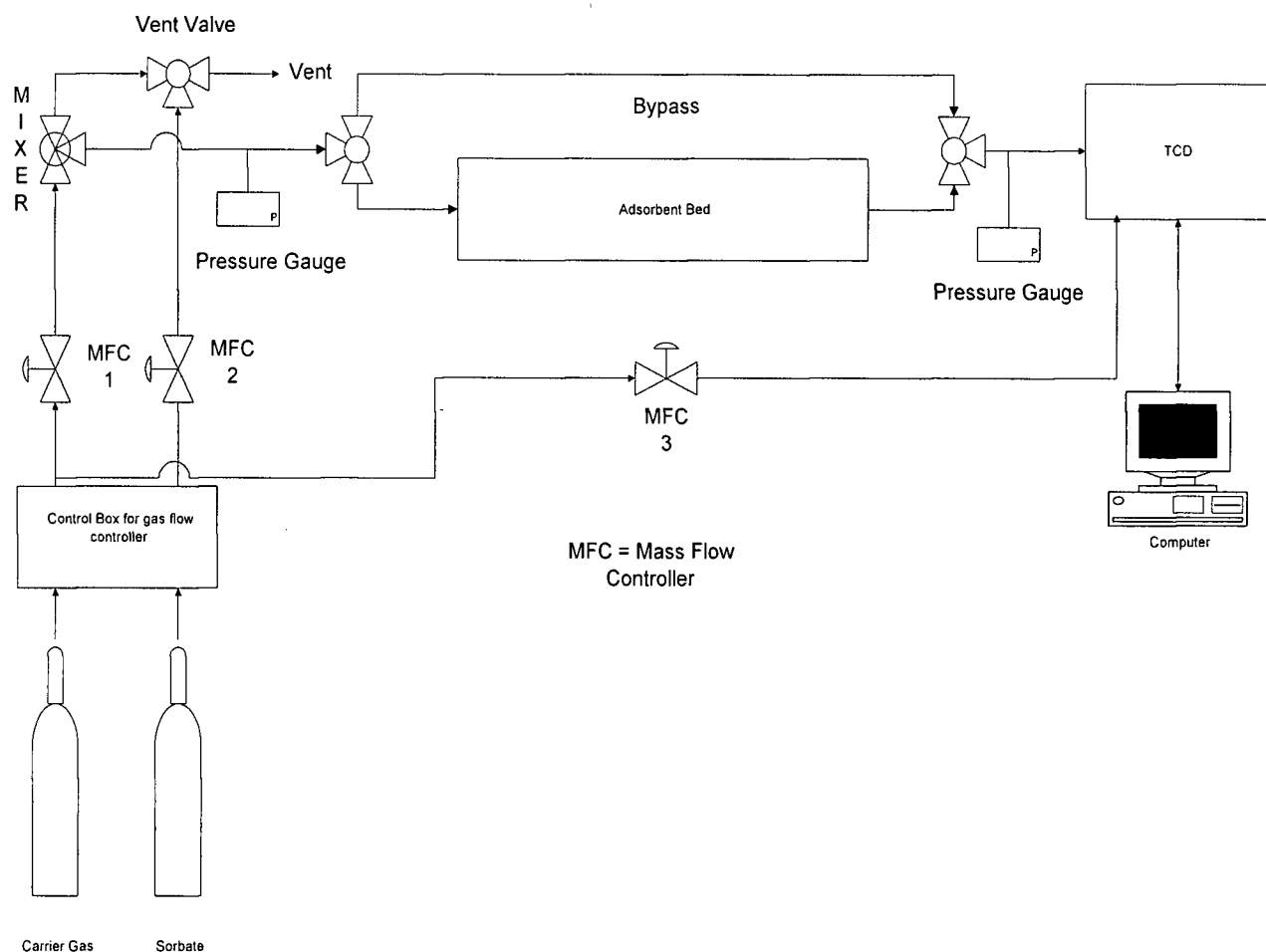


Figure 3.6 Breakthrough experimental set up with TCD for low flow rate experiments

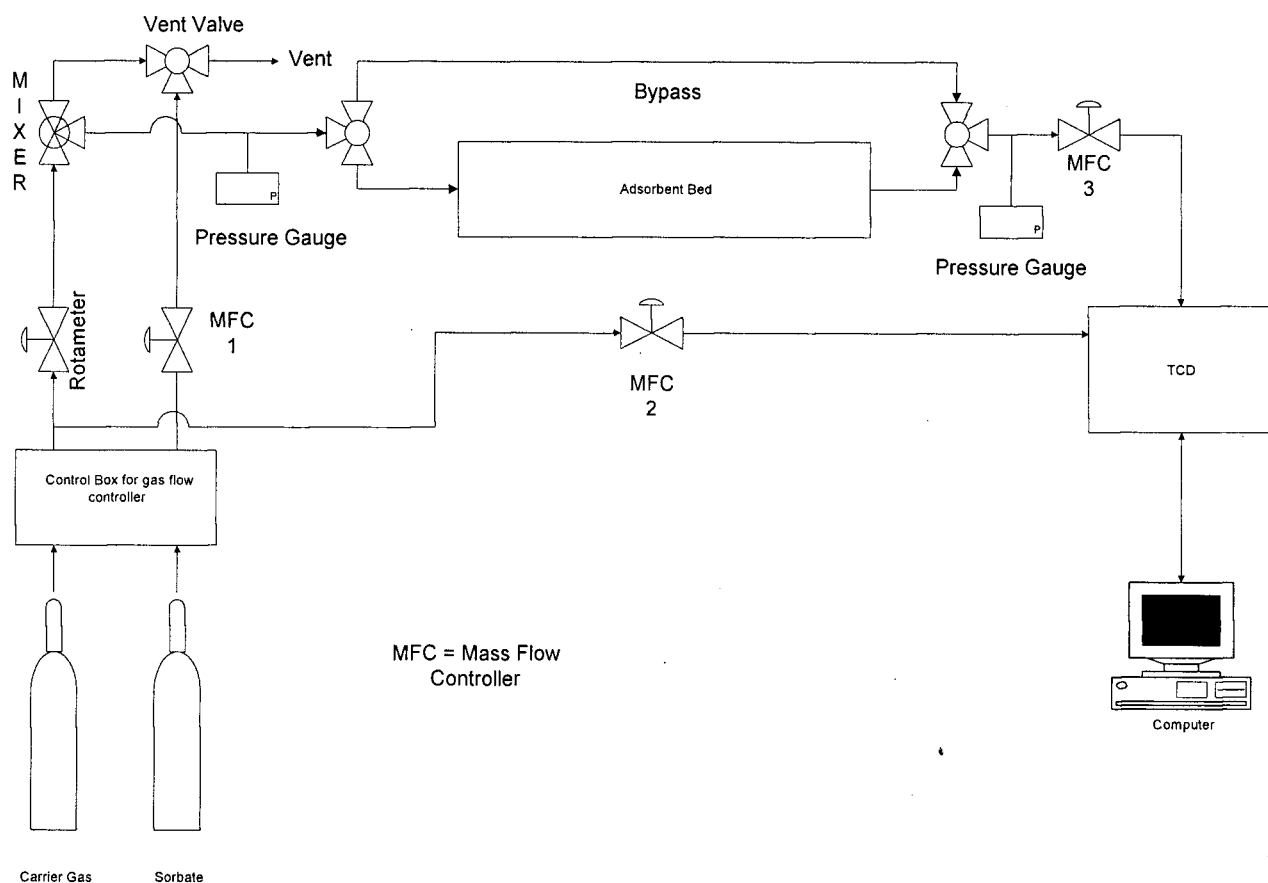


Figure 3.7 Breakthrough experiment set up with TCD for high flow rate experiments

3.1.3 Pressure Drop Through Structured Adsorbent Bed

The effect of pressure on the moments of the breakthrough response curve has been studied and later reviewed by Dixon and Ma (1988). According to these authors, the most useful analysis for the correction for pressure drop is that of Pazdernik and Schneider (1981) since by using approximations, they were able to derive a generally valid and simple closed form expression shown in Equation [3.1]

$$\frac{\sigma^2}{2\mu^2} \approx \frac{3\gamma}{2[(1+\gamma)^{3/2} - 1]} \left\{ \frac{D_L}{\nu L} + \frac{\varepsilon \nu}{L(1-\varepsilon)kK} \left[1 + \frac{\varepsilon}{(1-\varepsilon)K} \right]^{-2} \right\} \quad \text{Equation [3.1]}$$

where $\gamma = (p_o/p_L)^2 - 1$ and p_o and p_L are the inlet and outlet pressure, respectively

The term $\frac{3\gamma}{2[(1+\gamma)^{3/2} - 1]}$ is multiplied to the HETP value to correct for the pressure drop.

However, in the study the effect of pressure drop was negligible. For flow rates up to 260 SCCM (STP), the pressure drop was 0 to 0.69 kPa which was within the accuracy of the pressure transducer (± 0.69 kPa). At higher flows (1200 to 2500 SCCM), the maximum pressure drop was of the order 2-3 % of the inlet pressure. Consequently, the factor $\frac{3\gamma}{2[(1+\gamma)^{3/2} - 1]}$ only affected the HETP value by 1-2%. A representative set of corrected HETP values are shown in Appendix 6. From these data, we conclude that the effect of pressure drop on breakthrough response can be neglected and the negligible pressure drop assumption made for the axial dispersed plug flow model was indeed valid in the present study.

3.2 Materials

The materials used for the adsorption isotherm experiments were different than those used for the chromatographic method. The materials used for the gravimetric and volumetric experiments were powders (zeolite NaX, zeolite LiX, and a QuestAir proprietary adsorbent (QP)) while the materials used for the chromatographic method were beads that contained about 20 % inert binding material. These materials are discussed in the next two sections.

3.2.1 Adsorption Isotherm

Zeolite 13X and zeolite LiX were used for adsorption isotherm measurements. QuestAir proprietary adsorbent is a high temperature zeolite X adsorbent. The three different isotherm measurement techniques, (volumetric, gravimetric, and desorption breakthrough) were used to determine gas adsorption isotherms on these adsorbents as listed in Table 3.1.

Table 3. 1 Adsorbents used in the present study

Material	Gas	Temperature
Zeolite NaX	N ₂	30 °C and 50 °C
	CO	30 °C and 50 °C
	CO ₂	30 °C and 50 °C
Zeolite LiX	N ₂	30 °C, 40 °C, 50 °C, 60 °C and 80 °C
QP	N ₂	60 °C, 80 °C and 100 °C

3.2.2 Kinetic Parameters

Rectangular cross-sectional area sample packs consist of thin layers of substrate, on which LiX zeolite was deposited. The adsorbent structures, supplied by Questair Technologies, were used to extract kinetic parameters such as dispersion and mass transfer resistances. Figure 3.8 gives a graphical representation of a sample adsorbent structure. More detailed dimensions of the adsorbent structures can be found in Section 4.2.

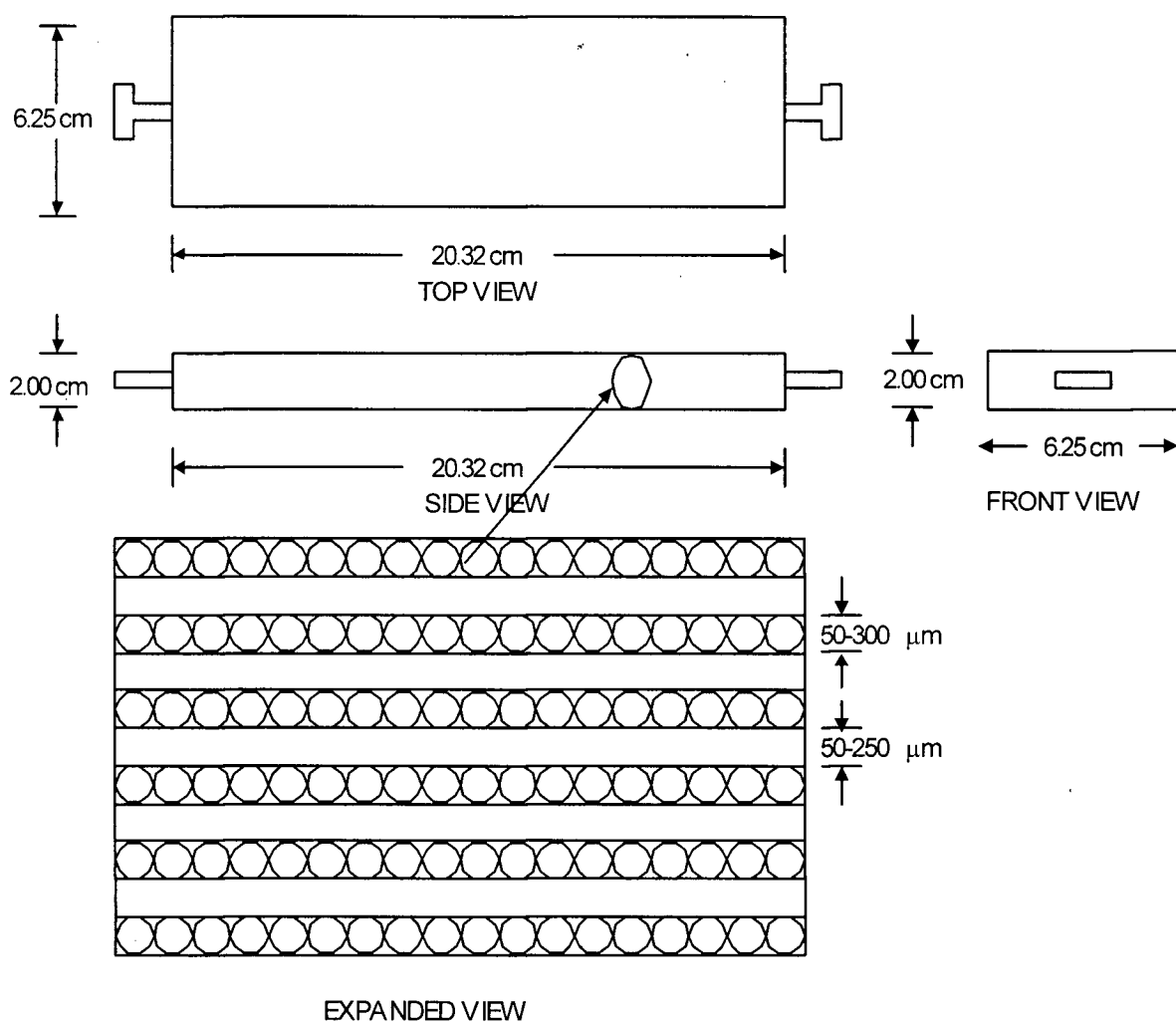


Figure 3.8 Graphical representation of the structured adsorbent

Chapter4: Adsorption Isotherm Measurements

4.1 Introduction

The results obtained from the present study are conveniently presented in two separate chapters. Chapter 4 describes and discusses the adsorption isotherm results while Chapter 5 focuses on the results obtained from the study of the dynamic response of the structured adsorbent.

4.2 CO and CO₂ adsorption isotherms

The CO and CO₂ adsorption isotherms for the zeolite NaX adsorbent, for pressures up to approximately 101 kPa, were determined using the volumetric, gravimetric, and desorption breakthrough methods. The volumetric and gravimetric methods directly generate adsorption capacity at different pressures, whereas the desorption breakthrough method generates data that allows calculation of the Langmuir adsorption isotherm constants. By measuring the desorption dynamics of a pre-adsorbed adsorbate from a bed of adsorbent, the adsorbate concentration profile through the bed can be determined. The concentration profile along the length of the bed yields Langmuir isotherm parameters, q_s and b where $q_s b = a$.

The adsorption isotherms obtained using the volumetric and gravimetric methods for CO and CO₂ at 30 °C are shown graphically in Figure 4.1.

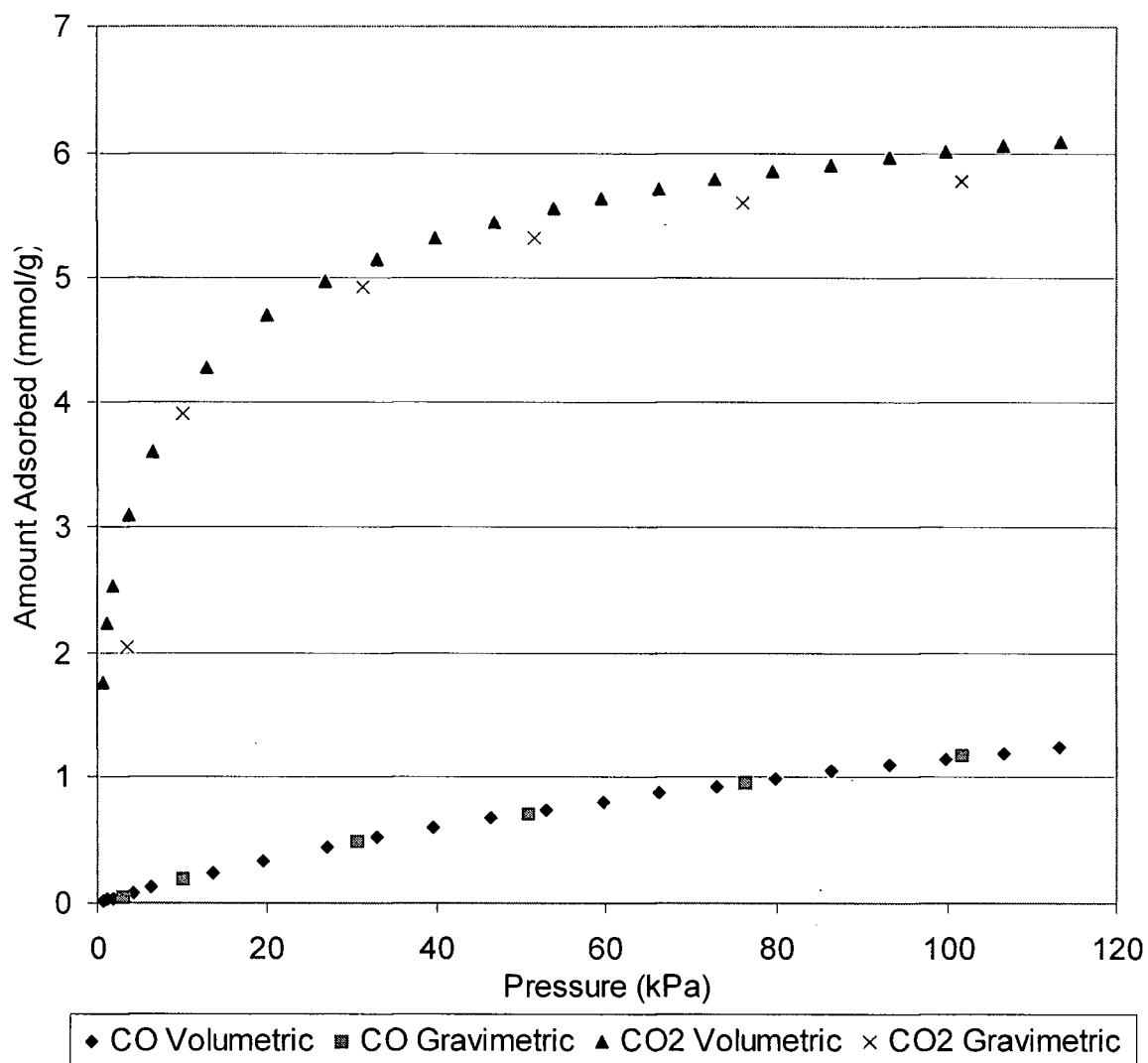


Figure 4.1 CO and CO₂ adsorption isotherms on zeolite NaX at 30 °C obtained by the volumetric and gravimetric methods.

As can be seen in Figure 4.1, the adsorption isotherms obtained from the volumetric and gravimetric methods are in reasonably good agreement. Slightly lower isotherm measured from the gravimetric method could be due to errors associated with the buoyancy force and the water adsorption rate correction (adsorbent is highly hydrophilic, i.e, the amount of water adsorbed that is not corrected for will result in a lower adsorption isotherm). The measured isotherm data were fitted to the Langmuir adsorption model using the Tablecurve2D program to extract the

Langmuir adsorption constants a and b according to Equation [2.06]. ($a = q_s \cdot b$). For the desorption breakthrough method, Langmuir adsorption constants were determined from the slope and intercept of the plot c/c_0 versus $1/\sqrt{vt - z}$ according to Equation [2.19]. Table 4.1 compares the Langmuir adsorption constants for CO and CO₂ extracted from the volumetric, and gravimetric isotherm data, and the desorption breakthrough data.

Table 4.1 Comparison of Langmuir adsorption constants at 30 °C determined using the volumetric gravimetric, and desorption breakthrough methods on zeolite NaX.

Gas	Measurement Method	Langmuir constant, a $\pm 95\% \text{ C.I.}^*$ (mmol g ⁻¹ kPa ⁻¹)	Langmuir constant, b $\pm 95\% \text{ C.I.}$ (kPa ⁻¹)
CO	Volumetric	0.01866 ± 0.00015	0.00620 ± 0.00015
	Gravimetric	0.01839 ± 0.00081	0.00582 ± 0.00082
	Desorption Breakthrough	0.08527	0.0234
CO ₂	Volumetric	1.8884 ± 0.4903	0.3192 ± 0.0895
	Gravimetric	1.2197 ± 0.1967	0.2075 ± 0.0376
	Desorption Breakthrough	2.6251	0.256

* C.I. is Confidence Interval

The adsorption isotherms for CO and CO₂, calculated from the Langmuir constants of Table 4.1, are compared to the measured adsorption isotherms for both the volumetric and gravimetric methods, in Figure 4.2 and Figure 4.3, respectively. Note that confidence intervals reported in Chapter 4 are the 95 % confidence intervals. A more accurate value of the Langmuir parameter b of CO adsorption isotherm may be obtained if the adsorption isotherm were to be measured up to higher pressure where adsorption saturation occurs.

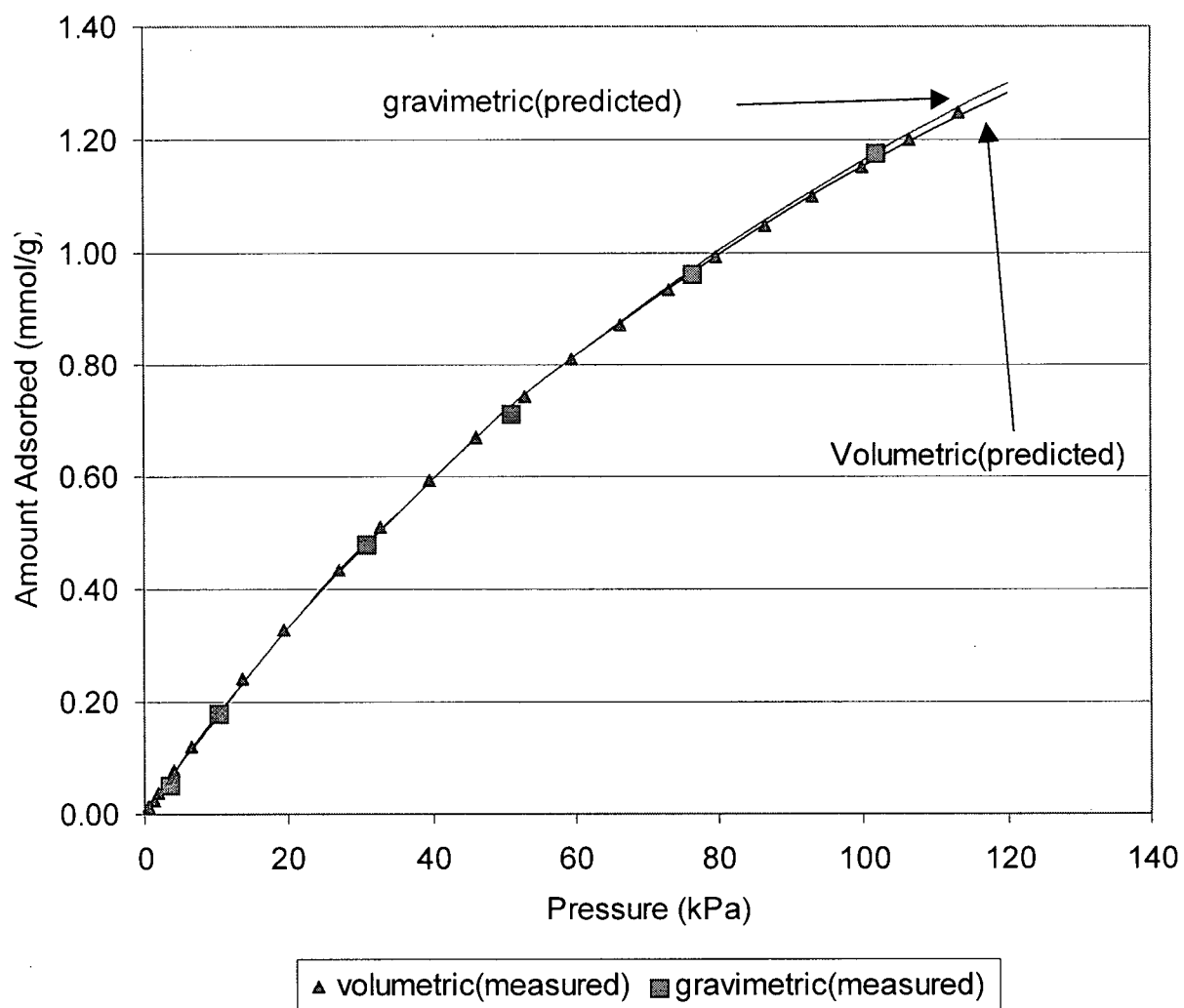


Figure 4.2 Measured and fitted adsorption isotherms for CO at 30 °C on zeolite NaX.

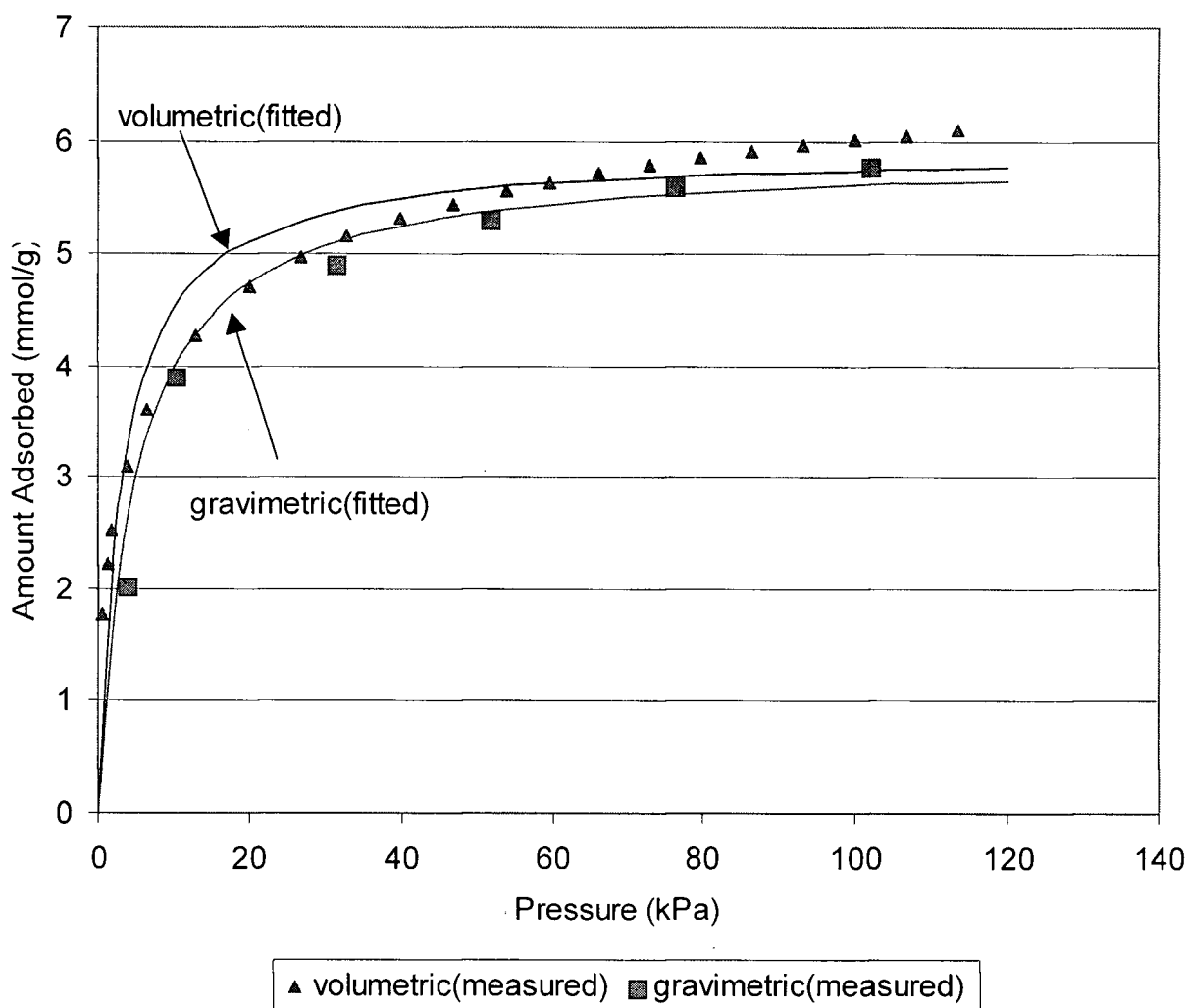


Figure 4.3 Measured and fitted adsorption isotherms for CO₂ at 30 °C on zeolite NaX.

Figures 4.2 and Figure 4.3 show that the Langmuir model fits the experimental data quite well, except for the adsorption isotherm predicted at low pressure (20-60 kPa) by the volumetric method, where the Langmuir model overpredicts the measured isotherm. Note that at pressures < 5 kPa the measurement error from the free space measurement (the measurement of the dead volume in the tubes and connections of the instrument) becomes significant and this may result in the higher than expected initial slope of the isotherm. Another possible explanation for the deviation of the fitted isotherm to the measured isotherm is that it is possible that the adsorption

system is a heterogeneous system, hence, Langmuir adsorption model may not be able to fit the isotherm. A generalized Langmuir model can be used to deal with the heterogeneous system.

The Langmuir adsorption constants obtained from all three methods were then used to generate adsorption isotherms for CO and CO₂, which are shown in Figure 4.4 and 4.5 respectively.

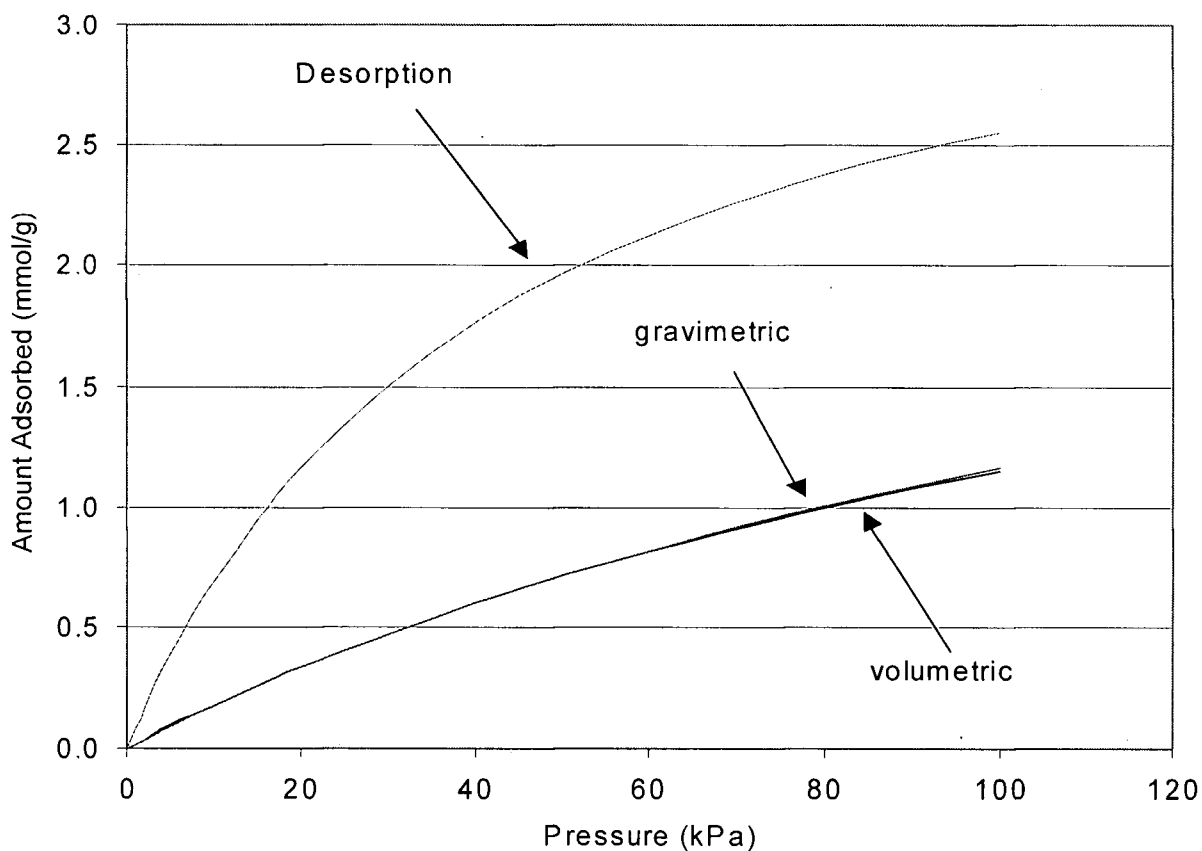


Figure 4.4 Comparison of the CO adsorption isotherms for zeolite NaX based on Langmuir parameters obtained from volumetric, gravimetric, and desorption breakthrough method at 30 °C.

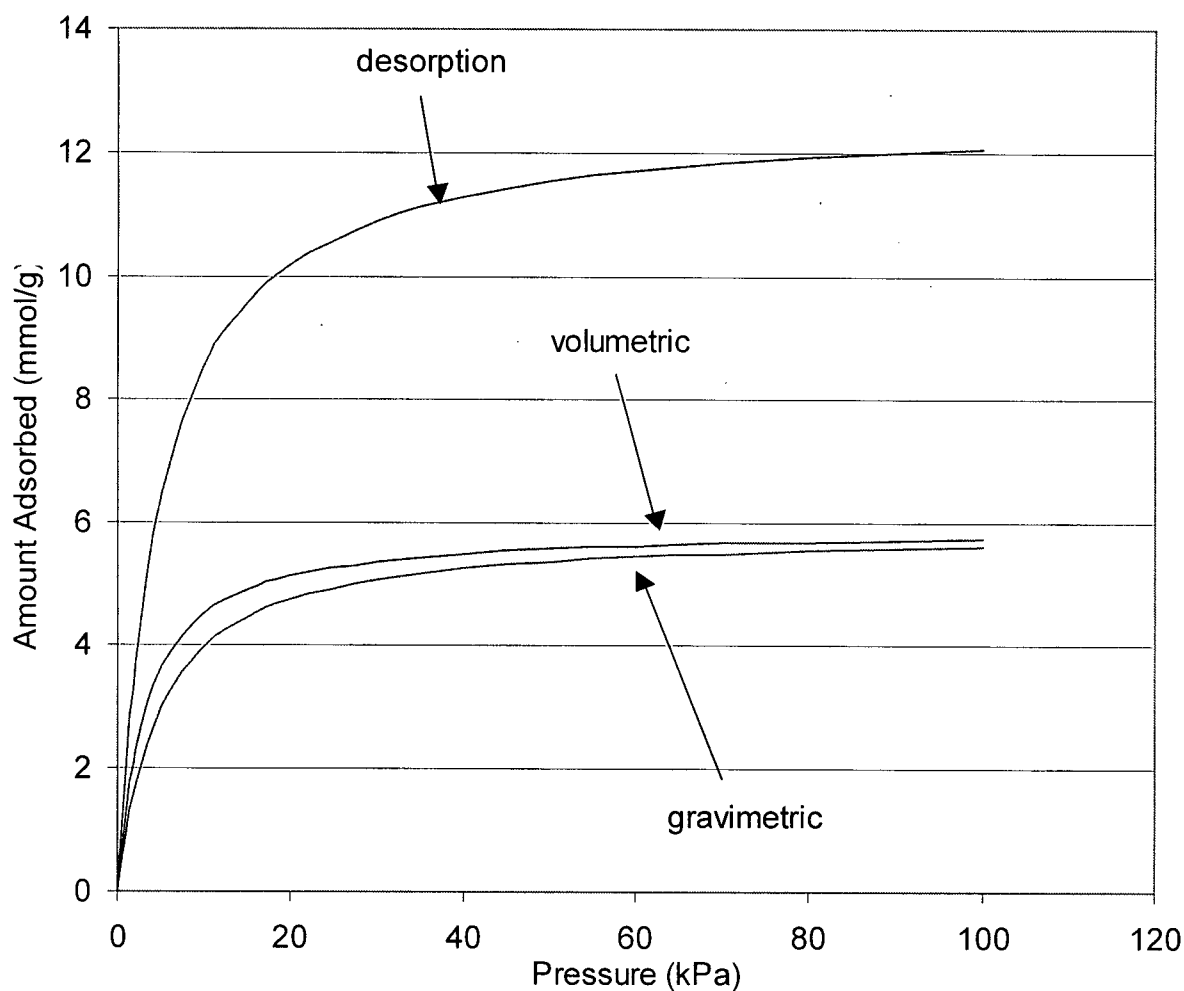


Figure 4.5 Comparison of the CO₂ adsorption isotherms at 30 °C for zeolite NaX based on Langmuir parameters obtained from volumetric, gravimetric, and desorption breakthrough method

Generally, adsorption isotherms obtained from the volumetric and gravimetric methods were in good agreement. Figure 4.4 shows that CO adsorption isotherms for the two methods almost perfectly match each other. For CO₂ adsorption isotherms, Figure 4.5 still shows reasonable agreement, but the gravimetric results appear to generate slightly lower adsorption capacity than the volumetric method. A possible explanation for this deviation is that fewer data

points were obtained from the gravimetric method at low pressure, hence, when fitted with the Langmuir model, the number of data points are inadequate to accurately define the curvature of the isotherm at low pressures, resulting in lower Langmuir parameters. Furthermore, for the gravimetric method, the adsorbate, which unavoidably contains a small quantity of water, is continuously flowing through the highly hydrophilic sample, until the sample reaches its maximum adsorption capacity at that pressure. In the present study, the amount of water adsorbed was accounted for and estimated assuming that the water adsorption rate was the same as that measured by flowing carrier gas (He) through the sample before the beginning of each experiment. However, it is possible that the amount of water adsorbed during the experiment is slightly less than corrected for since the water adsorption rate was measured for 10-15 minutes and it took 2-3 hours to measure an isotherm, i.e., the water adsorption rate over the extended period needed for the isotherm measurement could be lower than the initial water adsorption rate used. Furthermore, when the water adsorption rate was measured, it was measured with 100% He, but during the isotherm measurement, different partial pressures of the test gas mixed with He were used. Consequently, the adsorption isotherm from the gravimetric method was slightly lower than the volumetric method isotherm.

To quantify whether the Langmuir fit to the isotherm data for the volumetric and gravimetric methods were significantly different, F-tests were performed on the CO and CO₂ isotherm determined by both methods. The following hypothesis test was conducted:

$$H_0: \quad \sigma_1^2 = \sigma_2^2 \quad \text{if } F_{\text{stats}} < F_{\text{critical}, \alpha=0.05}$$

$$H_1: \quad \sigma_1^2 \neq \sigma_2^2 \quad \text{if } F_{\text{stats}} > F_{\text{critical}, \alpha=0.05}$$

where σ_1^2 and σ_2^2 are the variance of the two data sets from the two adsorption methods

$$F_{\text{stats}} \quad = \text{F factor defined as } F_1/F_2$$

$$F_1 \quad = \text{SSE/d.f. of data set 1}$$

F_2 = SSE/d.f. of data set 2

SSE = sum of square of errors defined as $[Y(\text{measured}) - Y(\text{average})]^2$

d.f. = degree of freedom

$F_{\text{critical}, \alpha=0.05}$ = F values from F distribution table at 95% confidence interval

The F factors and F-critical values for CO and CO₂ data are summarized in Table 4.2.

Table 4.2 F-test comparison between volumetric and gravimetric data for CO and CO₂

adsorption on zeolite NaX at 30 °C.

Gas	$F_{\text{stats}} = F_1/F_2$	$F_{\text{critical}, \alpha=0.05}$ for M_1/M_2
CO	1.46	1.96
CO ₂	0.94	1.96

F_1 = F factor for adsorption isotherm obtained from volumetric measurement

F_2 = F factor for adsorption isotherm obtained from gravimetric measurement

M_1 = Data obtained from volumetric method

M_2 = Data obtained from gravimetric method

From Table 4.2, we concluded that the fit to the isotherm data for CO and CO₂ obtained from the volumetric and gravimetric methods was not significantly different since the F factors are less than the F-critical values.

Adsorption isotherms derived from Langmuir parameters extracted from the desorption breakthrough curves were much higher than those obtained from the volumetric and gravimetric data, as can be seen in Figure 4.4 and Figure 4.5. Possible explanations for this discrepancy are as follows:

1. Sample differences: The sample used for the desorption breakthrough method was not in powder form, as was the case for the other two methods. The sample had been pelletized and contained approximately 20 percent “inert” binding materials.
2. The assumptions made for desorption breakthrough analysis may not all be valid. These assumptions include plug flow, negligible mass transfer resistance, and a favourable adsorption isotherm. The first two assumptions are more likely to introduce error in the Langmuir adsorption constants extracted. Axial dispersion is fairly significant in any packed bed system. According to Ruthven and Karger (1992), for N₂/He in 4A zeolite, the axial dispersion, D_L , is 0.7 cm²/sec at 35 °C. Mass transfer resistance may not be negligible as assumed since the particle diameter was quite large (approximately 2 mm), which results in significant macropore mass transfer resistance. The last assumption of a favorable isotherm is often valid since adsorption processes that can be fitted with Langmuir isotherm models should be favourable. Figure 4.6 and 4.7 confirms that both CO and CO₂ adsorption isotherms are indeed favourable. If $\frac{q^* - q_o}{q_o - q_o} > \frac{c - c_o}{c_o - c_o}$, i.e.,

$\frac{q^* - q_o}{q_o - q_o}$ vs. $\frac{c - c_o}{c_o - c_o}$ graph is above the diagonal or 45° line, then the isotherm is said to

be favourable.

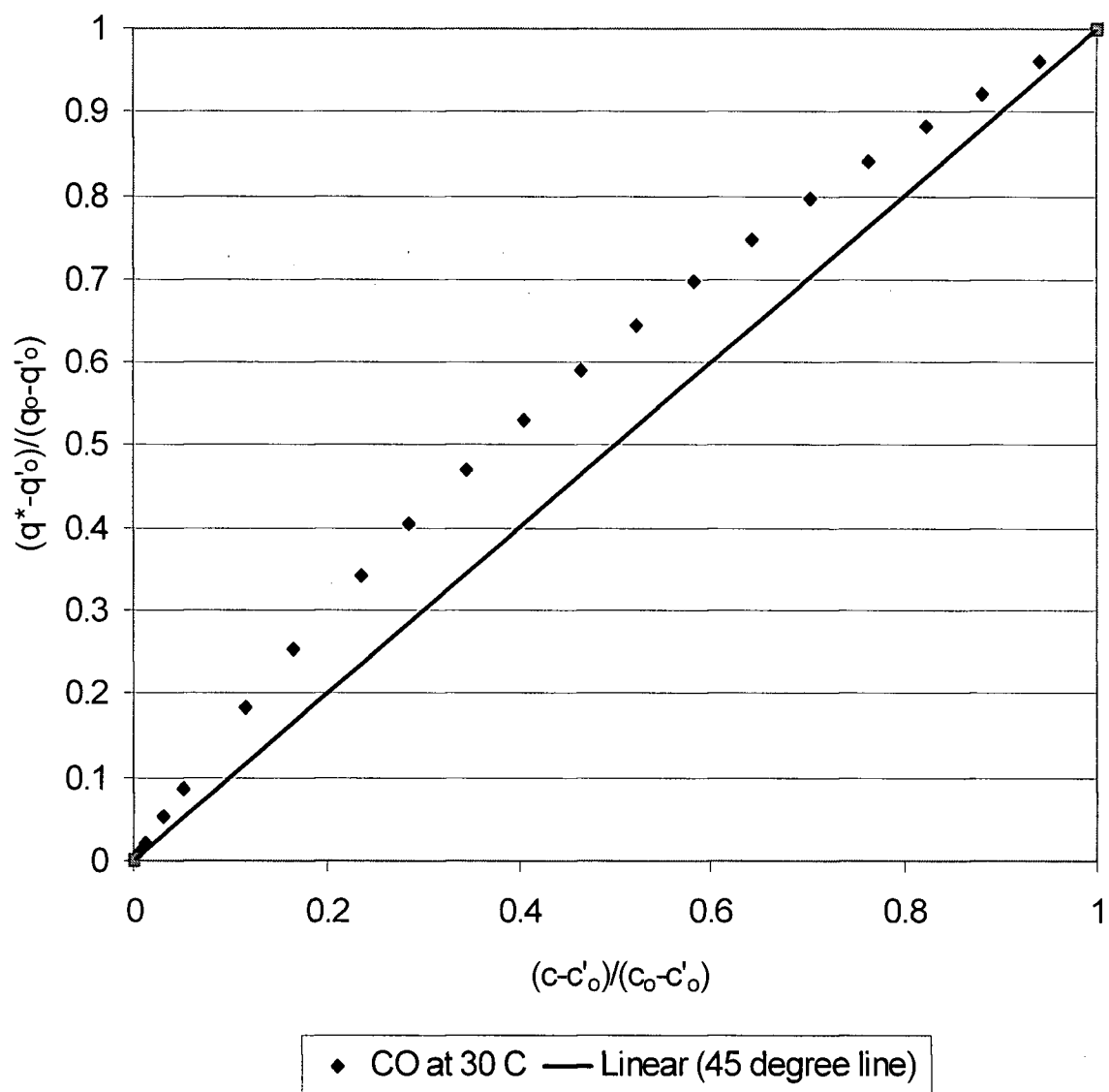


Figure 4.6 $(q^*-q'_o)/(q_o-q'_o)$ vs. $(c-c'_o)/(c_o-c'_o)$ for CO.

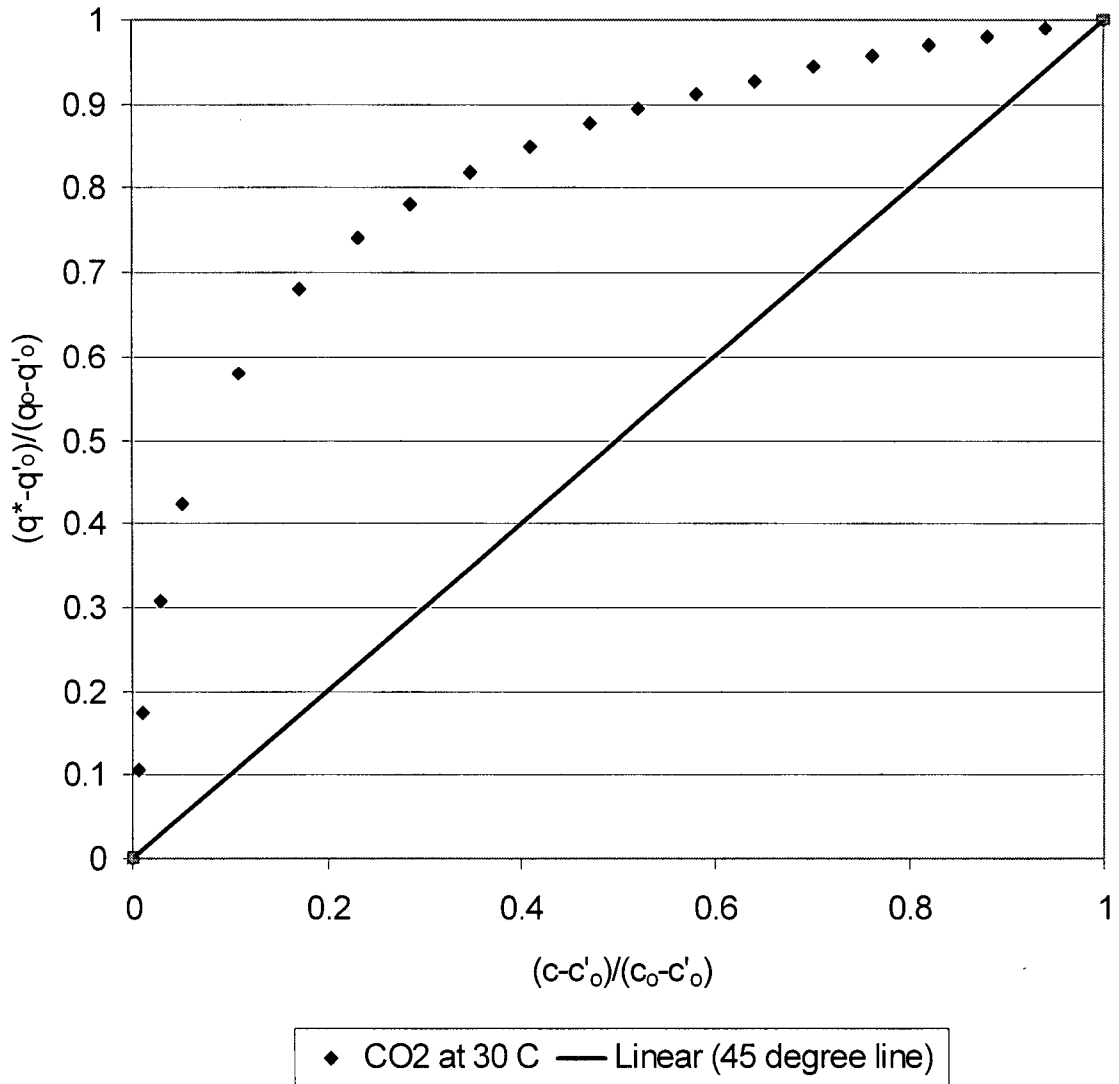


Figure 4.7 $(q^*-q'_0)/(q_0-q'_0)$ vs. $(c-c')/(c_0-c'_0)$ for CO₂.

3. Estimation of the Langmuir parameters is based on the slope and intercept of the c/c_0 versus $1/\sqrt{vt-z}$ plot, which may not be accurately extracted as shown in Figure 4.8.

The 95% confidence intervals for the slope and the intercept were determined to be $\pm 5\%$ and $\pm 30\%$, respectively

The results from the present study suggests that Desorption breakthrough method is not a suitable method in obtaining gas adsorption isotherms for the system under study.

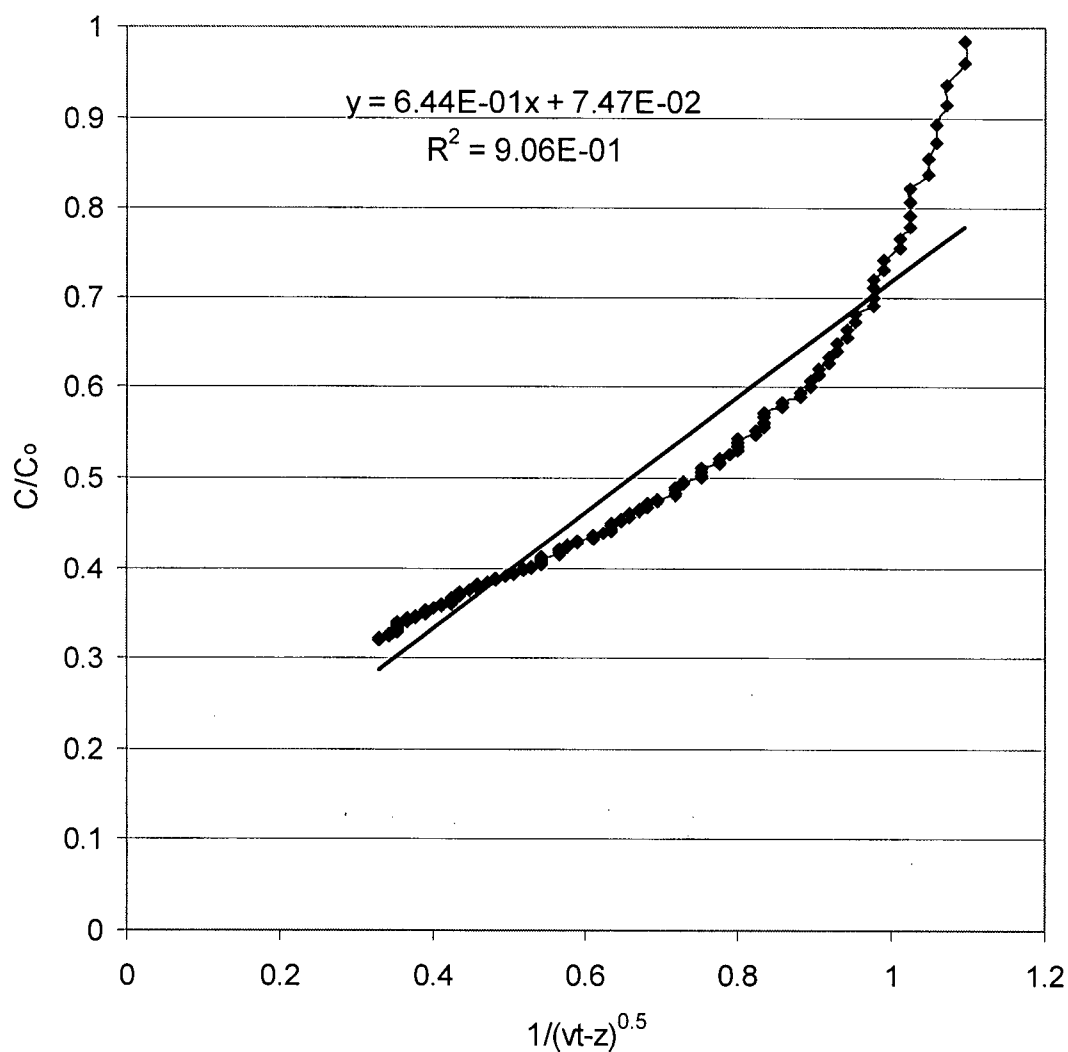


Figure 4.8 C/C_0 vs. $1/\sqrt{vt-z}$ plot for CO at 30 °C.

4.3 N_2 Adsorption Isotherms

N_2 adsorption isotherms on zeolite NaX were also obtained at 30 °C and 50 °C, as shown in Figure 4.9. These adsorption isotherms were fitted by the linear Henry's law equation. F tests were also performed for these data sets. The F_{stats} values, summarized in Table 4.3, indicate that

no significant difference existed between measured and fitted data for both sets of data obtained by the volumetric and gravimetric methods. Table 4.3 also lists the Henry's constants for N₂ adsorption isotherms on zeolite NaX at 30 °C and 50 °C. As can be seen in Figure 4.9, the adsorption process is temperature dependence as the process is exothermic. It follows that the adsorption decreases with increasing temperature.

Table 4.3 F-test comparison of N₂ adsorption on zeolite NaX by volumetric and gravimetric methods.

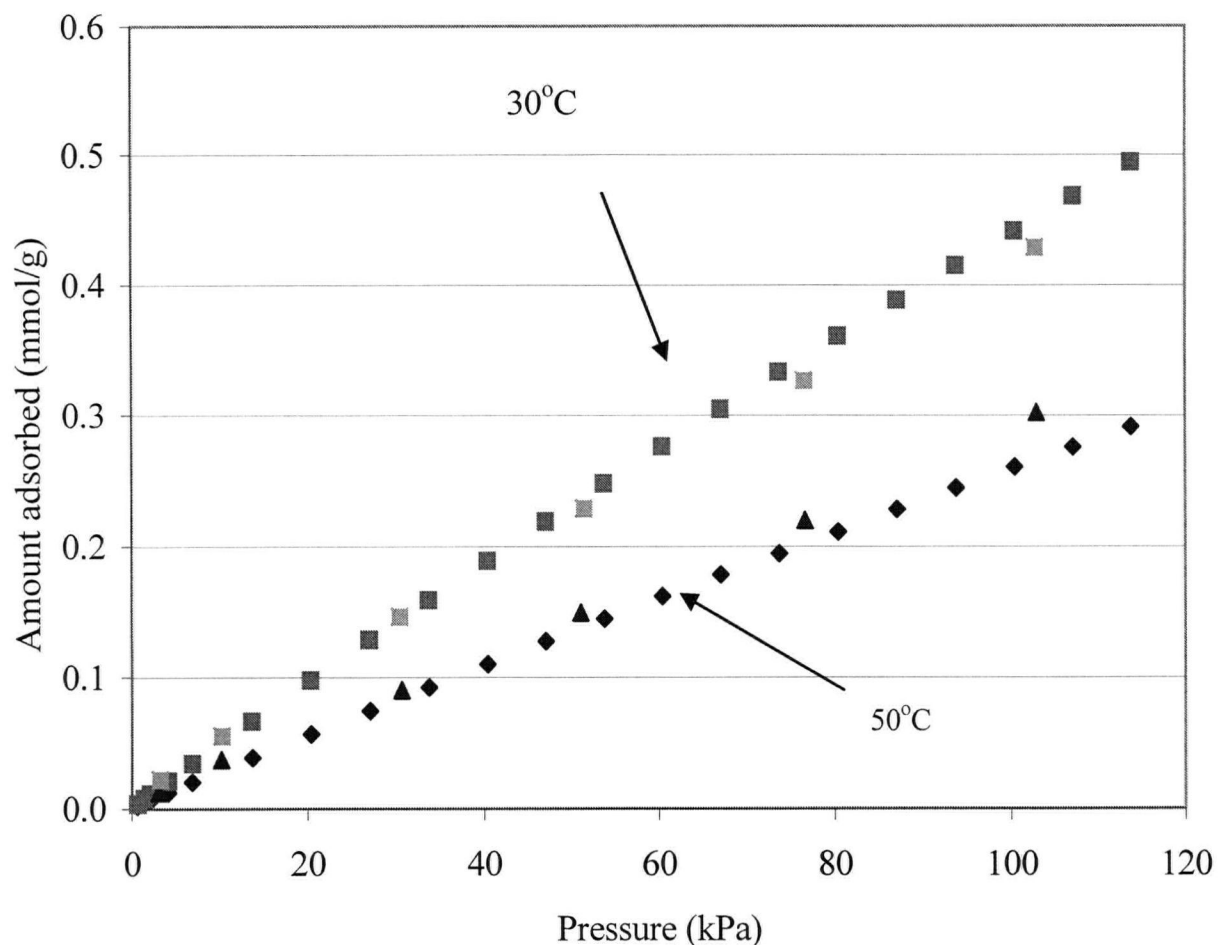
Temperature (°C)	Method	Henry's constant (mmol g ⁻¹ kPa ⁻¹)	F _{stats} = F ₁ /F ₂	F _{critical, α = 0.05} For M ₁ /M ₂
30	Volumetric	0.004460±0.000048	1.91	1.96
	Gravimetric	0.004279±0.000208		
50	Volumetric	0.002617±0.000023	0.78	1.96
	Gravimetric	0.002918±0.000075		

F₁ = F factor for adsorption isotherm obtained from volumetric measurement

F₂ = F factor for adsorption isotherm obtained from gravimetric measurement

M₁ = Data obtained from volumetric method

M₂ = Data obtained from gravimetric method



◆ Volumetric at 50 C ■ Volumetric at 30 C ▲ gravimetric at 50 C ▒ gravimetric at 30 C

Figure 4.9 Measured N_2 adsorption isotherms on zeolite NaX obtained by the volumetric and gravimetric methods.

Furthermore, N_2 adsorption isotherms were obtained at various temperatures for zeolite LiX adsorbent using the gravimetric method, as shown in Figure 4.10. The Langmuir parameters for the N_2 isotherm on zeolite LiX are listed in Table 4.4. When comparing the N_2 adsorption capacity of zeolite NaX and zeolite LiX adsorbents at 30 °C and 50 °C, the affinity for N_2 on zeolite LiX was approximately 3 times higher than that on zeolite NaX. This is consistent with literature reports. Zeolite LiX has been reported to give 3-4 times higher adsorption capacity than zeolite NaX (Mullhaupt and Stephenson, 1995). Also, N_2 adsorbs more strongly on zeolite

than zeolite NaX (Mullhaupt and Stephenson, 1995). Also, N₂ adsorbs more strongly on zeolite LiX since Li⁺ has the smallest ionic radius and hence the shortest distance between the nucleus of Li and the N₂ molecule (Yang et al., 1996).

Table 4.4 Langmuir constants for N₂ on zeolite LiX

Temperature (°C)	Langmuir Constant, a (mmol g ⁻¹ kPa ⁻¹)	Langmuir Constant, b (kPa ⁻¹)
30	0.02461± 0.00182	0.00775± 0.00151
40	0.01700± 0.00097	0.00576± 0.00100
50	0.00938± 0.00065	0.00343± 0.00102
60	0.00652± 0.00069	0.00176± 0.00144
80	0.00437± 0.00071	0.00041± 0.00193

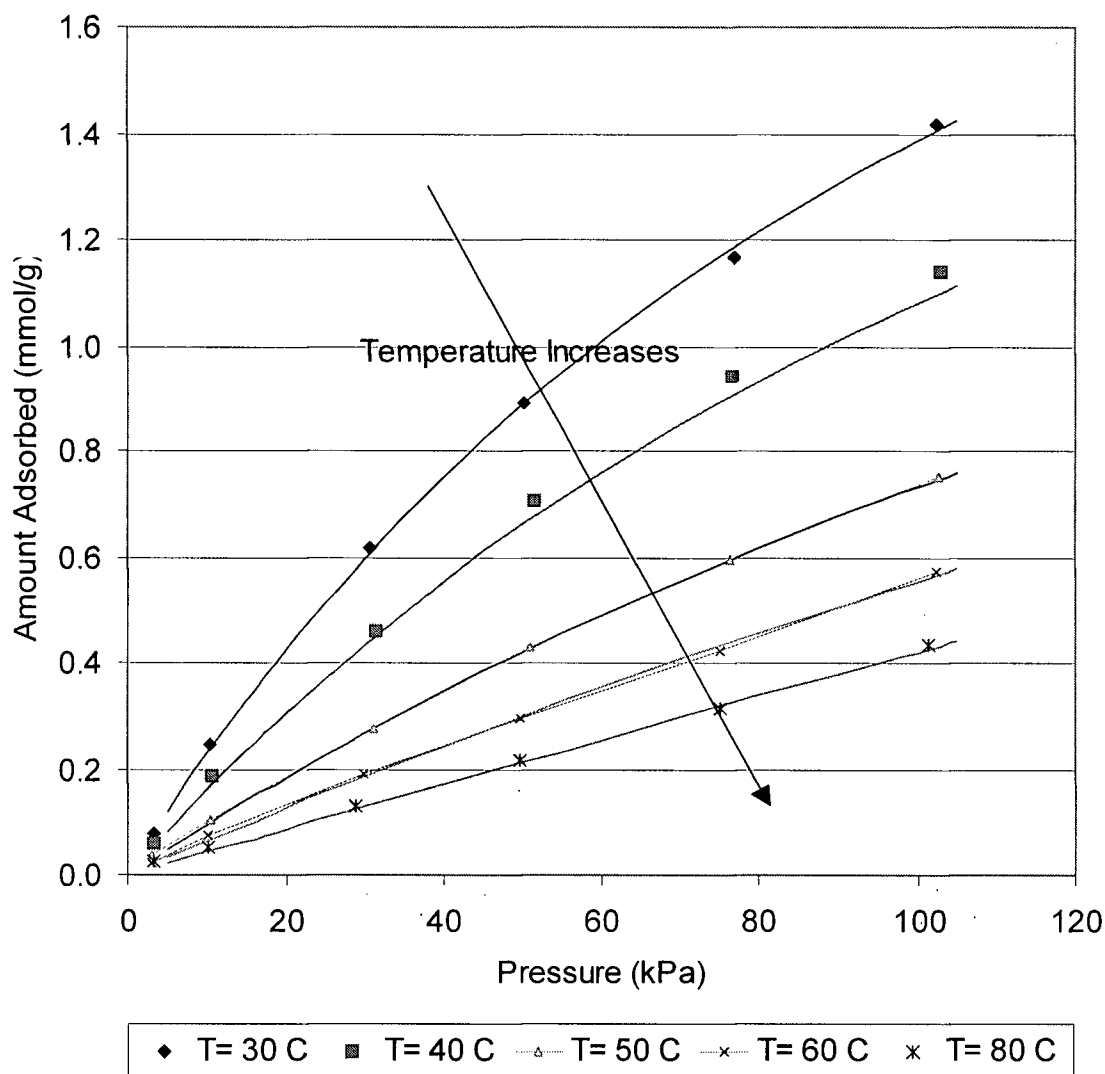


Figure 4.10 N_2 adsorption isotherms for zeolite LiX obtained by the gravimetric method.

After having determined N_2 adsorption isotherms on zeolite NaX and zeolite LiX, it is desirable to compare these isotherms to the reported literature values. However, since N_2 adsorption isotherms on NaX and LiX reported in the literature were obtained at 25 °C, the experimental N_2 adsorption isotherms on these adsorbents were extrapolated to give the isotherms at the same temperature. The extrapolation to determine the Henry's constant for the N_2 adsorption isotherm on zeolite NaX was done by plotting the $\ln K$ vs. $1000/T$ using the experimental data and extrapolating this plot to 25 °C using the slope and the intercept as shown

in Figure 4.11. The extrapolation for the Langmuir constant, b of N_2 adsorption isotherm on zeolite LiX was done using the plot of $\ln b$ vs. $1000/T$ as shown in Figure 4.12 while the Langmuir constant, a was calculated by determining the amount adsorbed at saturation, q_s at the temperatures listed in Table 4.4. Since q_s is independent of temperature, it should remain constant for all temperatures, however, q_s value for N_2 isotherm on zeolite LiX at 80°C was approximately 3 times larger than at other temperatures. This is due to the large error associated with the Langmuir constant, b at this temperature. Since the 95% confidence interval of the Langmuir constant is higher than the Langmuir constant, b at 80°C , this data point was discarded. As a result, q_s was determined to be the average q_s of the N_2 isotherm data at 30°C , 40°C , 50°C , and 60°C . After having determined b and q_s , the Langmuir constant, a can easily be determined since $a = q_s \cdot b$. N_2 adsorption isotherms on zeolite NaX and zeolite LiX at 25°C were then compared with the literature values in Figure 4.13 and 4.14. As can be seen in Figure 4.13, the experimental and literature adsorption isotherms (both obtained from N_2 on zeolite NaX in powder form (binderless)) agree within 12 percent. Again, an F test was performed at 95 percent confidence interval for these two sets of data. The F factor was determined to be 0.78, which is less than the F-critical value of 2.18. Hence, it can be concluded that there is no statistically significant difference between the two data sets.

Figure 4.14 compares the experimental results with two literature values for N_2 adsorption isotherms on LiX. N_2 adsorption isotherm on LiX reported by Rege and Yang (1997) is comparable with the experimental results of the present study. The F factor and F-critical value were determined to be 1.10 and 2.18, respectively, indicating that these two sets of isotherms are not significantly different. However, Yang et al. (1996) reported a much lower N_2 adsorption capacity than that of Rege and Yang (1997) and the experimental results. This is due to the Li content present in zeolite X. Zeolite LiX used in both Rege and Yang (1997) and this

study contained 100 percent Li on zeolite X whereas Zeolite LiX used in Yang et al. (1996) had Li content of 85 percent. Gaffney (1996) reported that N_2 capacity on LiX increased sharply as Li content was increased from 85 to 100 percent. Kimer (1993) reported N_2 capacity on LiX with 85 percent Li content as 0.85 mmol/g, which was slightly higher than 0.73 mmol/g of Yang et al. (1996). By comparing experimental results with the literature values, N_2 adsorption capacity increases with increasing Li content when Li content is 85% or higher.

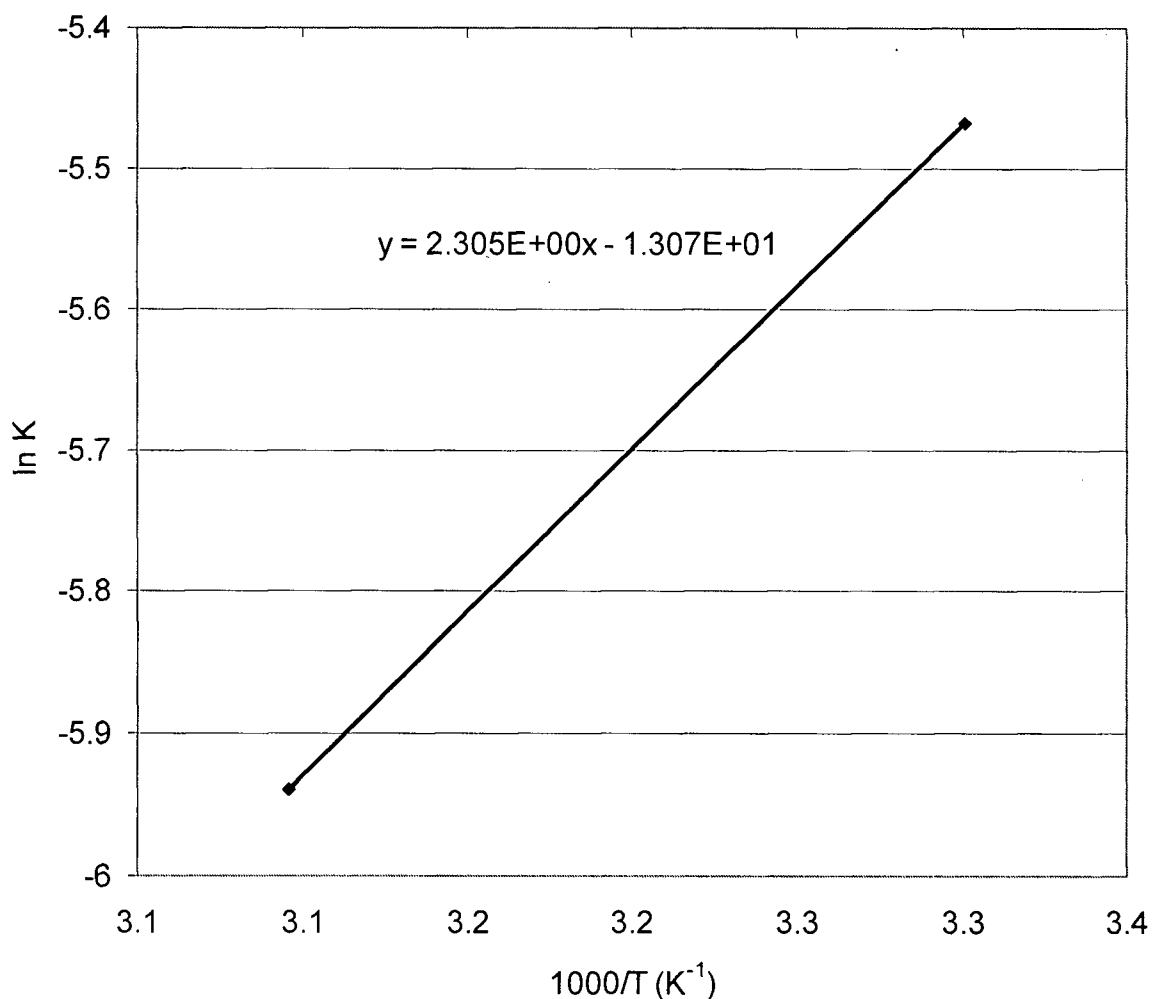


Figure 4.11 $\ln K$ vs. $1/T$ for the extrapolation of Henry's constant of N_2 isotherm on zeolite NaX.

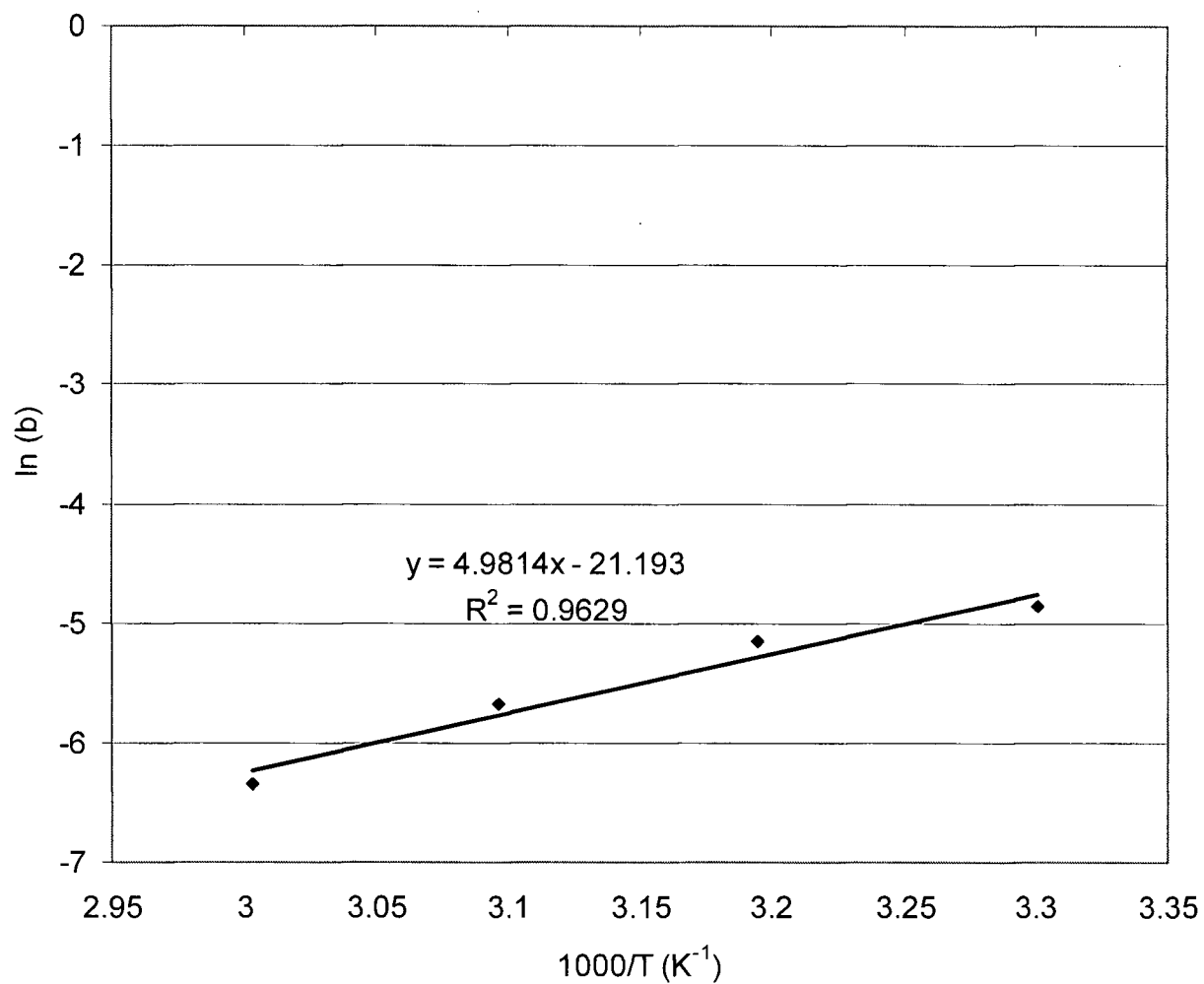


Figure 4. 12 $\ln b$ vs. $1/T$ for the extrapolation of Langmuir constant, b of N_2 isotherm on zeolite LiX.

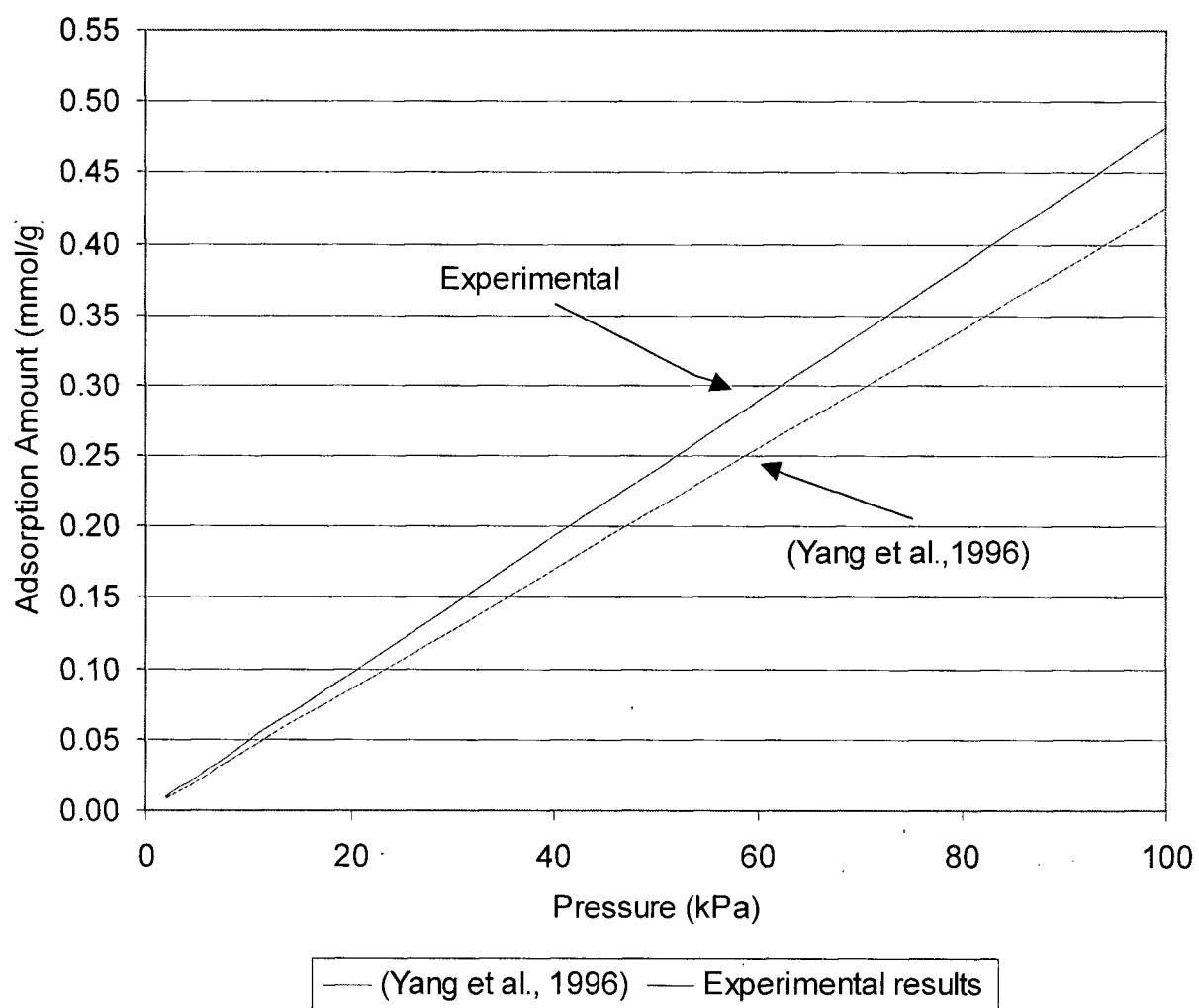


Figure 4.13 N_2 adsorption isotherm on NaX at 25 °C.

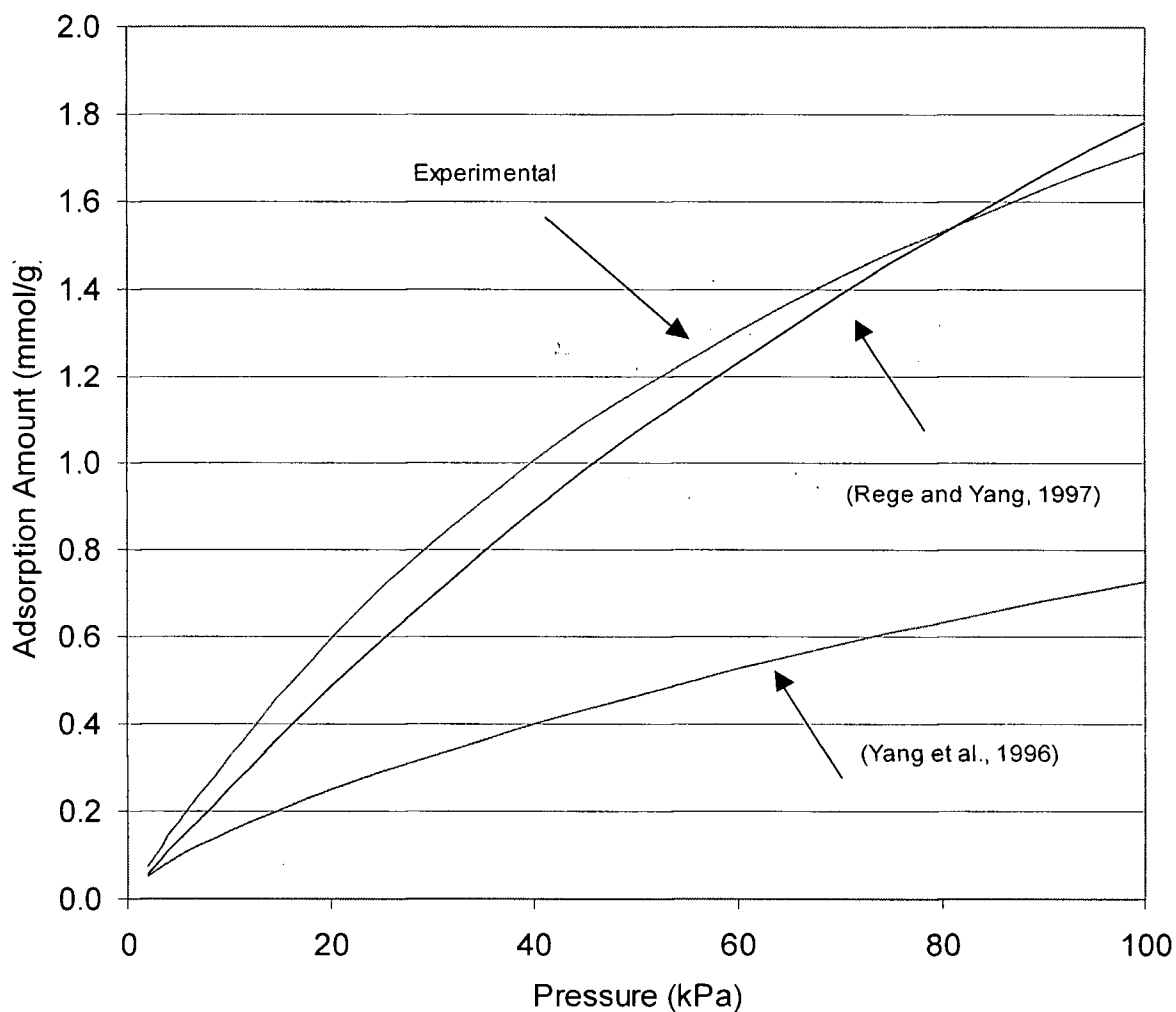


Figure 4.14 N₂ adsorption isotherm on LiX at 25 °C.

Having generated adsorption isotherms at low pressure and determined the Langmuir adsorption constants from these data, adsorption capacities at higher pressure were calculated using the Langmuir constants. However, in order to confirm that these extrapolated Langmuir adsorption capacities were valid, adsorption isotherms up to 300 kPa were measured using the gravimetric method in the high pressure gravimetric analyzer. Low pressure adsorption isotherms (0-101 kPa) measured using the volumetric method for QuestAir proprietary adsorbent (QP) were provided by Questair Technologies Inc. The extrapolation from low pressure data are

compared with low pressure and high pressure data in Figure 4.15 for N₂ on QP. Table 4.5 summarizes the Langmuir constants for QP.

Table 4.5 Langmuir constants for high and low pressure data for N₂ on QP

	Temperature (°C)	Langmuir Constant, a (mmol g ⁻¹ kPa ⁻¹)	Langmuir Constant, b (kPa ⁻¹)
Low pressure	60	0.0144± 0.0001	0.0079± 0.0001
	80	0.0086± 0.0001	0.0046± 0.0002
	100	0.0056± 0.0001	0.0033± 0.0002
High pressure	60	0.0127± 0.0025	0.0063± 0.0011
	80	0.0080± 0.0029	0.0039± 0.0015
	100	0.0056± 0.0011	0.0031± 0.0015

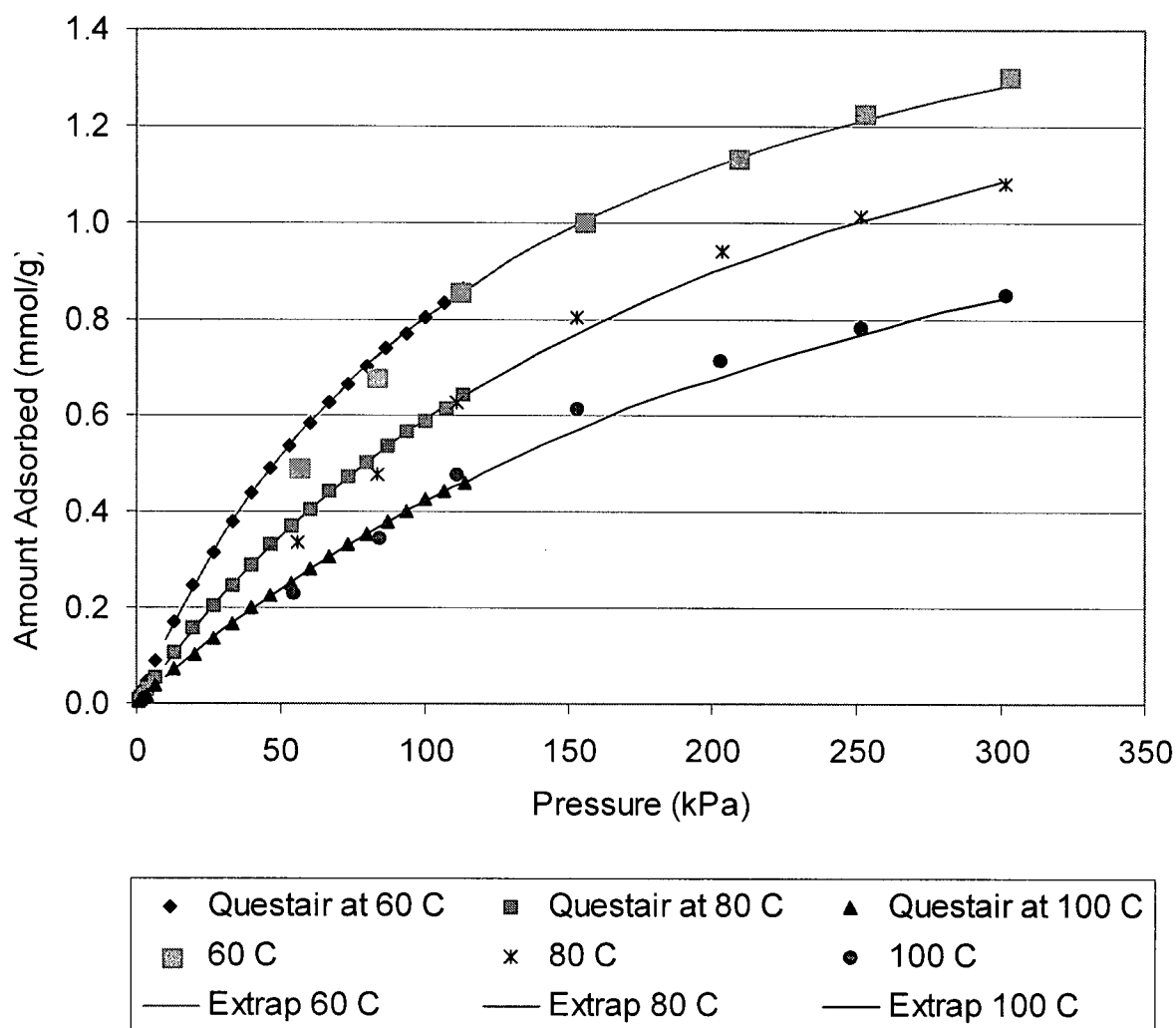


Figure 4.15 Comparison of extrapolated high pressure isotherm data with measured high pressure data for N_2 on QP.

Figure 4.15 shows that the Langmuir adsorption uptakes, calculated from low pressure adsorption isotherms can be extrapolated to higher pressure without significant errors. F tests similar to those described earlier were also performed on the data of Figure 4.15. The F factors, which are summarized in Table 4.6, were all less than the F-critical, and hence, there was no significant difference between fitted and measured data at low and high pressure.

Table 4.6 F-test comparison for significant difference between low and high pressure N₂ adsorption isotherms on QP vs. both sets of data.

Gas	Temperature (°C)	F ₁ /F ₃	F ₂ /F ₃	F _{critical,α =0.05} For M ₁ /M ₃	F _{critical,α =0.05} For M ₂ /M ₃
N ₂	60	1.05	1.00	1.95	2.36
	80	0.93	1.41	1.95	2.36
	100	0.84	1.68	1.95	2.36

F₁ = F factor for adsorption isotherm obtained from low pressure measurement

F₂ = F factor for adsorption isotherm obtained from high pressure measurement

F₃ = F factor for adsorption isotherm obtained from both the low and high pressure measurement

M₁ = Data obtained from low pressure method

M₂ = Data obtained from high pressure method

M₃ = Data obtained from both the low and high pressure method

The results suggest that the CO and CO₂ adsorption on zeolite NaX, N₂ adsorption on zeolite LiX and QP follow a simple Langmuir adsorption model while the N₂ adsorption on zeolite NaX follows Henry's law. Furthermore, the adsorption isotherm seems to fall into type I isotherm according to the Brunauer classification, indicating that the adsorption process follows a chemical adsorption on microporous adsorbent where the saturation point is limited by the monolayer coverage of adsorbed gas on the adsorbent surface.

4.4 Heats of Adsorption.

Heats of adsorption were also calculated from the measured adsorption data for N₂, CO, and CO₂ on zeolite NaX; and for N₂ on zeolite LiX. The slope of the plot $\ln(K)$ vs. $1000/T$ where K is the Langmuir constant b for the Langmuir model and K is Henry's constant for Henry's law, was used to calculate the apparent heat of adsorption according to equation [2.07] and are shown in Appendix 9.

The heats of adsorption for N_2 on zeolite NaX adsorbent determined using gravimetric and volumetric methods are 19.2 ± 0.6 kJ/mol and 21.6 ± 0.8 kJ/mol, respectively, which show consistency between volumetric and gravimetric values. There is only 11.5 percent error between the two values. According to Ruthven (1984) the heat of adsorption for N_2 on zeolite NaX is approximately 5 kcal/mol or 20.9 kJ/mol, which is in very good agreement with the heat of adsorption obtained from the present study. For CO and CO_2 on zeolite NaX, the heat of adsorption was obtained using the volumetric data since these sets of data have more data points. The heats of adsorption for CO and CO_2 on zeolite NaX measured volumetrically are 12.0 ± 5.2 kJ/mol and 22.2 ± 23.3 kJ/mol, respectively. However, when compared to the literature value, the heat of adsorption for CO_2 obtained from the volumetric method (22.2 kJ/mol) is much lower than the literature value (10 kcal/mol or 41.9 kJ/mol) (Ruthven, 1984). The difference is due to the errors in the Langmuir parameter b even though it was shown previously that data obtained from both the volumetric and gravimetric method were in good agreement. A slight change in the value of the initial slope in the linear region of the CO and CO_2 adsorption isotherm will not change the overall trend of the isotherm by much, but, this slight change in the initial slope or the Langmuir constant, b could affect the heats of adsorption's calculations considering that only two temperatures were used in these calculations. When considering the large error associated with the heats of adsorption for CO_2 on zeolite NaX adsorbent, the heats of adsorption obtained is not accurate.

When comparing the heat of adsorption of N_2 on zeolite NaX and zeolite LiX, the heat of adsorption for zeolite LiX (41.4 ± 24.8 kJ/mol) is higher than that of zeolite NaX (19.2 kJ/mol determined by the gravimetric method and 21.6 kJ/mol by the volumetric method). The higher heat of adsorption of N_2 on zeolite LiX is due to a stronger adsorption between the adsorbate and adsorbent surface. The heat of adsorption for N_2 on zeolite LiX of (41.4 ± 24.8 kJ/mol) obtained

in the study is comparable to the value of 23.5 kJ/mol reported by Rege and Yang (1997) when considering its 95% confidence interval. Figure 4.16 to Figure 4.18 show $\ln k$ vs. $1000/T$ plots used to determine the heat of adsorption.

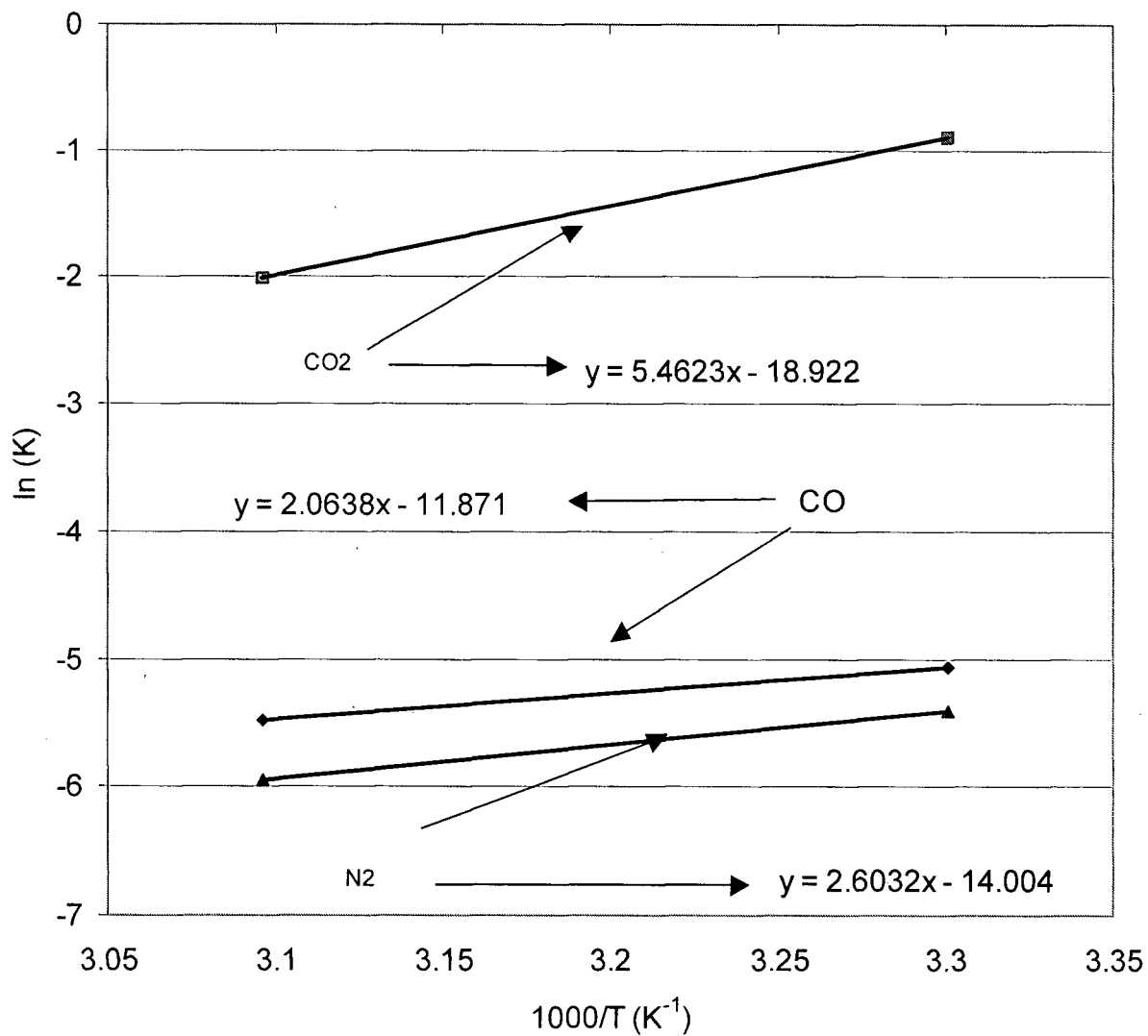


Figure 4.16 $\ln K$ vs. $1000/T$ used to determined heat of adsorption of N₂, CO, and CO₂ on zeolite NaX adsorbent from the data measured volumetrically.

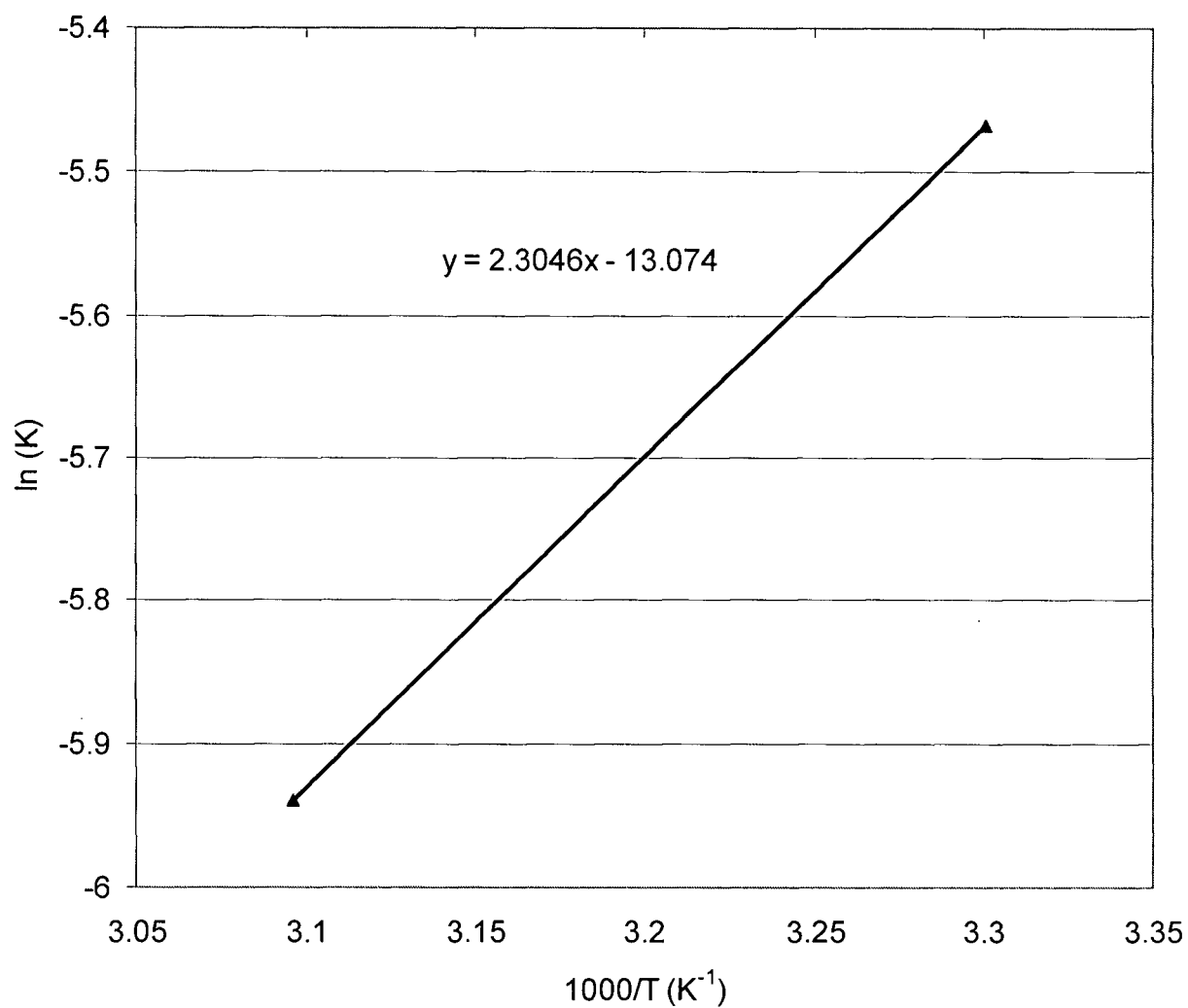


Figure 4.17 $\ln K$ vs. $1000/T$ used to determined heat of adsorption of N_2 on zeolite NaX adsorbent from the data measured gravimetrically.

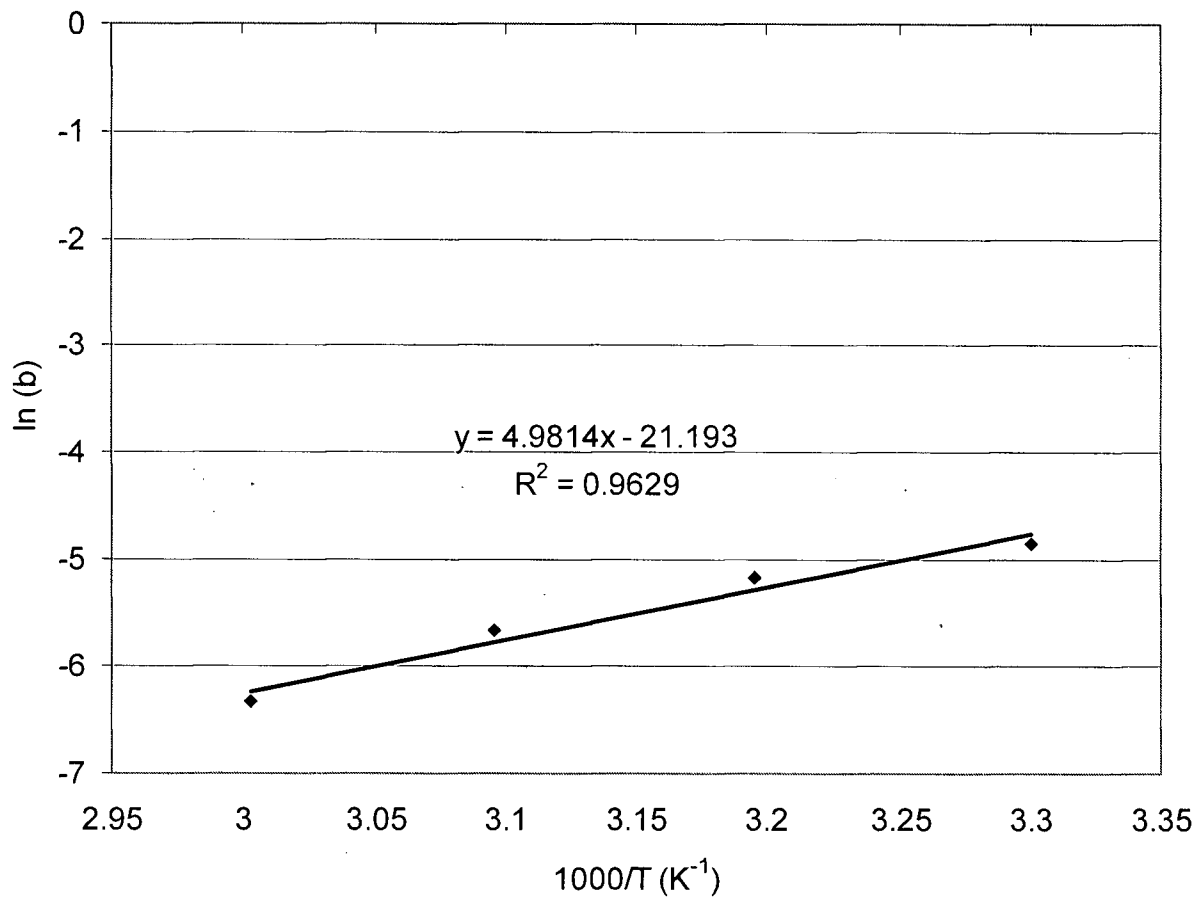


Figure 4.18 $\ln b$ vs. $1000/T$ used to determined heat of adsorption of N_2 on zeolite LiX adsorbent using Langmuir parameter, b .

Chapter 5: Dispersion and Mass Transfer in Structured Adsorbent Bed

5.1 Introduction

The dynamic response of an adsorbent structure is determined by such parameters as the gas dispersion and mass transfer resistances within the adsorbent structure. The value of these parameters can be estimated by measuring the dynamic response to a step change in inlet adsorbate concentration as a function of the particle size (particle diameter), the interstitial gas velocity, and by replacing the adsorbent of interest with inert particles. For a given adsorbent structure, two parameters can be determined: the axial dispersion coefficient and the lumped mass transfer coefficient.

Sometimes, the dispersion can mask the significance of mass transfer resistances. In order to separate the two effects, experiments must be done using two identical adsorbent structures, except that one structure is filled with non-adsorbing particles while the other is filled with the adsorbent of interest. The dynamic response to the non-adsorbing particles will directly give the dispersion since there is no micropore or macropore mass transfer resistance in this case. In addition, the magnitude of the dispersion coefficient of a non-adsorbing structure and other adsorbent structure can be compared to confirm if the values determined are correct. Furthermore, the external fluid film coefficient, which contributes to the lumped mass transfer coefficient, can also be estimated from the non-adsorbing structure dynamic response data.

The contributions to the lumped mass transfer coefficient can be accounted for from three individual mass transfer coefficients: external fluid film resistance, macropore mass transfer resistance, and micropore mass transfer resistance. In order to determine these individual mass transfer coefficients, particle size and interstitial velocities were varied. If $\frac{1}{kK}$ for two or more

different particle sizes are known, then the plot of $\frac{1}{kK}$ vs. R_p^2 can be used to determine the individual mass transfer coefficients (Equation [2.40]).

In order to determine the dispersion coefficient and the individual mass transfer coefficient, several adsorbent structures were studied. Table 5.1 lists the dimensions of the structures and the characteristics of these adsorbent structures were as follows:

1. High X-sectional area structure contained zeolite LiX adsorbent dispersed on a substrate with cross sectional area of 12.41 cm².
2. Mid X-sectional area structure contained zeolite LiX adsorbent dispersed on a substrate with cross sectional area of 6.29 cm². The cross sectional area of the mid X-sectional area structure is approximately half that of the high X-sectional area structure.
3. Low X-sectional area structure contained zeolite LiX adsorbent dispersed on a substrate with cross sectional area of 3.70 cm². The cross sectional area of the low X-sectional area structure was approximately one quarter of the high X-sectional area structure.
4. Non-adsorbing structure contained non-adsorbing solid dispersed on a substrate with cross sectional area of 6.14 cm².
5. High Voidage adsorbent structure contained zeolite LiX adsorbent dispersed on a substrate with cross sectional area of 6.22 cm². The high voidage adsorbent structure had similar cross-sectional area as the mid X-sectional area structure. However, the spacing between each adsorbent sheets, i.e. the spacer height used in this pack was approximately 40 percent less than that of the mid X-sectional area structure.

6. Thick adsorbent sheets structure contained zeolite LiX adsorbent dispersed on a substrate with cross sectional area of 6.22 cm^2 . The thick adsorbent sheets structure had similar cross sectional area as the mid X-sectional area structure. However, the adsorbent sheets thickness of this pack was twice that of the mid X-sectional area structure.

Note: X-sectional area refers to cross sectional area

Table 5.1 Summary of Adsorption structure dimensions.

Structure		1	2	3	4	5	6
Width (cm)		6.25	3.18	1.87	3.10	3.10	3.10
Height (cm)		1.99	1.98	1.98	1.98	2.01	2.01
Length (cm)		20.32	20.32	20.32	20.32	20.32	20.32
Spacer Tortuosity	High	x					
	Low		x	x	x	x	x
Voidage Ratio	High					x	
	Low	x	x	x	x		x
Cross Sectional Area	High	x					
	Mid		x		x	x	x
	Low			x			
Absorbent Sheet	Thick						x
	Thin	x	x	x	x	x	
N ₂ Adsorbing	Yes	x	x	x		x	x
	No				x		

5.2 Henry's Constant Estimates

In order to determine the dispersion and mass transfer resistances of an adsorbent structure, the gas adsorption constant or Henry's constant must first be determined since the model equations used to extract dispersion and mass transfer resistances are dependent on the amount of gas adsorbed or the Henry's constant, K . The Henry's constants and their 95 percent confidence intervals were obtained from the slope of the plot μ vs. $1/F$ using a curve fitting algorithm, and the values are summarized in Table 5.2. Figure 5.1 to Figure 5.5 shows the μ vs.

1/F plots used to obtain the Henry's constant reported in Table 5.2; in all cases two sets of data were obtained.

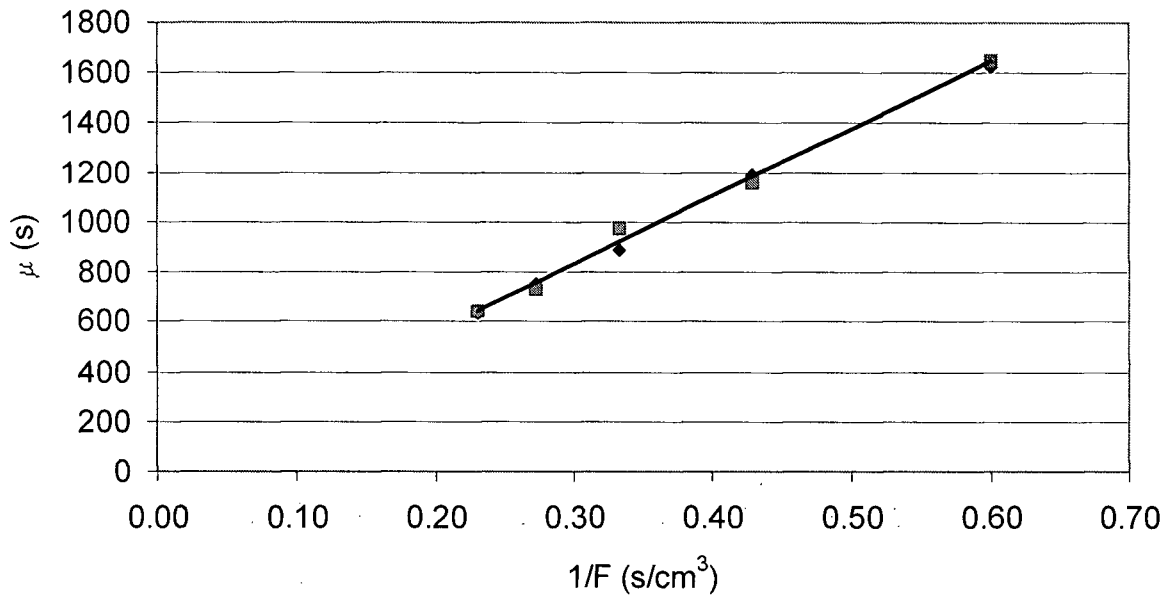


Figure 5.1 μ vs. $1/F$ for high X-sectional area structure for N₂ at 24 °C and 101 kPa.

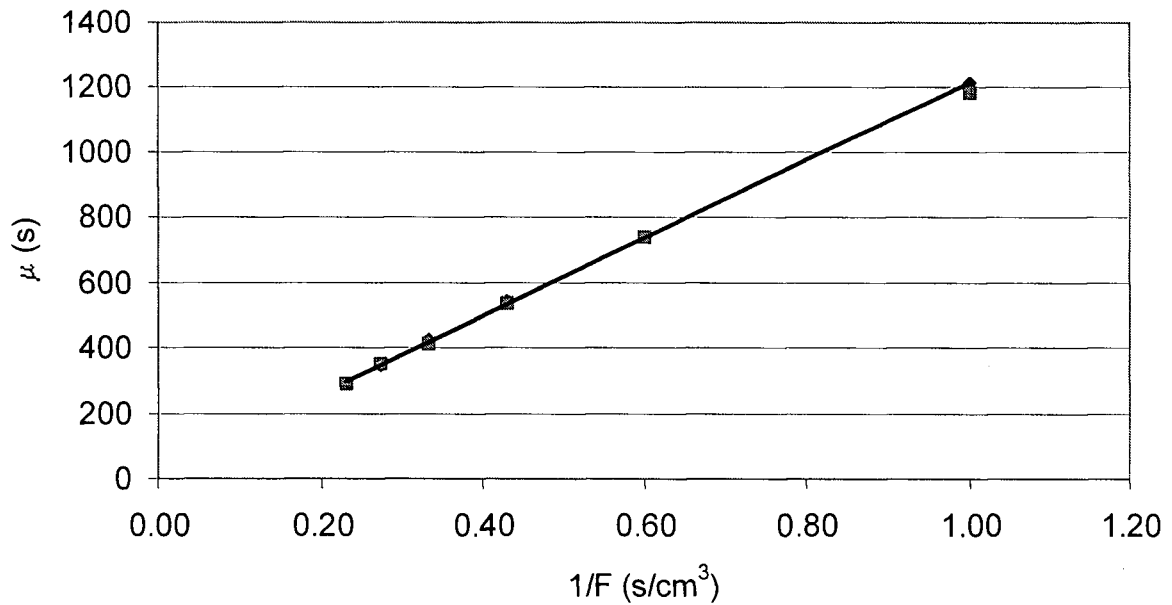


Figure 5.2 μ vs. $1/F$ for mid X-sectional area structure for N₂ at 24 °C and 101 kPa.

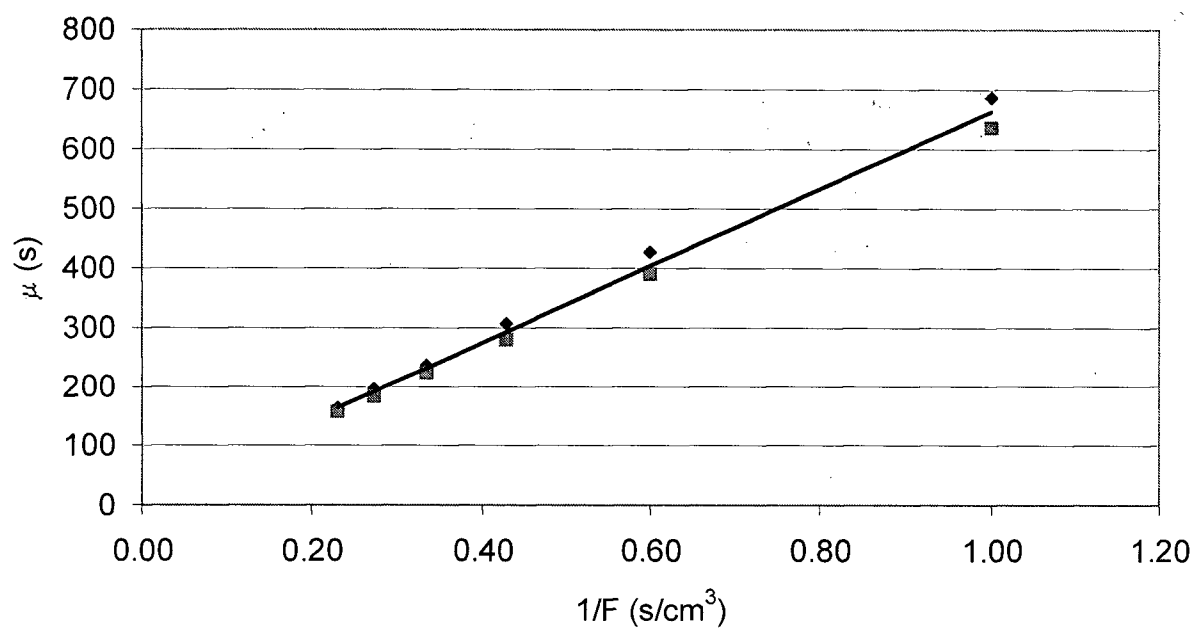


Figure 5.3 μ vs. $1/F$ for low X-sectional area structure for N_2 at 24°C and 101 kPa.

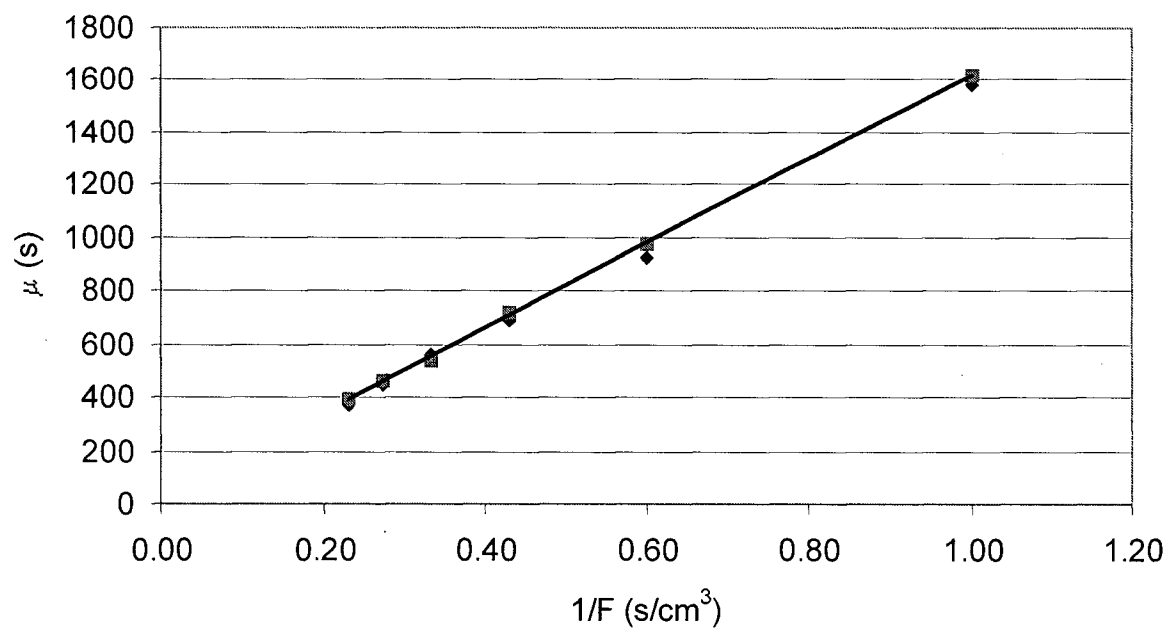


Figure 5.4 μ vs. $1/F$ for high voidage structure for N_2 at 24°C and 101 kPa.

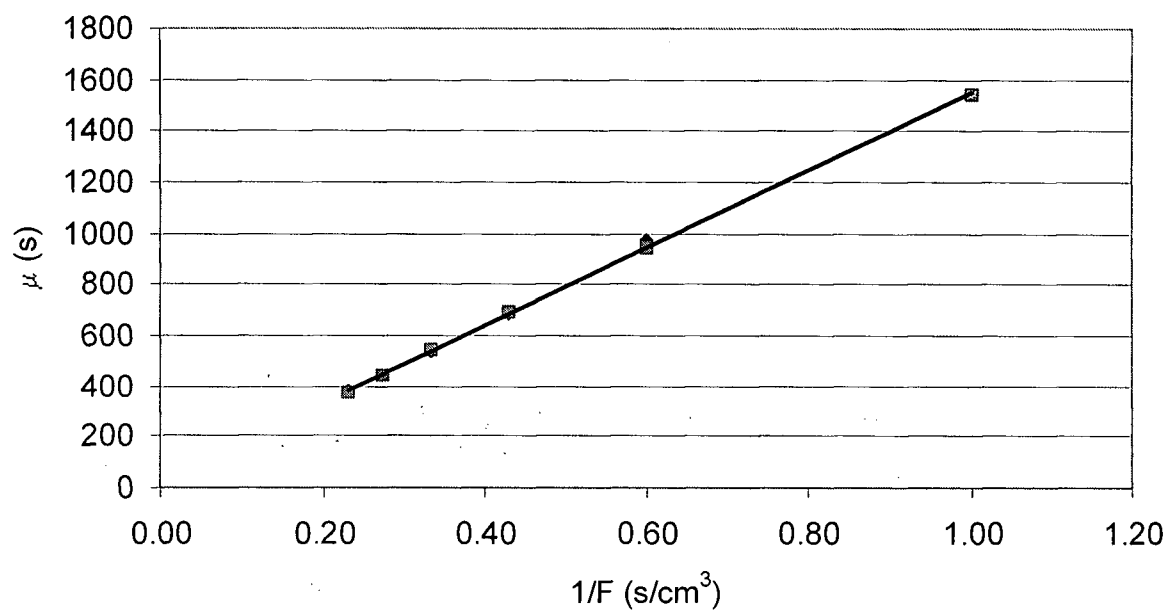


Figure 5.5 μ vs. $1/F$ for thick adsorbent sheets structure for N₂ at 24 °C and 101 kPa.

Table 5.2 Henry constants and their 95% confidence intervals.

Pack	High X-sectional Area	Mid X-sectional Area	Low X-sectional Area	High Voidage	Thick Adsorbent Sheets
Henry's constant	17.81±0.30	14.81±0.25	13.83±0.42	17.48±0.28	15.88±0.25

Henry's constants were calculated based on a volume per volume basis (volume adsorbed per volume of adsorbent). Henry's constants expressed in terms of volume, cannot be directly compared with other literature values or experimental values, since the amount of gas adsorbed is most often expressed in mmol/g. Hence, the amount of gas adsorbed at 101 kPa was calculated using Henry's law and the results are listed in mmol/g in Table 5.3. Table 5.3 below compares the amount of gas adsorbed from the gravimetric method (Chapter 4) to the values calculated from the Henry constants determined from the dynamic response measurement.

Table 5.3 Comparison of gas adsorbed at 101 kPa and 24 °C between gravimetric and chromatographic method

	N ₂ Adsorbed at 101 kPa and 24 °C (mmol/g)
Gravimetric Method (extrapolated to 24 °C from experimental data)	1.856
High X-sectional Area	1.834±0.031
Mid X-sectional Area	1.212±0.020
Low X-sectional Area	1.134±0.034
High Voidage	1.188±0.019
Thick Adsorbent sheets	1.615±0.025

From Table 5.3 the adsorbent uptake estimated from the chromatographic and gravimetric methods are comparable for the high X-sectional area structure. The thick adsorbent sheets structure had a 15% lower value than the gravimetric value. The amount of gas adsorbed for other adsorbent structures is significantly lower than that determined from the gravimetric method. The most likely explanation for this difference is that errors exist in the calculation of the adsorbent sheet thickness as well as the quantity of adsorbent contained within these prototype adsorbent structures. Furthermore, it might be possible that moisture exists within some of the adsorbent structures prior to the experiment because the adsorbent structures did not undergo thermal desorption treatment prior to each experiment. As a result, some of the adsorption sites might have been occupied by water molecules which could have led to lower adsorption data seen in some of the adsorbent structures.

5.3 Dispersion and Mass Transfer Estimates

Having estimated the Henry's constants, the 1st and 2nd moments were determined and used to calculate the dispersion and lumped mass transfer resistances from the plot $HETP/2v$ or $(\sigma^2/\mu^2)L/2v$ vs. $1/v^2$ (as per Equation [2.40]). The dispersions and their 95 % confidence intervals are summarized in Table 5.4. Figure 5.6 to Figure 5.11 show the $HETP/2v$ or $(\sigma^2/\mu^2)L/2v$ vs. $1/v^2$ plot (using two sets of data) used to calculate the dispersion and lumped mass transfer coefficients.

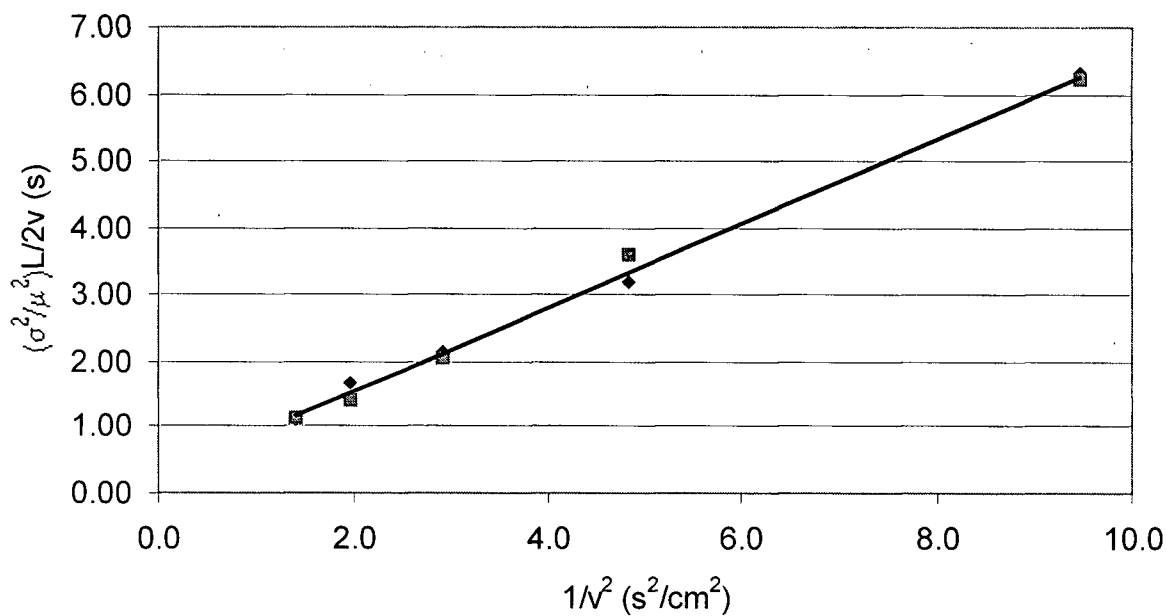


Figure 5.6 HETP/2v vs. $1/v^2$ for high X-section area structure for N_2 at 24 °C and 101 kPa.

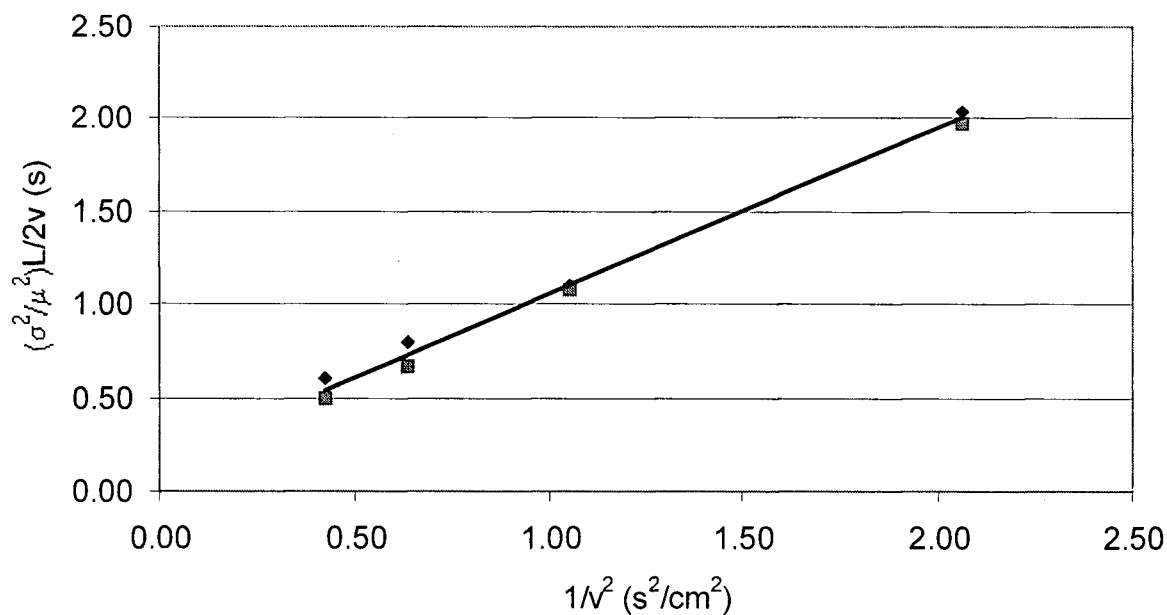


Figure 5.7 HETP/2v vs. $1/v^2$ for mid X-sectional area structure for N_2 at 24 °C and 101 kPa.

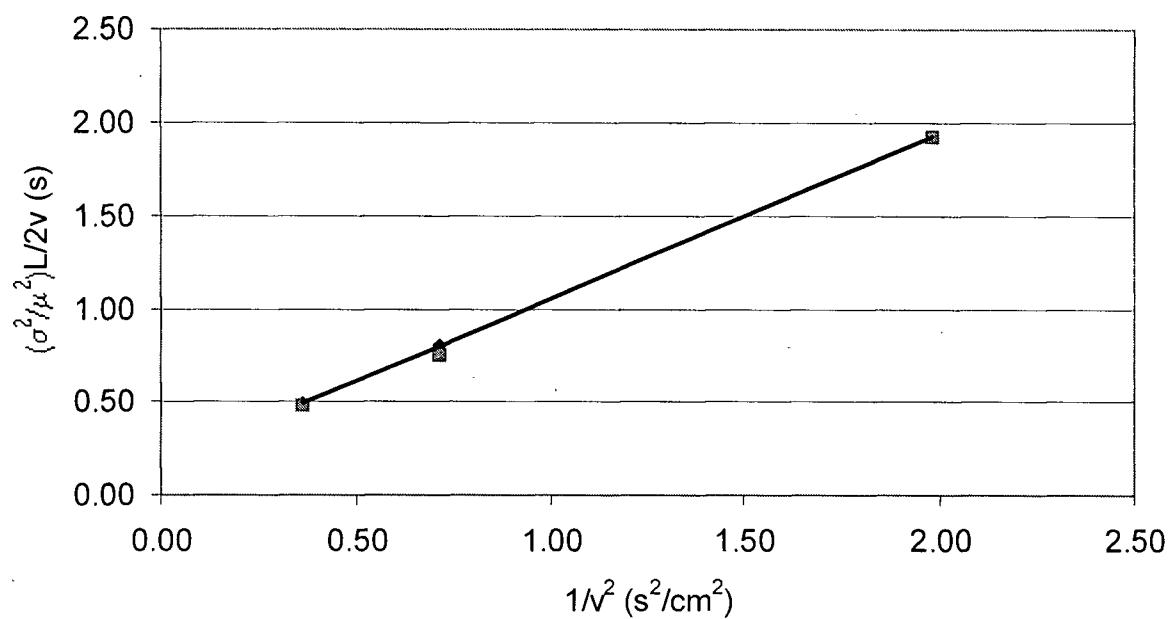


Figure 5.8 HETP/2v vs. $1/v^2$ for low X-sectional area structure for N_2 at 24 °C and 101 kPa.

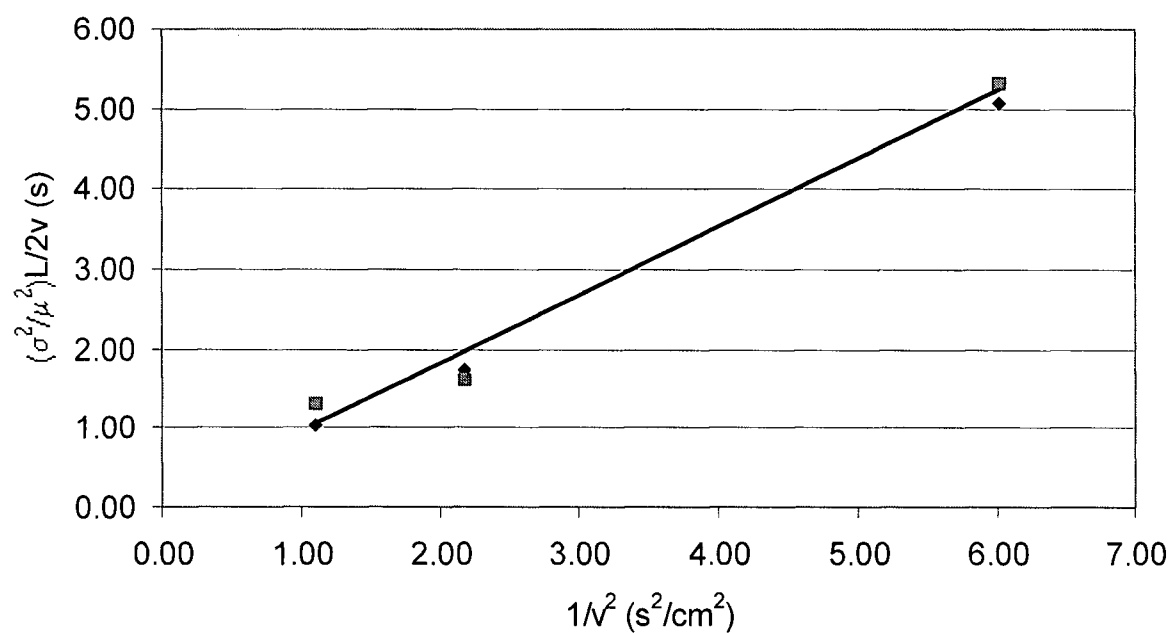


Figure 5.9 HETP/2v vs. $1/v^2$ for non adsorbing structure for N_2 at 24 °C and 101 kPa.

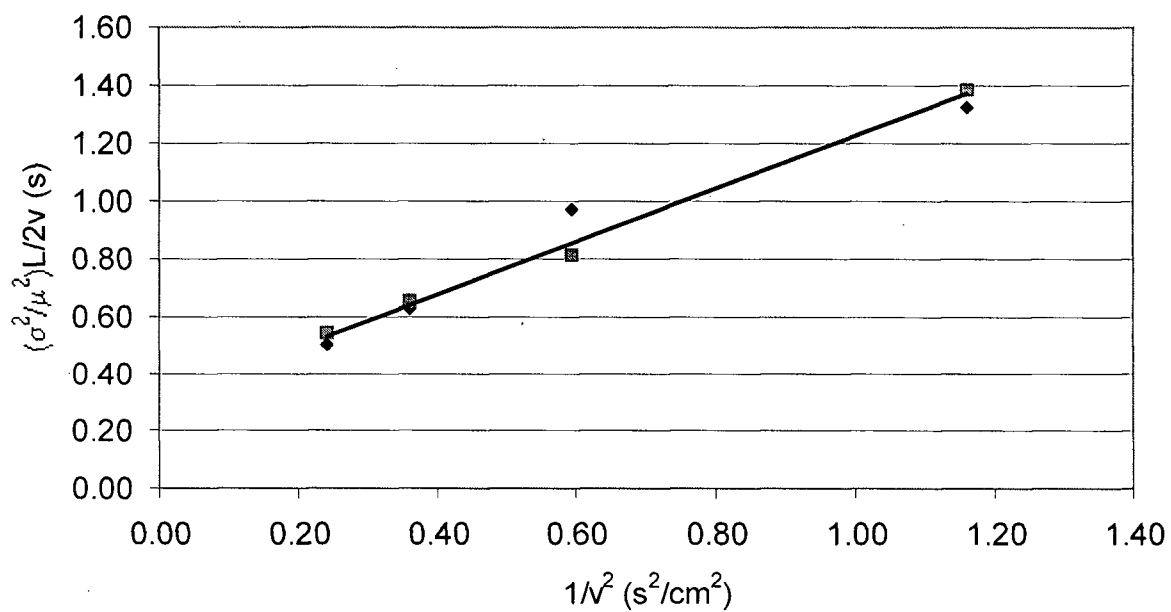


Figure 5.10 HETP/2v vs. $1/v^2$ for high voidage adsorbent structure for N_2 at 24 °C and 101 kPa.

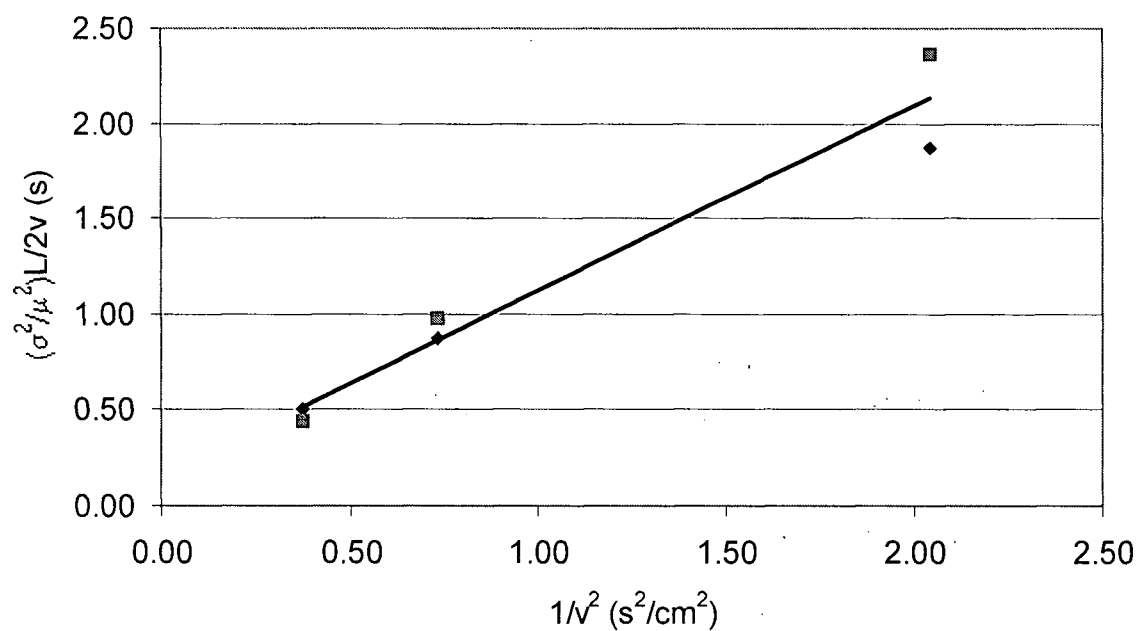


Figure 5.11 HETP/2v vs. $1/v^2$ for thick adsorbent sheets structure for N_2 at 24 °C and 101 kPa.

Table 5.4 Dispersion coefficients estimated for structured adsorbent beds.

Pack	Dispersion Coefficient (cm ² /s)
High X-sectional Area	0.635 ± 0.034
Mid X-sectional Area	0.894 ± 0.074
Low X-sectional Area	0.897 ± 0.037
Non-adsorbing	0.844 ± 0.133
High Voidage	0.896 ± 0.137
Thick Adsorbent Sheets	0.970 ± 0.295

The dispersion coefficients obtained from the mid X-sectional area, low X-sectional area, non adsorbing, and high voidage adsorbent structure show very good agreement. They are within 6 percent of each other. The thickness of adsorbent sheets and cross-sectional area are approximately equal for these four adsorbent structures (mid X-sectional area, non adsorbing, and high voidage adsorbent structure) except for the low X-sectional area structure where the cross-sectional area is half of the other three packs. The dispersion coefficient for the thick adsorbent sheets structure is slightly higher than the other adsorbent structures, but is still within the same range when considering the 95 % confidence interval of the estimated dispersion coefficient of these adsorbent structures. For the high X-sectional area structure, the dispersion coefficient was significantly lower at 0.635 cm²/sec compared to about 0.90 cm²/sec for the other packs.

One possible explanation for the difference in dispersion coefficient is that the substrate of the high X-sectional Area structure was made up of different materials from other adsorbent structures. The difference in the substrates may contribute to the higher dispersion observed in the mid X-sectional Area, low X-sectional Area, non-adsorbing, high voidage, and thick

adsorbent sheets structure compared to the high X-sectional area structure. The difference in the substrates could contribute to more mixing between channels which should be reflected in a higher dispersion coefficient.

The dispersion coefficients obtained were also compared with literature values by estimating the molecular dispersion, D_m from the dispersion coefficient. According to Kovacevic (2000), for N_2/He , the molecular dispersion was estimated as $0.86 \text{ cm}^2/\text{sec}$ at 35°C from dispersion coefficients obtained from a 13 X packed bed. This value is of the same magnitude as the $D_m = 0.91 \text{ cm}^2/\text{sec}$ estimated from the high X-sectional area structure dispersion of the present study, calculated from the equation $D_L = 0.7D_m$. Also, Satterfield (1970) reported the molecular dispersion of N_2 in He to be $0.69 \text{ cm}^2/\text{sec}$. The molecular dispersions estimated in the present study are within 25% of literature values.

The mass transfer resistances were also determined from the plot of $HETP/2v$ vs. $1/v^2$ at low flow rates ($v < 1.7 \text{ cm/s}$), and the values are summarized in Table 5.5.

Table 5.5 Lumped mass transfer resistances estimated using $HETP/2v$ vs. $1/v^2$ at low flow rate.

Pack	High X-sectional Area	Mid X-sectional Area	Low X-sectional Area	Non-adsorbing	High Voidage	Thick Adsorbent Sheets
$1/kK \text{ (sec)}$	0.411 ± 0.268	0.282 ± 0.160	0.268 ± 0.081	0.292 ± 2.000	0.842 ± 0.243	0.538 ± 1.307
$k \text{ (sec}^{-1}\text{)}$	0.137	0.239	0.270	N/A	0.068	0.117

Alternatively, chromatographic plate theory can be used to determine the lumped mass transfer rates at high velocities, $v > 7 \text{ cm/s}$ where mass transfer resistances dominate over the dispersion. According to Equation [2.48], the slope of the van Deemter plot equals $A_3 \approx 2[\epsilon/(1-$

$\epsilon)/kK$, from which the lump mass transfer resistance can be calculated knowing ϵ . The mass transfer rates for high X-sectional area, high voidage, and thick adsorbent sheets structures were determined from the slope of Figure 5.12 and are summarized in Table 5.6.

The lumped mass transfer resistance ($1/kK$) of the adsorbent structure ranges from 0.28 to 0.84 sec suggesting that short cycle PSA with cycle times 0.6 to 3 seconds is possible. The mass transfer resistance can be further reduced by reducing the size of the adsorbent structure, as seen from the values of $1/kK$ for the mid X-sectional area structure, to further decrease the cycle time needed for the short cycle PSA. Although the cycle time can be decreased by reducing the adsorbent structure size, N_2 adsorption capacity is reduced since less adsorbent is available for adsorption. A reduction in the adsorbent sheets thickness can also reduce $1/kK$ as shown in Table 5.5. However, by reducing the adsorbent sheets thickness, there will be less adsorbent present, i.e., less N_2 adsorption capacity as shown in the data of Table 5.3. The amount of gas adsorbed at 101 kPa and 24 °C for the thick adsorbent sheets structure and the mid X-sectional area structure were determined to be 1.615 ± 0.025 mmol/g and 1.212 ± 0.020 mmol/g, respectively.

$1/kK$ values cannot be compared directly to reported values since the lumped mass transfer resistances on LiX adsorbent are not available. However, $1/kK$ can be compared with reported values for N_2 on other zeolite X such as 13X. Kovacevic (2000) reported $1/kK$ for N_2 on 13X 8/12 mesh and 16/40 mesh for the interstitial velocity of 0.8 to 3.5 cm/sec as 0.09 and 0.02 second, respectively. $1/kK$ reported by Kavoccevic (2000) was obtained from similar experimental conditions as those used in the present study except that the adsorbent structures used by Kavoccevic (2000) was a packed bed of adsorbent beads. $1/kK$ values obtained in this study are 2 to 8 times higher than those reported by Kovacevic (2000), suggesting that the structured adsorbent bed configuration does not reduce the mass transfer resistance. However, the dispersion coefficient in the structured adsorbent bed is usually higher than in the packed

bed, which can mask the mass transfer resistance, i.e., resulting in higher mass transfer resistance. Furthermore, since the adsorbents used in the present study and literature are not the same, the comparison should only be considered qualitatively.

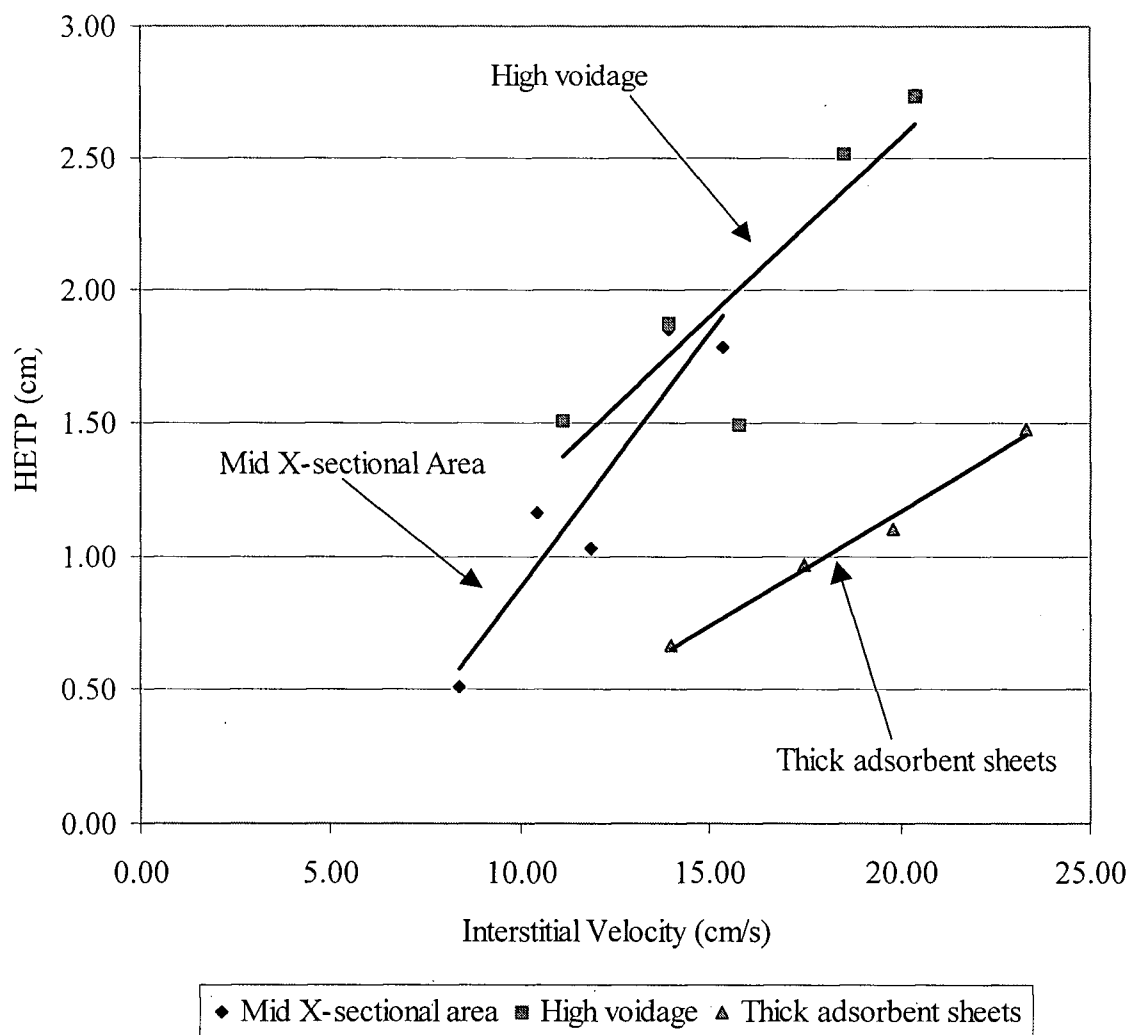


Figure 5.12 HETP vs. interstitial velocity plot used to determine the lumped mass transfer coefficient for $v > 7$ cm/s.

Table 5.6 Lumped mass transfer rates estimated using Plate theory at high flow rate and their 95% confidence intervals.

Pack	Mid X-Sectional Area	High Voidage	Thick Adsorbent Sheet
k (sec ⁻¹)	0.402 ± 0.174	0.328 ± 0.176	0.422±0.105

The lumped mass transfer rates obtained from both methods, as summarized in Table 5.5 and 5.6 show similar magnitude. The discrepancies between the two methods are most likely a result of both the scatter in data at high flow rates. At high flow rates, it becomes increasingly more difficult to correct for the mean and the variance of the dead volume in the system, the errors in the dead volume mean and variance ranges from 30-50% of the measured mean and variance. If comparison between the k values of the Mid X-sectional area at low and high velocity (Table 5.5 and 5.6) is made, the difference is approximately 68%. Since the errors associated with the measurement itself and the dead volume in the system can be up to 50%, there is no significant difference between the k values at low and high velocity given the large errors in the estimate of k at high velocity. The measurement is limited when the mean and variance of the dead volume approaches that of the measured mean and variance. Furthermore, at high velocity, the film layer thickness will decrease, which in turn increases film mass transfer rate. This may also contribute to high values of k.

5.4 Macropore and Micropore Mass Transfer

The mass transfer resistances listed in Table 5.5 are the lumped mass transfer resistances in the system, which consist of external fluid film mass transfer resistance, macropore mass transfer resistance, and micropore mass transfer resistance. From the slope and intercept of the plot of

$\frac{1}{kK}$ vs. R_p^2 , these individual mass transfer resistances can be separated when $\frac{1}{kK}$ are known for

two or more particle sizes, according to Equation [2.40]. Figure 5.13 shows the plot of $\frac{1}{kK}$ vs.

$(\alpha R_p)^2$ where α is an arbitrary constant used to conceal the actual particle size due to non-disclosure agreement. The intercept gives the micropore mass transfer coefficient and the slope gives a combination of external fluid film and macropore mass transfer coefficients. Calculation of the molecular diffusivity from any standard gas diffusion equation such as Equation [5.1] can

determine the external fluid film.
$$D_{12} = \frac{0.001858 T^{3/2} [(M_1 + M_2) / M_1 M_2]^{1/2}}{P \sigma_{12}^2 \Omega_D} \quad \text{Equation [5.1]}$$

Where T = temperature in K, M_1 , M_2 are the molecular weight of the two species, P is the total pressure (atm), Ω_D is the "collision integral," a function of kT/ϵ_{12} , ϵ , σ are the force constants in the Lennard-Jones potential function, and k is the Boltzmann constant.

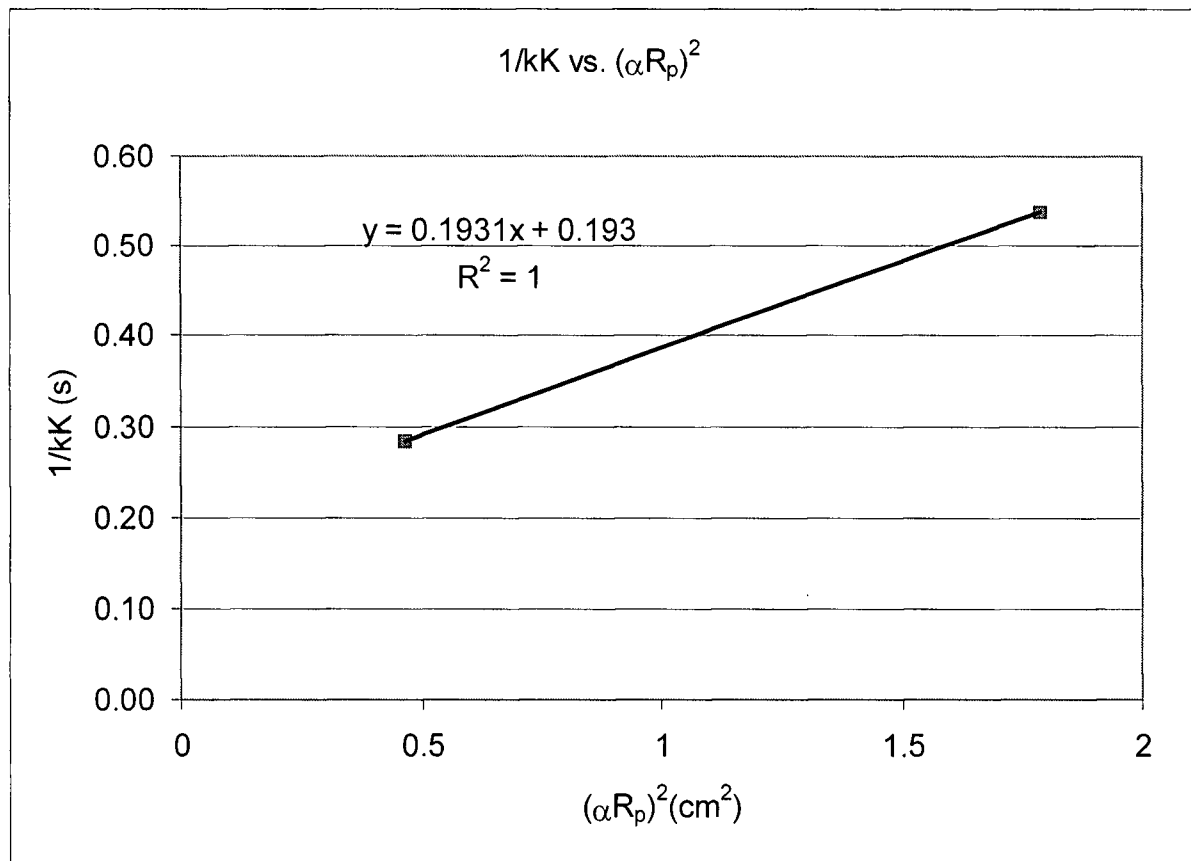


Figure 5.13 $\frac{1}{kK}$ vs. $(\alpha R_p)^2$ used to determine macropore and micropore mass transfer coefficients.

Macropore and micropore diffusivities obtained from Figure 5.13 are summarized in Table 5.7. Karger et al. (1997) reported micropore diffusivity of N₂ in zeolites NaX as 3×10^{-5} cm²/sec (using the pulsed field gradient n.m.r. method), which is 4 orders of magnitude different from the diffusivity found in this study. The difference could be due to the different methodology used and the difference in adsorbent (LiX in this study vs. NaX reported). However, micropore diffusivity of N₂ in zeolite LiX was determined from the intercept of Figure 5.13. The intercept is very sensitive to the error in $\frac{1}{kK}$. Suppose, if the $\frac{1}{kK}$ value for the smaller particle size adsorbent structure were to be decreased by 33 percent and $\frac{1}{kK}$ value for the larger particle size adsorbent structure were to be increased by 36 percent. The intercept will change dramatically as shown in Figure 5.14, resulting in the micropore diffusivity of 2.5×10^{-5} cm²/sec, which is almost the same as the micropore diffusivity obtained by Karger et al (1997). The error associated with the micropore diffusivity measurement is most likely due to the variability in the adsorbent sheet thickness or the particle size within the adsorbent structure. If three or more particle sizes were used instead of two, a more accurate micropore diffusivity could be determined. Only two adsorbent sheets thickness (particle sizes) were used because manufacturing adsorbent structures at different adsorbent sheets thickness were difficult and not feasible at the time of the present study.

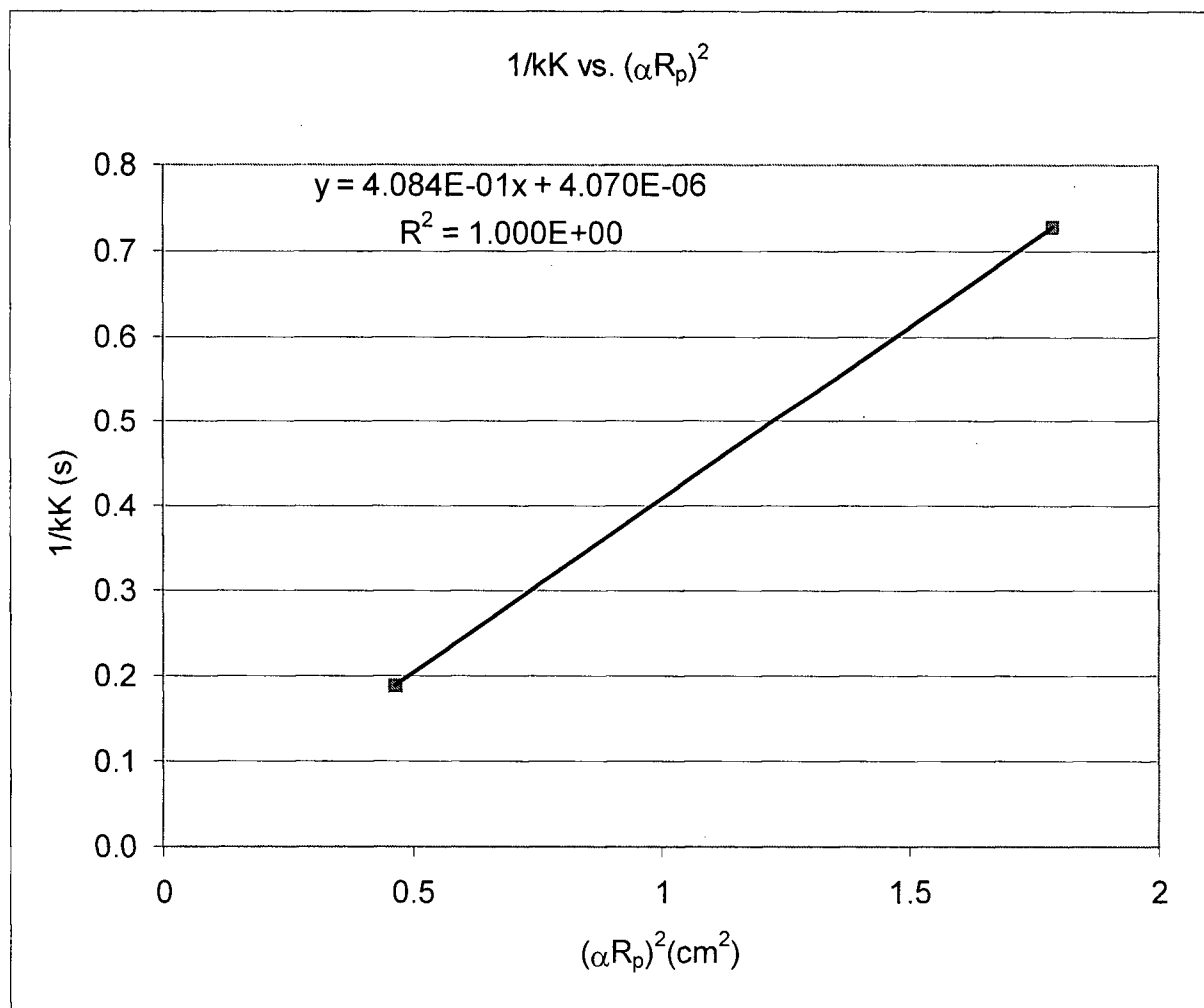


Figure 5.14 $\frac{1}{kK}$ vs. $(\alpha R_p)^2$ used to determine macropore and micropore mass transfer coefficients

Table 5.7 Individual mass transfer coefficients.

Macropore Diffusivity, D_p (cm ² /sec)	1.93×10^{-4}
Micropore Diffusivity, D_c (cm ² /sec)	5.25×10^{-10}

To determine the external fluid film mass transfer coefficient, the $Sh \equiv 2k_f R_p / D_m \approx 2$ approximation at low Reynolds is used. Hence, $k_f = D_m / R_p$ where D_m can taken as $0.7D_L$ at these

low flow rates and D_L was listed in Table 5.4. As a result k_f values are specific for each adsorbent structure and are listed in Table 5.8.

Table 5.8 Fluid film mass transfer coefficient.

Pack	High X-sectional Area	Mid X-sectional Area	Low X-sectional Area	Non-adsorbing	High Voidage	Thick Adsorbent Sheet
Fluid Film Mass Transfer coefficient (cm/sec)	84.1	125.8	126.1	128.1	138.3	69.5

The k_f values in Table 5.8 were then compared with k_f values calculated from the correlations listed in section 2.3.2. Table 5.9 lists the k_f obtained from various correlations and the percent difference between the experimental values and the values obtained from these correlations. As can be seen from Table 5.9, among all the correlations used, the fluid film mass transfer coefficient calculated from Ranz and Marshall (1952) seems to give the best agreement with the results of the present study. The difference between k_f obtained from Ranz and Marshall (1952) and the experimental values are within 10%. Furthermore, in order to calculate k_f , the Sherwood number must first be calculated. From Equation [2.27] to Equation [2.29], at low Reynolds number, the Sherwood number, Sh approaches the limiting value of 2.98, 2.69, and 3.53, respectively. These limiting values all correspond to the square monolith. However, the adsorbent structure used in this study contains plane monolith, i.e., each adsorbent sheet is separated by an empty space and there is no adsorbent material on the side wall of the adsorbent structure. As a result, the limiting values in Equation [2.27] to Equation [2.29] should be closer to 2.0 as in Ranz and Marshall (1952) correlation for the monolith geometry used in this study.

Table 5.9 Fluid film mass transfer coefficient compared with literature value.

Correlation	High X-sectional Area k_f (cm/s)	High X-sectional Area k_f (cm/s)	High X-sectional Area k_f (cm/s)	Non-adsorbing k_f (cm/s)	High Voidage k_f (cm/s)	Thick Adsorbent Sheet k_f (cm/s)
Ranz and Marshall (1952)	91	136	138	139	149	76
Percent difference (%)	8	8	10	8	7	9
Hawthorn (1974)	125	187	188	191	206	104
Percent difference (%)	49	49	49	49	49	49
Uberoi and Pereira (1996)	113	169	170	173	186	94
Percent difference (%)	35	35	35	35	35	35
Holmgren and Andersson (1998)	148	222	223	226	244	123
Percent difference (%)	76	76	77	77	76	76
Experimental	84	126	126	128	138	70

After having estimated the dynamics of the system: the dispersion and individual mass transfer coefficients, the relative magnitude of these resistances at different flow rates can be determined. From Equation [2.36], mass transfer will dominate when $\frac{v^2}{kKD_L} \gg 1$ because as the interstitial velocity increases, D_L/v^2 will decrease. This occurs at $v \gg 1.7$ cm/sec. At lower interstitial velocities, axial dispersion dominates. Moreover, as velocity increases, the relative magnitude of the various dynamic parameters shows that the macropore and micropore mass transfer resistances will dominate. Physically, at high gas velocity, the adsorption process may be limited due to the diffusion rate within the macropores and micropores since the gas retention time will significantly be decreased. As a result, some of the gas will not have sufficient time for adsorption since the gas have to diffuse through the macropores and micropores prior to adsorption. The calculations are shown in Appendix 4.

Furthermore, with the dispersion and the individual mass transfer coefficients identified, a simple linear rate model can be used to predict the breakthrough curves, according to Equation [2.51] with the effective rate coefficient being Equation [2.49]. Figure 5.15 to Figure 5.20 compares the predicted breakthrough curves with measured data at 100 SCCM for all adsorbent structures with the k_f value from Table 5.4, D_L value from Table 5.7, $D_p=0.000193 \text{ cm}^2/\text{s}$, $D_c=5.25 \times 10^{-10} \text{ cm}^2/\text{s}$, and $r_c=1.50 \times 10^{-4} \text{ cm}$.

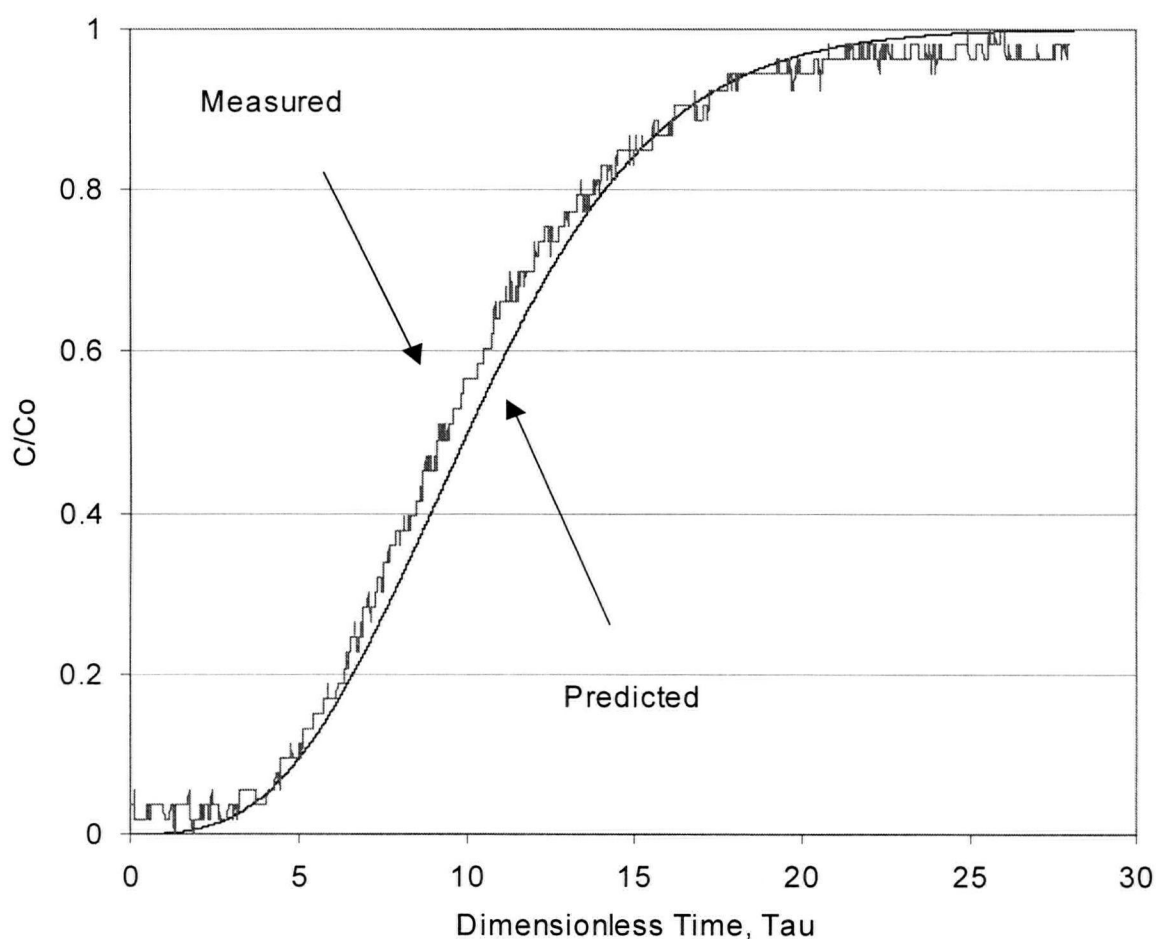


Figure 5.15 Predicted breakthrough curve and raw data for high X-section area structure with flow = 100 SCCM.

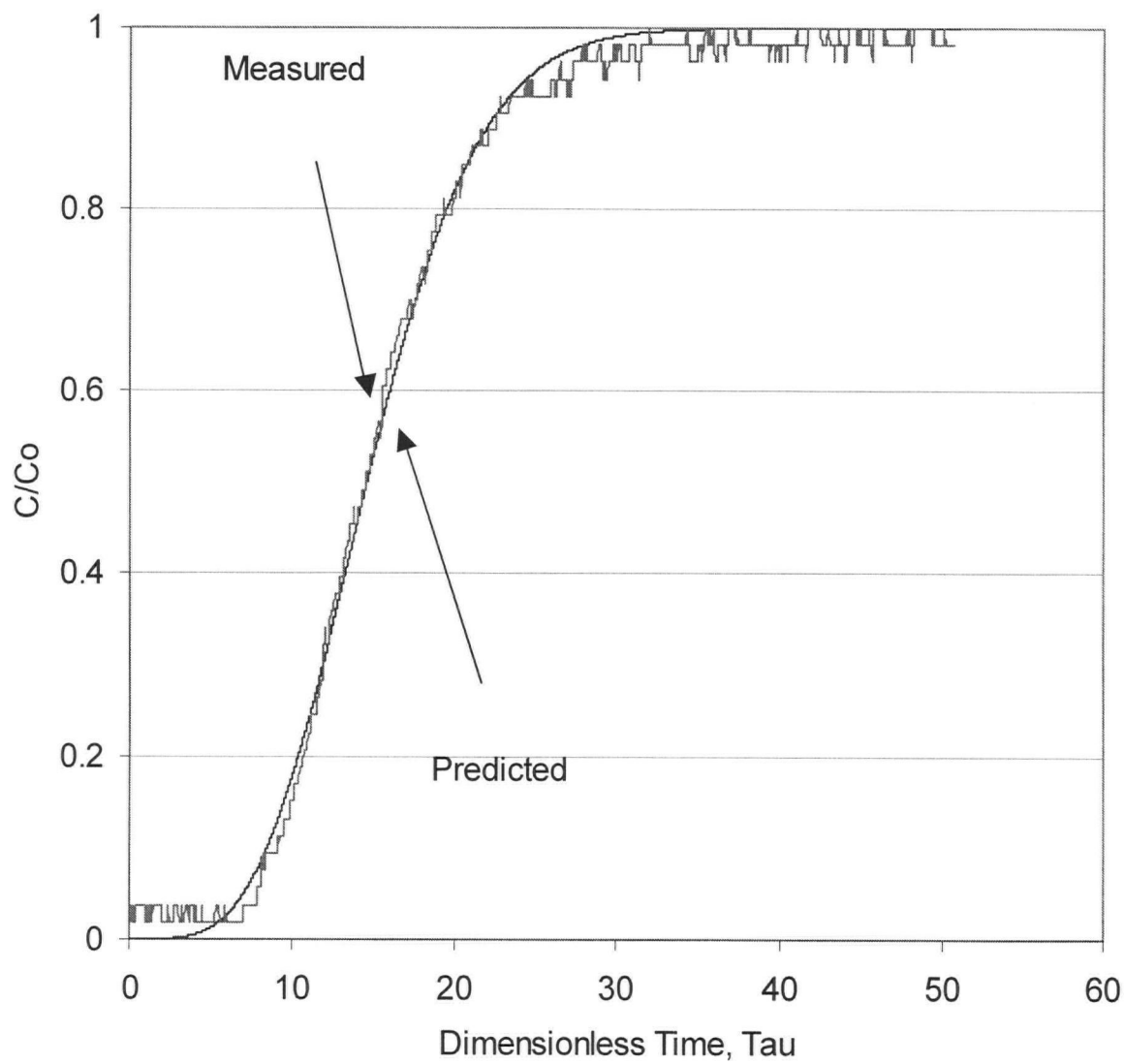


Figure 5.16 Predicted breakthrough curve and raw data for mid X-sectional area structure with flow = 100 SCCM.

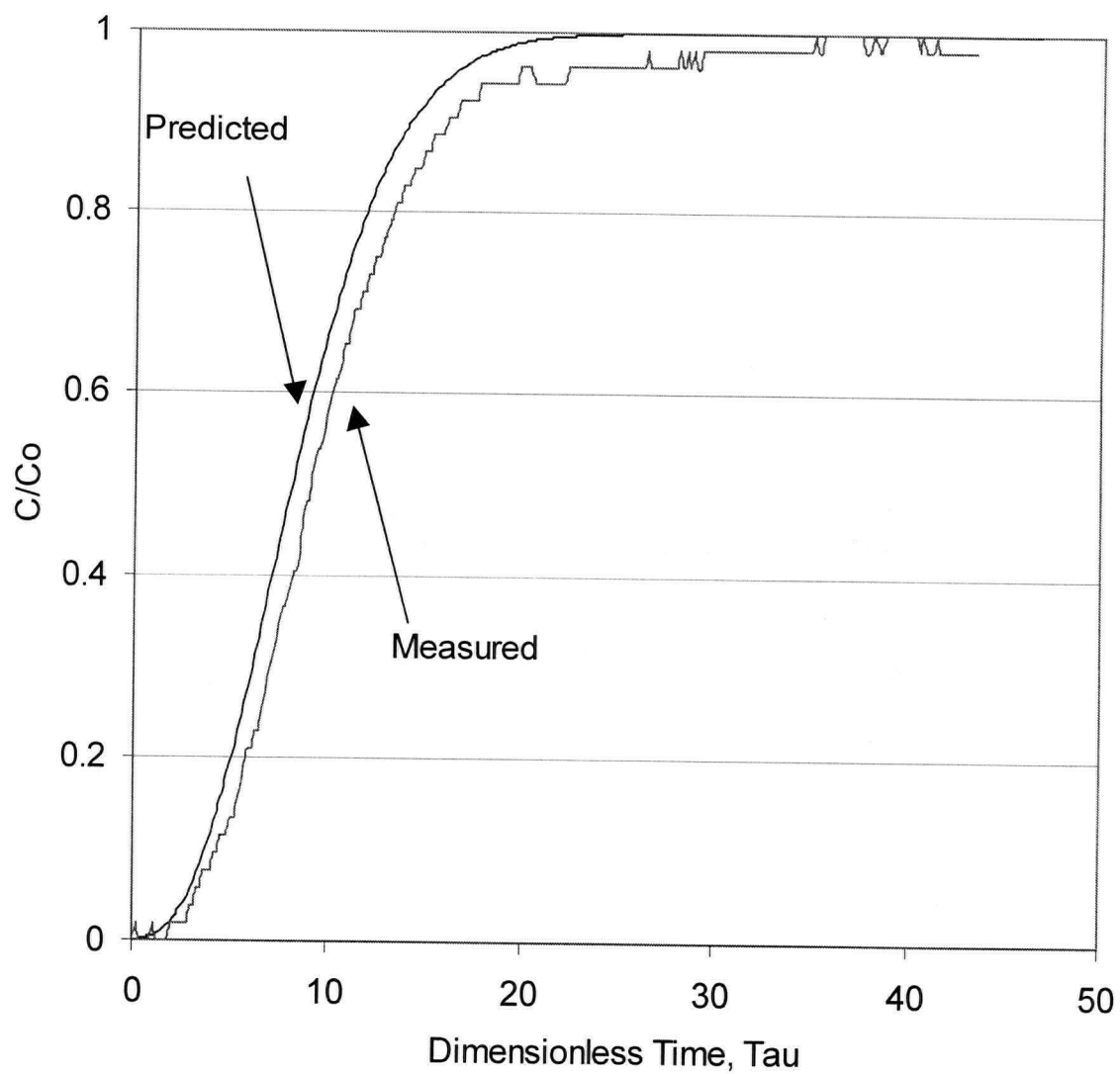


Figure 5.17 Predicted breakthrough curve and raw data for non-adsorbing structure with flow = 100 SCCM.

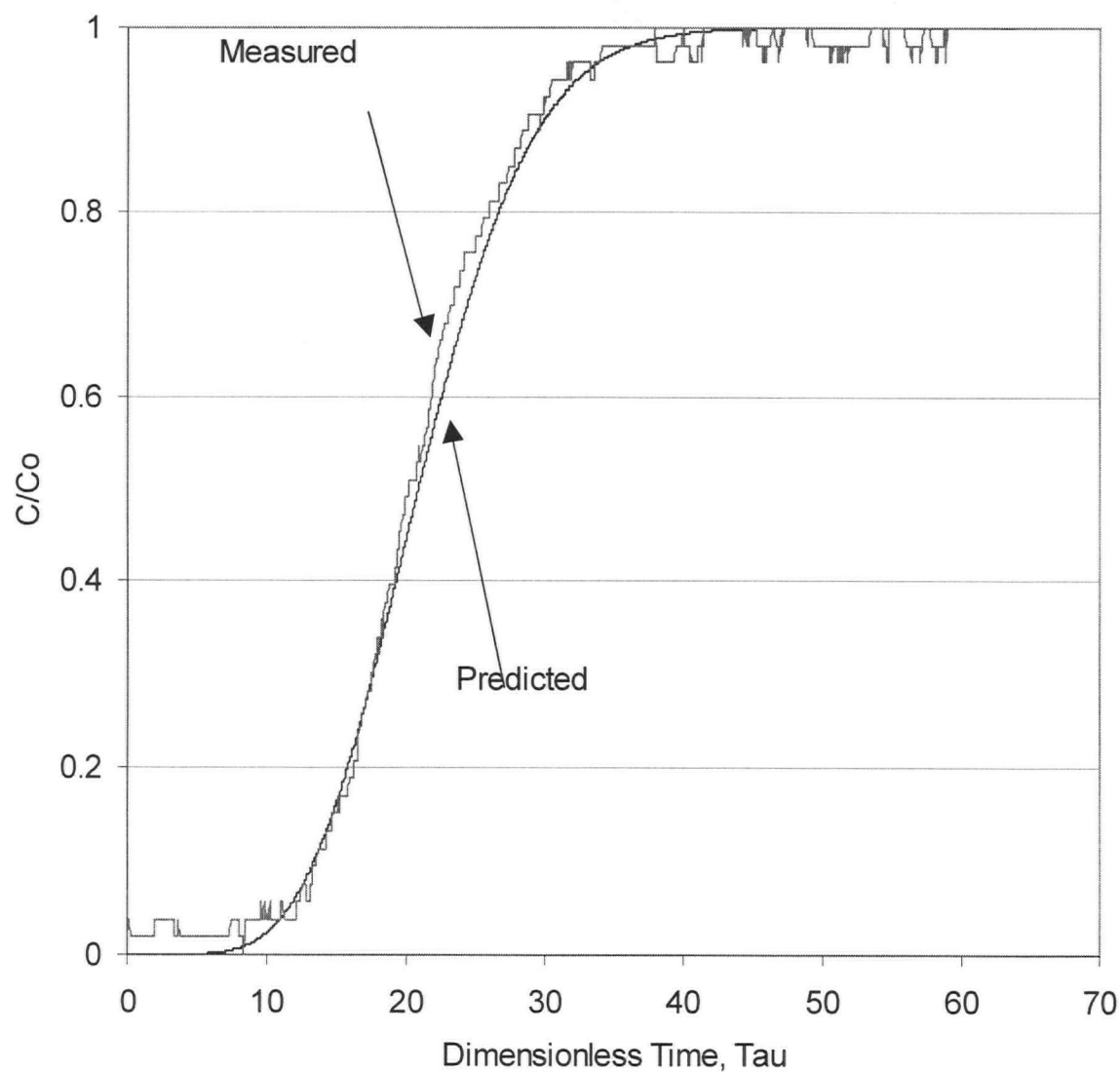


Figure 5.18 Predicted breakthrough curve and raw data for low X-sectional area structure with flow = 100 SCCM.

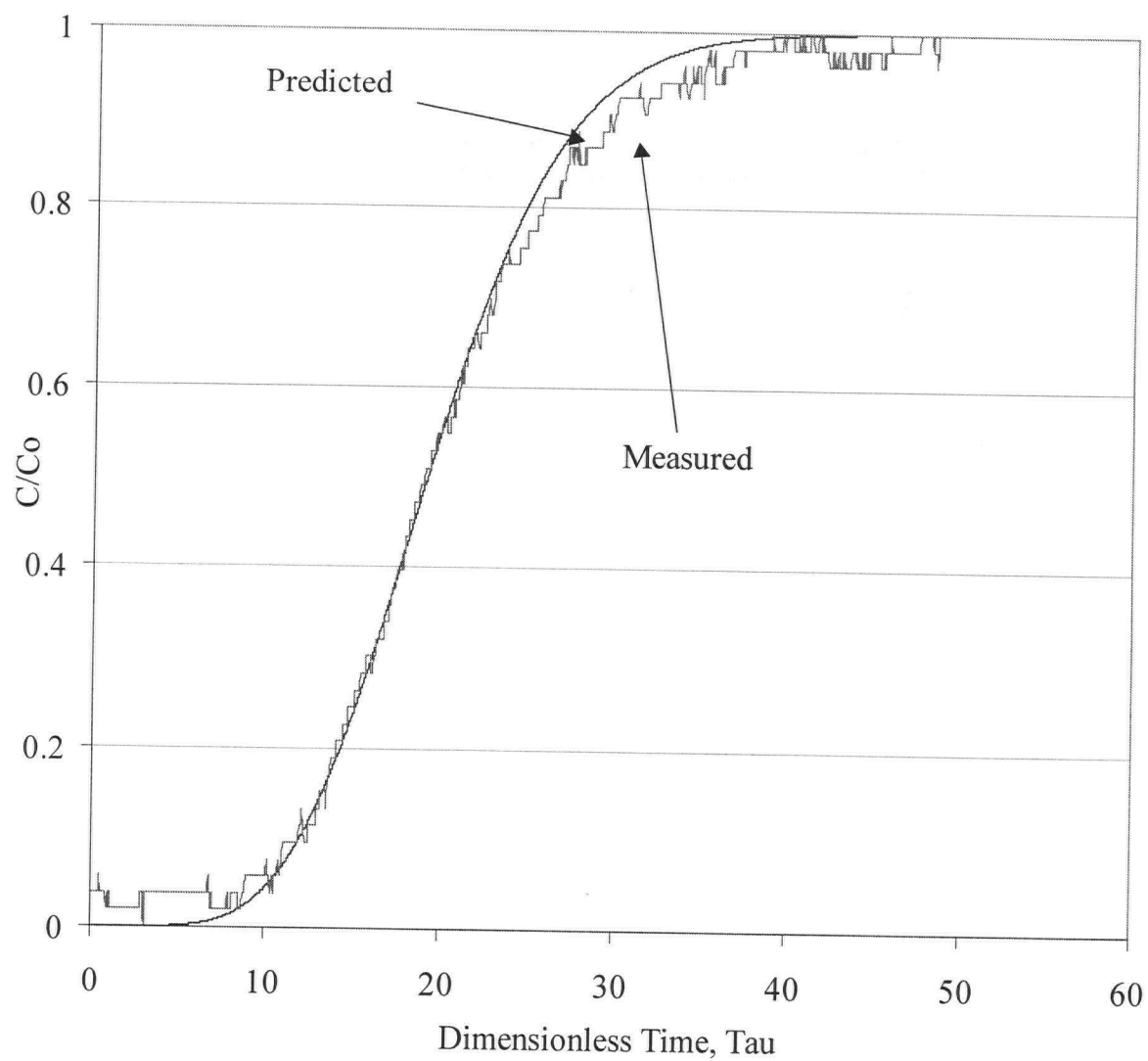


Figure 5.19 Predicted breakthrough curve and raw data for high voidage structure with flow = 100 SCCM.

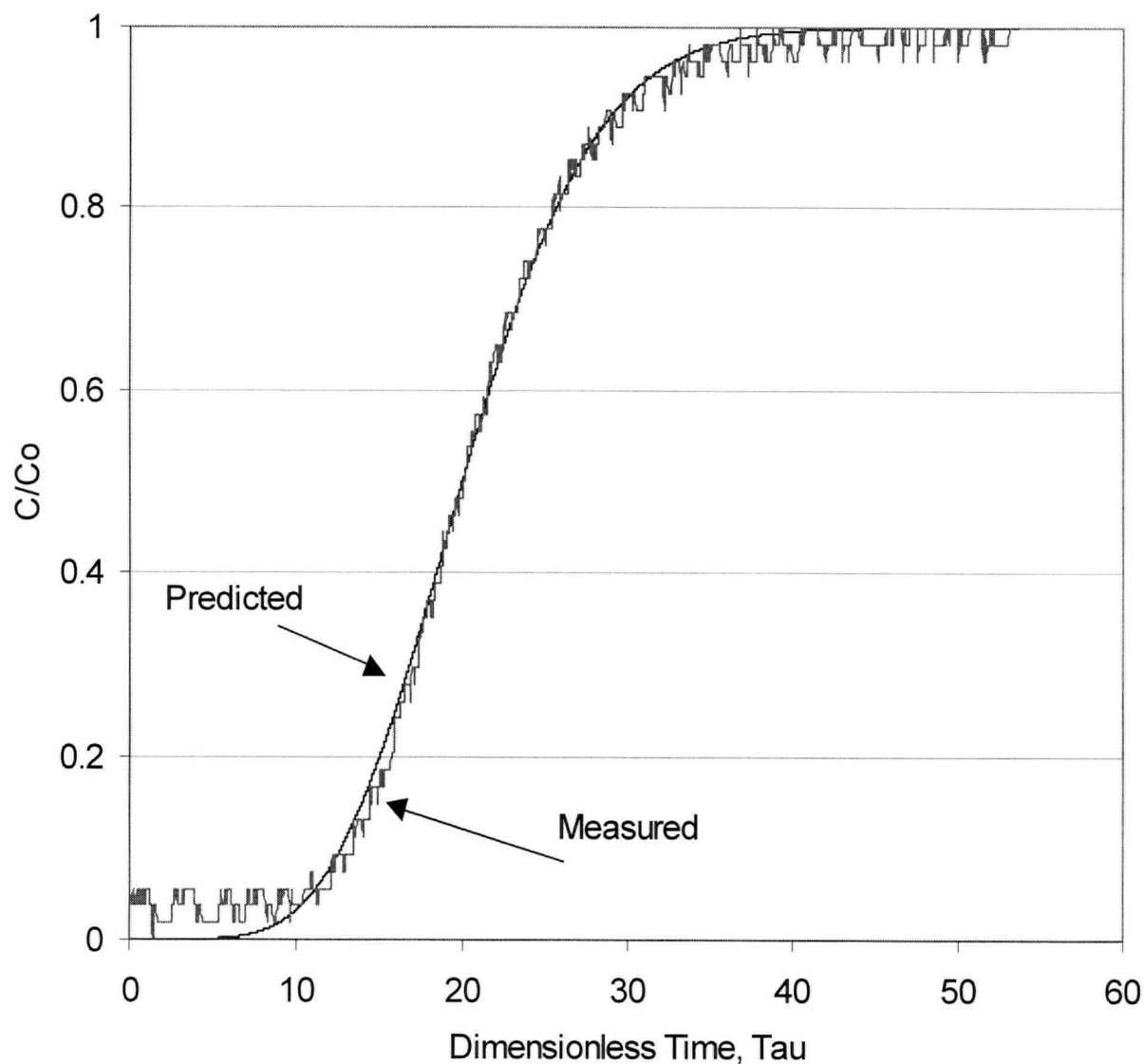


Figure 5.20 Predicted breakthrough curve and raw data for thick adsorbent sheets structure with flow = 100 SCCM.

Figures 5.15 to Figure 5.20 show that the first-order adsorption rate model can adequately described the measured breakthrough data for all adsorbent structures in this study. The sum of squares of errors (SSE) between the predicted data and measured data were calculated for Figure 5.15 to 5.20 and the values are summarized in Table 5.10. F-tests were also performed on these sets of data and are listed in Table 5.10. Small values of SSE and the F_{stats} less than that of the F-

critical values in Table 5.10 from 280 data points for non-adsorbing structure to 2500 data points for high X-sectional area structure suggest that the first-order adsorption rate model can describe the measured breakthrough data in this study.

Table 5.10 SSE and F_{stats} from the F-test for predicted data from Matlab™ program and measured data

Pack	SSE	F_{stats}	F-critical, $\alpha = 0.05$
High X-sectional Area	2.425	0.913	1.062
Mid X-sectional Area	0.536	0.952	1.084
Low X-sectional Area	0.605	0.966	1.086
Non-adsorbing	0.596	0.972	1.183
High Voidage	0.827	0.909	1.084
Thick Adsorbent Sheets	0.583	0.947	1.084

5.6 Parametric Study

A Matlab™ program was developed to investigate the effects of increasing and decreasing mass transfer coefficients and dispersion to assess the sensitivity of the adsorbent structures to these parameters at a fixed flow rate of 4000 SCCM or 13 cm/s for the full-size pack. The effects of increasing and decreasing mass transfer coefficients and dispersion are shown in Figure 5.21 to 5.24 where standard conditions refer to the following values for mass transfer coefficients and dispersion: $D_L = 0.64 \text{ cm}^2/\text{sec}$, $k_f = 84.7 \text{ cm/sec}$, $D_p = 1.93 \times 10^{-4} \text{ cm}^2/\text{sec}$, and $D_C = 5.25 \times 10^{-10} \text{ cm}^2/\text{sec}$. ξ and τ in Figure 5.21 to 5.24 refer to dimensionless bed length and dimensionless time, respectively (Equation [2.49]).

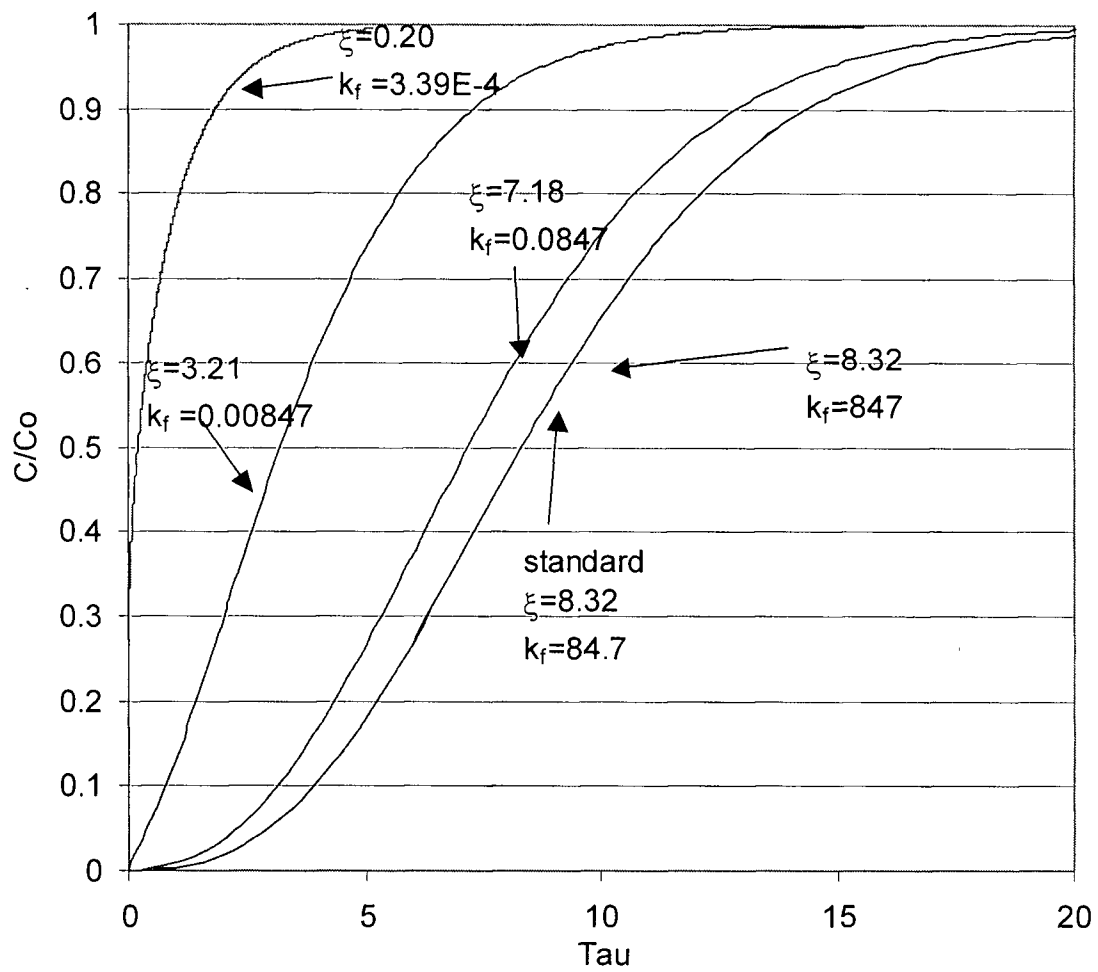


Figure 5.21 Predicted breakthrough curve for change in external fluid film coefficient, k_f .

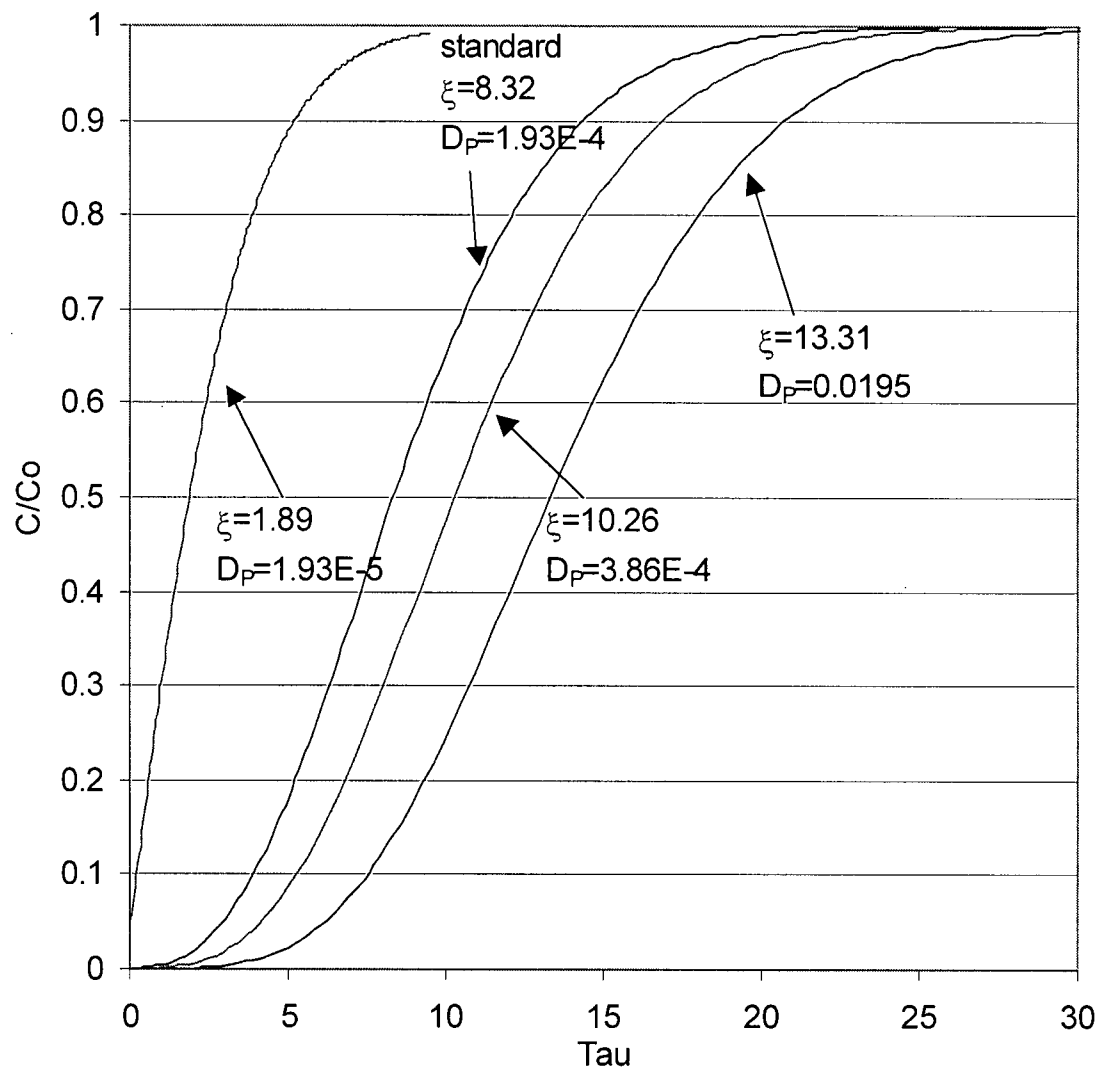


Figure 5.22 Predicted breakthrough curve for change in macropore mass transfer coefficient, D_p .

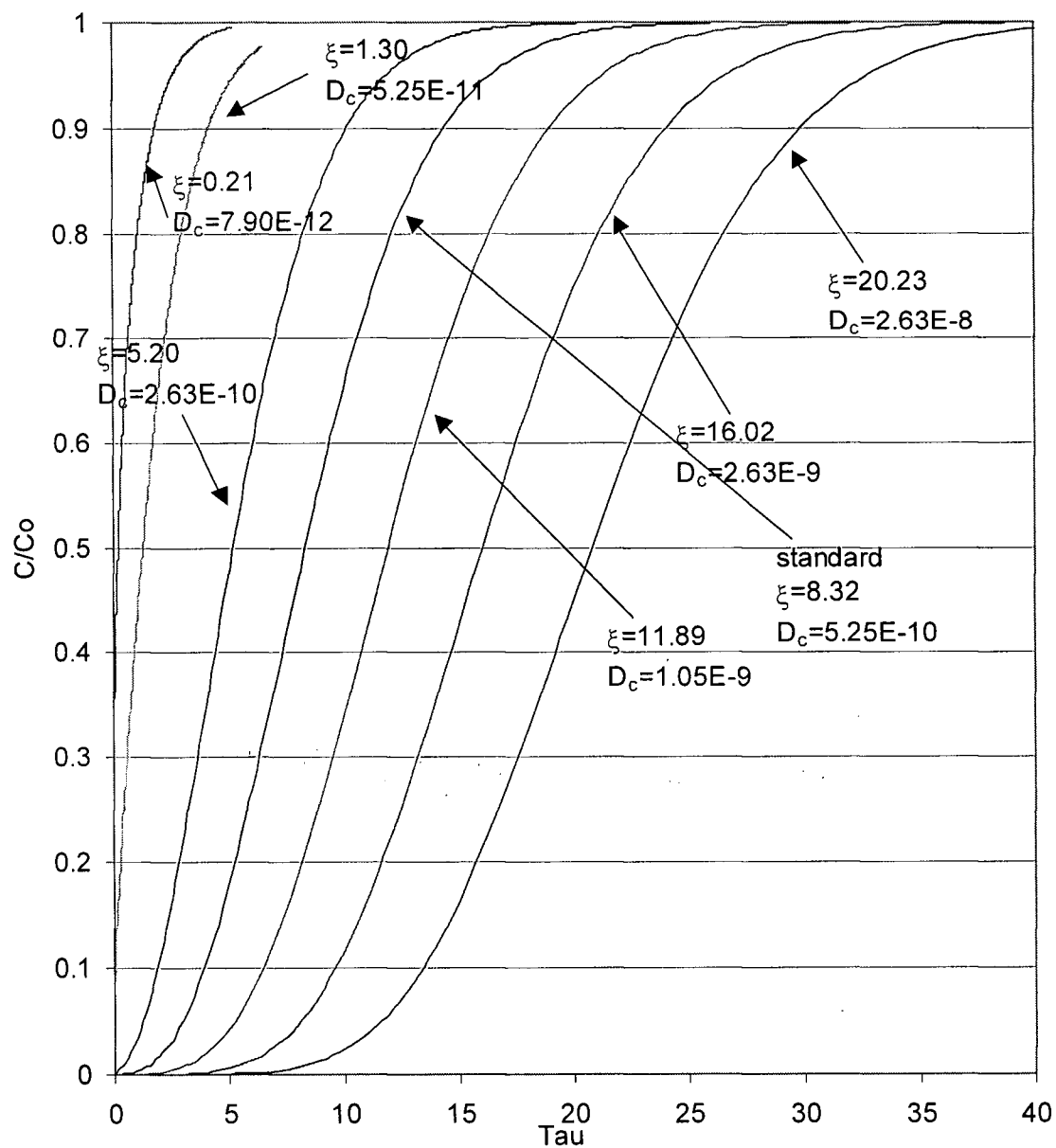


Figure 5.23 Predicted breakthrough curve for change in micropore mass transfer coefficient, D_c .

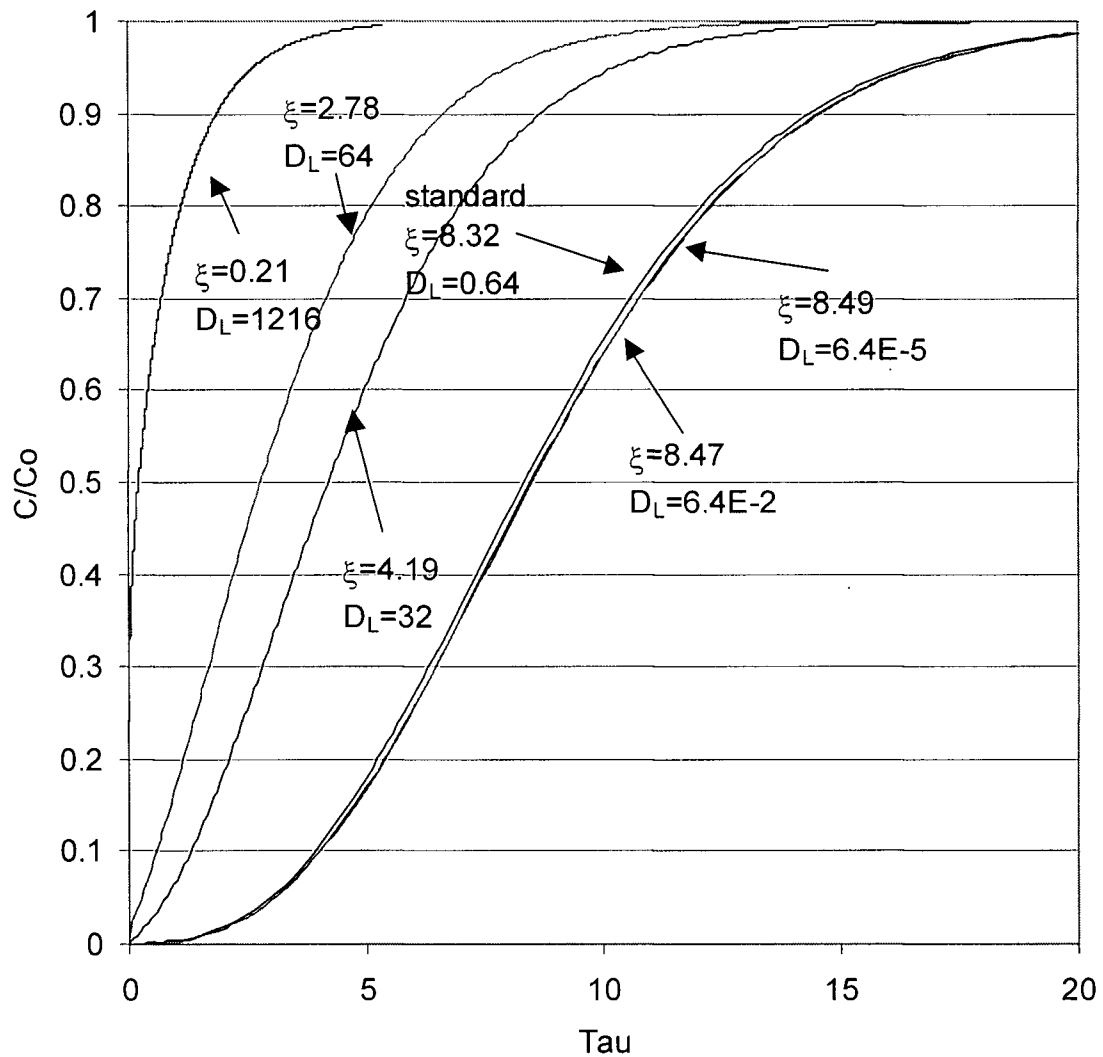


Figure 5.24 Predicted breakthrough curve for change in dispersion coefficient, D_L .

Figure 5.21 and 5.24 show that reducing the dispersion and fluid film mass transfer coefficient has little effect on the breakthrough since at the interstitial velocity used, the mass transfer dominates; moreover, the fluid film mass transfer coefficient does not contribute much to the overall mass transfer resistances as shown in Appendix 4. Significant increase in the magnitude of the dispersion will have a severe effect on the breakthrough. Figure 5.21 and 5.24 indicate that increasing the dispersion by two orders of magnitude or decreasing the fluid film

mass transfer coefficient by several orders of magnitude will greatly shift the dimensionless time of the breakthrough curve, resulting in less adsorption. Figure 5.22 and 5.23 shows that increasing both D_p and D_c , the rates of macropore and micropore diffusion by an order of magnitude or two will largely shift the breakthrough curve to the right, hence, improving the breakthrough characteristics. Hence, in order to improve the performance of the packs used in the present study, an increase in D_p and D_c by orders of magnitude must be achieved.

Chapter 6: Conclusions and Recommendations for Future Work

6.1 Conclusions

Accurate gas adsorption isotherms up to atmospheric pressure can be obtained gravimetrically or volumetrically. There was no significant difference between the measured data obtained using either method. However, gas adsorption isotherms generated using breakthrough analysis, which utilizes the desorption of gas in the non-linear region of the isotherm, appears to give much higher uptakes than those from either the gravimetric or volumetric method.

Buoyancy effects limit the accuracy of gravimetric adsorption isotherm measurements whereas the measurement of free space or dead volume limits the accuracy of measurements by the volumetric method.

Nitrogen adsorption capacity of LiX is far superior to that of NaX zeolite, the capacity of LiX being three times larger than that of NaX, is consistent with the literature reports.

The chromatographic method can be used to obtain estimates of dispersion and mass transfer coefficients present in a structured adsorbent bed. At low interstitial velocities, $u < 1.7$ cm/sec, dispersion dominates while at high interstitial velocities, $u \gg 1.7$ cm/sec, macropore and micropore mass transfer resistance dominates.

Estimated values of the dispersion and external fluid film mass transfer resistance were consistent with literature values. However, the estimated micropore diffusivity was much lower than the literature value and this difference is most likely due to the inaccuracy of the results obtained in the present study that were based on only two particle sizes. Furthermore, from the mass transfer resistances obtained for PSA with short cycle time using structured adsorbent beds, fast PSA with cycle time of 0.6 to 3 seconds are possible.

The simple linear rate model can be used to predict breakthrough curves at different flow rates. Dispersion and fluid film mass transfer coefficients do not affect breakthrough response at high flow rate used while increasing the macropore and micropore mass transfer coefficients by an order of magnitude will significantly improve the adsorption rate.

6.2 Recommendations for Future Work

- Adsorption of gas mixtures on inert porous solids like zeolites provide the basis for a variety of gas separation processes including the separation of air into nitrogen and oxygen enriched streams at ambient temperature. Pure component isotherms were measured in the present study; however, gas separation applications almost always involve multicomponent mixtures. Even though there exist several models that can predict multicomponent adsorption isotherms, the accuracy of the prediction is often less than desirable. As a result, there is a need for direct measurement of multicomponent isotherms. There are accurate models that can predict multicomponent isotherms once the binary component data are available. Hence, one of the recommendations for future work is to obtain binary gas adsorption isotherms at high pressure using the gravimetric method.
- The micropore and macropore mass transfer resistances measured in the present study had large errors associated with them since only two particle sizes (adsorbent sheets thickness) were used in the estimation of these values. Hence, it is recommended that further study should be done on measuring these mass transfer resistances using 3 or more particle sizes. If more accurate mass transfer resistances are obtained, they can be use to predict breakthrough curves and consequently optimize the PSA cycle. Also, it would be interesting to make a comparison between individual mass transfer resistances obtained from the chromatography method and other methods such as frequency response method, permeation, and zero length chromatography.

Reference:

- Alpay, E., Kenney, C.N. and Scott, D. M., *Chem. Eng. Sci.* **49**(18), 3059 (1994).
- Ansel, J.G.H. "Oxygen"; Air Products and Chemicals Inc, New York, 1996
- Bar, N.K., McDaniel, P.L., Coe, C.G., Seiffert, G. and Karger J., *Zeolites*. **18**, 71 (1997).
- Bennett, C.J., Kolaczowski, S.T. and Thomas, W.J., *Trans. Instn Chem. Engrs..* **69**, 209 (1991).
- Berlin, N. H. U.S. Patent 3 280 536, 1966.
- Boniface, H.A. and Ruthven D. M., *Chem. Eng. Sci.* **40**, 2053 (1985).
- Brunauer, S., Emmett, P. H. and Teller, E., *J. Am. Chem. Soc.* **60**, 309 (1938).
- Chemical Manufacturers Association, "U.S. Chemical Industry Statistical Handbook," CMA, Arlington, VA, 1992.
- Chemical Manufacturers Association, "U.S. Chemical Industry Statistical Handbook," CMA, Arlington, VA, 1996.
- Chilton, T. H. and Colburn, A. P., *Trans. Am. Inst. Chem. Eng.* **26**, 178 (1931).
- Choudary, N. V., Jarsa, R.V. and Bhat S.G.T. U.S. Patent 6 087 289, 2000.
- Coe, C. G. In *Gas Separation Techonology*; Vansant and Dewolfs, R., Ed.; Elsevier, Amsterdam, 1990; p.149.
- Coe, C. G., Kirner, J. F. and Pierantozzi, R. U.S. Patent 5 258 058, 1993.

- Dixon, A. G. and Ma, Y. H., *Chem. Eng. Sci.* **43**, 1297 (1988).
- Eic, M. and Ruthven, D. M., *Zeolites*. **8**, 40 (1988).
- Eisfeld, B. and Schnitzlein, K., *Chem. Eng. Sci.* **56**, 4321 (2001).
- Ergun, S., *Chem. Eng. Prog.* **48**, 89 (1952).
- Fitch, F. R., Bulow, M. and Ojo, A. F. U.S. Patent 5 464 467, 1995.
- Gaffney, T.R., *Curr. Opin. Solid. St. M.* **1**(1), 69 (1996).
- Glueckauf, E., *Trans. Faraday Soc.* **51**, 1540 (1955).
- Hardenburger, T.L., *Kirk-Othmer Encyclopedia of Chemical Technology*. (1996).
- Hawthorn, R.D., *A.I.Ch.E. Symp. Ser.* **70**(137), 428 (1974).
- Hayashi, S., Kawai, M. and Kaneko, T., *Gas. Sep. Purif.* **10**, 19 (1996).
- Hayes, R.E. and Kolaczowski, S.T., *Chem. Eng. Sci.* **49**(21), 3587 (1994).
- Haynes, H. W. and Sarma, P. N., *AIChE J.* **19**, 1043 (1973).
- Heck, R. M., Gulati, S. and Farrauto, R.J., *Chem. Eng. Jour.* **82**, 149 (2001).
- Holmgren, A. and Andersson, B., *Chem. Eng. Sci.* **53**(13), 2285 (1998).
- Jones, R. L., Keller, G. E. and Wells, R. C. US Patent 4 194 892, 1980.
- Jones, R. L. and Keller, G. E., *J. Separ. Proc. Tech.* **2**(3), 17 (1981).
- Keefer, B.G. U.S. Patent 5 082 473, 1992.

Keefer, B.G. and Doman D.G. U.S. Patent 6 051 050, 1992.

Keefer, B.G. and McLean C.R. U.S. Patent 6 056 804, 1992.

Kimer, J.F. U.S. Patent 5 268 023, 1993.

Kovacevic, S. M.A.Sc Thesis, University of British Columbia, 2000.

Lipinsky, E.; Ingham, J.D. *Final Task Report on Brief Characterizations of the Top 50 U.S. Commodity Chemicals*; A Pacific Northwest National Laboratory report submitted to the U.S. Department of Energy, Biological and Chemical Technology Research Program, 1994.

Martin, M. J. P. and Synge, R. L. M., *Biochem. J.* **35**, 1359 (1941).

Mattia, M.M. U.S. Patent 4 452 612, 1984.

Mullhaupt, J. T. and Stephenson, P. C. E.P. Patent 658 364, 1995.

Pazdernik, O. and Schneider, P., *J. Chromatogr.* **207**, 181 (1981).

Published unexamined patent application of Japan, 52-52181, To BOC, 1996.

Published unexamined patent application of Japan, 64-43327, To Sumitomo Seika Co, Ltd., 1996.

Ranz, W.E. and Marshall W.R., *Chem Eng. Prog.* **48**, 173 (1952).

Rege, S.U. and Yang, R.T., *Ind.Eng.Chem.Res.* **36**(12), 5358 (1997)

Reichelt, W., *Chemie-In-genier-Technik.* **44**, 1068 (1972).

Robens, E., Keller, J. U., Massen, C.H. and Staudt, R. *J. Therm. Anal. Calorim.* **5**, 383 (1999).

- Ruthven, D. M. *Principles of Adsorption and Adsorption Processes*; John Wiley & Sons: New York, 1984.
- Ruthven et al., *Chem. Eng. Sci.* **49**, 3052 (1994)
- Ruthven, D. M. and Derrah, R.I, *J. Chem. Soc. Faraday Trans. I.* **71**, 2031 (1971).
- Ruthven D. M., Farooq, S. and Knaebel, K. S. *Pressure Swing Adsorption*; VCH: New York, 1994
- Ruthven D. M. and Karger, J. *Diffusion in Zeolites*; John Wiley & Sons: New York, 1992
- Satterfield, C.N., *Mass Transfer in Heterogeneous. Catalysis*, M.I.T. Press, Cambridge, 1970.
- Sircar, S. and Hanley, B. F., *Adsorption* **1**, 313, (1995).
- Skarstrom, C. W. U.S. Patent 2 944 627, 1960.
- Sorial, G. A., Granville, W. H. and Daley, W. O., *Chem. Eng. Saci.* **38**, 1517 (1983).
- Storm, G.E. "Oxygen Dissolution Technologies for Biotreatment Applications"; Praxair Inc., New York, 1997.
- Talu, O. *Adv. Colloid. Interac.* **77**, 227 (1998).
- Turnock, P.H. and Kadlec, R.H., *AIChE J.* **17**, 335 (1971).
- Ullah, U., Waldram, S.P., Bennett, C.J. and Truex, T., *Chem. Eng. Sci.* **47**(9-11), 2413 (1992).
- Uberoi, M. and Pereira, C.J., *Ind. Engng Chem. Res.* **35**, 113 (1996).
- Van der Laan, E. Th., *Chem. Eng. Sci.*, **7**, 187 (1958).

Wicke, E., and Kallenbach, R., *Kolloid Z.* **97**, 135 (1941).

William, F., Baade, Uday N., Parekh, Venkat S., and Raman, "Hydrogen"; Air Products and Chemicals Inc., New York, 2001.

Xu, Z. and Ruthven, D. M. *Proc. Ninth Internat. Zeolite Conf. Montreal*, July 1992.

Yang, R.T., Chen, N., Chen Y.D. and Peck, J.D., *Ind. Engng Chem. Res.* **35**, 3093 (1996).

Yang, R.T., Jayaraman, A., Cho, S.H., Bhat, T.S.G. and Choudary, V.N., *Adsorption*. **8**, 271 (2002).

Yasuda, Y., *Heterog. Chem. Rev.* **1**, 103 (1994).

Zhang, Z.X., Guan, J.Y. and Ye, Z.H., *Adsorption* **4**(2), 173 (1998).

<http://www.eren.doe.gov/hydrogen/faqs.html#cost>, 2002.

<http://www.tosoh.com/EnglishHomePage/tcnew/news1999/0722.htm>, 1999.

APPENDIX

Appendix 1 :Isotherm Measurements Data

Table A.1.1 Nitrogen Isotherm data on NaX at 50 °C


Temperature (°C)	Volumetric		TGA	
	Pressure (kPa)	Amount (mmol adsorbed/g)	Pressure (kPa)	Amount (mmol adsorbed/g)
50	0.7	0.002	3	0.013
	1.4	0.004	10	0.037
	2.1	0.007	31	0.090
	4.2	0.012	51	0.149
	6.9	0.020	77	0.220
	13.8	0.039	103	0.302
	20.4	0.057		
	27.1	0.074		
	33.8	0.092		
	40.4	0.110		
	47.1	0.127		
	53.8	0.145		
	60.4	0.162		
	67.1	0.178		
	73.8	0.195		
	80.4	0.211		
	87.1	0.228		
	93.8	0.244		
	100.4	0.260		
	107.1	0.276		
	113.8	0.291		

Table A.1.2 Nitrogen Isotherm data on NaX at 30 °C

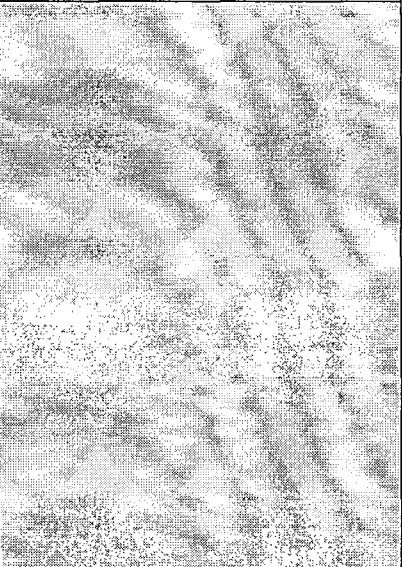
Temperature (°C)	Volumetric		TGA	
	Pressure (kPa)	Amount (mmol adsorbed/g)	Pressure (kPa)	Amount (mmol adsorbed/g)
30	0.6	0.003	3	0.022
	1.4	0.007	10	0.055
	2.1	0.011	30	0.146
	4.1	0.021	51	0.229
	6.9	0.034	77	0.327
	13.7	0.066	103	0.429
	20.3	0.098		
	27.0	0.129		
	33.7	0.159		
	40.4	0.189		
	47.0	0.219		
	53.7	0.248		
	60.4	0.276		
	67.0	0.305		
	73.7	0.333		
	80.4	0.361		
	87.1	0.388		
	93.7	0.415		
	100.4	0.442		
	107.1	0.469		
	113.7	0.494		

Table A.1.3 Carbon Monoxide Isotherm data on NaX at 50 °C

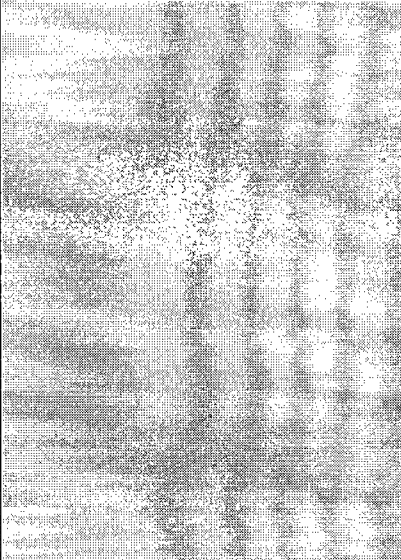
Temperature (°C)	Volumetric		TGA	
	Pressure (kPa)	Amount (mmol adsorbed/g)	Pressure (kPa)	Amount (mmol adsorbed/g)
50	0.7	0.010	3	0.043
	1.3	0.018	10	0.100
	2.0	0.027	30	0.277
	4.0	0.049	50	0.433
	6.8	0.064	76	0.625
	12.7	0.169	101	0.817
	19.8	0.243		
	26.5	0.313		
	33.2	0.376		
	39.9	0.437		
	46.6	0.497		
	53.3	0.553		
	60.0	0.606		
	66.7	0.656		
	73.4	0.704		
	80.1	0.752		
	86.7	0.801		
	93.4	0.846		
	100.1	0.891		
	106.8	0.931		
	113.5	0.972		

Table A.1.4 Carbon Monoxide Isotherm data on NaX at 30 °C

Temperature (°C)	Volumetric		TGA	
	Pressure (kPa)	Amount (mmol adsorbed/g)	Pressure (kPa)	Amount (mmol adsorbed/g)
30	0.7	0.014	3	0.055
	1.3	0.025	10	0.184
	2.0	0.039	31	0.482
	4.1	0.079	51	0.714
	6.4	0.120	76	0.965
	13.7	0.240	102	1.179
	19.4	0.327		
	27.1	0.436		
	32.9	0.511		
	39.5	0.592		
	46.2	0.669		
	52.9	0.741		
	59.6	0.810		
	66.3	0.874		
	73.0	0.936		
	79.8	0.994		
	86.5	1.049		
	93.2	1.101		
	99.9	1.151		
	106.5	1.200		
	113.2	1.247		

Table A.1.5 Carbon Dioxide Isotherm data on NaX at 50 °C


Temperature (°C)	Volumetric		TGA	
	Pressure (kPa)	Amount (mmol adsorbed/g)	Pressure (kPa)	Amount (mmol adsorbed/g)
50	0.6	1.148	3	1.880
	1.3	1.552	10	2.940
	1.9	1.826	30	4.029
	3.8	2.344	51	4.523
	6.5	2.779	76	4.953
	13.0	3.437	103	5.252
	20.0	3.869		
	26.7	4.153		
	32.8	4.357		
	39.6	4.540		
	46.5	4.692		
	53.5	4.821		
	60.4	4.932		
	66.2	5.008		
	72.8	5.091		
	79.5	5.167		
	86.3	5.235		
	93.1	5.296		
	99.8	5.354		
	106.5	5.406		
	113.2	5.455		

Table A.1.6 Carbon Dioxide Isotherm data on NaX at 30 °C

Temperature (°C)	Volumetric		TGA	
	Pressure (kPa)	Amount (mmol adsorbed/g)	Pressure (kPa)	Amount (mmol adsorbed/g)
30	0.6	1.768	4	2.038
	1.3	2.230	10	3.903
	1.9	2.525	31	4.918
	3.8	3.098	51	5.319
	6.5	3.597	76	5.605
	12.9	4.275	102	5.778
	20.0	4.705		
	26.8	4.971		
	32.9	5.150		
	39.8	5.310		
	46.7	5.444		
	53.8	5.554		
	59.5	5.631		
	66.1	5.712		
	72.9	5.783		
	79.6	5.849		
	86.5	5.904		
	93.1	5.959		
	99.9	6.008		
	106.6	6.053		
	113.3	6.093		

Table A.1.7 Nitrogen Isotherm data on LiX using TGA method

Temperature (°C)	N2 pressure (kPa)	Amount adsorbed (mmol/g)
30	3.38	0.079
	10.46	0.247
	30.67	0.616
	50.31	0.891
	76.85	1.166
	102.46	1.419
40	3.19	0.061
	10.71	0.188
	31.31	0.460
	51.39	0.707
	76.62	0.943
	102.98	1.141
50	3.06	0.039
	10.42	0.106
	30.99	0.275
	50.90	0.430
	76.46	0.594
	102.56	0.753
60	3.07	0.023
	10.24	0.075
	29.92	0.191
	49.71	0.295
	75.13	0.424
	102.50	0.571
80	3.25	0.025
	10.14	0.054
	28.90	0.130
	49.59	0.216
	75.24	0.316
	101.37	0.435

Table A.1.8 Nitrogen Isotherm data on QP at 60 °C

Low Pressure		High Pressure	
Pressure (kPa)	Measured Amount (mmol adsorbed/g)	Pressure (kPa)	Measured Amount (mmol adsorbed/g)
0.7	0.011	56	0.495
1.3	0.020	83	0.680
2.0	0.030	112	0.859
3.3	0.047	155	1.005
6.4	0.089	209	1.135
12.8	0.168	252	1.230
19.7	0.247	302	1.308
26.5	0.316		
33.2	0.379		
39.9	0.436		
46.6	0.489		
53.2	0.538		
59.9	0.583		
66.6	0.625		
73.3	0.665		
79.9	0.702		
86.6	0.739		
93.3	0.772		
99.9	0.805		
106.6	0.835		
113.3	0.862		

Table A.1.9 Nitrogen Isotherm data on QP at 80 °C

Low Pressure		High Pressure	
Pressure (kPa)	Measured Amount (mmol adsorbed/g)	Pressure (kPa)	Measured Amount (mmol adsorbed/g)
0.7	0.007	56	0.336
1.4	0.013	83	0.477
2.0	0.018	111	0.624
3.3	0.029	153	0.805
6.5	0.056	204	0.942
13.1	0.108	251	1.011
19.9	0.158	302	1.079
26.6	0.203		
33.3	0.245		
39.9	0.290		
46.6	0.331		
53.3	0.368		
59.9	0.405		
66.6	0.441		
73.3	0.472		
79.9	0.504		
86.6	0.535		
93.3	0.565		
100.1	0.586		
107.2	0.615		
113.3	0.643		

Table A.1.10 Nitrogen Isotherm data on QP at 100 °C

Low Pressure		High Pressure	
Pressure (kPa)	Measured Amount (mmol adsorbed/g)	Pressure (kPa)	Measured Amount (mmol adsorbed/g)
0.6	0.004	54	0.230
1.4	0.008	84	0.344
2.0	0.012	111	0.476
3.4	0.019	153	0.613
6.6	0.036	203	0.716
13.2	0.070	251	0.784
20.0	0.103	302	0.853
26.6	0.136		
33.3	0.167		
40.0	0.199		
46.7	0.227		
53.4	0.252		
60.0	0.279		
66.7	0.305		
73.4	0.330		
80.0	0.354		
86.7	0.378		
93.3	0.400		
100.0	0.425		
106.8	0.443		
114.1	0.458		

Appendix 2: Summary of Breakthrough Data

Table A.2.1 Summary of breakthrough data for high X-section area adsorbent structure

Bed voidage 0.413
Length (L) 20.32cm
X_Sect_Area 12.41cm²

Volumetric Flow Rate (cc/min)	Interstitial Velocity (cm/s)	μ (s)	σ^2 (s ²)	HETP (σ^2/μ^2)L (cm)	HETP/2v (σ^2/μ^2)L/2v (s)	1/F (s/cm ³)	1/v ² (s ² /cm ²)	Temperature (°C)
60	0.19	2437	1453762	4.97	12.76	1.00	26.3	23.2
100	0.32	1624	531337	4.09	6.30	0.60	9.5	21.5
140	0.45	1189	201472	2.90	3.18	0.43	4.8	22.7
180	0.58	890	97456	2.50	2.14	0.33	2.9	22.7
220	0.71	749	66173	2.39	1.67	0.27	2.0	23.2
260	0.84	631	36737	1.87	1.11	0.23	1.4	23.2
60	0.19	2437	1453762	4.97	12.76	1.00	26.3	23.2
100	0.32	1653	543372	4.04	6.22	0.60	9.5	22.7
140	0.45	1157	216707	3.29	3.62	0.43	4.8	22.7
180	0.58	971	111072	2.39	2.04	0.33	2.9	22.3
220	0.71	727	52593	2.02	1.41	0.27	2.0	23.2
260	0.84	640	38230	1.90	1.12	0.23	1.4	23.2

Table A.2.2 Summary of breakthrough data for mid X-section area adsorbent structure

Bed voidage 0.380
Length (L) 20.32cm
X_Sect_Area 6.29cm²

Volumetric Flow Rate (cc/min)	Interstitial Velocity (cm/s)	μ (s)	σ^2 (s ²)	HETP (σ^2/μ^2)L (cm)	HETP/2v (σ^2/μ^2)L/2v (s)	1/F (s/cm ³)	1/v ² (s ² /cm ²)	Temperature (°C)
60	0.42	1212	292217	4.04	4.83	1.00	5.72	23.8
100	0.70	740	76692	2.84	2.04	0.60	2.06	23.8
140	0.98	544	31099	2.13	1.09	0.43	1.05	23.7
180	1.25	425	17859	2.01	0.80	0.33	0.64	23.5
220	1.53	343	10629	1.84	0.60	0.27	0.43	23.5
260	1.81	287	6322	1.56	0.43	0.23	0.30	24.0
60	0.42	1185	302798	4.38	5.24	1.00	5.72	23.3
100	0.70	743	74792	2.75	1.98	0.60	2.06	23.7
140	0.98	537	29710	2.09	1.07	0.43	1.05	23.7
180	1.25	416	14272	1.67	0.67	0.33	0.64	23.5
220	1.53	353	9292	1.51	0.49	0.27	0.43	23.6
260	1.81	288	5647	1.38	0.38	0.23	0.30	23.3

Table A.2.3 Summary of breakthrough data for low X-section area adsorbent structure

Bed voidage 0.380
 Length (L) 20.32cm
 X_Sect_Area 3.70cm²

Volumetric Flow Rate (cc/min)	Interstitial Velocity (cm/s)	μ (s)	σ^2 (s ²)	HETP ($(\sigma^2/\mu^2)L$) (cm)	HETP/2v ($(\sigma^2/\mu^2)L/2v$) (s)	1/F (s/cm ³)	1/v ² (s ² /cm ²)	Temperature (°C)
60	0.71	686	63384	2.74	1.93	1.00	1.98	21.0
100	1.18	427	17248	1.92	0.81	0.60	0.71	21.0
140	1.66	308	7550	1.62	0.49	0.43	0.36	21.0
180	2.13	236	2651	0.96	0.23	0.33	0.22	21.0
220	2.61	196	2128	1.13	0.22	0.27	0.15	21.0
260	3.08	165	1046	0.78	0.13	0.23	0.11	21.0
60	0.71	637	61229	3.06	2.15	1.00	1.98	22.3
100	1.18	390	13344	1.78	0.75	0.60	0.71	22.5
140	1.66	282	6174	1.58	0.48	0.43	0.36	22.5
180	2.13	224	2418	0.98	0.23	0.33	0.22	22.6
220	2.61	184	1942	1.16	0.22	0.27	0.15	22.4
260	3.08	157	1361	1.13	0.18	0.23	0.11	22.5

Table A.2.4 Summary of breakthrough data for non-adsorbing structure

Bed voidage 0.399
 Length (L) 20.32cm
 X_Sect_Area 6.14cm²

Volumetric Flow Rate (cc/min)	Interstitial Velocity (cm/s)	μ (s)	σ^2 (s ²)	HETP ($(\sigma^2/\mu^2)L$) (cm)	HETP/2v ($(\sigma^2/\mu^2)L/2v$) (s)	1/F (s/cm ³)	1/v ² (s ² /cm ²)	Temperature (°C)
60	0.41	125	3182	4.13	5.07	1.000	6.01	
100	0.68	79	732	2.35	1.73	0.600	2.16	
140	0.95	55	298	1.97	1.04	0.429	1.10	
180	1.22	46	135	1.32	0.54	0.333	0.67	
220	1.50	38	66	0.94	0.31	0.273	0.45	
260	1.77	28	87	2.34	0.66	0.231	0.32	
60	0.41	126	3373	4.34	5.32	1.000	6.01	
100	0.68	77	644	2.21	1.62	0.600	2.16	
140	0.95	56	395	2.52	1.32	0.429	1.10	
180	1.22	45	115	1.15	0.47	0.333	0.67	
220	1.50	38	74	1.07	0.36	0.273	0.45	
260	1.77	28	56	1.49	0.42	0.231	0.32	

Table A.2.5 Summary of breakthrough data for high voidage adsorbent structure

Bed voidage 0.289
 Length (L) 20.32cm
 X_Sect_Area 6.22cm²

Volumetric Flow Rate (cc/min)	Interstitial Velocity (cm/s)	μ (s)	σ^2 (s ²)	HETP (σ^2/μ^2)L (cm)	HETP/2v (σ^2/μ^2)L/2v (s)	1/F (s/cm ³)	1/v ² (s ² /cm ²)	Temperature (°C)
60	0.56	1581	465762	3.79	3.40	1.00	3.23	24.5
100	0.93	925	103361	2.46	1.32	0.60	1.16	24.5
140	1.30	686	58358	2.52	0.97	0.43	0.59	N/A
180	1.67	559	32128	2.09	0.63	0.33	0.36	24.5
220	2.04	445	20100	2.06	0.50	0.27	0.24	N/A
260	2.41	373	13793	2.01	0.42	0.23	0.17	N/A
60	0.56	1616	432265	3.37	3.02	1.00	3.23	22.7
100	0.93	977	120747	2.57	1.39	0.60	1.16	22.7
140	1.30	721	54099	2.11	0.81	0.43	0.59	22.7
180	1.67	534	30821	2.19	0.66	0.33	0.36	N/A
220	2.04	463	23521	2.23	0.55	0.27	0.24	22.6
260	2.41	394	13680	1.79	0.37	0.23	0.17	22.7

Table A.2.6 Summary of breakthrough data for thick adsorbent sheets structure

Bed voidage 0.230
 Length (L) 20.32cm
 X_Sect_Area 6.22cm²

Volumetric Flow Rate (cc/min)	Interstitial Velocity (cm/s)	μ (s)	σ^2 (s ²)	HETP (σ^2/μ^2)L (cm)	HETP/2v (σ^2/μ^2)L/2v (s)	1/F (s/cm ³)	1/v ² (s ² /cm ²)	Temperature (°C)
60	0.70	1546	308771	2.63	1.87	1.00	2.04	23.9
100	1.17	976	95879	2.05	0.88	0.60	0.73	23.8
140	1.63	689	38736	1.66	0.51	0.43	0.37	23.9
180	2.10	540	21914	1.53	0.36	0.33	0.23	24.1
220	2.57	444	12353	1.27	0.25	0.27	0.15	24.2
260	3.03	380	7661	1.08	0.18	0.23	0.11	24.0
60	0.70	1545	389469	3.31	2.37	1.00	2.04	23.8
100	1.17	943	99552	2.27	0.97	0.60	0.73	23.9
140	1.63	693	33761	1.43	0.44	0.43	0.37	23.6
180	2.10	544	18803	1.29	0.31	0.33	0.23	23.7
220	2.57	446	10409	1.06	0.21	0.27	0.15	23.7
260	3.03	372	7471	1.10	0.18	0.23	0.11	24.0

Table A.2.7 Summary of breakthrough data for high flow rate

Pack	FlowRate	Interstitial	Residence	Variance	HETP
		Velocity	Time		
	(SCCM)	(cm/s)	(s)	(s ²)	(cm)
mid X-section area	1200	8.37	114	321	0.50
adsorbent structure	1500	10.46	89	452	1.17
	1700	11.85	84	358	1.03
	2000	13.95	76	520	1.85
	2200	15.34	72	455	1.78
High voidage	1200	11.13	136	1372	1.51
	1500	13.91	104	1003	1.88
	1700	15.77	97	693	1.49
	2000	18.55	87	932	2.52
	2200	20.40	81	883	2.73
Thick adsorbent	1200	13.98	138	621	0.66
sheets	1500	17.48	107	542	0.97
	1700	19.81	97	510	1.10
	2000	23.31	87	556	1.48

Appendix 3: Breakthrough Curves for Breakthrough Experiments

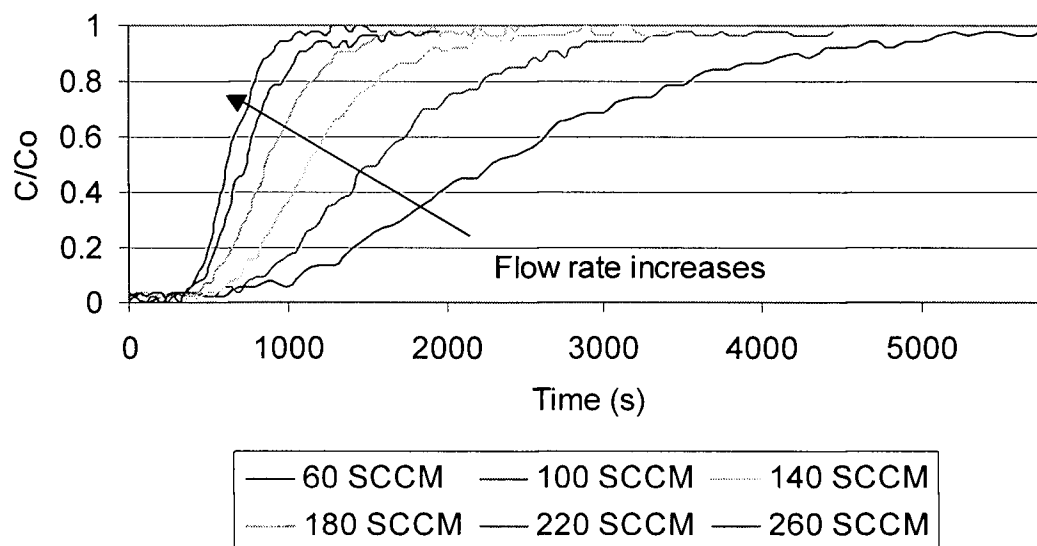


Figure A.3.1 Breakthrough curves for high X-sectional area structure

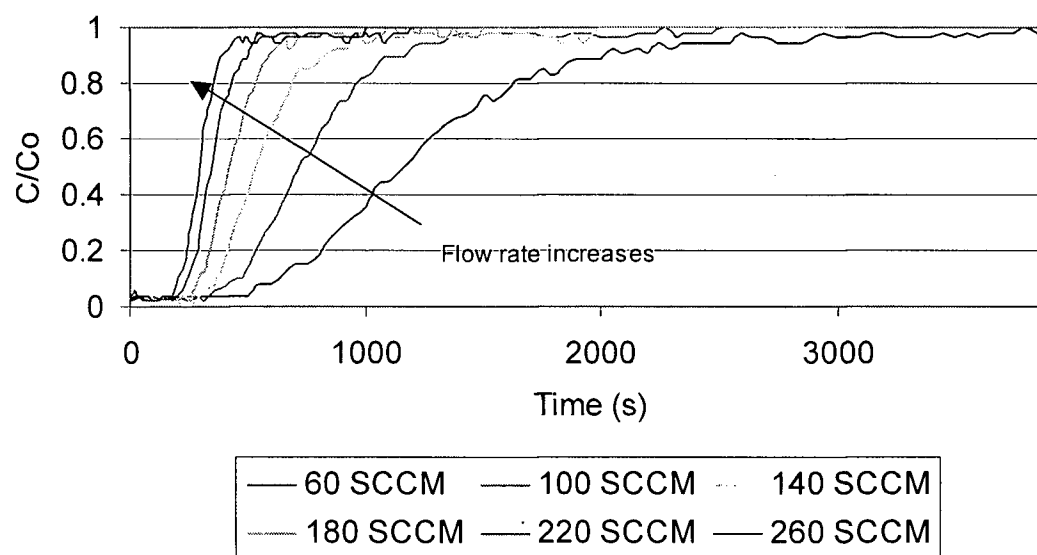


Figure A.3.2 Breakthrough curves for mid X-sectional area structure

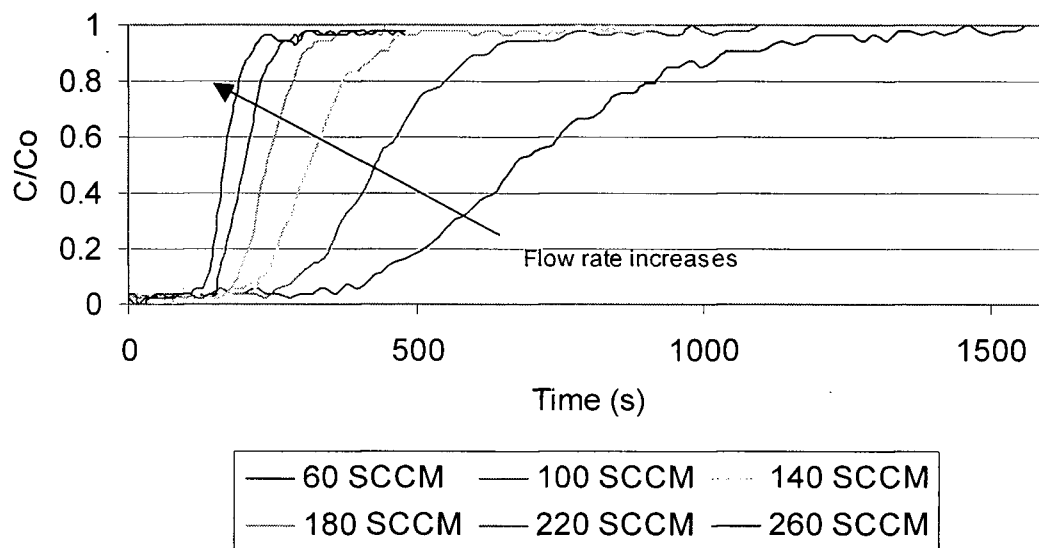


Figure A.3.3 Breakthrough curves for low X-sectional area structure

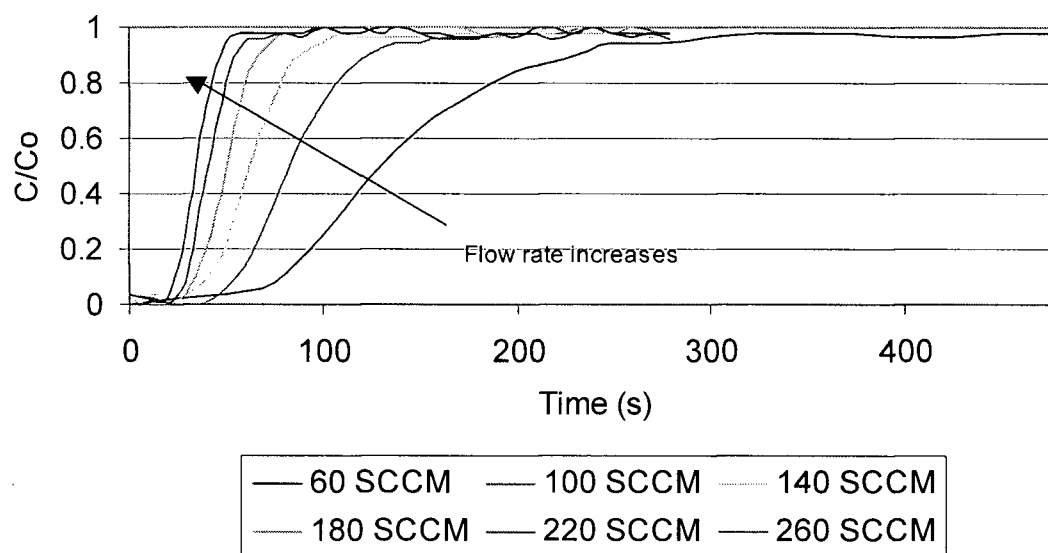


Figure A.3.4 Breakthrough curves for non-adsorbing structure

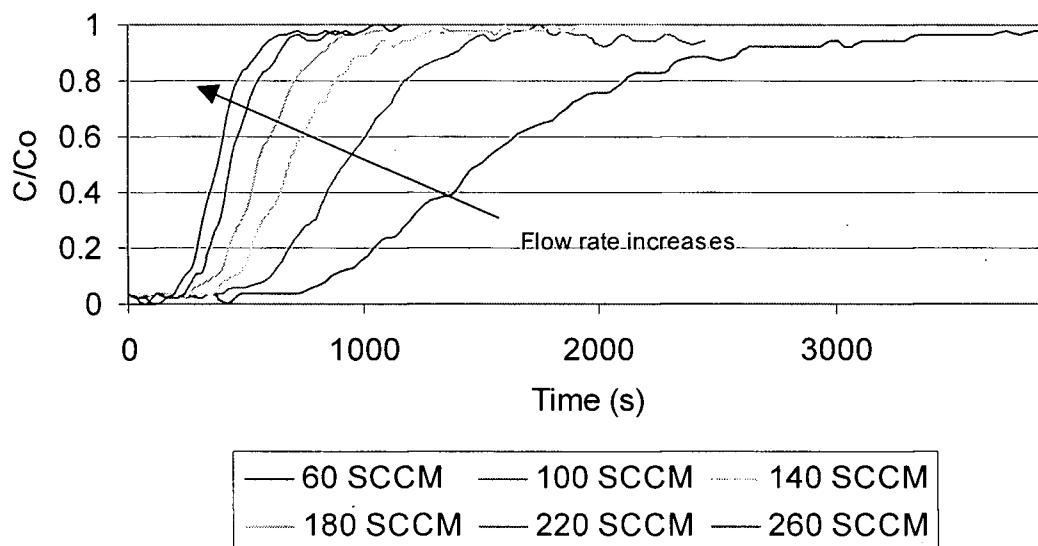


Figure A.3.5 Breakthrough curves for high voidage adsorbent structure

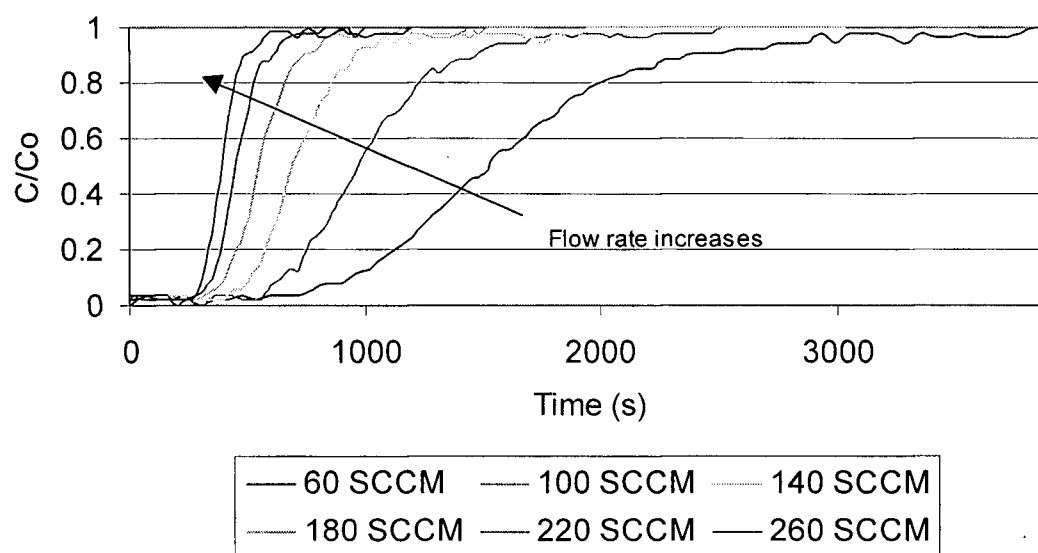


Figure A.3.6 Breakthrough curves for thick adsorbent sheets structure

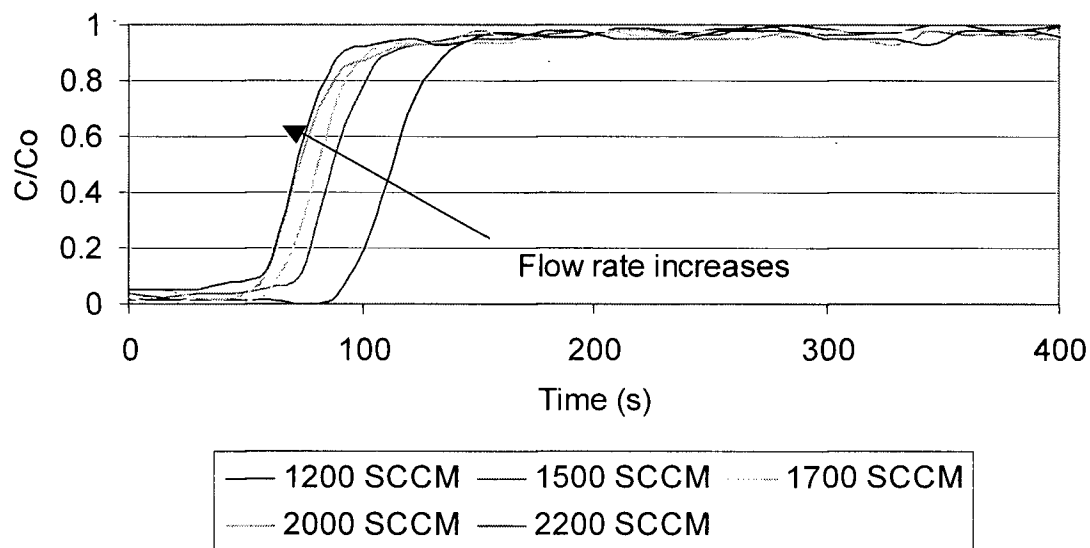


Figure A.3.7 Breakthrough curves for mid X-sectional area structure at high flow rates

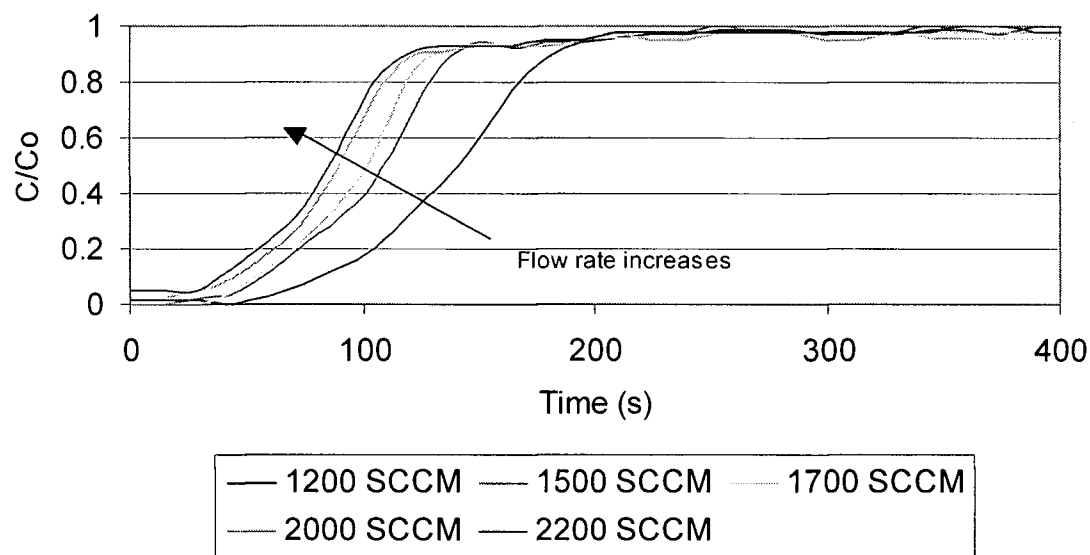


Figure A.3.8 Breakthrough curves for high voidage structure at high flow rates

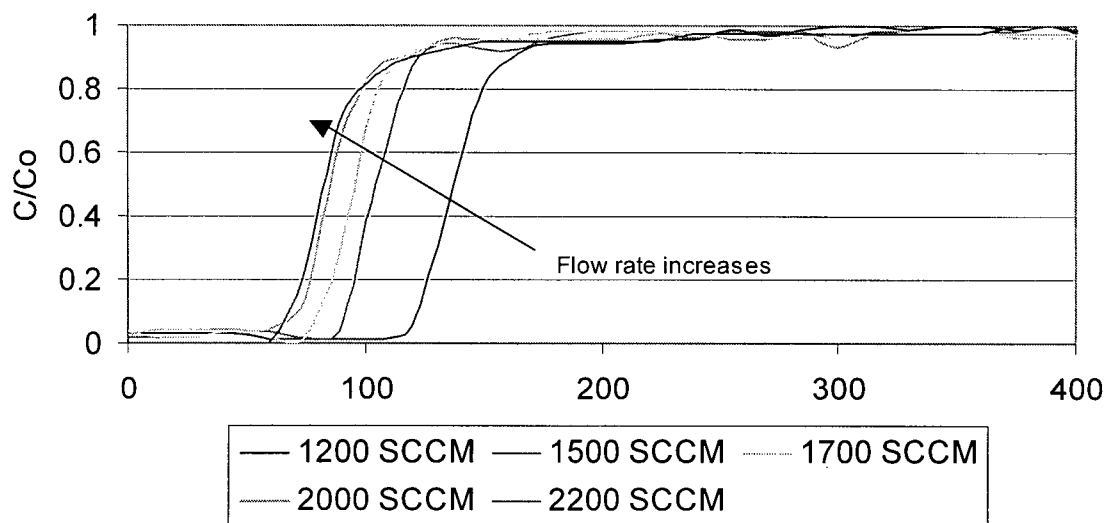


Figure A.3.9 Breakthrough curves for thick adsorbent sheets structure at high flow rates

Appendix 4: Mass Transfer Resistance Comparison

				Particle voidage	0.398							
Dm	1.229			Length	20.32							
Dp	1.93E-04			Pack voidage	0.38e/(1-e)		0.613	(1+e/1-e)/K)			1.04	
Dc	5.25E-10											
				K	14.81							
v	DL/v2	DL	Film	Macro	Micro	L/v	DL/v2	1/kK	HETP/2v	1/v2	V2/DiKk	
cm/sec				sec								
0.1	86.0	0.860	1.58E-05	0.2117	0.1090	203.2	86.03	0.5675	86.5976	100.00	0.007	
0.2	21.5	0.860	1.58E-05	0.2117	0.1090	101.6	21.51	0.5675	22.0751	25.00	0.026	
0.3	9.6	0.860	1.58E-05	0.2117	0.1090	67.7	9.56	0.5675	10.1264	11.11	0.059	
0.5	3.4	0.860	1.58E-05	0.2117	0.1090	40.6	3.44	0.5675	4.0088	4.00	0.165	
0.75	1.5	0.860	1.58E-05	0.2117	0.1090	27.1	1.53	0.5675	2.0970	1.78	0.371	
1	0.9	0.860	1.58E-05	0.2117	0.1090	20.3	0.86	0.5675	1.4279	1.00	0.66	
1.25	0.6	0.860	1.58E-05	0.2117	0.1090	16.3	0.55	0.5675	1.1181	0.64	1.031	
2	0.2	0.860	1.58E-05	0.2117	0.1090	10.2	0.22	0.5675	0.7826	0.25	2.639	
2.5	0.1	0.860	1.58E-05	0.2117	0.1090	8.1	0.14	0.5675	0.7052	0.16	4.123	
3	0.1	0.860	1.58E-05	0.2117	0.1090	6.8	0.10	0.5675	0.6631	0.11	5.936	
3.5	0.1	0.861	1.58E-05	0.2117	0.1090	5.8	0.07	0.5675	0.6378	0.08	8.079	
4	0.1	0.861	1.58E-05	0.2117	0.1090	5.1	0.05	0.5675	0.6213	0.06	10.55	
4.5	0.0	0.861	1.58E-05	0.2117	0.1090	4.5	0.04	0.5675	0.6100	0.05	13.35	
5	0.0	0.861	1.58E-05	0.2117	0.1090	4.1	0.03	0.5675	0.6020	0.04	16.48	
5.5	0.0	0.861	1.58E-05	0.2117	0.1090	3.7	0.03	0.5675	0.5960	0.03	19.94	
6	0.0	0.861	1.58E-05	0.2117	0.1090	3.4	0.02	0.5675	0.5915	0.03	23.73	
6.5	0.0	0.861	1.58E-05	0.2117	0.1090	3.1	0.02	0.5675	0.5879	0.02	27.85	
7	0.0	0.861	1.58E-05	0.2117	0.1090	2.9	0.02	0.5675	0.5851	0.02	32.29	
7.5	0.0	0.861	1.58E-05	0.2117	0.1090	2.7	0.02	0.5675	0.5829	0.02	37.07	
8	0.0	0.861	1.58E-05	0.2117	0.1090	2.5	0.01	0.5675	0.5810	0.02	42.17	
8.5	0.0	0.861	1.58E-05	0.2117	0.1090	2.4	0.01	0.5675	0.5795	0.01	47.6	
9	0.0	0.862	1.58E-05	0.2117	0.1090	2.3	0.01	0.5675	0.5782	0.01	53.35	
9.5	0.0	0.862	1.58E-05	0.2117	0.1090	2.1	0.01	0.5675	0.5771	0.01	59.44	
10	0.0	0.862	1.58E-05	0.2117	0.1090	2.0	0.01	0.5675	0.5762	0.01	65.84	
12	0.0	0.863	1.58E-05	0.2117	0.1090	1.7	0.01	0.5675	0.5735	0.01	94.74	
15	0.0	0.864	1.58E-05	0.2117	0.1090	1.4	0.00	0.5675	0.5714	0.00	147.8	
18	0.0	0.866	1.58E-05	0.2117	0.1090	1.1	0.00	0.5675	0.5702	0.00	212.4	
20	0.0	0.867	1.58E-05	0.2117	0.1090	1.0	0.00	0.5675	0.5697	0.00	261.9	
25	0.0	0.870	1.58E-05	0.2117	0.1090	0.8	0.00	0.5675	0.5689	0.00	407.5	

Appendix 5: Calculation of Mass Transfer Resistance

laminate thickness, (αR_p)	0.0068m	mid X-sectional area structure
	0.0134m	Thick adsorbent sheets structure
1/kK	0.2825s	mid X-sectional area structure
	0.5376s	Thick adsorbent sheets structure
$(\alpha R_p)^2$	4.634E-05m ²	mid X-sectional area structure
	1.785E-04m ²	Thick adsorbent sheets structure
$(\alpha R_p)^2$	0.4634cm ²	mid X-sectional area structure
	1.7847cm ²	Thick adsorbent sheets structure
r_c	1.50E-04cm	

From the 1/kK vs. $(\alpha R_p)^2$ plot

slope	0.1931	
intercept	0.193	
laminate voidage	0.398	
Dm	1.278cm ² /s	by using correlations to estimate Dm
ϵ_p is 0.398	<==laminate voidage	
$D_p = 1/(\text{slope} - 0.33D_m)/15/\square$	0.000193cm ² /s	
$D_c/r_c^2 = 1/(15K(\text{intercept}))$	0.0233s ⁻¹	micropore
D_c	5.25E-10cm ² /s	

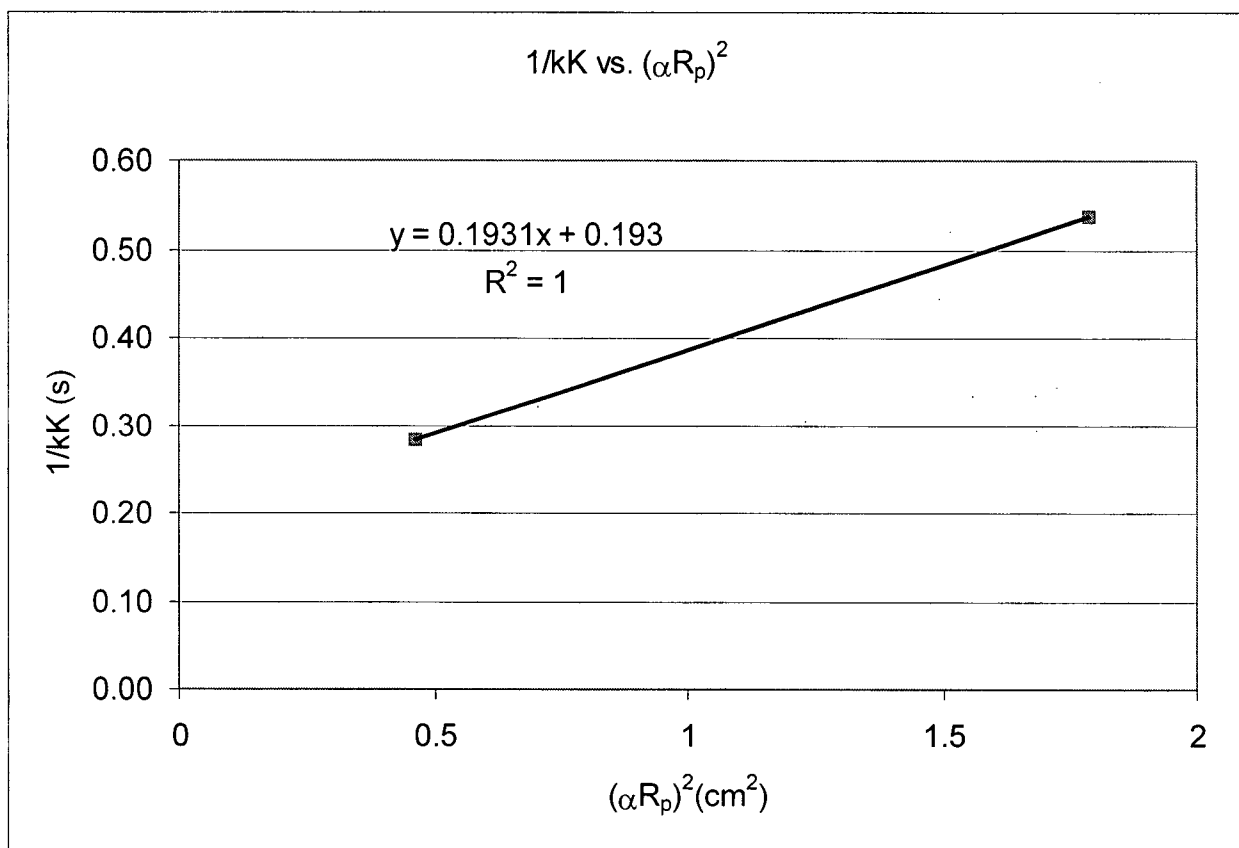


Figure A.5.1 $1/kK$ vs. $(\alpha R_p)^2$ plot used to calculate macropore and micropore mass transfer coefficient

Appendix 6: Pressure Drop Through the Structure Adsorbent Bed

Table A.6.1 Sample Pressure drop for high flow breakthrough experiments

HighFlow Pack Description	Flow rate (SCCM)	After breakthrough Inlet Pressure (psi)	Outlet Pressure (psi)	Δp (psi)	γ $(P_o/P_L)^2 - 1$	HETP correction (approximate)	HETP correction
High X-	1200	28.9	28.4	0.5	0.036	1.018	1.009
Sectional	1500	42.9	42.1	0.8	0.038	1.019	1.010
Area	2000	76.5	75.2	1.3	0.035	1.017	1.009
	2500	114.5	112.7	1.8	0.032	1.016	1.008
	3000	160.5	158.3	2.2	0.028	1.014	1.007
Mid X-	1200	28.2					
Sectional	1500	40.7					
Area	2000	69.3					
	2500	107.2					
	3000	154.4					
Low X-	1200	29.2	28.7	0.5	0.035	1.018	1.009
Sectional	1500	42.7	42	0.7	0.034	1.017	1.008
Area	2000	73.8	72.5	1.3	0.036	1.018	1.009
Non-adsorb	1200	29.1	28.6	0.5	0.035	1.018	1.009
	1500	42.1	41.4	0.7	0.034	1.017	1.008
	2000	73.8	72.7	1.1	0.030	1.015	1.008
	2500	112.7	111.1	1.6	0.029	1.015	1.007
	3000	161	159	2	0.025	1.013	1.006
bypass	1200	29.4	28.5	0.9	0.064	1.032	1.016
	1500	43.3	41.8	1.5	0.073	1.037	1.018
	2000	75.1	72.7	2.4	0.067	1.034	1.017
	2500	114.4	111.2	3.2	0.058	1.029	1.014
	3000	160.8	156.6	4.2	0.054	1.027	1.013

Table A.6.2 Sample Pressure drop for high flow breakthrough experiments

Pack Description	Flow rate (SCCM)	After breakthrough Inlet Pressure (psi)	Outlet Pressure (psi)	Δp (psi)	$\gamma (P_o/P_L)^2 - 1$	HETP correction (approximate)	HETP correction
New Data High flow							
Mid X-	1200	26	25.6	0.4	0.031	1.016	1.008
Sectional	1500	40	39.3	0.7	0.036	1.018	1.009
Area	2000	49.8	49.1	0.7	0.029	1.014	1.007
	2500	70.3	69.2	1.1	0.032	1.016	1.008
	3000	86.1	84.9	1.2	0.028	1.014	1.007
High voidage	1200	25.8	25.3	0.5	0.040	1.020	1.010
	1500	39.6	38.8	0.8	0.042	1.021	1.010
	2000	49.6	48.5	1.1	0.046	1.023	1.011
	2500	69.7	68.3	1.4	0.041	1.021	1.010
	3000	84.9	83.3	1.6	0.039	1.019	1.010
Thick adsorbent sheets	1200	25.8	25.3	0.5	0.040	1.020	1.010
	1500	39.8	39.1	0.7	0.036	1.018	1.009
	2000	49.4	48.6	0.8	0.033	1.017	1.008
	2500	70.5	69.3	1.2	0.035	1.017	1.009
	3000	85.6	84.3	1.3	0.031	1.016	1.008
Bypass	1200	28.6	27.6	1	0.074	1.037	1.018
	1500	45.7	44.2	1.5	0.069	1.035	1.017
	2000	56.9	55	1.9	0.070	1.035	1.017
	2500	78.5	76	2.5	0.067	1.033	1.017
	3000	95.6	92.8	2.8	0.061	1.031	1.015

Table A.6.3 Sample Pressure drop for low flow breakthrough experiments

Pack Description	Flow rate (SCCM)	Inlet Pressure (psi)	Outlet Pressure (psi)	Δp (psi)	$\gamma (P_o/P_L)^2 - 1$	HETP correction (approximate)	HETP correction
all packs	260	10.1	10	0.1	0.020	1.010	1.005
all packs	260	10	10	0	0.000	N/A	N/A

Appendix 7: Detailed Experimental Procedures

Low pressure (atmospheric) gravimetric method

1. Clean the sample pan from previous run
2. Put approximately 20-25 mg of sample in the pan
3. Load the sample in the TGA
4. Measure the weight of the sample (wet mass) on bypass
5. Establish He flow of 400 mL/min through the unit overnight
6. Program the TGA to heat up the sample to 450 °C at 10 °C/min
7. Hold the temperature at 450 °C for 4 hours
8. Cool down to measurement temperature, e.g., 30 °C
9. Wait until the weight signal is stable
10. Measure the weight of the sample on both bypass and with gas going through (dry mass)
11. Introduce a mixture of test gas in He with a flow rate of 400 mL/min into the TGA
12. Open the program to record the weight changes of the sample
13. Wait until the weight signal is stable, then record the weight of the sample
14. Repeat steps 11-13 for other compositions of gas until the entire isotherm is obtained (up to 1 atmospheric pressure)

High pressure (up to 3 bar) gravimetric method

1. Clean the sample pan from previous run
2. Put approximately 20-25 mg of sample in the pan
3. Load the sample in the TGA
4. Measure the weight of the sample (wet mass) on bypass
5. Establish He flow of 400 mL/min through the unit
6. Program the TGA to heat up the sample to 450 °C at 10 °C/min
7. Hold the temperature at 450 °C for 3 hours
8. Cool down to measurement temperature, e.g., 60 °C
9. Wait until the weight signal is stable
10. Record sample weight on bypass and while gas going through the unit
11. Establish a mixture of test gas and He at 400 mL/min through the unit

12. Open a file to record weight changes of the sample
13. When the weight signal is stable, record the sample weight

Repeat steps 11-13 for other compositions of gas up to the pressure of 3 bars

Volumetric method

A detailed experimental procedure including programming a sample file for volumetric measurement is as follows:

1. Obtain a clean sample tube and put quartz/glass wool in the tube to support the sample.
2. Degas the empty tube at 150 °C under vacuum for 2 hrs to drive off the moisture in the tube.
3. After the empty tube is degassed, weigh the empty tube, then, put approximately 350 mg of sample into the tube.
4. Degas the sample tube with the sample at 350 °C under vacuum for 14 hrs.
5. Weigh the sample tube again (the difference between the empty tube weight and the tube with sample yields the dry sample weight)
6. Load sample tube onto the chemisorption port.
7. Connect the two ends of the sample tube to the chemisorption unit.
8. Bring up the furnace and insulate the top of the furnace with glass wool to keep constant temperature in the furnace.
9. Turn on the fan to help cool down and stabilize the temperature at lower experimental temperature. (30 °C)
10. Program a sample file to set up the pre-treatment and experiment conditions.
11. Start the program.

Programming a sample file

The following gives a rough description of a typical pre-treatment and experiment conditions to be programmed into a sample file.

1. Evacuate the sample tube for about 30 minutes to establish vacuum. (test if the o-rings seal at both end of the sample tube)

2. Heat up the sample tube from 30 °C under vacuum to 450 °C under vacuum to drive off moisture when loading up the sample tube.
3. Hold the temperature at 450 °C under vacuum for 3 ½ hrs.
4. Cool down the sample to the experimental temperature (either 30 or 50 °C) under vacuum.
5. Continue evacuation for 30 minutes.
6. Test for leak to see if 5 µm Hg can be reached.
7. Continue evacuation for 30 minutes.
8. Begin collecting the adsorption isotherm.
9. Backfill the sample tube with He.

Desorption breakthrough experiment

A detailed experimental procedure for the desorption (breakthrough) experiment is as follows:

Loading up the laminate bed into the column

1. Uncap the black rubber cap on one end of the bed.
2. Quickly put on the adaptor and cap the end of the adaptor with the 1/8-inch cap.
3. Follow step 1-2 to put on the adaptor on the other end of the bed.
4. Bring the bed to the experimental equipment set up.
5. Uncap one end of the bed, then, quickly connect it to the 1/8-inch tube.
6. Uncap the other end of the bed, then, connect it to the 1/8-inch tube.
7. Immediately flow 30 cc/min of He through the system (i.e., through the bed) to keep moisture from getting into the adsorbent in the bed.

Running breakthrough measurements

Note: Before beginning an experiment, a flow of 30 cc/min He was established through the system after the laminate bed was attached.

1. Open the adsorbent gas cylinder.
2. Set V1 to vent.

3. Set absorbent gas flow to 50 cc/min to flush the line.
4. Turn on the mass spectrometer.
5. Turn on the protect feature in the mass spectrometer. (to automatically turn off the filament if the pressure exceeds 5×10^{-5} torr)
6. Turn on the filament.
7. Enable total pressure detector on mass spectrometer.
8. View bar graph on the mass spectrometer.
9. Wait for about 30 minutes for the pressure in the chamber of the mass spectrometer to reduce and stabilize.
10. Open the black valve to let gas from the system enters the mass spec chamber.
11. Go to the peak selection mode in the mass spectrometer.
12. Disable all peak selections except for channel two.
13. Adjust the scanning mass to an appropriate value depending on the adsorbate gas (e.g., 28 for N_2)
14. Wait until the display pressure value on channel 2 stabilizes.
15. Turn on the computer.
16. Enter Labtech notebook program.
17. Set an appropriate sampling time by adjusting the data logging frequency.
18. Set total flow rate to be tested with 5% adsorbate gas in He, for example, for the total flow rate of 100 SCCM, set adsorbate flow rate to 5 SCCM and He flow rate to 95 SCCM.
19. Wait until the flow rates stabilize.
20. Start the data logging program.
21. After having collected 25 data points, switch valve V1 from vent to the system.
22. Wait until the pressure increases until breakthrough occurs.
23. After breakthrough is reached, i.e., when the pressure does not change anymore, stop the data logging.
24. Switch valve V1 to vent.
25. Set He flow rate to 500 SCCM to flush the adsorbate gas from the laminate bed.
26. Wait until the adsorbate has been flushed out, i.e., the pressure returns to roughly the same value as before the experiment.
27. Change the total flow rate of the gas for the 5% absorbent in He mixture.
28. Repeat step 19 to 26.

Shutting down

1. Adjust the He flow rate to 30 SCCM.
2. Turn off the computer.
3. Close the black valve connecting the system to the mass spectrometer.
4. Switch valve V1 to vent.
5. Turn off adsorbate gas flow.
6. Turn off the mass spectrometer's filament.
7. Turn off the mass spectrometer.

Breakthrough method used to estimate dispersion and mass transfer coefficients

A detailed experimental procedure for the breakthrough experiment is as follows:

Loading up the laminate bed (adsorbent pack) into the column and running the experiment

1. Uncap the cap on one end of the pack
2. Bring the bed to the experimental equipment set up
3. Uncap one end of the bed, then, quickly connect it to the 1/8-inch tube
4. Uncap the other end of the bed, then, connect it to the 1/8-inch tube
5. Immediately flow 100 cc/min of He through the system (i.e., through the bed) to keep moisture from getting into the adsorbent in the bed
6. Open the adsorbate (N₂) cylinder
7. Set vent valve to vent
8. Flush the line with adsorbate gas
9. Turn on the GC and set up the data logging program.
10. Set an appropriate sampling time by adjusting the data logging frequency.
11. Set total flow rate to be tested with 5% adsorbate gas in He, for example, for the total flow rate of 1000 SCCM, set adsorbate flow rate to 50 SCCM and He flow rate to 950 SCCM.

Note: For high flow rate system: Set the reference gas (MFC2) flow rate to 30 SCCM, then set MFC3 flow rate to 30 SCCM

For low flow rate system: Set the reference gas to as close to the flow rate of the total test gas (carrier + sorbate)

12. Wait until the flow rates stabilize
13. Start the data logging program
14. After 25 seconds, switch vent valve from vent to the system
15. Wait until the TCD signal increases until breakthrough occurs
16. After breakthrough is reached, i.e., when the TCD signal does not change anymore, stop the data logging
17. Switch vent valve to vent
18. Set He flow rate to 500 SCCM to flush the absorbate gas from the laminate bed
19. Wait until the absorbate has been flushed out, i.e., the TCD signal returns to roughly the same value as before the experiment
20. Change the total flow rate of the gas for the 5% absorbent in He mixture
21. Repeat step 11 to 20 to perform experiment at different flow rate.

Shutting down

1. Turn computer off
2. Turn off the TCD
3. Take out the adsorbent pack
4. Turn off all flows and turn off the mass flow controller box
5. Close all the gas cylinders

Appendix 8: F test

Table A.8.1 F test for N₂ on NaX at 30 °C for measured and predicted values.

Volumetric			TGA			[Y(measured) - Y(average)] ²	
Pressure	Measured Amount		Pressure	Measured Amount (mmol adsorbed/g)		Volumetric	TGA
(kPa)	(mmol adsorbed/g)		(kPa)				
0.6	0.003		3	0.022		4.79E-02	3.22E-02
1.4	0.007		10	0.055		4.61E-02	2.14E-02
2.1	0.011		30	0.146		4.46E-02	3.04E-03
4.1	0.021		51	0.229		4.05E-02	7.63E-04
6.9	0.034		77	0.327		3.53E-02	1.57E-02
13.7	0.066		103	0.429		2.43E-02	5.18E-02
20.3	0.098					1.55E-02	
27.0	0.129					8.79E-03	
33.7	0.159					4.02E-03	
40.4	0.189					1.10E-03	
47.0	0.219					1.25E-05	
53.7	0.248					6.53E-04	
60.4	0.276					2.90E-03	
67.0	0.305					6.79E-03	
73.7	0.333					1.23E-02	
80.4	0.361					1.92E-02	
87.1	0.388					2.76E-02	
93.7	0.415					3.72E-02	
100.4	0.442					4.82E-02	
107.1	0.469					6.07E-02	
113.7	0.494					7.41E-02	
average	0.222		average	0.202	SSE	5.58E-01	7.30E-02
		ratio of			SSE / (d.F.)	2.79E-02	1.46E-02
		SSE/d.f.					
		vol/TGA			F-critical, $\alpha = 0.05$		
		1.91			1.96		

Table A.8.2 F test for N₂ on NaX at 50 °C for measured and predicted values.

Volumetric			TGA			[Y(predicted) - Y(average)] ²	
Pressure	Measured Amount		Pressure	Measured Amount		Volumetric	TGA
(kPa)	(mmol adsorbed/g)		(kPa)	(mmol adsorbed/g)			
0.7	0.002		3	0.013		1.64E-02	1.50E-02
1.4	0.004		10	0.037		1.58E-02	9.62E-03
2.1	0.007		31	0.090		1.53E-02	2.02E-03
4.2	0.012		51	0.149		1.39E-02	1.94E-04
6.9	0.020		77	0.220		1.21E-02	7.16E-03
13.8	0.039		103	0.302		8.38E-03	2.79E-02
20.4	0.057					5.41E-03	
27.1	0.074					3.14E-03	
33.8	0.092					1.45E-03	
40.4	0.110					4.14E-04	
47.1	0.127					7.75E-06	
53.8	0.145					2.06E-04	
60.4	0.162					9.82E-04	
67.1	0.178					2.31E-03	
73.8	0.195					4.13E-03	
80.4	0.211					6.55E-03	
87.1	0.228					9.57E-03	
93.8	0.244					1.31E-02	
100.4	0.260					1.70E-02	
107.1	0.276					2.12E-02	
113.8	0.291					2.60E-02	

average	0.130	average	0.135	SSE	1.93E-01	6.19E-02
				SSE / (d.F.)	9.66E-03	1.24E-02

ratio of
SSE/d.f.
vol/both F-critical, α = 0.05

0.78 1.96

Table A.8.3 F test for CO on NaX at 30 °C for measured and predicted values.

Volumetric		TGA			[Y(measured) - Y(average)] ²	
Pressure (kPa)	Measured Amount (mmol adsorbed/g)	Pressure (kPa)	Measured Amount (mmol adsorbed/g)		Volumetric	TGA
0.7	0.014	3	0.055		3.75E-01	2.94E-01
1.3	0.025	10	0.184		3.61E-01	1.70E-01
2.0	0.039	31	0.482		3.45E-01	1.31E-02
4.1	0.079	51	0.714		3.00E-01	1.39E-02
6.4	0.120	76	0.965		2.56E-01	1.35E-01
13.7	0.240	102	1.179		1.49E-01	3.40E-01
19.4	0.327				8.99E-02	
27.1	0.436				3.64E-02	
32.9	0.511				1.32E-02	
39.5	0.592				1.18E-03	
46.2	0.669				1.79E-03	
52.9	0.741				1.32E-02	
59.6	0.810				3.36E-02	
66.3	0.874				6.12E-02	
73.0	0.936				9.57E-02	
79.8	0.994				1.35E-01	
86.5	1.049				1.79E-01	
93.2	1.101				2.26E-01	
99.9	1.151				2.76E-01	
106.5	1.200				3.29E-01	
113.2	1.247				3.85E-01	
average	0.626	average	0.596	SSE	3.66E+00	6.26E-01
				SSE / (d.F.)	1.83E-01	1.25E-01

ratio of
SSE/d.f.
vol/TGA

F-critical, $\alpha = 0.05$

1.46 1.96

Table A.8.4 F test for CO₂ on NaX at 30 °C for measured and predicted values.

Volumetric		TGA			[Y(predicted) - Y(average)] ²	
Pressure (kPa)	Measured Amount (mmol adsorbed/g)	Pressure (kPa)	Measured Amount (mmol adsorbed/g)		Volumetric	TGA
0.6	1.768	4	2.038		9.43E+00	6.53E+00
1.3	2.230	10	3.903		6.81E+00	4.77E-01
1.9	2.525	31	4.918		5.35E+00	1.05E-01
3.8	3.098	51	5.319		3.03E+00	5.27E-01
6.5	3.597	76	5.605		1.54E+00	1.02E+00
12.9	4.275	102	5.778		3.18E-01	1.40E+00
20.0	4.705				1.81E-02	
26.8	4.971				1.75E-02	
32.9	5.150				9.68E-02	
39.8	5.310				2.22E-01	
46.7	5.444				3.66E-01	
53.8	5.554				5.11E-01	
59.5	5.631				6.28E-01	
66.1	5.712				7.62E-01	
72.9	5.783				8.90E-01	
79.6	5.849				1.02E+00	
86.5	5.904				1.13E+00	
93.1	5.959				1.25E+00	
99.9	6.008				1.37E+00	
106.6	6.053				1.47E+00	
113.3	6.093				1.57E+00	
average	4.839	average	4.594	SSE	3.78E+01	1.01E+01
				SSE / (d.F.)	1.89E+00	2.01E+00

ratio of
SSE/d.f.
vol/both

F-critical, $\alpha = 0.05$

0.94 1.96

Table A.8.5 F test for N₂ on QP at 60 °C for measured and predicted values.

Low Pressure			High Pressure			[Y(measured) - Y(predicted)] ²		[Y(predicted) - Y(average)] ²	
Pressure (kPa)	Measured Amount (mmol/g)	Predicted Amount (mmol/g)	Pressure (kPa)	Measured Amount (mmol/g)	Predicted Amount (mmol/g)	Low Pressure	High Pressure	Low Pressure	High Pressure
0.7	0.011	0.010	56	0.495	0.523	5.85E-07	8.00E-04	1.90E-01	1.90E-01
1.3	0.020	0.019	83	0.680	0.688	1.32E-06	6.36E-05	1.82E-01	7.33E-02
2.0	0.030	0.028	112	0.859	0.829	1.92E-06	8.94E-04	1.74E-01	1.69E-02
3.3	0.047	0.046	155	1.005	0.991	3.13E-06	1.81E-04	1.60E-01	1.06E-03
6.4	0.089	0.087	209	1.135	1.140	3.95E-06	3.02E-05	1.29E-01	3.30E-02
12.8	0.168	0.167	252	1.230	1.232	1.36E-06	1.34E-06	7.76E-02	7.44E-02
19.7	0.247	0.245	302	1.308	1.316	3.50E-06	5.93E-05	4.02E-02	1.27E-01
26.5	0.316	0.315				1.34E-06		1.71E-02	
33.2	0.379	0.378				1.75E-06		4.58E-03	
39.9	0.436	0.436				3.27E-07		9.60E-05	
46.6	0.489	0.489				3.02E-08		1.90E-03	
53.2	0.538	0.539				4.68E-07		8.67E-03	
59.9	0.583	0.585				3.32E-06		1.93E-02	
66.6	0.625	0.627				5.37E-06		3.30E-02	
73.3	0.665	0.667				5.49E-06		4.91E-02	
79.9	0.702	0.705				5.65E-06		6.70E-02	
86.6	0.739	0.739				2.83E-08		8.63E-02	
93.3	0.772	0.773				5.12E-07		1.07E-01	
99.9	0.805	0.803				1.99E-06		1.28E-01	
106.6	0.835	0.833				6.79E-06		1.50E-01	
113.3	0.862	0.860				2.38E-06		1.72E-01	

average 0.446 average 0.959SSE 5.12E-05 2.03E-03 1.80 0.52

SSE / (d.F.) 2.56E-06 3.38E-04 0.09 0.09

ratio of ratio of

SSE/d.f. SSE/d.f.

both high and low P low P/both High P/both

SSE 2.31

SSE / (d.F.) 0.09 1.05 1.00

F-critical, $\alpha = 0.05$ 1.95 2.36

Table A.8.6 F test for N₂ on QP at 80 °C for measured and predicted values.

Low Pressure			High Pressure			[Y(measured) - Y(predicted)] ²		[Y(predicted) - Y(average)] ²	
Pressure (kPa)	Measured Amount (mmol/g)	Predicted Amount (mmol/g)	Pressure (kPa)	Measured Amount (mmol/g)	Predicted Amount (mmol/g)	Low Pressure	High Pressure	Low Pressure	High Pressure
0.7	0.007	0.006	56	0.336	0.366	2.47E-07	9.10E-04	9.48E-02	1.50E-01
1.4	0.013	0.012	83	0.477	0.505	6.24E-07	7.71E-04	9.12E-02	6.18E-02
2.0	0.018	0.017	111	0.624	0.621	9.67E-07	1.01E-05	8.80E-02	1.76E-02
3.3	0.029	0.028	153	0.805	0.767	9.78E-07	1.46E-03	8.17E-02	1.77E-04
6.5	0.056	0.055	204	0.942	0.909	2.21E-06	1.13E-03	6.72E-02	2.40E-02
13.1	0.108	0.106	251	1.011	1.015	4.64E-06	2.00E-05	4.31E-02	6.85E-02
19.9	0.158	0.157	302	1.079	1.108	1.58E-07	8.46E-04	2.46E-02	1.26E-01
26.6	0.203	0.204				1.71E-06		1.20E-02	
33.3	0.245	0.249				1.32E-05		4.25E-03	
39.9	0.290	0.290				1.87E-07		5.57E-04	
46.6	0.331	0.331				1.25E-08		2.86E-04	
53.3	0.368	0.369				1.88E-07		3.00E-03	
59.9	0.405	0.405				6.30E-11		8.26E-03	
66.6	0.441	0.439				5.66E-06		1.57E-02	
73.3	0.472	0.472				2.51E-08		2.51E-02	
79.9	0.504	0.503				1.16E-06		3.58E-02	
86.6	0.535	0.533				3.52E-06		4.82E-02	
93.3	0.565	0.562				7.51E-06		6.16E-02	
100.1	0.586	0.590				1.74E-05		7.62E-02	
107.2	0.615	0.618				8.99E-06		9.24E-02	
113.3	0.643	0.641				4.22E-06		1.07E-01	

average 0.314 average 0.753SSE 7.36E-05 5.15E-03 0.98 0.45

SSE / (d.F.) 3.68E-06 8.59E-04 0.05 0.07

ratio of ratio of
SSE/d.f. SSE/d.f.

both high and low P

low P/both High P/both

SSE 1.43

SSE / (d.F.) 0.05 0.93 1.41

F-critical, $\alpha=0.05$ 1.95 2.36

Table A.8.7 F test for N₂ on QP at 100 °C for measured and predicted values.

Low Pressure			High Pressure			[Y(measured) - Y(predicted)] ²		[Y(predicted) - Y(average)] ²	
Pressure (kPa)	Measured Amount (mmol/g)	Predicted Amount (mmol/g)	Pressure (kPa)	Measured Amount (mmol/g)	Predicted Amount (mmol/g)	Low Pressure	High Pressure	Low Pressure	High Pressure
0.6	0.004	0.004	54	0.230	0.261	7.88E-08	9.43E-04	4.66E-02	9.79E-02
1.4	0.008	0.008	84	0.344	0.373	1.79E-07	8.27E-04	4.48E-02	4.04E-02
2.0	0.012	0.011	111	0.476	0.462	2.70E-07	1.96E-04	4.33E-02	1.25E-02
3.4	0.019	0.019	153	0.613	0.581	2.77E-07	1.06E-03	4.03E-02	4.59E-05
6.6	0.036	0.036	203	0.716	0.696	8.39E-09	3.97E-04	3.36E-02	1.49E-02
13.2	0.070	0.071	251	0.784	0.790	4.98E-07	2.84E-05	2.20E-02	4.66E-02
20.0	0.103	0.105	302	0.853	0.872	1.72E-06	3.49E-04	1.32E-02	8.87E-02
26.6	0.136	0.137				3.32E-07		6.81E-03	
33.3	0.167	0.168				3.02E-07		2.65E-03	
40.0	0.199	0.197				1.48E-06		4.82E-04	
46.7	0.227	0.226				9.55E-07		4.58E-05	
53.4	0.252	0.254				2.50E-06		1.18E-03	
60.0	0.279	0.280				9.33E-07		3.67E-03	
66.7	0.305	0.306				1.08E-07		7.44E-03	
73.4	0.330	0.330				7.02E-09		1.23E-02	
80.0	0.354	0.354				1.02E-08		1.81E-02	
86.7	0.378	0.377				6.66E-07		2.48E-02	
93.3	0.400	0.399				6.65E-07		3.23E-02	
100.0	0.425	0.421				2.19E-05		4.04E-02	
106.8	0.443	0.442				1.53E-06		4.94E-02	
114.1	0.458	0.464				2.93E-05		5.97E-02	

average 0.219 average 0.574SSE 6.38E-05 3.80E-03 0.50 0.30
SSE / (d.F.) 3.19E-06 6.33E-04 0.03 0.05

ratio of ratio of
SSE/d.f. SSE/d.f.
High
low P/both P/both

both high and low P
SSE 0.80
SSE / (d.F.) 0.03

0.84 1.68

F-critical, $\alpha = 0.05$ 1.95 2.36

Table A.8.8 F test for N₂ on NaX at 25 °C between literature and experimental results.

Pressure (kPa)	Amount Adsorbed (mmol/g)			[Y(experiment) - Y(literature)] ²	[Y(predicted) - Y(average)] ²	
	(Rege and Yang, 1997)	Experimental			Low Pressure	High Pressure
2.0	0.009	0.010		1.28E-06	3.57E-02	4.58E-02
5.0	0.021	0.024		7.99E-06	3.10E-02	3.98E-02
10.0	0.043	0.048		3.20E-05	2.40E-02	3.08E-02
20.0	0.085	0.096		1.28E-04	1.26E-02	1.62E-02
30.0	0.128	0.145		2.88E-04	4.88E-03	6.26E-03
40.0	0.170	0.193		5.11E-04	7.45E-04	9.56E-04
50.0	0.213	0.241		7.99E-04	2.32E-04	2.98E-04
60.0	0.255	0.289		1.15E-03	3.34E-03	4.28E-03
70.0	0.298	0.337		1.57E-03	1.01E-02	1.29E-02
80.0	0.340	0.386		2.05E-03	2.04E-02	2.62E-02
90.0	0.383	0.434		2.59E-03	3.44E-02	4.41E-02
100.0	0.425	0.482		3.20E-03	5.19E-02	6.67E-02
average	0.197	0.224	SSE	1.23E-02	0.2293	0.2943
			SSE / (d.F.)	1.12E-03	0.02085	0.02676

F factor 0.78

F-critical, α
=0.05 2.18

Table A.8.9 F test for N₂ on LiX at 25 °C between literature and experimental results.

				[Y(measured) - Y(predicted)] ²	[Y(predicted) - Y(average)] ²	
Pressure (kPa)	Amount Adsorbed (mmol/g) (Rege and Yang, 1997)		Experimental		Low	High
					Pressure	Pressure
2.0	0.053	0.071		3.38E-04	7.71E-01	8.25E-01
5.0	0.130	0.173		1.78E-03	6.41E-01	6.51E-01
10.0	0.255	0.328		5.34E-03	4.57E-01	4.25E-01
20.0	0.486	0.595		1.19E-02	1.98E-01	1.48E-01
30.0	0.698	0.817		1.43E-02	5.44E-02	2.63E-02
40.0	0.891	1.005		1.29E-02	1.57E-03	6.37E-04
50.0	1.069	1.165		9.20E-03	1.92E-02	3.45E-02
60.0	1.234	1.304		4.95E-03	9.18E-02	1.05E-01
70.0	1.386	1.425		1.56E-03	2.07E-01	1.99E-01
80.0	1.527	1.532		2.53E-05	3.56E-01	3.05E-01
90.0	1.659	1.627		9.99E-04	5.30E-01	4.19E-01
100.0	1.782	1.712		4.83E-03	7.24E-01	5.36E-01
average	0.931	0.980	SSE	6.81E-02	4.0496	3.6756
			SSE / (d.F.)	6.19E-03	0.36815	0.33415

F factor 1.10

F-critical, $\alpha=0.05$ 2.18

Appendix 9: Heat Adsorption Calculations

Table A.9.1 Adsorption Isotherm parameters for NaX

Method	Linear Isotherm		Langmuir Isotherm	
		$q=KP$	$q=aP/(1+bP)$	
		K, mmol/(g·kPa)	a, mmol/(g·kPa)	b, kPa ⁻¹
QA2 adsorbent				
Gravimetric	N ₂ at 30°C	0.00422		
Gravimetric	N ₂ at 50°C	0.00264		
Volumetric	N ₂ at 30°C	0.00446		
Volumetric	N ₂ at 50°C	0.00262		
Volumetric	CO at 30°C		0.01866	0.00620
Volumetric	CO at 50°C		0.01249	0.00462
Volumetric	CO ₂ at 30°C		1.88840	0.31916
Volumetric	CO ₂ at 50°C		0.99910	0.18508

Method	Gas	Temperature (K)	Henry constant or Langmuir constant, b		
				1000/T (K ⁻¹)	ln b
Gravimetric	N ₂	303	0.00422	3.30	-5.468
		323	0.00264	3.10	-5.939
Volumetric	N ₂	303	0.00446	3.30	-5.413
		323	0.00262	3.10	-5.945
Volumetric	CO	303	0.00620	3.30	-5.083
		323	0.00462	3.10	-5.377
Volumetric	CO ₂	303	0.31916	3.30	-1.142
		323	0.18508	3.10	-1.687

Method	Gas	From graph, slope =	Langmuir using b
Gravimetric	N ₂	2.3046ΔH =	19.2kJ/mol
Volumetric	N ₂	2.6032ΔH =	21.6kJ/mol
Volumetric	CO	1.4394ΔH =	12.0kJ/mol
Volumetric	CO ₂	2.6665ΔH =	22.2kJ/mol

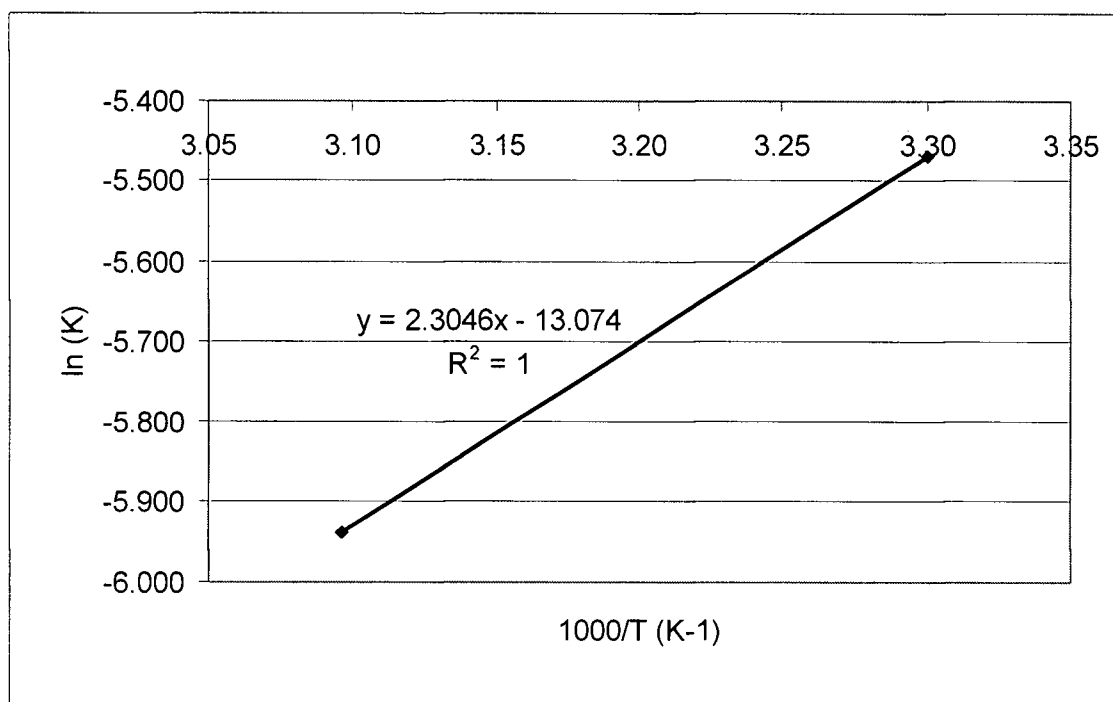


Figure A.9.1 N_2 on NaX:ln(K) vs. $1000/T$ measured gravimetrically.

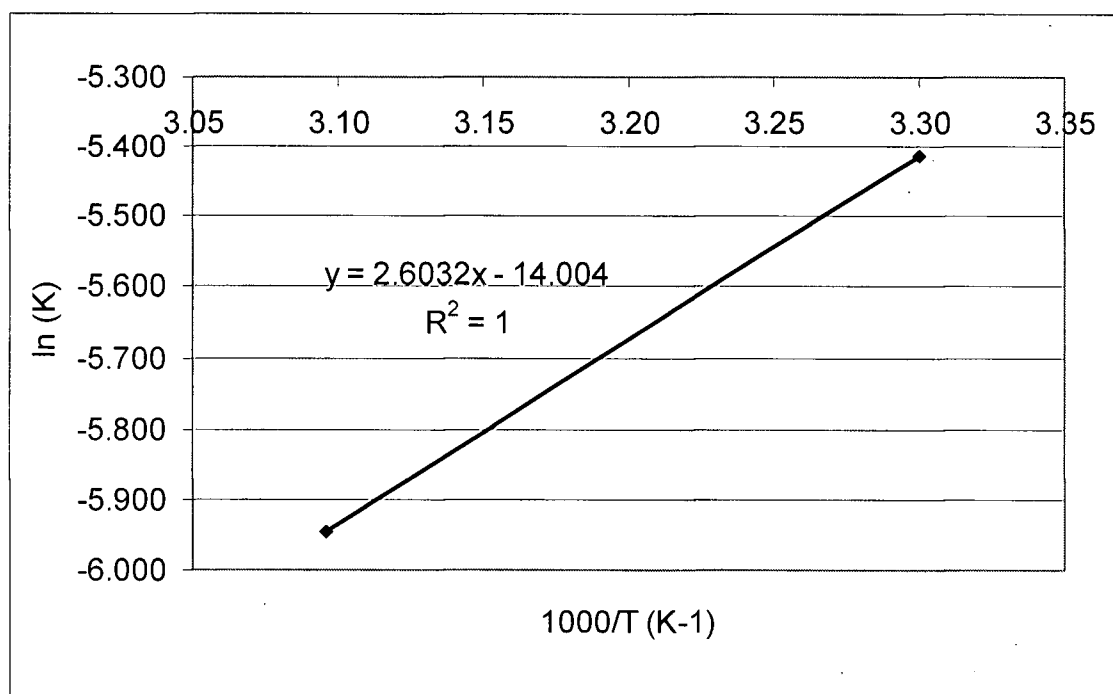


Figure A.9.2 N_2 on NaX:ln(K) vs. $1000/T$ measured volumetrically

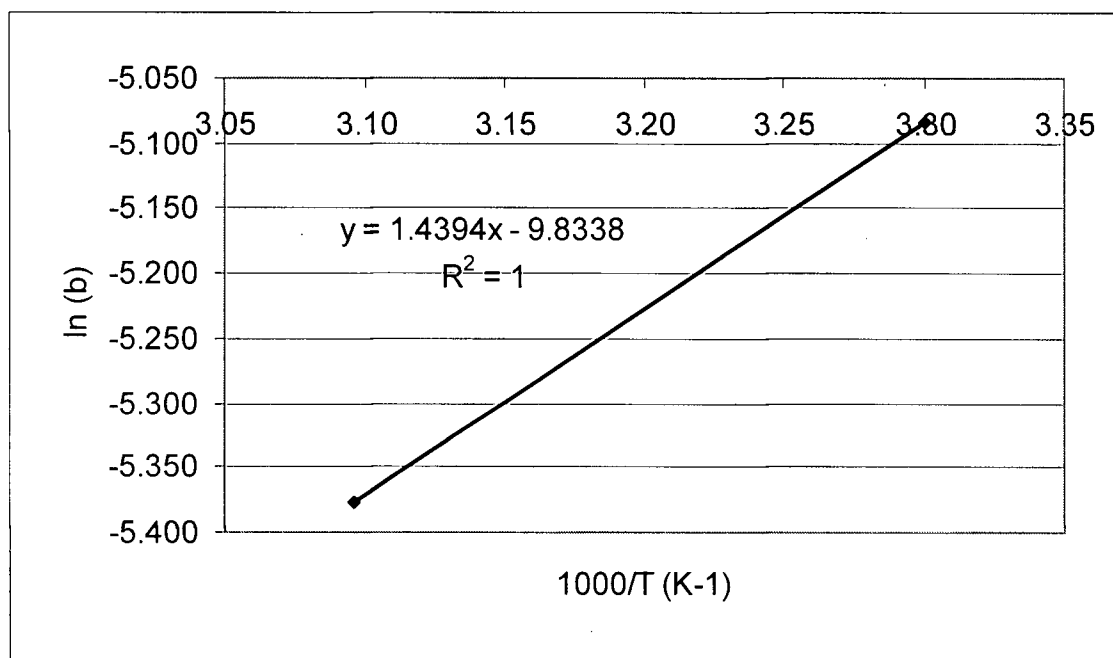


Figure A.9.3 CO on NaX: $\ln(b)$ vs. $1000/T$ measured volumetrically

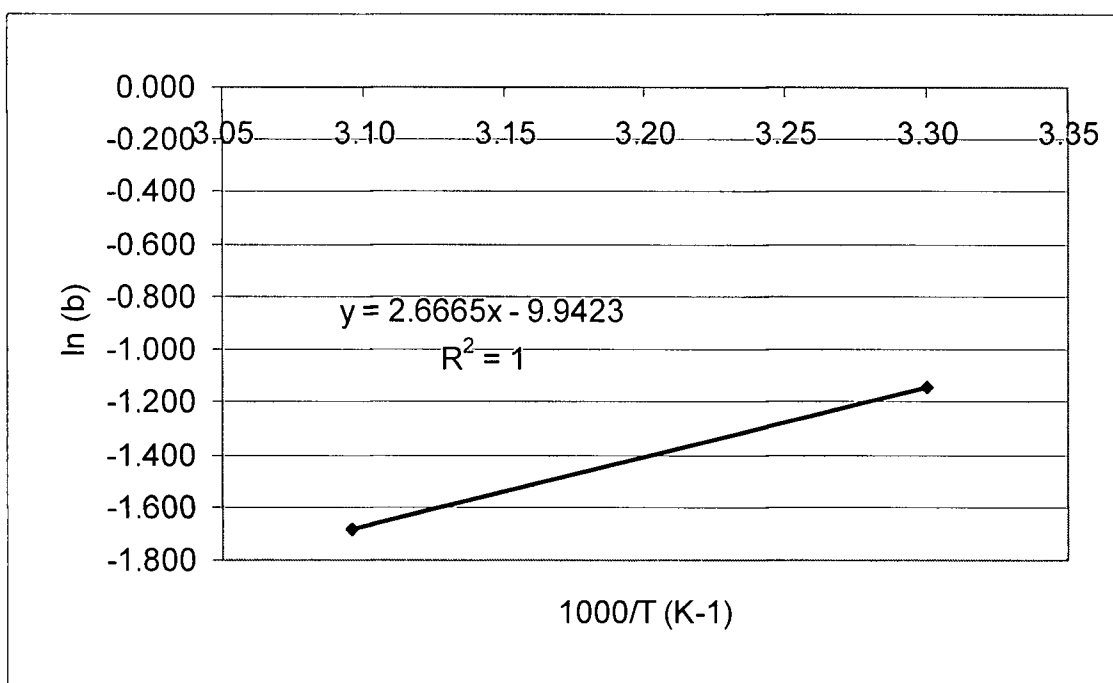


Figure A.9.4 CO₂ on NaX: $\ln(b)$ vs. $1000/T$ measured volumetrically

Table A.9.2 Adsorption Isotherm parameters for LiX

	Langmuir Isotherm $q=aP/(1+bP)$	
	a, mmol/(g·kPa)	b, kPa ⁻¹
QA N₂ adsorbent		
N ₂ at 30°C	0.02461	0.00775
N ₂ at 40°C	0.01700	0.00576
N ₂ at 50°C	0.00983	0.00343
N ₂ at 60°C	0.00652	0.00176
N ₂ at 80°C	0.00437	0.00041

Temperature (K)	Langmuir constant, b	1000/T (K ⁻¹)	ln b
303	0.00775	3.30	-4.861
313	0.00576	3.19	-5.158
323	0.00343	3.10	-5.676
333	0.00176	3.00	-6.342
353	0.00041	2.83	-7.790

From graph, slope = $\Delta H =$ 41.4 kJ/mol

Langmuir using b 4.9814

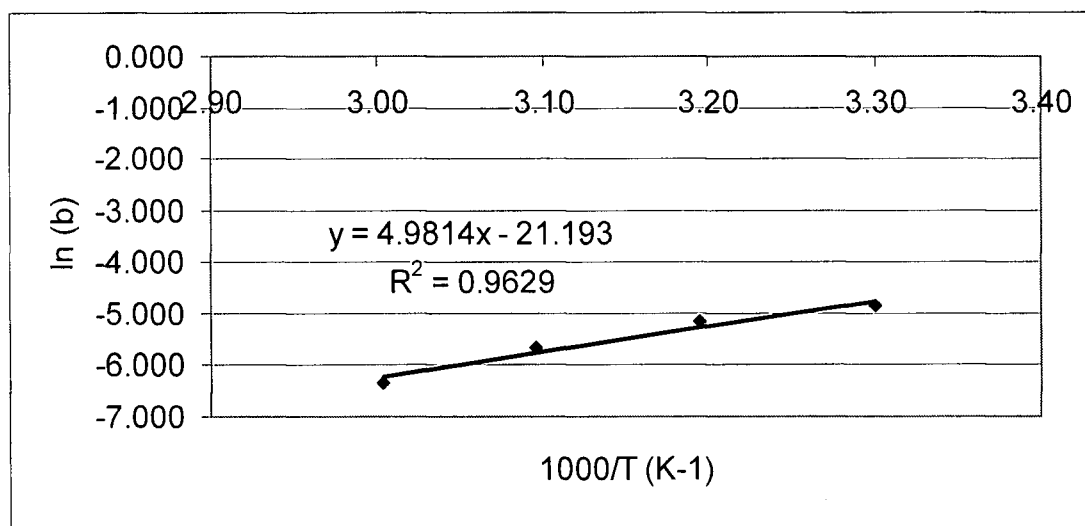


Figure A.9.5 N₂ on LiX:ln(b) vs. 1000/T measured gravimetrically

Appendix 10: Matlab™ Program

Comparison of predicted and measured C/Co

```
clear;
clear all;
clc;

tic;

%bks3_model3TaueiditJune14_03.m is a m-file that predicts breakthrough curve based on
extracted values
%and compare it with raw data at flow rates where raw data is available.
%Parameters extracted used here are derived based on using the bed voidage without the
laminar voidage

%defining some values

%Length of adsorption pack (in cm)

z = 20.32;

%Laminar voidage

ep = 0.398;

%Mass transfer resistances

%kf (in cm/s) Dp (in cm2/s) Dc (in cm2/s) rc (cm)

%Dm = 0.64/0.7; %cm2/s
%Rpfull = 0.02159/2; %cm
%Sh = 2*kf*Rp/Dm = 2, kf = Dm/Rp;

%kf = Dm/Rpfull; %kf = 0.0107;

Dc = 5.25e-10;
rc = 1.5e-4;

Number = input('Please enter the number of times you want to run the program \n');
for c=1:Number

    totaltime = input('Please enter the total time for breakthrough (sec) \n');

    if totaltime > 20000
        fprintf('Maximum Simulation time exceeded');
        break
    elseif totaltime <= 0
```

```

    fprintf('Simulation time can not be less than or equal to zero');
    break
end

Q = input('Please enter the volumetric flowrate of gas (SCCM) \n');

    if Q > 10000
        fprintf('Maximum Simulation flowrate exceeded');
        break
    elseif Q <= 0
        fprintf('Simulation flowrate can not be less than or equal to zero');
        break
    end

    pack = input(' Please enter which pack you want to run the simulation for\n 1 = Full-size
    pack (A244)\n 2 = Half-size pack (A267)\n 3 = Quarter-size pack\n 4 = non-adsorbing pack\n 5
    = space-height pack\n 6 = laminate-thickness pack\n');

%cross-sectional area of different packs (in cm2)

    cross        = [12.41 6.29 3.70 6.14 6.22 6.22];

%including laminate voidage of different packs

    voidage      = [0.413 0.380 0.380 0.399 0.289 0.230];

    lam_thick(1,1:6) = lam_thick/2;
%Henry constant (vol/vol) for (including laminate voidage in calculating interstitial velocity)

    Henry = [17.81 14.81 13.83 1.04 17.48 15.88];

%Dispersion coefficient (cm2/sec) (including laminate voidage in calculating interstitial
velocity)

    Disperse = [0.64 0.89 0.90 0.84 0.90 0.97];

    for n = 1:6
        if pack == n
            xsect = cross(n);
            void = voidage(n);
            Rp = lam_thick(n);
            K = Henry(n);
            DL = Disperse(n);
        end
    end

v = Q/(xsect*void*60);
Dm = DL/0.7;

```

```

kf = Dm/Rp;                                %kf = 0.0107;

% 1/Kk'

mass_x_fer = (DL/v^2)*((1-void)/void)+((Rp/(3*kf))+
(Rp^2/(15*ep*Dp)))+(rc^2/(15*K*Dc)));

%k'

kprime = 1/(mass_x_fer*K);

%Calculating Xi (the dimensionless bed length

Xi = (kprime*K*z/v)*((1-void)/void);

%Calculating the predicted C/Co

for t = b:1:totaltime
    if t < z/v
        b=t+1;
    else
        Tau(t) = kprime*(t-z/v);
        X = sqrt(Xi)-sqrt(Tau(t));
        storetime(t)=t;
        conc3(t) = (1/2)*erfc(X);
    end

end

%Initializing adsorption time vector

Time1=0;

%Initializing Total time to read the raw data (number of data required) for comparison

totaltimeraw = totaltime;

%Reading raw data for adsorption time from 0 to saturation and concentration up to saturation
and/or
%reading adsorption time and concentration (C/Co) up to the time inputted by user to run the
simulation

if pack == 1
    if Q==60
        totaltimeraw=totaltime/2;
        [Time1,concrow]=textread('FullA244_C_over_Co_60.txt','%d %f',totaltimeraw);
    elseif Q==100

```

```

    totaltimeraw=totaltime/2;
    [Time1,concrow]=textread('FullA244_C_over_Co_100.txt','%d %f',totaltimeraw);
elseif Q==140
    totaltimeraw=totaltime/2;
    [Time1,concrow]=textread('FullA244_C_over_Co_140.txt','%d %f',totaltimeraw);
    elseif Q==180
    totaltimeraw=totaltime/2;
    [Time1,concrow]=textread('FullA244_C_over_Co_180.txt','%d %f',totaltimeraw);
    elseif Q==220
    totaltimeraw=totaltime/2;
    [Time1,concrow]=textread('FullA244_C_over_Co_220.txt','%d %f',totaltimeraw);
    elseif Q==260
    totaltimeraw=totaltime/2;
    [Time1,concrow]=textread('FullA244_C_over_Co_260.txt','%d %f',totaltimeraw);
    end
end

if pack == 2
    if Q==60
        totaltimeraw=totaltime/2;
        [Time1,concrow]=textread('Half_C_over_Co_60.txt','%d %f',totaltimeraw);
        elseif Q==100
        totaltimeraw=totaltime/2;
        [Time1,concrow]=textread('Half_C_over_Co_100.txt','%d %f',totaltimeraw);
        elseif Q==140
        totaltimeraw=totaltime/2;
        [Time1,concrow]=textread('Half_C_over_Co_140.txt','%d %f',totaltimeraw);
        elseif Q==180
        totaltimeraw=totaltime/2;
        [Time1,concrow]=textread('Half_C_over_Co_180.txt','%d %f',totaltimeraw);
        elseif Q==220
        totaltimeraw=totaltime/2;
        [Time1,concrow]=textread('Half_C_over_Co_220.txt','%d %f',totaltimeraw);
        elseif Q==260
        totaltimeraw=totaltime/2;
        [Time1,concrow]=textread('Half_C_over_Co_260.txt','%d %f',totaltimeraw);
    elseif Q==1200
        totaltimeraw=totaltime/0.5;
        [Time1,concrow]=textread('Half_C_over_Co_1200to2200.txt','%f %f %*f %*f %*f
%*f',totaltimeraw);
    elseif Q==1500
        totaltimeraw=totaltime/0.5;
        [Time1,concrow]=textread('Half_C_over_Co_1200to2200.txt','%f %*f %f %*f %*f
%*f',totaltimeraw);
    elseif Q==1700
        totaltimeraw=totaltime/0.5;
        [Time1,concrow]=textread('Half_C_over_Co_1200to2200.txt','%f %*f %*f %f %*f
%*f',totaltimeraw);
    elseif Q==2000

```

```

        totaltimeraw=totaltime/0.5;
        [Time1,concrow]=textread('Half_C_over_Co_1200to2200.txt','%f%f%f%f%f%f%f%f',totaltimeraw);
    elseif Q==2200
        totaltimeraw=totaltime/0.5;
        [Time1,concrow]=textread('Half_C_over_Co_1200to2200.txt','%f%f%f%f%f%f%f%f',totaltimeraw);
    end
end

if pack == 3
    if Q==60
        totaltimeraw=totaltime;
        [Time1,concrow]=textread('Quarter_C_over_Co_60.txt','%d%f',totaltimeraw);
    elseif Q==100
        totaltimeraw=totaltime;
        [Time1,concrow]=textread('Quarter_C_over_Co_100.txt','%d%f',totaltimeraw);
    elseif Q==140
        totaltimeraw=totaltime;
        [Time1,concrow]=textread('Quarter_C_over_Co_140.txt','%d%f',totaltimeraw);
    elseif Q==180
        totaltimeraw=totaltime;
        [Time1,concrow]=textread('Quarter_C_over_Co_180to260.txt','%d%f%f',totaltimeraw);
    elseif Q==220
        totaltimeraw=totaltime;
        [Time1,concrow]=textread('Quarter_C_over_Co_180to260.txt','%d%f%f',totaltimeraw);
    elseif Q==260
        totaltimeraw=totaltime;
        [Time1,concrow]=textread('Quarter_C_over_Co_180to260.txt','%d%f%f',totaltimeraw);
    end
end

if pack == 4
    if Q==60
        totaltimeraw=totaltime/0.5;
        [Time1,concrow]=textread('nonadsorb_C_over_Co_60.txt','%f%f',totaltimeraw);
    elseif Q==100
        totaltimeraw=totaltime/0.5;
        [Time1,concrow]=textread('nonadsorb_C_over_Co_100to260.txt','%f%f%f%f%f%f%f',totaltimeraw);
    elseif Q==140
        totaltimeraw=totaltime/0.5;
        [Time1,concrow]=textread('nonadsorb_C_over_Co_100to260.txt','%f%f%f%f%f%f',totaltimeraw);
    elseif Q==180
        totaltimeraw=totaltime/0.5;

```

```

[Time1,concrow]=textread('nonadsorb_C_over_Co_100to260.txt','%f%f%f%f%f%f%f%f%f');
elseif Q==220
totaltimeraw=totaltime/0.5;
[Time1,concrow]=textread('nonadsorb_C_over_Co_100to260.txt','%f%f%f%f%f%f%f%f%f');
elseif Q==260
totaltimeraw=totaltime/0.5;
[Time1,concrow]=textread('nonadsorb_C_over_Co_100to260.txt','%f%f%f%f%f%f%f%f%f');
end
end

if pack == 5
if Q==60
totaltimeraw=totaltime/2;
[Time1,concrow]=textread('spaceheight_C_over_Co_60.txt','%d%f',totaltimeraw);
elseif Q==100
totaltimeraw=totaltime/2;
[Time1,concrow]=textread('spaceheight_C_over_Co_100.txt','%d%f',totaltimeraw);
elseif Q==140
totaltimeraw=totaltime/2;
[Time1,concrow]=textread('spaceheight_C_over_Co_140.txt','%d%f',totaltimeraw);
elseif Q==180
totaltimeraw=totaltime/2;
[Time1,concrow]=textread('spaceheight_C_over_Co_180.txt','%d%f',totaltimeraw);
elseif Q==220
totaltimeraw=totaltime/2;
[Time1,concrow]=textread('spaceheight_C_over_Co_220.txt','%d%f',totaltimeraw);
elseif Q==260
totaltimeraw=totaltime/2;
[Time1,concrow]=textread('spaceheight_C_over_Co_260.txt','%d%f',totaltimeraw);
elseif Q==1200
totaltimeraw=totaltime/0.5;
[Time1,concrow]=textread('spaceheight_C_over_Co_1200to2200.txt','%f%f%f%f%f%f%f%f%f');
elseif Q==1500
totaltimeraw=totaltime/0.5;
[Time1,concrow]=textread('spaceheight_C_over_Co_1200to2200.txt','%f%f%f%f%f%f%f%f%f');
elseif Q==1700
totaltimeraw=totaltime/0.5;
[Time1,concrow]=textread('spaceheight_C_over_Co_1200to2200.txt','%f%f%f%f%f%f%f%f%f');
elseif Q==2000
totaltimeraw=totaltime/0.5;
[Time1,concrow]=textread('spaceheight_C_over_Co_1200to2200.txt','%f%f%f%f%f%f%f%f%f');
elseif Q==2200

```



```

        totaltimeraw=totaltime/0.5;
        [Time1,concrow]=textread('spaceheight_C_over_Co_1200to2200.txt','%f %f %f %f %f %f %f',totaltimeraw);
    end
end

if pack == 6
    if Q==60
        totaltimeraw=totaltime/2;
        [Time1,concrow]=textread('thickness_C_over_Co_60.txt','%d %f',totaltimeraw);
    elseif Q==100
        totaltimeraw=totaltime/2;
        [Time1,concrow]=textread('thickness_C_over_Co_100.txt','%d %f',totaltimeraw);
    elseif Q==140
        totaltimeraw=totaltime/2;
        [Time1,concrow]=textread('thickness_C_over_Co_140.txt','%d %f',totaltimeraw);
    elseif Q==180
        totaltimeraw=totaltime/2;
        [Time1,concrow]=textread('thickness_C_over_Co_180.txt','%d %f',totaltimeraw);
    elseif Q==220
        totaltimeraw=totaltime/2;
        [Time1,concrow]=textread('thickness_C_over_Co_220.txt','%d %f',totaltimeraw);
    elseif Q==260
        totaltimeraw=totaltime/2;
        [Time1,concrow]=textread('thickness_C_over_Co_260.txt','%d %f',totaltimeraw);
    elseif Q==1200
        totaltimeraw=totaltime/0.5;
        [Time1,concrow]=textread('thickness_C_over_Co_1200to2200.txt','%f %f %f %f %f %f %f',totaltimeraw);
    elseif Q==1500
        totaltimeraw=totaltime/0.5;
        [Time1,concrow]=textread('thickness_C_over_Co_1200to2200.txt','%f %f %f %f %f %f %f',totaltimeraw);
    elseif Q==1700
        totaltimeraw=totaltime/0.5;
        [Time1,concrow]=textread('thickness_C_over_Co_1200to2200.txt','%f %f %f %f %f %f %f',totaltimeraw);
    elseif Q==2000
        totaltimeraw=totaltime/0.5;
        [Time1,concrow]=textread('thickness_C_over_Co_1200to2200.txt','%f %f %f %f %f %f %f',totaltimeraw);
    elseif Q==2200
        totaltimeraw=totaltime/0.5;
        [Time1,concrow]=textread('thickness_C_over_Co_1200to2200.txt','%f %f %f %f %f %f %f',totaltimeraw);
    end
end

```

%inputting flow rates that raw data are available for comparison for each pack

```

if pack == 1
    flowmat = [60 100 140 180 220 260];
elseif pack == 2
    flowmat = [60 100 140 180 220 260 1200 1500 1700 2000 2200];
elseif pack == 3
    flowmat = [60 100 140 180 220 260];
elseif pack == 4
    flowmat = [60 100 140 180 220 260];
elseif pack == 5
    flowmat = [60 100 140 180 220 260 1200 1500 1700 2000 2200];
elseif pack == 6
    flowmat = [60 100 140 180 220 260 1200 1500 1700 2000 2200];
end

%Initializing variables required to plot model in case the inputted flow rates does not match
%raw data flow rates

realtimeraw = 0;
d = 1;

for e = 1:length(flowmat)
    if Q == flowmat(e)
        for d=2:length(Time1)
            if Time1(d)<Time1(d-1)
                realtimeraw = d-4;
                break
            end
        end
    end
end

if realtimeraw ~= d-4
    realtimeraw = totaltimeraw;
end

realtimeraw = fix(realtimeraw);

if realtimeraw == 0
    realtimeraw = totaltimeraw
end

testing = realtimeraw;

if Time1 == 0
    realtimeraw = realtimeraw;
elseif Time1(2)-Time1(1) == 1
    realtimeraw = realtimeraw;
elseif Time1(2)-Time1(1) == 0.5

```

```

temp = 1;
realtimeraw = realtimeraw/2;
for g = 1:2:length(Time1)
    Time1temp(temp) = Time1(g);
    concrawtemp(temp) = concraw(g);
    temp = temp + 1;
end

```

```

concraw = concrawtemp;
Time1 = Time1temp;
end

```

```

realtimeraw = fix(realtimeraw);

if realtimeraw > length(Time1)
    realtimeraw = length(Time1);
end

```

```

h = realtimeraw;
bb=0;
for g=1:h

    Tau2(g) = kprime*(Time1(g)-z/v);

end

```

```

end

```

```

p=b;

```

```

%Plotting the predicted C/Co and raw data to compare

```

```

if totaltime < b
    fprintf('Insufficient totaltime specified');
    break
end

```

```

rawda = 0;
if length(flowmat)>1
    for f = 1:length(flowmat)
        if Q == flowmat(f)
            figure(c)
            plot(Tau(b:t),conc3(b:t),'b^',Tau2(b:realtimeraw),concraw(b:realtimeraw),'mo');
            xlabel('Tau');
            ylabel('C/Co');
            title('C/Co vs. Tau');
            legend('model3','raw');
            rawda = 1;
        end
    end
end

```

```

        end
    end
end

if rawda ~=1
    figure(c)
    plot(Tau(b:t),conc3(b:t),'b^');
    xlabel('Tau');
    ylabel('C/Co');
    title('C/Co vs. Time');
    legend('model3');

end

Xi

end

toc

Tau2temp=Tau2';
conc3temp=conc3';
Tautemp=Tau';
concrawtemp=concraw';

for o=1:length(conc3temp)
    p=2*o;
    if p>length(conc3temp)
        break
    end
    conc3temp2(o) = conc3temp(p);
end

%writing the results to text file to be used to plot the C/Co vs. Tau for predicted and measured
values
%in Microsolf Excel

y = [Time1;concraw;storetimetemp;conc3temp2];
fid = fopen('Thickness100June14.txt','wt');
fprintf(fid,'%6.4f\n',y);
fclose(fid);

```

Comparison of the effects of changing dispersion, film mass transfer coefficient, macropore mass transfer coefficient, and micropore mass transfer coefficient

```

clear;
clear all;
clc;

tic;

%bk_para_mod_Dec12Tauedit.m is a m-file that predicts breakthrough curve based on extracted
values and compare it with
%raw data at flow rates where raw data is available.
%Parameters extracted used here are derived based on using the bed voidage without the
laminar voidage

%Testing for changing in packing

%defining some values

%Length of adsorption pack (in cm)

z = 20.32;

%Laminar voidage

ep = 0.398;

%Mass transfer resistances

%kf (in cm/s) Dp (in cm2/s) Dc (in cm2/s) rc (cm)

Dp(1) = 0.000193;           %Dp(1) = 0.000775;
Dc(1) = 5.25e-10;
rc(1) = 1.5e-4;

Number = input('Please enter the number of times you want to run the program \n');
for c=1:Number

    totaltime = input('Please enter the total time for breakthrough (sec) \n');

    if totaltime > 20000
        fprintf('Maximum Simulation time exceeded');
        break
    elseif totaltime <= 0
        fprintf('Simulation time can not be less than or equal to zero');
        break
    end

    Q = input('Please enter the volumetric flowrate of gas (SCCM) \n');

```

```

if Q > 10000
    fprintf('Maximum Simulation flowrate exceeded');
    break
elseif Q <= 0
    fprintf('Simulation flowrate can not be less than or equal to zero');
    break
end

pack = input(' Please enter which pack you want to run the simulation for\n 1 = Full-size
pack (A244)\n 2 = Half-size pack (A267)\n 3 = Quarter-size pack\n 4 = non-adsorbing pack\n 5
= space-height pack\n 6 = laminate-thickness pack\n');

    if pack > 6
        nottrue = 1;
    elseif pack < 1
        nottrue = 1;
    else
        nottrue = 0;
    end

    if nottrue == 1
        fprintf('Must select the number from 1 to 6');
        break
    end

%cross-sectional area of different packs (in cm2)

    cross = [12.41 6.29 3.70 6.14 6.22 6.22];

%including laminate voidage of different packs

    voidage(1,1:6) = [0.413 0.380 0.380 0.399 0.289 0.230];

    lam_thick(1,1:6) = lam_thick/2;

%Henry constant (vol/vol) for (including laminate voidage in calculating interstitial velocity)

    Henry = [17.81 14.81 13.83 1.04 17.48 15.88];

%Dispersion coefficient (cm2/sec) (including laminate voidage in calculating interstitial
velocity)

Disperse = [0.64 0.89 0.90 0.84 0.90 0.97];

    for n = 1:6
        if pack == n

```

```

        xsect = cross(n);
        void(1) = voidage(1,n);
        Rp(1) = lam_thick(1,n);
        K = Henry(n);
        DL = Disperse(n);
    end
end

Dm = DL/0.7;
kf(1) = Dm/Rp(1);

per_lam = input('Please enter the percentage that the laminate thickness changes by \n positive
number = increase in laminate thickness \n negative number = decrease in laminate thickness
\n');

if per_lam ~= 0
    perc = 1+per_lam/100;
elseif per_lam == 0
    perc = 1;
end

if per_lam <= -100
    fprintf('changed in laminate thickness can not exceed -100%');
    break
end

per_spac = input('Please enter the percentage that the space height changes by \n positive
number = increase in space height \n negative number = decrease in space height \n');

if per_spac ~= 0
    perc2 = 1+per_spac/100;
elseif per_spac == 0
    perc2 = 1;
end

if per_spac <= -100
    fprintf('changed in space height can not exceed -100%');
    break
end

Rp(2) = perc*Rp(1);

%Pack dimension (m)

width = [6.248e-2 3.175e-2 1.867e-2 3.099e-2 3.099e-2 3.099e-2];
height = [1.986e-2 1.981e-2 1.981e-2 1.981e-2 2.007e-2 2.007e-2];

```

```

% New(changed) space height

newspacer = perc2*spacer(1,pack);

%Defining total volume of laminate (m3)

vollam(1,1:6) = [1.480e-4 7.341e-5 4.317e-5 8.059e-5 8.861e-5 1.004e-4];

totallhtemp = totallh(pack)-Rp(2)/100;

%thickness or height of one laminate sheet and one spacer (m)

onelayer = Rp(2)/100+newspacer;

%changed(new) number of spacers and sheets

numspac = totallh(pack)/onelayer;
numlam = numspac + 1;

%changed(new) volume of spacers and sheets

newvollam = width(pack)*height(pack)*(Rp(2)/100)*numlam;
newvolspac = width(pack)*height(pack)*newspacer*numspac;

%changed(new) total volume (spacers + laminates)(m3)

newtotvol = newvollam+newvolspac;

%void(2) = 1 - newvollam/newtotvol;

void(2) = void(1);

per_kf = input('Please enter the percentage that the external fluid film changes by \n positive
number = increase in parameter value \n negative number = decrease in parameter value \n');
per_Dp = input('Please enter the percentage that the macropore diffusivity changes by \n
positive number = increase in parameter value \n negative number = decrease in parameter value
\n');
per_Dc = input('Please enter the percentage that the micropore diffusivity changes by \n
positive number = increase in parameter value \n negative number = decrease in parameter value
\n');
per_rc = input('Please enter the percentage that the zeolite crystal diameter changes by \n
positive number = increase in diameter \n negative number = decrease in diameter \n');
per_DL = input('Please enter the percentage that the dispersion changes by \n positive number
= increase in dispersion number \n negative number = decrease in dispersion number \n');

if per_kf ~= 0
    perc_kf = 1+per_kf/100;
elseif per_kf == 0

```



```

    perc_kf = 1;
    end

    if per_kf <= -100
        fprintf('changed in laminate thickness can not exceed -100%');
        break
    end

    if per_Dp ~= 0
        perc_Dp = 1+per_Dp/100;
    elseif per_Dp == 0
        perc_Dp = 1;
    end

    if per_Dp <= -100
        fprintf('changed in laminate thickness can not exceed -100%');
        break
    end

    if per_Dc ~= 0
        perc_Dc = 1+per_Dc/100;
    elseif per_Dc == 0
        perc_Dc = 1;
    end

    if per_Dc <= -100
        fprintf('changed in laminate thickness can not exceed -100%');
        break
    end

    if per_rc ~= 0
        perc_rc = 1+per_rc/100;
    elseif per_rc == 0
        perc_rc = 1;
    end

    if per_rc <= -100
        fprintf('changed in laminate thickness can not exceed -100%');
        break
    end

    if per_DL ~= 0
        perc_DL = 1+per_DL/100;
    elseif per_DL == 0
        perc_DL = 1;
    end

    if per_DL <= -100
        fprintf('changed in laminate thickness can not exceed -100%');

```

```

    break
end

kf(2) = perc_kf*kf(1);
Dp(2) = perc_Dp*Dp(1);
Dc(2) = perc_Dc*Dc(1);
rc(2) = perc_rc*rc(1);
DL(2) = perc_DL*DL(1);

for d = 1:2

v(d) = Q/(xsect*void(d)*60);

% 1/Kk'

    mass_x_fer = (DL(d)/v(d)^2)*((1-
void(d))/void(d))+((Rp(d)/(3*kf(d)))+(Rp(d)^2/(15*ep*Dp(d)))+(rc(d)^2/(15*K*Dc(d))));

%k'

    kprime(d) = 1/(mass_x_fer*K);

%Calculating Xi (the dimensionless bed length)

    Xi(d) = (kprime(d)*K*z/v(d))*((1-void(d))/void(d));


for t = b:1:totaltime
    if t < z/v(d)
        b=t+1;
    else
        Tau(d,t) = kprime(d)*(t-z/v(d));
        X = sqrt(Xi(d))-sqrt(Tau(d,t));
        storetime(t)=t;
        conc3(d,t) = (1/2)*erfc(X);
    end

end

end

%Plotting the predicted C/Co and raw data to compare

if totaltime < b
    fprintf('Insufficient totaltime specified');
    break
end

```

```

figure(c)
plot(Tau(1,b:t),conc3(1,b:t),'b^',Tau(2,b:t),conc3(2,b:t),'go');
xlabel('Tau');
ylabel('C/Co');
title('C/Co vs. Tau');
legend('model3_standard','model3_changed');

```

Xi

end

toc

```

Tautemp=Tau';
Tautemp1=Tautemp(1:length(storetime),1);
Tautemp2=Tautemp(1:length(storetime),2);
conc3stand=conc3(1,1:length(storetime))';
conc3chang=conc3(2,1:length(storetime))';

```

%writing the results to a text file to be used in Excel to plot C/Co vs. Tau graphs

```

y = [Tautemp1;conc3stand;Tautemp2;conc3chang];
fid = fopen('disper99.99neg.txt','wt');
fprintf(fid,'%6.4f\n',y);
fclose(fid);

```